Title
Deciphering Mechanisms of Early Meiotic Gene Expression Through Ume6 and Ime1

Author
Harris, Anthony

Publication Date
2023

Peer reviewed|Thesis/dissertation

Deciphering Mechanisms of Early Meiotic Gene Expression Through Ume6 and Ime1

by

Anthony Harris

A dissertation submitted in partial satisfaction of the

requirements for the degree of

Doctor of Philosophy

in

Molecular and Cell Biology

in the

Graduate Division

of the

University of California, Berkeley

Committee in charge:

Professor Elçin Ünal, Chair
Professor Douglas Koshland
Professor Barbara Meyer
Professor Kathleen Ryan

Summer 2023

Deciphering Mechanisms of Early Meiotic Gene Expression Through Ume6 and Ime1

Abstract

Deciphering Mechanisms of Early Meiotic Gene Expression Through Ume6 and Ime1

by

Anthony Harris

Doctor of Philosophy in Molecular and Cell Biology

University of California, Berkeley

Professor Elçin Ünal, Chair

The process of gametogenesis is orchestrated by a dynamic gene expression program, where a vital subset constitutes the early meiotic genes (EMGs). In budding yeast, the transcription factor Ume6 represses EMG expression during mitotic growth. However, during the transition from mitotic to meiotic cell fate, EMGs are activated in response to the transcriptional regulator Ime1 through its interaction with Ume6. While it is known that binding of Ime1 to Ume6 promotes EMG expression, the mechanism of EMG activation remains elusive. Two competing models have been proposed whereby Ime1 either forms an activator complex with Ume6 or promotes Ume6 degradation. Here, we resolve this controversy using a combination of depletion and tethering strategies to functionally characterize both Ume6 and Ime1 (Chapter 2 and Chapter 3).

Much of the research surrounding Ume6 function, and the genes it regulates, has come from using a null allele (*ume6*Δ). Accordingly, constitutive loss of *UME6* function leads to derepression of several meiosis specific genes during mitosis. Expression of these meiotic genes during the mitotic cell cycle causes conflicts in cellular machinery and leads to pleiotropic consequences. Instead of *ume6*Δ to assess *UME6* function, here we leverage the auxin inducible degron (AID) system to construct a depletable allele of *UME6* (Ume6-AID). This allele of *UME6* maintains repression of its targets during the mitotic cell cycle. Using this approach, we identify the set of genes that are directly regulated by Ume6, including *UME6* itself (Chapter 2).

With the development of Ume6-AID, we next investigated the functional relationship between Ume6 and Ime1 by combining our Ume6-AID with a method of synchronizing expression for *IME1*, which encodes the meiotic transcription factor, and *IME4*, which encodes an mRNA N6-adenosine methyltransferase (Chapter 3). This increased control allowed careful monitoring of how Ume6 responds to *IME1* and *IME4* expression and allowed functional dissection of Ume6's role in the mechanism of early

meiotic gene (EMG) expression. We find that, while Ume6 protein levels increase in response to Ime1, Ume6 degradation occurs much later in meiosis, in a manner dependent on another meiotic transcription factor called Ndt80. Importantly, we found that depletion of Ume6 shortly before meiotic entry is detrimental to EMG activation and gamete formation. Finally, to explore the functional role of Ime1 in EMG expression, we employed a tethering strategy. We find that tethering of Ume6 to a heterologous activation domain is sufficient to trigger EMG expression and produce viable gametes in the absence of Ime1. These data indicate that Ime1 and Ume6 form an activator complex in meiosis. While Ume6 is indispensable for EMG expression, Ime1 primarily serves as a transactivator for Ume6.

This dissertation unifies observations from two disparate models involving Ime1 and Ume6 and their involvement in meiotic initiation. Our work unveils the impact Ime1 has on Ume6 through its binding to Ume6 and how this influences EMG expression. In doing so we elevate Ume6 to a primary determinant of cell state through its exchange of transcriptional cofactors and significantly advance our understanding of meiotic gene regulation.

To my Mom, Carrie, Son Eli, and Daughter Zoey

Contents

List of Figures

List of Tables

Acknowledgements

I would like to thank all members of the Brar and Ünal laboratories past and present for creating a positive and stimulating environment that has made my scientific pursuits enjoyable, fulfilling, and full of lasting friendships. I would also like to thank those who played a central role in the development, refinement, and execution of this work: Gloria Brar, Christiane Brune, Leon Chan, Jingxun Chen, Jay Goodman, Andrea Higdon, Jessica Leslie, Kate Morse, Emily Powers, Cyrus Ruediger, Eric Saywer, Tina Sing, Ben Styler, Amanda Su, Peter Sudmant, Jeremy Thorner, Folkert van Werven, Alec Uebersohn. In addition to this, I'd like to thank Amy Tresenrider for her training and guidance during my introduction to the Ünal laboratory. Amy's patience and passion for science were inspiring and I'm honored to have carried her legacy of investigating Ume6 and meiotic entry further. I'm proud to call her friend and wish her the best. I'd like to thank Tina Sing, for being a phenomenal bay mate. Her encouragement always lifted me up and our scientific conversations were always stimulating. I'd like to thank Chris Mugler for his instruction of performing wet protein transfers, which significantly improved my immunoblotting of Ume6. I'd like to thank Grant King for his guidance in performing time-lapse microscopy for the visualization of chromosomes. Thank you Lizet Reyes Rodas for being a wonderful student during the NSF-REU. It was a pleasure having a partner on the journey for Ume6 discoveries. I'd also like to thank QB3 Genomics Facility at the University of California, Berkeley, for technical assistance and guidance in processing and analyzing RNAseq samples.

I'd like to specifically thank my thesis committee members: Doug Koshland, Barbara Meyer, and Kathleen Ryan. They made committee meetings a challenging and intellectually rewarding experience. For their oversight in the development of this work over the years and their intellectual contributions. I wouldn't be where I am without your guidance, and I intend to take the lessons given with me moving forward. In addition to this, I'd like to thank Doug Koshland for his attendance of seminars and level of engagement with speakers. His questions have always come from a place of honest curiosity for the science and inspires me to ask questions of my own. Thank you, Doug Koshland, for being a phenomenal scientist.

Most of all, I'd like to thank an amazing influence on both my personal and scientific development during my graduate education, Elçin Ünal. Her energy knows no limits, her passion knows no bounds, and her compassion has no reservation. Elçin's unwavering respect and confidence in my abilities is a fundamental reason this work exists. I can't

image having gone through this experience without the support of such a phenomenal mentor. The lessons she endowed in me will be carried high and passed to many.

I'd like to thank my family who supported me during the development of this work. To my mom, your encouragement, love, and support over the years has always taught me to believe in myself, even when things are at their hardest. These lessons are why I made it to graduate school and have achieved this PhD. To my uncle, Daniel Harris, whose life was cut short, thank you for teaching me what it means to be a curious explorer and having a little too much tenacity. You taught me that it's ok to take risks and always push myself just a little further than I believed I could go. To my wife, Carolyn Harris, who gave up so much to come on this journey with me, I couldn't have done this without you. Throughout graduate school you've always been a glimmer of light, always reminding me to smile, remember how far we've come, and where we still have yet to go. That sometimes we need to take a moment to step away from it all together and come back anew. I couldn't have asked for a more perfect partner in this journey, and I know the life ahead will be even greater as we take on the next adventure together. To my children, Eli Daniel Harris and Zoey Aria Harris, thank you for keeping me moving, for getting me to climb a playground, jump in a pool, and reminding me to not take things too seriously. Thank you for listening to my stories and showing me that just because the lesson is hard doesn't mean it can't be learned.

Chapter 1

Introduction

Genetic diversity has been a cornerstone in species survivability and a driving force for evolutionary progress. One manner of achieving genetic diversity is the cellular differentiation program of gametogenesis (also termed meiotic differentiation due to its intimate relationship with meiosis), whereby a progenitor cell doubles and shuffles its DNA content before undergoing meiotic divisions. These meiotic divisions are triggered by a coordinated response to a variety of context specific cues from both internal and external sources. Successful execution of gametogenesis requires the coordinated expression of a plethora of genes that must be properly regulated. When properly regulated, these genes influence chromatin architecture and cellular morphology to produce genetically distinct gametes (Mitchell 1994; Neiman 2011). Conversely, misregulation of these genes results in loss of overall fitness and inability to properly initiate meiosis. Because of their impact on organismal survival, the control of meiotic gene expression is of paramount importance. Fine-tuning expression patterns for meiotic genes occur through regulation by transcription factors (TFs). TFs are a superfamily of proteins that bind and influence chromatin to aid in and initiate transcription. In meiosis, TFs are responsible for a fundamental decision made by cells, whether to initiate meiosis and activate these genes. Once made, this decision triggers waves of genes to work in concert and initiate the meiotic program.

1.1 Structural Dynamics Within DNA Organization that Help Regulate Transcription

DNA is organized at many levels to ensure integrity and transmissibility as the genetic information. At the first level of organization, DNA itself is a highly negative phosphodiester string of adenine (A), thymine (T), cytosine (C), and guanine (G) nucleic acid bases (Chargaff 1950). Each nucleic acid carries unique biochemical properties, one of which is to recognize a complementary nucleic acid in the opposite orientation and hydrogen bond (A to T and C to G). Association between nucleic acids forms the double stranded DNA (dsDNA) structure and due to the nature of this opposing complementarity, sister strands in dsDNA run antiparallel giving the dsDNA directionality (Watson and Crick 1953). This antiparallel dsDNA structure forms a double helix with ~10 nucleic acids per 34 Å turn with several major and minor grooves that establish the second level of organization for DNA. As the genetic material, DNA must be transmissible but also

contain the codes for an astonishing number of protein structures. Indeed, even a smaller eukaryotic genome like that of budding yeast consists of ~ 12 million base pairs (bps) of DNA containing the ~6,500 protein coding genes that must be consolidated into a nucleus ~ 2μm across (Duina et al. 2014). Consolidating these long strands of DNA into nuclei leads to the third level of organization by using four core histone proteins called: H2A, H2B, H3, and H4. These core histone proteins dimerize to form an octameric complex with two copies of each core histone protein (Cutter and Hayes 2015). Through electrostatic interactions, ~ 147 bps of DNA wrap tightly around this octamer to form a nucleosome. These nucleosomes are stacked in their own helical structure and with the aid of histone H1, can be condensed into helices ~30 nm in diameter that appear as chromosome structures. These three levels of organization help cells maintain and fit the tremendous amount of DNA into the nucleus for use by a variety of factors and lay the foundation for DNA regulation.

Influencing DNA expression patterns using these three levels of organization requires a variety of factors, particularly TFs, that are capable of navigating a highly dynamic DNA structure. By manipulating nucleosome positioning and recognition of DNA landmarks strategically positioned across the genome, TFs are able to identify sites of relevance to further influence DNA architecture and ultimately tune patterns of gene expression (Maston et al. 2006). In yeast, regions that exist within ~200 bps upstream of a transcriptional start site (TSS) called promoters, are important sites of recognition for TFs. Metazoans have adopted additional regulatory elements called enhancers whose distances from their TSSs vary greatly. For example, an enhancer involved in limb development, the *ZRS* enhancer, can exist ~900,000 bps away from a TSS while the *ß*-globin LCR is ~100,000 bps away from its TSS (Williamson et al. 2016). These promoters and enhancers serve to direct the many TFs necessary to recruit the transcriptional machinery to start transcription.

A variety of core elements exist in promoters that allow developmental signals to control binding propensity of RNA Pol II and the general transcription factors (GTFs): TFIIA, TFIIB, TFIIE, TFIIF, and TFIIH, which together can form the transcription preinitiation complex (PIC) (Sainsbury et al. 2015). These elements include the TATA element, initiator (INR), downstream promoter element (DPE), motif 10 element (MTE), and the TFIIB recognition element (BRE), and although not ubiquitous in all promoters, these elements direct landing, assembly, and orientation of the GTFs and RNA Pol II. The INR defines the region over which the TSS occurs. The TATA element, located ~ -30 bp from the TSS, is recognized by the TATA-binding protein (TBP) and serves as the foundation for GTF landing. The DPE, ~ +30 bp from the TSS, also serves to properly orient the PIC. The BRE, ~ -35 bp from the TSS, is used by TFIIB to accurately position RNA Pol II. Finally, an MTE located ~ +25 bp from the TSS, operates synergistically with

the TATA and DPE to enhance transcription initiation (Lim et al. 2004; Hahn and Young 2011). Together, these elements play a critical role in establishing the TSS and dictating the basal activity of gene expression through assembly of the PIC.

Along with establishing PIC orientation and assembly, promoters also contain DNA motifs recognized and bound by other TFs. These sequence motifs are termed upstream activation sequences (UASs) or upstream repressive sequences (URSs) depending on their use by transcriptionally activating or repressing TFs, respectively, and are strong predictors of TF binding. Since the initial discovery and structural resolution of the TFs Lac and λ repressors, the UAS and URS were thought to be chiefly recognize by TFs using sequence specific context (Kribelbauer et al. 2019). However, compared to the palindromic DNA recognition scheme used by restriction enzymes, these TF motifs contained many degenerate sequences (Stormo 2013). With the characterization of additional TFs like Gal4, Sp1, and many more, it became increasingly apparent many TFs recognize degenerate versions of their DNA recognition motifs (Dynan and Tjian 1983; Pabo and Sauer 1984; Bram et al. 1986). These degeneracies resulted in variable binding across the genome that was highly situational. Summaries of these binding profiles were subsequently represented in position weight matrixes (PWMs) to capture these degeneracies and provide an overall consensus sequence still used today (Stormo 2013).

Alternative to sequence mediated regulation of DNA, nucleosome occupancy within promoters can further influence transcriptional potential at these sites. Histone consolidation of DNA into the nucleus naturally impacts DNA density and accessibility by TFs. Chromatin exists as long DNA strings linking nucleosome beads. Positioning of these nucleosome beads can either reveal or mask regions with transcriptional potential through their degree of occupancy. Regions of high nucleosome occupancy and, by extension, densely packed DNA are frequently associated with inactive or silenced chromatin. These heterochromatic regions contain dormant genes unable to be expressed (Henikoff 2000). Conversely, regions with fewer and more sporadically positioned histones are termed euchromatic, and are frequently associated with active transcription, especially when cued by a developmental response. Initiation of transcription at euchromatic regions involves shifting of these loose nucleosomes away from sites of transcription within promoters to create nucleosome depleted regions (NDRs). These NDRs contain exposed chromatin and are flanked by a nucleosome upstream (-1) and downstream (+1). The shifting of nucleosomes across the DNA plays a fundamental role in toggling the transcription activity of genes ensuring appropriate and timely response to developmental signals.

Shifting of nucleosomes away from sites of active transcription to form NDRs occurs in part through post-translational modifications to the flexible nucleosome “tail”.

These nucleosome tails are peptide strings protruding from each histone core protein that are subject to covalent alterations. The histone H3 tail is extensively modified and plays a more significant role in transcriptional regulation compared to the other histone tails (Kouzarides 2007; Zhao and Garcia 2015). Modifications frequently involve the addition or removal of acetyl or methyl groups by histone acetyltransferases (HATs) or histone deacetylases (HDACs) and histone methyltransferases (HMTs) or histone demethylases (HDMs), respectively. Acetylation, correlated with sites of transcriptional upregulation, is a chemical modification to lysine that neutralizes the positive charge and loosens its electrochemical bond to DNA to create sites of open chromatin. Methylation on the other hand, often associated with transcriptional downregulation, is a chemical modification made either to lysine or arginine that needn't disrupt the charge but does often recruit HDACs (Kouzarides 2007; Clapier and Cairns 2009). Additionally, other modifications exist including ubiquitylation, sumoylation, and phosphorylation that are implicated in transcription, but also other events like DNA repair and cell cycle (Zhao 2015). Together, these marks coalesce in architectural rearrangements that impact transcription and the developmental response (Clapier and Cairns 2009).

1.2 Transcription Factors Initiate Developmental Responses

TFs make up a highly diverse family of proteins with domains conserved across many species. In prokaryotes, the number of TFs varies widely between species with *Bacillus subtilis* having 113 confirmed TFs and *Rickettsia prowazekii* containing only nine (Andersson et al. 1998; Moreno-Campuzano et al. 2006). However, the shift from prokaryotes to eukaryotes, and even metazoans, experienced a marked increase in the number of TFs. To date, TFs comprise nearly 183 characterized members in yeast and in humans reaches ~ 1,600 and additional experimentation will likely only increase these numbers (Lambert et al. 2018; Monteiro et al. 2020). Despite their abundance, this group of proteins can be classified by a limited number of similar structural features they utilize to associate with DNA, termed a DNA-binding domain (DBD). Three major classes of DBDs found in nature populate the family of TFs (Hahn and Young 2011). The most abundant are the zinc (Zn^{2+}) finger proteins that stabilize DNA-TF complexes through a cysteine or histidine bound Zn^{2+} ion. The zipper-type DBDs are the next most abundant and they form a dimeric structure with motifs rich in leucine (bZIP) or highly basic stretches (bHLH). Helix-turn-helix (HTH) DBDs are the third most abundant and also form homo- or heterodimeric structures with a combination of exposed peptides that contact DNA in unique ways (Hahn and Young 2011). Using these DBDs TFs are able to navigate to unique DNA sites and influence transcription.

Along with DBDs, TFs also employ embedded or associating regulatory domains termed activating domains (ADs) or repressive domains (RDs) whether they encourage or discourage active transcription, respectively. ADs and RDs mediate transcription initiation using a combination of methods that (1) alter chromatin structure through histone remodeler/modifying enzyme activity, (2) recruit transcriptional machinery such as the GTFs, and (3) improve downstream transcriptional efficiency of the PIC post transcription initiation (Hahn et al. 2011). Despite the abundance of TFs that contain both a regulatory domain and DBD together, TFs more frequently exist as a multimeric structure of associating and disassociating subunits (Hahn and Young 2011). Because of this, a single DBD can adopt different situationally specific AD or RD and vice versa an AD or RD can bind a variety of DBDs expanding their influence. This promiscuity within TF structures helps TFs regulate genes in a variety of methods to coordinate large-scale genetic responses. Furthermore, these large-scale responses often form intricate regulatory networks of many TF interactions that further fine-tune both metabolic and developmental responses.

To transform extranuclear signals into an appropriate metabolic/developmental response, TFs often use crosstalk between expansive networks of different TFs. Studies of galactose utilization in yeast have been instrumental in understanding these regulatory networks(Johnston 1987; Weinhandl et al. 2014). The galactose sensing pathway, which assesses galactose/glucose availability and relays that signal to the galactose responsive genes involves many factors including the glucose sensing repressor Mig1 bound to Cyc8-Tup1 (an HDAC), the galactose sensor Gal3, the transcriptional activator (TA) Gal4, and the transcriptional repressor (TR) Gal80 (Weinhandl et al. 2014). The glucose and galactose-based signals can converge at many genes involved in galactose usage as follows. In glucose-rich and galactose-limiting conditions, glucose is used as the primary carbon source and any Gal4 activity is masked through Gal80 binding while Mig1 binds the promoter of galactose responsive genes and deacetylates histones. This deacetylation leads to a more compact chromatin state restricting access to activating factors. Absence of glucose triggers dissociation of Mig1 and with it the restrictive compact chromatin state. Subsequently, the addition of galactose is sensed by Gal3 which localizes to the nucleus. Gal3 then binds Gal80 to sequester it in the cytoplasm and unmask Gal4's activation domain (Hahn and Young 2011). Convergence of glucose-limiting and galactose-rich signals through TFs then leads to the expression of several other classes of proteins involved in galactose metabolism. Thus, regulatory networks like galactose metabolism are an example of genetic on/off switches for toggling large subsets of genes involved in complex networks.

Along with a glimpse of the intricacies of regulatory networks, the galactose pathway also provided insights into the modularity of TFs using Gal4 as a model. The first

important insight came from the Ptashne group who found Gal4 had two functionally distinct domains, the C-terminal DBD and the N-terminal AD, that could be dissected and reconstituted (Keegan et al. 1986). Furthermore, Gal4's activation potential was found to transfer to other systems, a testament to the conservation of these mechanisms (Fischer et al. 1988; Kakidani and Ptashne 1988; Ma et al. 1988; Webster et al. 1988). Inspired by this modularity, the yeast two-hybrid (Y2H) technique was then developed, whereby the Gal4(DBD) and Gal4(AD) could be tethered to distinct protein domains. Association between these protein domains would recombine Gal4(DBD) and Gal4(AD) to initiate transcription. This protein-protein interaction could then be determined using a reporter gene and novel protein interactions could be determined (Fields and Song 1989). Since then, this system has been exploited to interrogate a vast number of protein-protein interactions and analogous inducible systems have arisen that allow conditional expression of genes. (Quintero et al. 2007; Brückner et al. 2009; Ottoz et al. 2014). This potential for modulating TF domains has been grossly exploited in biological systems where a single DBD can associate and exchange an egregious number of factors to help coordinate many regulatory and developmental responses.

By combining modulation and crosstalk, TF subdomains can react and relay a variety of signals through large associating and dissociating interconnected structures. An example of this modularity and crosstalk is the highly conserved TF Sin3 (*Drosophila* Sin3.187, Sin3.220, and Sin3.190; Mammalian Sin3A and Sin3B; Kadamb et al. 2013). First discovered as a negative regulator of mating-type switching in yeast, Sin3 would later also be identified in screens for meiotic and metabolic mutants (Nasmyth et al. 1987; Sternberg et al. 1987; Strich et al. 1989; Chaubal and Pile 2018). Sin3 exercises its modular function by providing docking sites for a number of TFs. The most studied of which is the also highly conserved associated factor Rpd3 (Mammalian HDAC1 and HDAC2), which provides Sin3 a RD in the form of an HDAC that removes acetyl groups to effectively compact nucleosomes. Some less studied RDs adopted by Sin3 have been documented that increase its repressive capabilities and form either the Rpd3L or Rpd3S complexes on Sin3 along with Rpd3. The Rpd3L complex conditionally acquires Rxt1, Rxt2, Dep1, Sds3, Pho23, and Sap30, while the Rpd3S complex can adopt Eaf3 and Rco1 (Kadamb et al. 2013). To serve as a TF in a variety of pathways, Sin3 also contains a DBD docking site. In yeast, Sin3 docking has been confirmed at Ume6, Ash1, and Opi1, which allows repression of meiotic genes, homothallic endonuclease (HO) transcription, and phospholipid biosynthesis, respectively (Jäschke et al. 2011; Chaubal and Pile 2018). Analogous structures have been found in other species including human p53-Sin3A at the *Nanog* promoter, which has been shown to repress embryonic stem cell differentiation under nonproliferating conditions (Chaubal and Pile 2018). Relieving this Sin3-mediate repression often involves a variety of pathway specific alterations to Sin3 binding and interactions. For example, alleviation of Ash1/Sin3 repression in mate-type switching

occurs through Ash1 localization. During the yeast cell cycle, two TFs, Swi5 and Ash1, play an important role in expression or repression, respectively, of the HO endonuclease involved in initiating mating-type switching. To initiate this process, yeast begin manufacturing Swi5 during G2 where it remains cytosolically localized. Shortly after anaphase, Swi5 is localized to the nucleus of the mother and daughter cell, while *ASH1* transcripts are actively shuttled to only the daughter-cell's nucleus. The presence of Ash1 allows Ash1/Sin3-mediated repression of HO in the daughter preventing mating-type switching. As this daughter reenters the cell cycle, Ash1 levels rapidly decrease and are more-or-less gone by late G1/S phase. By fluctuating levels of its DBD Ash1, cells can not only regulate Sin3 activity in a cell specific manner, but also independently of the other DBDs where Sin3 is bound (Amon 1996; Haber 2012).

Through leveraging both promoter elements and the swapping of RDs and ADs, TFs can quickly switch from transcriptional repression to activation and in doing so recruit a variety of coactivators, GTFs, and RNA Pol II as follows. Initially, TFIIA promotes TBP transport to the core promoter by either of two distinct pathways involving TFIID or SAGA. TBP then interacts with the DNA minor groove in a TFIIB-dependent manner using BRE to coordinate binding. Along with TFIIF and RNA Pol II, an important coactivator called the Mediator complex is also recruited to serve as a bridge between the TFs, GTFs, and the PIC, establishing the core PIC that spans ~ 60 bps of DNA. Once formed, TFIIE and TFIIH are then loaded onto the core PIC, at which point the Mediator stimulates TFIIH-mediated phosphorylation of the PolI II carboxy-terminal domain (CTD) to further stabilize the PIC. TFIIE connects TFIIH to the PIC and permits TFIIH-mediated strand separation by means of its helicase activity and phosphorylation of the CTD at Ser5 and -7 using its kinase activity. TFIIH addition creates a transcriptional bubble where RNA Pol II can begin forming the nascent RNA chain. Shortly after the formation of this nascent chain, Pol II's CTD is phosphorylated once more at Ser2 and RNA Pol II is converted from the PIC to an elongation complex to transcribe the full RNA (Hahn and Young 2011; Sainsbury et al. 2015; Soutourina 2018).

How TFs, particularly their ADs, initiate this tremendous series of events is still a subject of debate. ADs generally exist structurally distinct from their DBD as intrinsically disordered proteins carrying acidic and hydrophobic stretches. At first, it was unclear which domains were important for activation and how such highly disordered proteins could associate with their DBDs so effectively. Initial insights came from experiments with Gcn4, in which the Mediator protein Med15 interacts with the AD of Gcn4 at two distinct sites in an additive way (Park et al. 2000; Majmudar et al. 2009; Herbig et al. 2010; Jedidi et al. 2010). Additional work regarding Gcn4 where all 10 acidic peptides were swapped with Ala, an aliphatic peptide, had transcription of *ARG3* and *HIS4* only minimally effected (Brzovic et al. 2011). This suggested that despite their prevalence, the acidic residues of

Gcn4 seemed dispensable for transcription. Alternatively, NMR data collected by this group revealed that binding of Gcn4 to its coactivator Med15 in a purely hydrophobic interaction allows Gcn4 to adopt two equally probable and distinct conformations termed a “fuzzy complex”. Prior to this binding, Gcn4 exists as eight unstructured conformations, however binding to Med15 permits the Gcn4 fuzzy complex to bind at the two distinct Med15 domains. This conversion to a stable structure through hydrophobic bonding between TF-coactivator had also been previously confirmed in another activator, CREB. Through phosphorylation and binding to CBP, CREBs coactivator, CREB also transitions from an unstable structure to a lower energy highly structured conformation (Turjanski et al. 2008). Furthermore, many nuclear proteins have been found to contain low-complexity domains, also called intrinsically disordered regions (IDRs), capable of creating liquid-liquid phase separated micro-environments (Banani et al. 2017). Increasing appreciation for phase separated compartments and their biological relevance has revealed a number of functional roles for this phenomenon including mRNA shuttling between compartments and organization of the actin cytoskeleton (Mitrea et al. 2016; Su et al. 2016; Hondele et al. 2019). Along with these demonstrations of function for phase separation, pockets of high TF and RNA Pol II activity have been observed (Liu et al. 2020). Additionally, TAs like Gcn4 that have had their IDRs disrupted fail to initiate transcription (Boija et al. 2018). Strikingly, decapeptides containing poly-glutamic acid stretches were able to be incorporated into phase-separated droplets (Boija et al. 2018). Taken together, these results suggest that TF IDRs and hydrophobic stretches, instead of acidic stretches, lead to phase separated micro-compartments that recruit and bind coactivators to influence gene expression.

1.3 Meiotic Regulatory Circuits

Through their ability to influence the transcriptional machinery, and with it the expression of diverse collections of proteins, TFs coordinate large-scale developmental programs that reorganize and reshape the chromatin landscape. One such program is gametogenesis (or meiotic differentiation), and is responsible for the formation of sex cells, also called gametes. Executing meiotic differentiation is energy intensive and requires the coordination of large subsets of genes that are under the control of master regulatory TFs. In meiotic differentiation, these master regulatory TFs set into motion a sequence of events that are often difficult or impossible to reverse. This irreversibility makes meiotic differentiation a non-cyclic terminal differentiation program and results in gametes that are genetically distinct from the progenitor cell. Thus, entry into this program is highly regulated and often requires the convergence of multiple signals to trigger expression of these master regulatory TFs. Upon their expression and entry into meiotic differentiation, gametes are generated that contain unique combinations of alleles, or

gene isoforms. Formation of these gametes and their reunion to form progeny by sexual reproduction allow a near infinite combination of alleles to occur, many of which can dramatically increase an organism's fitness. This fitness advantage has led to meiotic differentiation being highly conserved within many eukaryotes, especially multicellular eukaryotes where not many examples exist of non-meiotic multicellular eukaryotes. Even within the unicellular branches of eukaryotic life, many examples of meiotic differentiation can be found such as within the ciliated *Paramesium* and *Tetrahymena*, the fungi *Saccharomyces cerevisiae* and *Schizosaccharomyces pombe*, and more recently *Salpingoeca rosetta*, a member of the choanoflagellates that are thought to be the closest unicellular ancestor of animals (Woznica et al. 2017). Due to the nature of meiotic differentiation, its study has been invaluable in understanding the complexity of transcriptional regulation and the events they can unfold.

Meiotic differentiation is characterized by several regulatory and morphological events. The exposure to meiotically favorable signals encourages exit from the mitotic cycle in G1, forgoing mitotic S phase and instead opts cells into meiotic S phase (Marston and Amon 2004). Concomitantly, much of the mitotic machinery is shutdown or repurposed to fulfill the meiotic program. During S phase the DNA is replicated to produce sister chromatids and effectively doubles ploidy. Around the same time, hundreds of programmed double- strand breaks (DSBs) are introduced to the genome. After S phase, cells enter a prolonged prophase where DSBs are repaired and homologs form linkages in order to pair and ensure proper alignment. The first linkage joining homologs, the synaptonemal complex (SC), is a series of proteinaceous interactions that behave as a liquid crystalline bilayer (Rog et al. 2017). The second linkage formed in prophase results from meiotic recombination. Resolution of DSBs occurs through exchange of homologous DNA strands to form physical crossovers (COs) that mix chromosomes. Upon completion of recombination and proper alignment of chromosomes cells undergo two rounds of nuclear divisions. The first nuclear division, termed meiosis I, segregates homologous chromosomes while the second, termed meiosis II, segregates sisters. After these two rounds of segregation, each gamete contains one copy of the genetic material (1n) compared to the progenitor (2n). Restoring the genetic content back to 2n requires union of two gametes and forms the basis for genetic diversity in progeny of sexual reproduction.

Strides have been made in understanding events surrounding meiotic entry across species. In *Caenorhabditis elegans* gonads, meiotic entry is dictated by a concentration gradient between two FBF (FBF-1 and -2) and three GLD (GLD-1, -2, and -3) RNA binding proteins (Kimble and Crittenden 2007). This gradient is established by distal tip cells (DTCs) that, through activation of GLP-1/Notch signaling, increase FBF levels and decrease GPD levels. As cells migrate away from GLP-1/Notch signals these

concentrations invert until cells encounter the transition zone (TZ) and trigger the cascade of events for entry into the meiotic program. The TZ thus demarcates the boundary between mitotic and meiotic programs and appears thus far controlled chiefly through post-transcriptional means. Mutations that disrupt these proteins can produce sterile cells (*glp-1* nulls) or shift the TZ (*fbf-1* and *-2* nulls; Lamont et al. 2004). Despite an understanding of this post-transcriptional mechanism for meiotic entry no master TF have been identified (Lamont et al. 2004; Kimble and Crittenden 2007). Alternatively, mammalian meiotic entry is influenced thus far by three TFs: Max, Meiosin, and *Stra8*. Max is a bHLH family TF that possess both repressive and activating properties depending on its heterodimeric association to *Mad/mSin3* or *Myc*, respectively (Ayer et al. 1993). Knock-down of Max causes derepression of many meiosis specific genes including another bHLH family TF called *Stra8* (Suzuki et al. 2016; Ferder et al. 2019; Grandori et al. 2000). *Stra8* expression is regulated by levels of retinoic acid (RA). RA is an active metabolite of vitamin A and its levels play an important role in many developmental events. Because of this, RA levels are highly regulated by RA-degrading enzymes like cytochrome P450 (CYP26; Reviewed in Spiller et al. 2017). Indeed, it's been shown that *Cyp26b1-KO* mouse embryos, where RA accumulates, shows *Stra8* becomes ectopically expressed (Bowles et al. 2006). Furthermore, treatment of mammalian germ cells with RA is sufficient to drive meiotic genes expression (Tedesco et al. 2013). Like many ADs, *Stra8*'s AD doesn't contain much homology but does contain stretches of acidic residues that, in subsequent work, cemented *Stra8* as a transcriptional activator both *in vitro* and *in vivo* (Tedesco et al. 2009; Ferder et al. 2019; Kojima et al. 2019). More recently, it's been found that Stra8 is coexpressed in male and female germ cells with another bHLH TF called Meiosin (Reviewed in Ishiguro 2023). Interestingly, Meiosin contains a high mobility group (HMG)-box, which are domains often associated with DNA binding(Ishiguro et al. 2020). Further probing revealed Stra8 and Meiosin share a DNA binding motif by ChIP-Seq as well as many overlapping targets, *Meiosin KO* and/or *Stra8 KO* lines fail to initiate meiosis, and both TFs respond to increases in RA (Ishiguro et al. 2020). Taken together, Meiosin and Stra8 appear to work in concert to promote EMG expression in mammalian systems.

In the budding yeast *Saccharomyces cerevisiae*, gametogenesis is characterized by the activation of a series of temporally distinct gene expression clusters. The first cluster, known as the early meiotic genes (EMGs), contains evolutionarily conserved meiosis-specific genes required for DNA replication, recombination, and synapsis that ensure proper segregation of chromosomes into gametes. The coordinated expression of EMGs during gametogenesis is achieved through the common upstream regulatory sequence 1 (URS1) motif found in their promoters, which is recognized by the transcription factor Ume6 (Park et al. 1992). Ume6 interacts with three other factors – Sin3, Rpd3, and Ime1 – to toggle the expression of EMGs on or off in different

developmental contexts (Bowdish and Mitchell 1993; Park et al. 1992; Washburn and Esposito 2001; Figure 1.1). This is achieved through three distinct regions in Ume6: the DNA-binding domain, the Sin3-Rpd3 histone deacetylase binding domain, and the Ime1 binding domain. Thus, Ume6 facilitates the repression and expression of EMGs by recruiting these factors to EMG promoters.

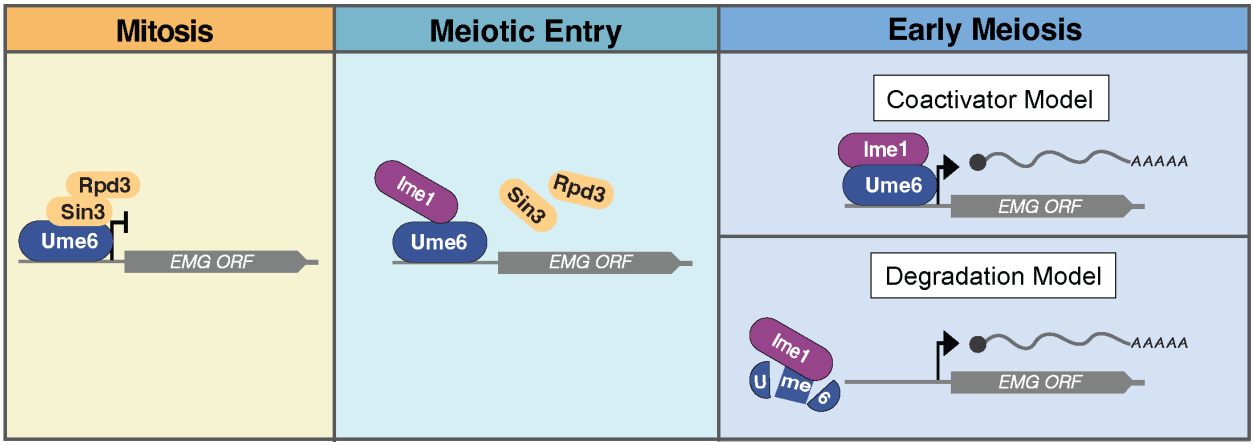

Figure 1.1: Two models of early meiotic gene (EMG) expression through Ume6 and Ime1 interaction. During vegetative growth, Ume6 associates with the Sin3-Rpd3 complex ensuring quiescence of the EMGs. The decision to enter meiosis requires exposure to nutrient and mating-type specific cues that help drive many events including: (1) dissociation of Sin3-Rpd3 from Ume6 and (2) expression of the Ime1 TF. Once expressed, Ime1 associates with Ume6. This association is critical to initiating meiotic initiation through EMG expression. However, how Ime1 binding influences Ume6 to promote EMG expression remains unclear. Two models have been presented to explain how Ime1 binding to Ume6 stimulates EMG expression. In the "Coactivator model", Ime1 serves as a transactivator, and its binding converts Ume6 to an activator complex. In the "Degradation model", Ime1 acts as a signal for Ume6 degradation, and its binding displaces Ume6 from EMG promoters.

Despite the importance in recruitment of Ime1 to EMG promoters through its interaction with Ume6, the influence Ime1 has on Ume6 itself to initiate EMG expression and enter cells into the meiotic program remains unclear. Two conflicting models have been proposed to explain Ime1's role in the expression of EMGs. The first model suggests that Ime1, with its activation domain, binds Ume6 to convert it from a transcriptional repressor to an activator, and this conversion drives EMG expression (Rubin-Bejerano et al. 1996; Smith et al. 1993; Washburn and Esposito 2001; Bowdish et al. 1995). More recently, Raithatha et al. supported this model through finding that Ume6 remains bound to EMG promoters when these genes are activated (Raithatha et al. 2021). Conversely, the second model of EMG expression posits that Ime1 binding to Ume6 functions as the signal which leads to the subsequent degradation of Ume6, and in turn, the derepression of EMGs (Mallory et al. 2007; Law et al. 2014; Mallory et al. 2012). Discrepancies between each model likely stem from a number of factors. Firstly, the *IME1* promoter spans over two kilobases and receives signal input from a variety of internal and external cues related

to carbon source, nitrogen availability, and mating (Reviewed in van Werven and Amon 2011). This complex regulatory network that converges at the *IME1* promoter results in highly variable expression of *IME1*. Because *IME1* is a major driver of meiotic initiation, this variable expression culminates in asynchronous entry of cells into the meiotic program. This heterogeneity in initiation significantly blurs developmental boundaries within meiosis, namely the timing of EMG expression and how it coincides with the timing of drops in Ume6 levels. Furthermore, interrogating questions related to Ime1 and Ume6 role in meiotic entry in a non-meiotically optimized strain background that increases both the variability of *IME1* expression and duration of meiosis only serves to exacerbate the issue. Finally, much of what is known about Ume6 comes from the use of Ume6 null strains (*ume6*Δ). Strains harboring *ume6*Δ are unable to enter meiosis, relegating much of the findings related to Ume6 to mitosis. However, even during mitosis these *ume6*Δ suffer from pleiotropic consequences that leave cells sick. Thus, asynchronous entry and the lack of a system with which to ask more functional questions of Ume6 have prevent resolution between these two models.

Here, we apply a combinatorial strategy to overcome many of the aforementioned limitations and resolve these two models while also providing additional insights into the roles of both Ume6 and Ime1. In Chapter 2, the Ume6 regulon is interrogated using a depletion strategy to reduce Ume6 protein levels conditionally and acutely during mitosis. As a consequence of Ume6's repressive role in mitosis, its depletion derepresses its targets. Thus, we then identify genes that respond to this depletion and, by combining it with a previously acquired Ume6 ChIP-Seq dataset, identify direct Ume6 targets (Tresenrider et al. 2021). In Chapter 3, we probe the interaction between Ime1 and Ume6 using a variety of strategies to ask functional questions of both Ume6 and Ime1. The work then concludes in Chapter 4 with a perspective on how Ime1 and Ume6 facilitate EMG expression, which includes unique insights into functional roles for Ime1 and Ume6. Finally, we provide an outlook on future avenues of exploration.

Chapter 2

The Mitotic Repression of Early Meiotic Genes by Ume6

Introduction

During mitotic growth, EMGs are repressed by a complex made of Ume6 and Sin3-Rpd3 (Figure 1.1). Ume6-dependent targeting of Sin3-Rpd3 to EMG promoters creates a repressive chromatin state, partly through the deacetylation of histone H4 lysine 5 (Rundlett et al. 1998; Strich et al. 1989; Vidal et al. 1991; Wang et al. 1990). In parallel, the *IME1* promoter is strongly repressed by nutritional cues, and any Ime1 protein produced is kept outside the nucleus in a cyclin-dependent kinase (CDK) and target of rapamycin (TOR)-dependent manner (Colomina et al. 2003, 1999; van Werven and Amon 2011). These conditions produce cells that cannot enter meiosis and ensure separation between mitotic and meiotic events. Disruptions to Ume6, Sin3, or Rpd3 result in prolonged misregulation of EMGs during mitosis and are detrimental to cellular health. Despite this, much of the functional analysis of *UME6* during mitosis has largely relied on the characterization of a null allele, *ume6*∆, which manifests pleiotropic phenotypes and gene expression patterns resulting from constitutive loss of EMG repression (Park et al. 1992; Strich et al. 1994; Bowdish et al. 1995; Williams et al. 2002). This accumulation of secondary effects from prolonged exposure to EMG expression largely masks many Ume6 specific effects. Therefore, the subset of genes that are directly regulated by Ume6 remains unclear.

Here we show that, by using an inducible protein depletion approach, Ume6 maintains regulation of its targets during mitosis prior to depletion. This abolishes many of the secondary effects associated with *ume6*∆ resulting in better overall growth of cells. In response to depletion, Ume6 levels drop rapidly and dramatically. In parallel, genes under Ume6 regulation also become derepressed. Interestingly, one such target is *UME6* itself indicating Ume6 autoregulates its own promoter. Additionally, we functionally

validate many long undecoded transcript isoforms (LUTIs) implicated as being under Ume6 regulation. Further, exploration of the transcriptome to identify genes responsive to Ume6 depletion and combining this with a previously acquired Ume6 ChIP-Seq dataset, we identify 144 genes that become derepressed upon acute removal of Ume6 during mitotic growth, thereby revealing its direct transcriptional targets. Consistent with Ume6's role in regulating early meiotic machinery, many of these 144 genes were components important in executing DNA replication, recombination, synaptonemal complexing. However, we also find Ume6 regulates several genes involved in energy production. Taken together, this study bypasses the consequences associated with *ume6*Δ to better define genes directly under Ume6 control, while also revealing a new mode of regulation for *UME6* itself.

Results

Inducible depletion of Ume6 prevents the pleiotropic phenotypes associated with constitutive loss of *UME6* function.

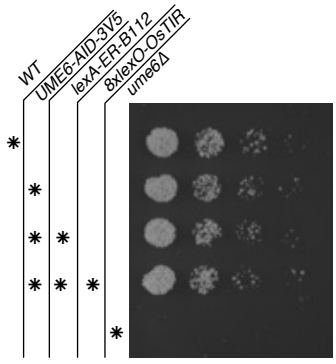

Figure 2.1: Growth phenotype associated with Ume6-AID compared to *ume6*Δ. Growth phenotype of the haploid strains *UME6* (UB17716), *UME6-AID-3V5* (UB18216), *UME6-AID-3V5; lexA-ER-B112* (UB18287), *UME6-AID-3V5; lexA-ER-B112; 4xlexO-OsTIR* (UB17646), *ume6*Δ (UB17718). Strains were serially diluted onto plates containing nutrient-rich media with agar (YPD) and allowed to grow at 30˚C for 48 h before images were acquired.

In mitotically dividing cells, Ume6 acts as part of a repressive complex leading to the silencing of EMGs (Strich et al. 1994; Williams et al. 2002). Attempts to understand Ume6's role during mitotic growth have revealed hundreds of genes involved in both meiotic and metabolic functions (Park et al. 1992; Strich et al. 1994; Bowdish et al. 1995; Williams et al. 2002). However, these studies primarily relied on the use of a null mutant, *ume6*Δ, which has prolonged exposure to meiosis-specific machinery during the mitotic cell cycle, rendering it extremely sick (Figure 2.1) and possibly leading to indirect effects in gene expression.

To overcome the limitations exerted by constitutive loss of *UME6* function, we utilized the auxin inducible degron system (AID, Nishimura et al. 2009), which enables rapid depletion of Ume6 carrying an AID tag (Ume6-AID) in response to the plant hormone auxin and the F-box receptor OsTIR1, which is induced by a ß-estradiol activatable transcription factor (Figure 2.2, see material and methods for technical details). Cells carrying the *UME6-AID* allele grew similarly to wild type in the absence of auxin and ß-estradiol (Figure 2.1), suggesting that degron tagging of *UME6* at the endogenous locus does not interfere with its function.

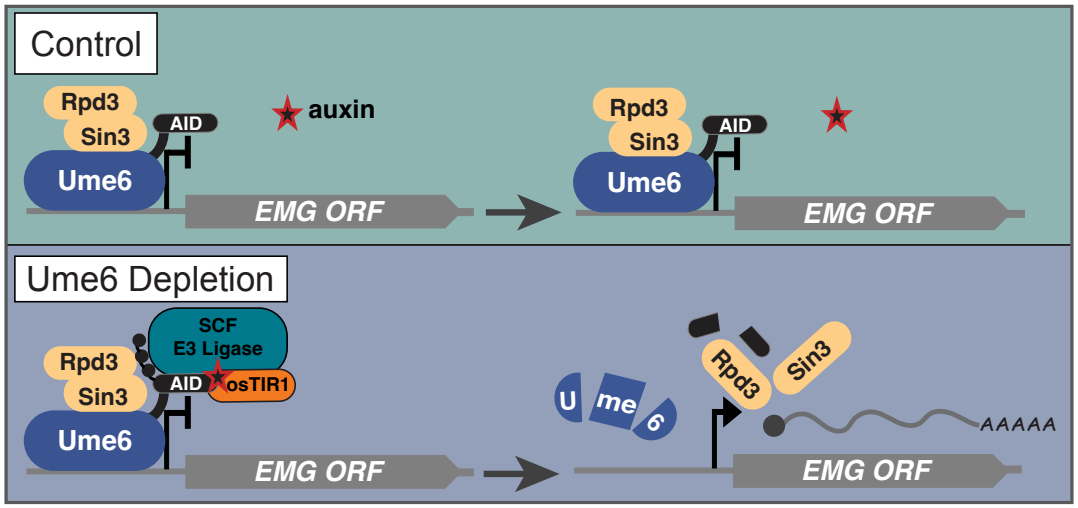

Figure 2.2: Schematic for Ume6-AID depletion strategy. Acute depletion of Ume6 results in the derepression of EMGs in mitotically dividing cells. Illustration of Ume6 depletion scheme using the auxin-inducible degron system. The Ume6-Sin3-Rpd3 repressive complex occupies the EMG promoters. In the absence of *osTIR* (control; light blue), the introduction of auxin doesn't trigger Ume6 degradation and the EMG genes that it regulates remain repressed. Conversely, cells expressing *osTIR* (Ume6 depletion; dark blue) in the presence of auxin recruit the E3 Ligase to the auxin-inducible degron tag associated with Ume6 for poly-ubiquitylation and subsequent degradation of Ume6-AID, which also displaces Sin3-Rpd3. Degradation of Ume6 derepresses EMGs resulting in their expression. Note that *osTIR* is under the control of *lexO* promoter, which can be induced by LexA-ER-B112 (mitotic depletion) or LexA-ER-GAL4$^{770\text{-}881}$ (meiotic depletion) upon addition of beta-estradiol. Please refer to Materials and Methods for further details.

To test the effectiveness of the *UME6-AID* system, we compared Ume6 levels by immunoblotting in the absence or presence of the F-box receptor OsTIR1 (from here on referred to as "control" and "Ume6 depletion", respectively). In control cells, addition of ß-estradiol and auxin had no detectable influence on Ume6 levels (Figure 2.3A and 2.3B). In contrast, the same drug regimen resulted in the rapid depletion of Ume6 in cells carrying the F-box receptor (Figure 2.3A and 2.3B). Ume6 abundance was reduced to ~13% of the initial levels within 15 min and remained low afterwards (Figure 2.3A and 2.3B).

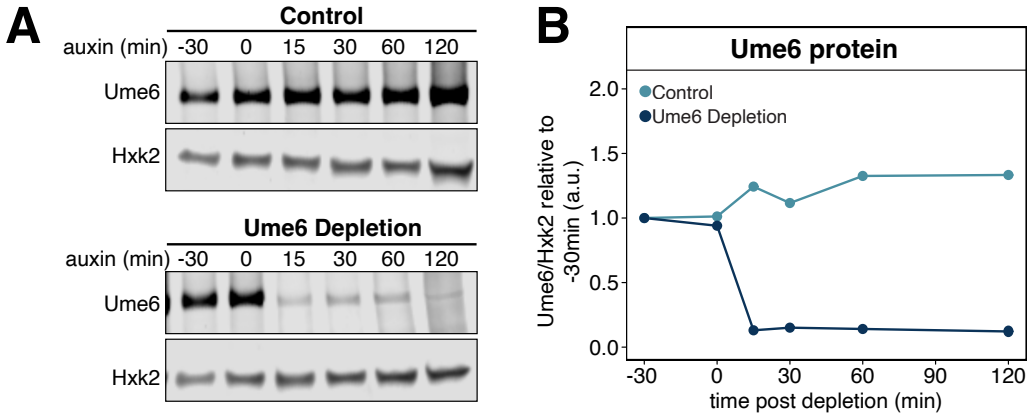

Figure 2.3: Immunoblotting for Ume6 levels in depletion system. Ume6 protein levels were monitored in response to addition of auxin and beta-estradiol in the presence or absence of *osTIR* (Ume6 depletion or control, respectively). Strains possessing (UB17646) or lacking (UB18287) the *osTIR* construct or strains with wild-type *UME6* (WT; UB17716) or *ume6*Δ (*ume6*Δ; UB17718) were inoculated in YPD. Cultures were grown overnight to OD_{600} > 10 and then back diluted to OD_{600} = 0.25. Once cells reached log phase (OD_{600} = 0.5) ß-estradiol (40 nM) was added to all cultures (t_{auxin} = -30 min). Cells were allowed to continue shaking for 30 min before auxin (200 µM) was added to all cultures, initiating Ume6-AID degradation only in the *osTIR* containing strains (t_{auxin} = 0 min). Samples for protein and RNA were then collected at the designated time points. Note, cultures for wild-type *UME6* and *ume6*Δ were collected at t_{auxin} = -30 min prior to chemical treatments. (A) Ume6 protein levels were monitored by anti-V5 immunoblotting and using Hxk2 as a loading control. Representative blots from one of three biological replicates are shown. (B) Quantification of immunoblots in A.

To measure the transcriptomic response to Ume6 depletion, we performed RNA-seq. We initially analyzed global changes in gene expression by pairwise comparison using Spearman's rank correlation coefficient (ρ; Figure 2.4A). We found that control and Ume6 depletion samples were initially very similar to one another (-30 min; ρ = 0.995). The correlation decreased, albeit slightly, following induction of Ume6 depletion (ρ = 0.978, 0.982, 0.984, and 0.984 for 15, 30, 60 and 120 min, respectively). This is perhaps not surprising given that even in the case of the *ume6*Δ, global differences in transcript levels were relatively subtle compared to wild type (ρ = 0.917). We additionally monitored sample-to-sample variation across time points using principal component analysis (PCA; Figure 2.4B). PC1 (58%) and PC2 (17%) accounted for 75% of the variation. Initially (-30 min), control and Ume6 depletion samples formed a distinct group, highlighting sample relatedness. After treatment with ß-estradiol and auxin, control and Ume6 depletion samples separated, with control samples only slightly shifting away from 0 min along PC1 and Ume6 depletion samples spreading along PC1 and PC2. Altogether, these transcriptome-wide comparisons indicate that gene expression patterns diverge only after

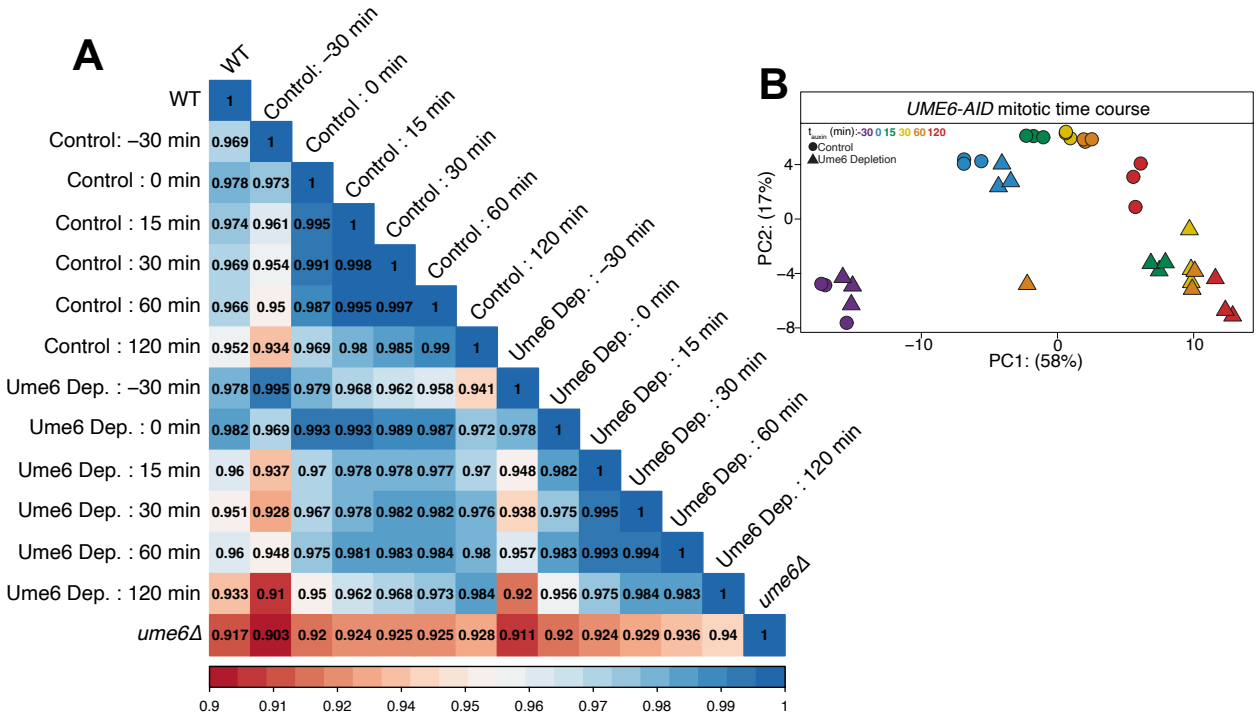

Figure 2.4: Using DESeq2, counts data were analyzed for the control and Ume6 deplete time course data. Measuring the impact of Ume6 depletion using Spearman correlation and PCA (A and B) Sample-to-sample variation was analyzed using Spearman rank order correlation (ρ) with the corrplot package and the variance stabilizing transformation (VST) and plotPCA function associated with DESeq2. (A) Results of Spearman analysis. Colors denote sample similarities or dissimilarities. (B) A PCA plot was then generated from these data using the ggplot2 package to visualize the influence of PC1 (x-axis) and PC2 (y-axis) on samples. To distinguish between samples, control (UB18287) and Ume6 deplete (UB17646) conditions were differentiated by shapes while specific time points were assigned colors. We note that replicate 3 from Ume6 depletion sample (60 min time point) is separated from the other two replicates. This is possibly due to the higher read depth in this sample.

induction of Ume6 depletion, thereby corroborating the temporally controlled nature of the AID system.

We next focused on the expression patterns of a subset of meiotic genes. First, we analyzed *IME2* and *ZIP1*, two well-characterized EMGs known to be repressed by Ume6 during mitotic growth (Figure 2.5; Mitchell 1994). In the control strain where Ume6 protein levels remained high, we observed no noticeable change in either *IME2* or *ZIP1* expression relative to wild type across all time points. However, upon Ume6 depletion, we observed a 10- and 5-fold upregulation for *IME2* and *ZIP1*, respectively (Figure 2.5, 15 min). *IME2* and *ZIP1* transcripts reached similar levels to that of *ume6*Δ mutant following Ume6 depletion. Furthermore, Ume6 depletion did not affect the expression of mid meiotic (e.g., *NDT80*, *SMK1*) or late meiotic (e.g., *SPS100*) genes (Figure 2.5). Together, these data suggest that the *UME6-AID* system can specifically cause

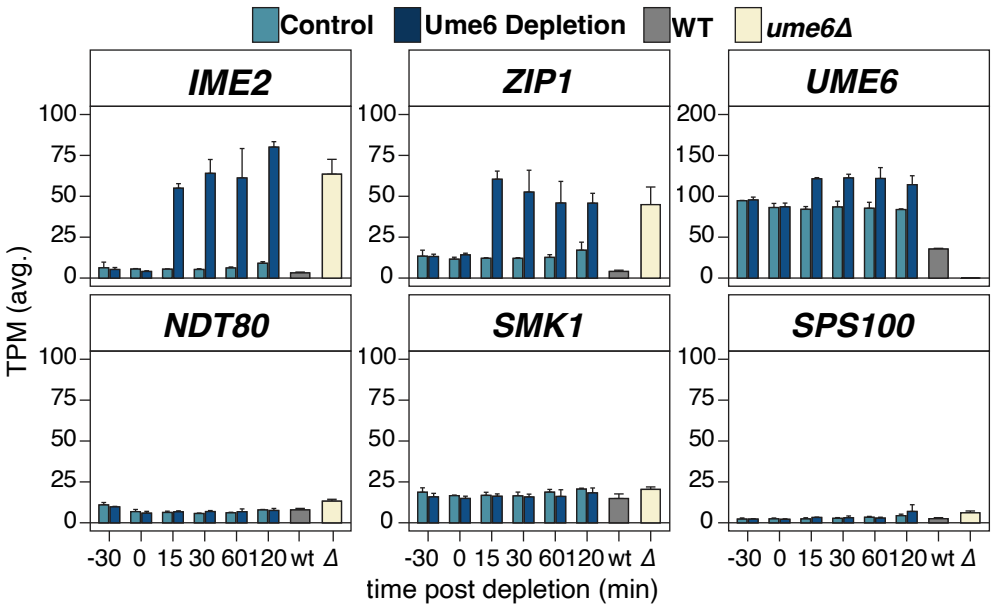

Figure 2.5: Visualizing transcript levels for key meiotic genes. Acute depletion of Ume6 results in the derepression of EMGs in mitotically dividing cells. To investigate the EMG response to Ume6 degradation, RNA was extracted, and cDNA libraries were generated, sequenced, and analyzed as described in materials and methods. Time series data for control (light blue) and Ume6 depletion (dark blue) are shown as well as for *UME6* (grey) and *ume6*Δ (ivory). The average TPM for *IME2*, *ZIP1*, *UME6*, *NDT80*, *SMK1*, and *SPS100* are presented with standard error for three biological replicates.

derepression of EMGs in mitotic cells. Finally, we noticed reproducible upregulation of *UME6* transcripts in response to Ume6 depletion (~30% increase between control and Ume6 depletion, Figure 2.5), suggesting that Ume6 autoregulates its own expression.

Mitotic depletion of Ume6 enables the identification of its direct targets.

We next identified differentially expressed genes (DEGs) responsive to acute Ume6 depletion using two complementary approaches (see Materials and Methods for details). This analysis resulted in a composite list of 165 Ume6-responsive genes (Figure 2.6; Table 1.1). This list of targets was further curated using a previously published Ume6 ChIP-Seq dataset, which was acquired in the absence of *IME1* expression when Ume6 should be bound to its targets (Tresenrider et al. 2021). This resulted in 144 Ume6-responsive genes that were also enriched for a Ume6 ChIP peak, indicating direct targets (Figure 2.7, Table 1.1; Tresenrider et al. 2021). To corroborate these results, we employed Multiple EM for Motif Elicitation (MEME) analysis to look for common motifs within or adjacent to the gene bodies of the 144 Ume6-responsive genes (Bailey et al. 2015; Bailey and Elkan 1994). MEME identified the core URS1 sequence (5'-GGCGGC-3) in 119 of the 144 genes (83%; Figure 2.8). Further inspection of the Ume6 depletion

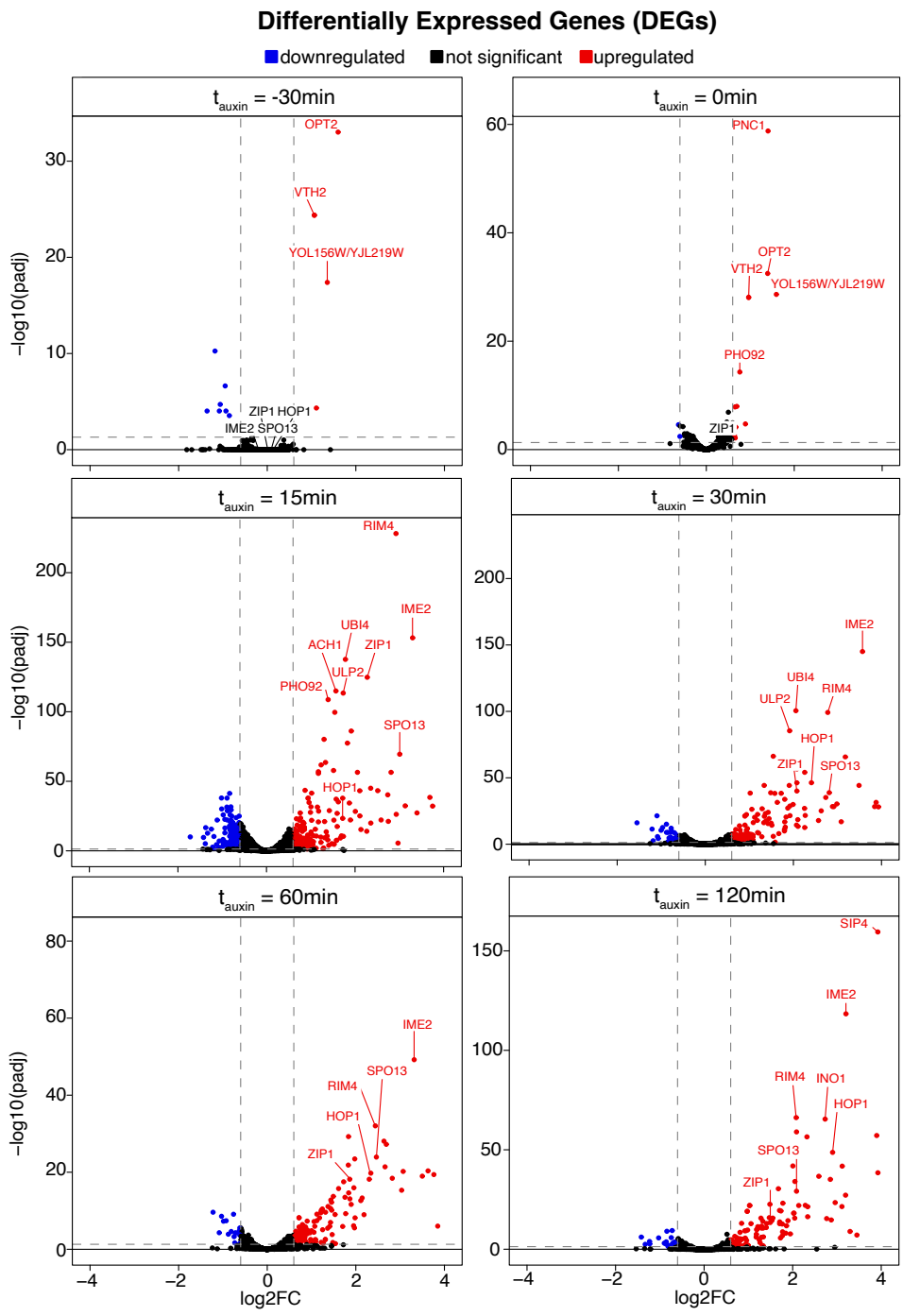

Figure 2.6: DESeq2 analysis to identify differentially expressed genes for Ume6-AID system. Volcano plots were used to observe significance with which genes were derepressed (y-axis) and how this corresponded to log2FC (x-axis). Genes were either considered down- or upregulated if padj < 0.05 and log2FC > 0.6. Otherwise, changes were deemed not significant. Dots represent a gene and are color matched to their differential expression profile. Relevant dots are provided a box denoting their gene name.

Table 1.1: Ume6 Responsive Gene Targets

Systematic Name	Gene	MEME Peak Identified	Ume6 ChIP Peak
YBL015W	*ACH1*	Yes	Yes
YJL200C	*ACO2*	NA	No
YAL054C	*ACS1*	Yes	Yes
YMR120C	*ADE17*	NA	No
YOR128C	*ADE2*	NA	No
YMR009W	*ADI1*	No	Yes
YCR010C	*ADY2*	Yes	Yes
YDL239C	*ADY3*	Yes	Yes
YGL032C	*AGA2*	NA	No
YOR374W	*ALD4*	Yes	Yes
YNL270C	*ALP1*	Yes	Yes
YGR225W	*AMA1*	Yes	Yes
YNR019W	*ARE2*	No	Yes
YGL180W	*ATG1*	Yes	Yes
YBL078C	*ATG8*	No	Yes
YDL070W	*BDF2*	Yes	Yes
YAL061W	*BDH2*	NA	No
YGR142W	*BTN2*	Yes	Yes
YPL111W	*CAR1*	Yes	Yes
YLR438W	*CAR2*	Yes	Yes
YML042W	*CAT2*	Yes	Yes
YMR280C	*CAT8*	Yes	Yes
YLR346C	*CIS1*	No	Yes
YJR161C/ YDL248W	*COS5*	No	No
YGR295C	*COS6*	No	Yes
YHL048W	*COS8*	No	Yes
YKL219W	*COS9*	No	Yes
YLL018C-A	*COX19*	No	Yes
YOR303W	*CPA1*	Yes	Yes
YOR100C	*CRC1*	Yes	Yes
YPL018W	*CTF19*	Yes	Yes
YPR158W	*CUR1*	Yes	Yes
YNL155W	*CUZ1*	Yes	Yes
YER179W	*DMC1*	Yes	Yes

Table 1.1: Ume6 Responsive Gene Targets (continued)

Systematic Name	Gene	MEME Peak Identified	Ume6 ChIP Peak
YDR273W	*DON1*	Yes	Yes
YOR114W	*DPI34*	NA	No
YDR359C	*EAF1*	Yes	Yes
YDR446W	*ECM11*	Yes	Yes
YOR388C	*FDH1*	Yes	Yes
YMR306W	*FKS3*	No	Yes
YKR009C	*FOX2*	Yes	Yes
YDR506C	*GMC1*	Yes	Yes
YLR445W	*GMC2*	Yes	Yes
YLL031C	*GPI13*	Yes	Yes
YBR014C	*GRX7*	NA	No
YJL103C	*GSM1*	Yes	Yes
YDR014W-A	*HED1*	Yes	Yes
YMR207C	*HFA1*	Yes	Yes
YGL251C	*HFM1*	Yes	Yes
YIL072W	*HOP1*	Yes	Yes
YGL033W	*HOP2*	Yes	Yes
YDR171W	*HSP42*	Yes	Yes
YPL240C	*HSP82*	Yes	Yes
YJR036C	*HUL4*	Yes	Yes
YFR017C	*IGD1*	Yes	Yes
YJL106W	*IME2*	Yes	Yes
YJL153C	*INO1*	Yes	Yes
YNL106C	*INP52*	Yes	Yes
YPL017C	*IRC15*	Yes	Yes
YKL217W	*JEN1*	Yes	Yes
YLR096W	*KIN2*	No	Yes
YLR260W	*LCB5*	Yes	Yes
YPL054W	*LEE1*	Yes	Yes
YJR005C-A	*LSO1*	Yes	Yes
YGR053C	*MCO32*	Yes	Yes
YBR136W	*MEC1*	Yes	Yes
YJL102W	*MEF2*	Yes	Yes

Table 1.1: Ume6 Responsive Gene Targets (continued)

Systematic Name	Gene	MEME Peak Identified	Ume6 ChIP Peak
YER044C-A	*MEI4*	Yes	Yes
YPL121C	*MEI5*	Yes	Yes
YOR351C	*MEK1*	Yes	Yes
YIR033W	*MGA2*	Yes	Yes
YGL183C	*MND1*	Yes	Yes
YOR177C	*MPC54*	Yes	Yes
YPL168W	*MRX4*	NA	No
YFL003C	*MSH4*	Yes	Yes
YDL154W	*MSH5*	Yes	Yes
YIL144W	*NDC80*	No	Yes
YOL104C	*NDJ1*	Yes	Yes
YHR133C	*NSG1*	NA	No
YOL032W	*OPI10*	NA	No
YBR295W	*PCA1*	Yes	Yes
YLR151C	*PCD1*	No	No
YBR186W	*PCH2*	Yes	Yes
YLR134W	*PDC5*	No	No
YOR360C	*PDE2*	No	No
YNL231C	*PDR16*	Yes	Yes
YMR018W	*PEX9*	Yes	Yes
YOL084W	*PHM7*	No	Yes
YDR374C	*PHO92*	Yes	Yes
YLR273C	*PIG1*	Yes	Yes
YOL100W	*PKH2*	Yes	Yes
YJR006W	*POL31*	Yes	Yes
YGL205W	*POX1*	No	Yes
YBL064C	*PRX1*	Yes	Yes
YDR055W	*PST1*	Yes	Yes
YLR376C	*PSY3*	NA	No
YLR414C	*PUN1*	Yes	Yes
YKL015W	*PUT3*	Yes	Yes
YPL147W	*PXA1*	Yes	Yes
YGL062W	*PYC1*	Yes	Yes

Table 1.1: Ume6 Responsive Gene Targets (continued)

Systematic Name	Gene	MEME Peak Identified	Ume6 ChIP Peak
YIL121W	*QDR2*	Yes	Yes
YLR329W	*REC102*	No	Yes
YHR157W	*REC104*	Yes	Yes
YPR007C	*REC8*	Yes	Yes
YLR263W	*RED1*	Yes	Yes
YHL024W	*RIM4*	Yes	Yes
YLL046C	*RNP1*	Yes	Yes
YML091C	*RPM2*	Yes	Yes
YDL020C	RPN4	Yes	Yes
YDR427W	*RPN9*	NA	No
YOR077W	*RTS2*	Yes	Yes
YHR079C-A	*SAE3*	Yes	Yes
YMR127C	*SAS2*	No	Yes
YDR180W	*SCC2*	Yes	Yes
YJR095W	*SFC1*	Yes	Yes
YLR058C	*SHM2*	NA	No
YJL089W	*SIP4*	Yes	Yes
YNL196C	*SLZ1*	Yes	Yes
YNL012W	*SPO1*	Yes	Yes
YHL022C	*SPO11*	Yes	Yes
YHR014W	*SPO13*	Yes	Yes
YHR153C	*SPO16*	Yes	Yes
YIL073C	*SPO22*	Yes	Yes
YMR101C	*SRT1*	Yes	Yes
YKL086W	*SRX1*	Yes	Yes
YAL005C	*SSA1*	Yes	Yes
YER103W	*SSA4*	No	Yes
YGL184C	*STR3*	Yes	Yes
YPR151C	*SUE1*	Yes	Yes
YPL016W	*SWI1*	NA	No
YML100W	*TSL1*	Yes	Yes
YLL039C	*UBI4*	Yes	Yes
YLR024C	*UBR2*	Yes	Yes
YIL031W	*ULP2*	Yes	Yes

Table 1.1: Ume6 Responsive Gene Targets (continued)

Systematic Name	Gene	MEME Peak Identified	Ume6 ChIP Peak
YDR207C	*UME6*	Yes	Yes
YLR132C	*USB1*	Yes	Yes
YGL258W	*VEL1*	No	No
YLR417W	*VPS36*	Yes	Yes
YGL104C	*VPS73*	Yes	Yes
YOR359W	*VTS1*	NA	No
YDR374W-A	*WIP1*	Yes	Yes
YGR194C	*XKS1*	No	Yes
YBR184W	*YBR184W*	Yes	Yes
YBR284W	*YBR284W*	Yes	Yes
YDR018C	*YDR018C*	No	Yes
YDR222W	*YDR222W*	Yes	Yes
YEL025C	*YEL025C*	Yes	Yes
YGL036W	*YGL036W*	Yes	Yes
YGL081W	*YGL081W*	Yes	Yes
YGR079W	*YGR079W*	Yes	Yes
YHL044W	*YHL044W*	No	Yes
YHR202W	*YHR202W*	Yes	Yes
YIL024C	*YIL024C*	Yes	Yes
YKR005C	*YKR005C*	Yes	Yes
YMR085W	*YMR085W*	No	Yes
YOL131W	*YOL131W*	Yes	Yes
YOR389W	*YOR389W*	No	Yes
YPL034W	*YPL034W*	No	Yes
YPL077C	*YPL077C*	No	Yes
YPR145C-A	*YPR145C-A*	No	Yes
YPR172W	*YPR172W*	NA	No
YIL063C	*YRB2*	No	Yes
YOR003W	*YSP3*	Yes	Yes
YDR285W	*ZIP1*	Yes	Yes
YGL249W	*ZIP2*	Yes	Yes

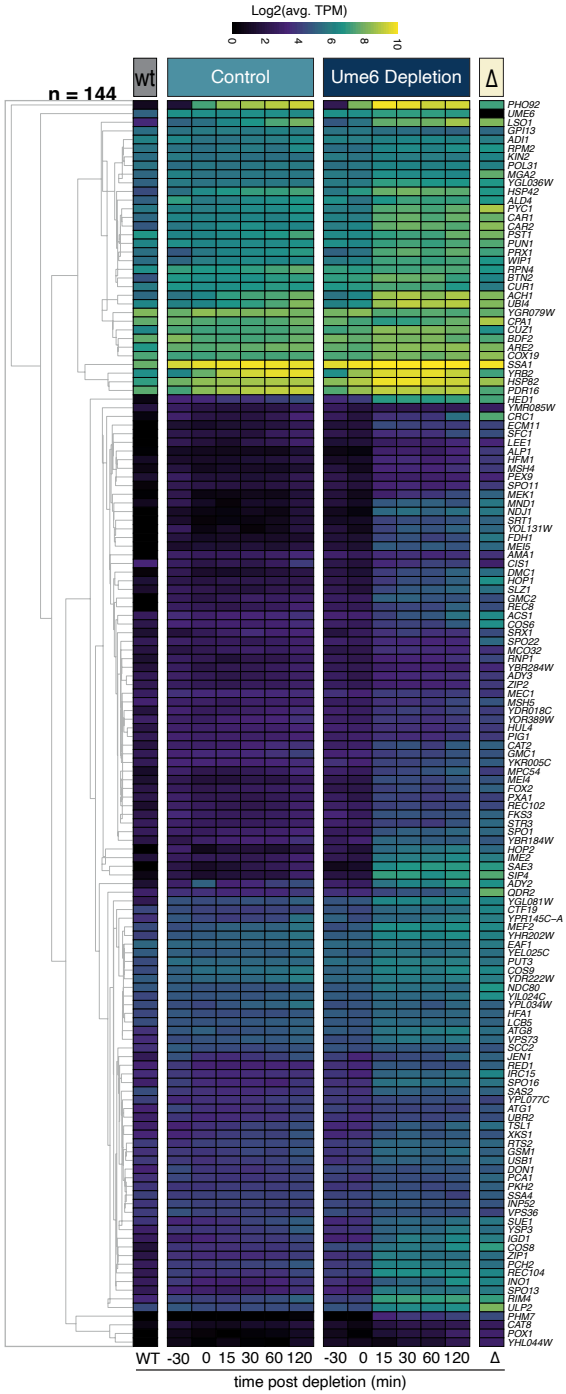

Figure 2.7: Heatmap of differentially expressed Ume6 targets. Differentially expressed genes (DEGs) between Ume6 depletion and control as well as WT and *ume6*Δ conditions were identified with the R package DESeq2 using Kallisto generated counts tables. The log2 of mean TPMs across three biological replicates are shown for the 144 DEGs identified ranging from no expression to high expression. DEGs were clustered by Euclidian distance (centroid) and partitioned vertically by strain background.

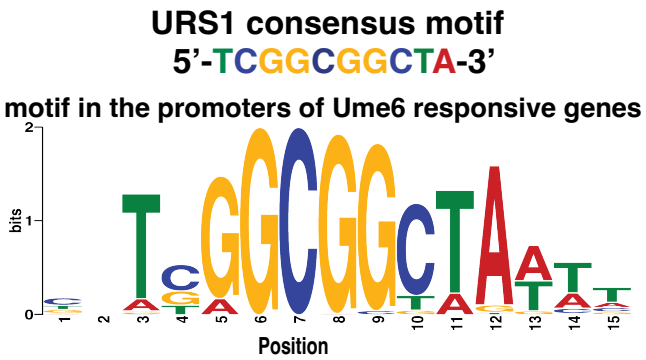

Figure 2.8: The URS1 motif present in Ume6 targets. The URS1 motif identified in the regions flanking or internal to the CDS of a subset of the 144 DEGs.

samples revealed that all of the 144 genes were derepressed rapidly, within 15 min following auxin administration, with 58% (83/144) having a log2FC ≥ 1. Additionally, 56% (81/144) maintained a log2FC ≥ 1 at 30 min indicating a sustained expression. (Figure 2.9, Table 1.1). In conclusion, this comparative analysis enabled the identification of a refined gene set that is directly regulated by Ume6.

Many of the Ume6 targets identified in this study are transcriptionally regulated during meiosis (Brar et al. 2012; Tresenrider et al. 2021). Brar et al. (2012) has rigorously categorized the dynamic changes in gene expression with respect to the chronology of meiotic events. Using this dataset, we determined when the Ume6 targets were expressed during meiosis. Doing so, we found that a majority reached their highest expression during meiotic entry (49/144; 34%), DNA replication (12/144; 8%), and recombination (66/144; 46%). This indicates that 88% (127/144) of our Ume6 targets are EMGs. The remaining 12% (17/144) were expressed throughout meiosis, but expression didn't peak until mid and late meiosis suggesting additional possible layers of regulation. GO enrichment analysis for the 144 Ume6 targets was largely composed of genes involved in meiotic machinery and metabolism (Figure 2.10). However, other functional classes were also revealed, including protein synthesis, trafficking, RNA processing, and cell wall maintenance. Finally, 18 genes of unknown function were present, and it is possible these genes are involved in one of the abovementioned functions that Ume6 regulates. Altogether, the comparison to the published dataset from Brar et al. confirms that the targets identified by the *UME6-AID* system represent meiotically expressed genes.

Mitotic depletion of Ume6 derepresses meiotically expressed LUTIs.

A pervasive mechanism of gene regulation has recently been characterized in meiosis, whereby expression of a Long Undecoded Transcript Isoform (LUTI) from a

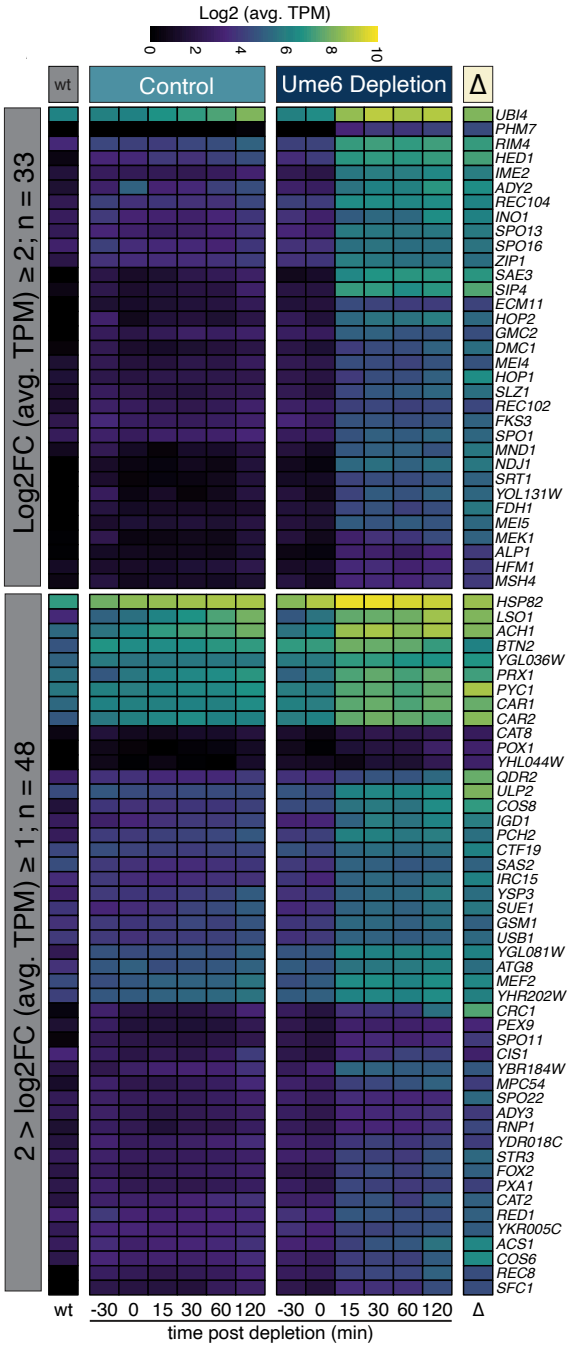

Figure 2.9: Heatmap of differentially expressed genes showing log2FC ≥ 1 in response to Ume6 depletion. Acute depletion of Ume6 results in the derepression of EMGs in mitotically dividing cells. A heatmap as in Figure S1E highlighting a subset of DEGs that showed the greatest response to Ume6 depletion at t = 30min. This resulted in 33 DEGs with a log2FC ≥ 2 (top) and 48 DEGs with a log2FC ≥ 1 and < 2.

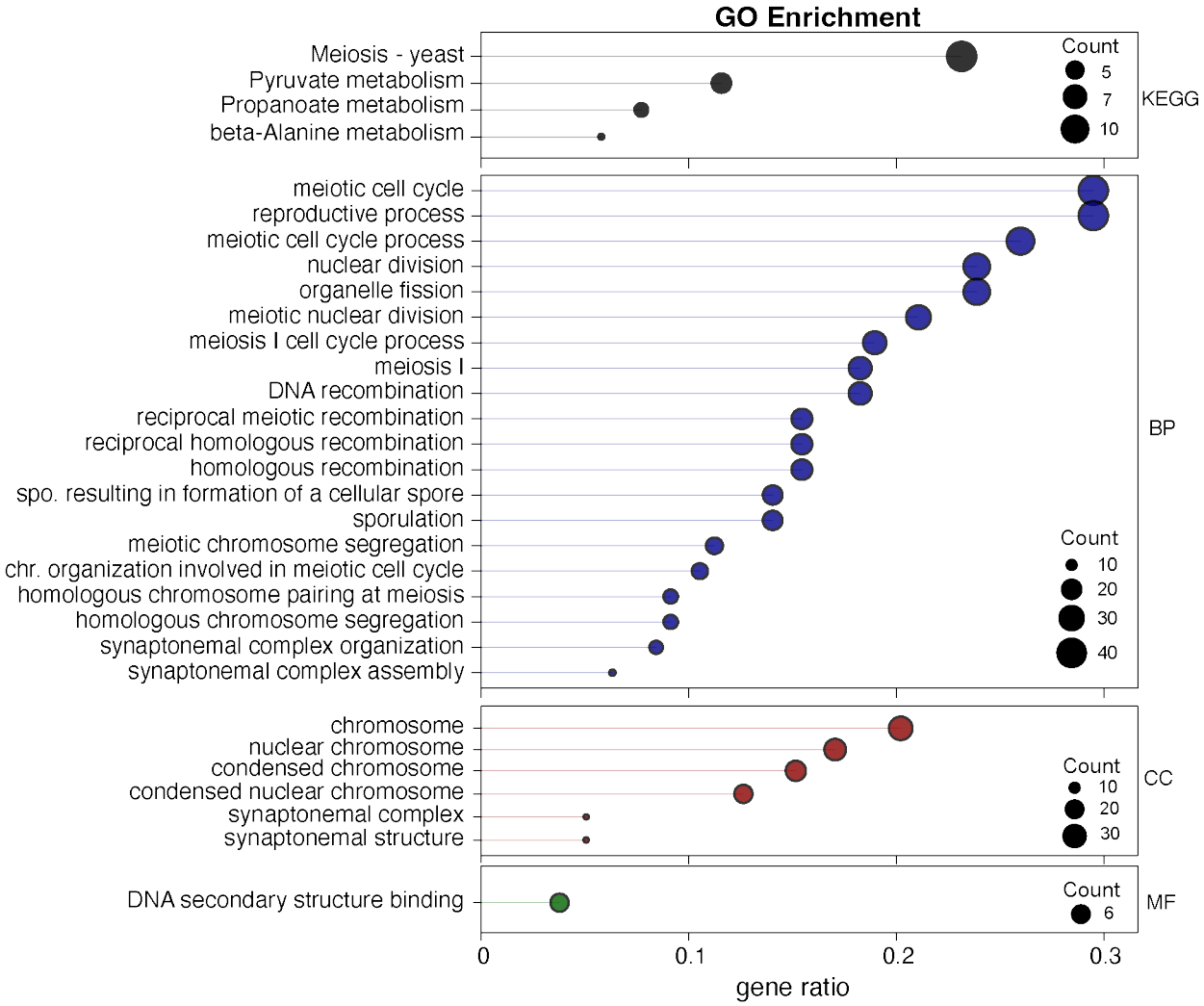

Figure 2.10: GO terms associated with Ume6 targets. Acute depletion of Ume6 results in the derepression of EMGs in mitotically dividing cells. GO enrichment analysis of the 144 DEGs that responded to Ume6 depletion. The gene ratio is shown on the x-axis and is the percent of genes in a given GO term out of the total 144 genes total. Point size denotes the number of genes in that GO term and color signifies category: KEGG, KEGG pathway database; BP, biological process; CC, cellular component; MF, molecular function.

distal gene promoter causes downregulation of the canonical, protein-coding transcript from the proximal promoter through the combined act of transcriptional and translational interference (Chia et al. 2017; Chen et al. 2017; Cheng et al. 2018). Among the meiotically expressed LUTIs, 72 were found to be controlled by Ume6 based on ChIP-seq (Tresenrider et al. 2021). However, a more direct interrogation of Ume6's role in regulating these LUTIs remains unclear. Using the *UME6-AID* depletion system, we asked whether the Ume6-regulated LUTIs became derepressed in response to acute loss of *UME6* function during mitotic growth. Reads wer e aligned to a reference genome using

Table 1.2: LUTIs Responsive to Ume6 Depletion

Systematic Name	Gene	LUTI Detected Post-Ume6 Depletion in Mitosis	LUTI Detected Post-*IME1* Induction (Meiosis)	LUTI Expression Disrupted by Ume6 Depletion (Meiosis)
YJL084C	*ALY2*	Yes	Yes	Yes
YPR029C	*APL4*	Yes	Yes	Yes
YLR114C	*AVL9*	Yes	Yes	Yes
YBL085W	*BOI1*	Yes	Yes	Yes
YPL160W	*CDC60*	Yes	Yes	Yes
YLR115W	*CFT2*	Yes	Yes	Yes
YBR281C	*DUG2*	Yes	Yes	Yes
YLL031C	*GPI13*	Yes	Yes	Yes
YML075C	*HMG1*	Yes	Yes	Not Detected
YLR259C	*HSP60*	Yes	Yes	Yes
YJR138W	*IML1*	Yes	Yes	Not Detected
YLR260W	*LCB5*	Yes	Yes	Not Detected
YDR060W	*MAK21*	Yes	Yes	Not Detected
YBR185C	*MBA1*	Yes	Yes	Yes
YOR020W-A	*MCO10*	Yes	Yes	Yes
YGR264C	*MES1*	Yes	Yes	Yes
YCL057C-A	*MIC10*	Yes	Yes	Yes
YPR164W	*MMS1*	Yes	Yes	Yes
YOR354C	*MSC6*	Yes	Yes	Yes
YMR100W	*MUB1*	Yes	Yes	Yes
YIL144W	*NDC80*	Yes	Yes	Yes
YOL100W	*PKH2*	Yes	Yes	Yes
YOR321W	*PMT3*	Yes	Yes	Not Detected
YBR257W	*POP4*	Yes	Yes	Yes
YBR114W	*RAD16*	Yes	Yes	Yes
YGL103W	*RPL28*	Yes	Yes	Not Detected
YFL036W	*RPO41*	Yes	Yes	Not Detected
YPL274W	*SAM3*	Yes	Yes	Not Detected
YBL011W	*SCT1*	Yes	Yes	Yes
YOR076C	*SKI7*	Yes	Yes	Yes
YOR290C	*SNF2*	Yes	Yes	Not Detected
YGL097W	*SRM1*	Yes	Yes	Not Detected
YKL122C	*SRP21*	Yes	Yes	Yes

Table 1.2: LUTIs Responsive to Ume6 Depletion (continued)

Systematic Name	Gene	LUTI Detected Post-Ume6 Depletion in Mitosis	LUTI Detected Post-*IME1* Induction (Meiosis)	LUTI Expression Disrupted by Ume6 Depletion (Meiosis)
YHR006W	*STP2*	Yes	Yes	Not Detected
YER111C	*SWI4*	Yes	Yes	Yes
YJL083W	*TAX4*	Yes	Yes	Yes
YGR194C	*XKS1*	Yes	Yes	Not Detected
YGR266W	*YGR266W*	Yes	Yes	Not Detected
YGR281W	*YOR1*	Yes	Yes	Not Detected
YCL050C	*APA1*	Not Detected	Yes	Not Detected
YHR013C	*ARD1*	Not Detected	No	NA
YDL070W	*BDF2*	Not Detected	Yes	Not Detected
YML111W	*BUL2*	Not Detected	Yes	Not Detected
YNL305C	*BXI1*	Not Detected	Yes	Not Detected
YPR013C	*CMR3*	Not Detected	Yes	Not Detected
YJL003W	*COX16*	Not Detected	Yes	Not Detected
YBR112C	*CYC8*	Not Detected	No	NA
YDL174C	*DLD1*	Not Detected	Yes	Not Detected
YEL015W	*EDC3*	Not Detected	No	NA
YJL196C	*ELO1*	Not Detected	No	NA
YOR246C	*ENV9*	Not Detected	No	NA
YMR208W	*ERG12*	Not Detected	Yes	Not Detected
YOR320C	*GNT1*	Not Detected	Yes	Not Detected
YOL103W	*ITR2*	Not Detected	Yes	Not Detected
YOL002C	*IZH2*	Not Detected	No	NA
YLR274W	*MCM5*	Not Detected	No	NA
YOL135C	*MED7*	Not Detected	Yes	Not Detected
YJR077C	*MIR1*	Not Detected	Yes	Yes
YOR350C	*MNE1*	Not Detected	Yes	Not Detected
YMR122W-A	*NCW1*	Not Detected	Yes	Yes
YNL015W	*PBI2*	Not Detected	No	NA
YHR071W	*PCL5*	Not Detected	Yes	Not Detected
YDR501W	*PLM2*	Not Detected	No	NA
YLR325C	*RPL38*	Not Detected	Yes	Yes
YPL152W	*RRD2*	Not Detected	Yes	Yes
YPL163C	*SVS1*	Not Detected	Yes	Not Detected

Table 1.2: LUTIs Responsive to Ume6 Depletion (continued)

Systematic Name	Gene	LUTI Detected Post-Ume6 Depletion in Mitosis	LUTI Detected Post-*IME1* Induction (Meiosis)	LUTI Expression Disrupted by Ume6 Depletion (Meiosis)
YOR352W	*TFB6*	Not Detected	Yes	Not Detected
YNR017W	*TIM23*	Not Detected	Yes	Yes
YGR260W	*TNA1*	Not Detected	Yes	Not Detected
YIL031W	*ULP2*	Not Detected	No	NA
YPL120W	*VPS30*	Not Detected	Yes	Not Detected
YDR222W	*YDR222W*	Not Detected	No	NA
YEL025C	*YEL025C*	Not Detected	No	NA
YPL088W	*YPL088W*	Not Detected	No	NA

HISAT2 and LUTI expression was monitored for all Ume6 regulated LUTIs. Of the 72 LUTIs, we identified 39 (54.2%) as being mitotically derepressed after Ume6 degradation (Table 1.2). The remaining 35 failed to produce a detectable signal, possibly due to low expression and/or reduced transcript stability. Thus, our depletion system has validated a functional role for Ume6 in repressing at least 39 meiotically expressed LUTIs during mitotic growth, indicating that its activity as a transcriptional repressor can lead to both decreased and increased protein levels.

Discussion

UME6-AID system refines the Ume6 regulon.

In this study, we have shown that use of the AID system allows conditional and acute depletion of Ume6. This allele of *UME6* is able to avoid many of the pleiotropic effects associated with *ume6*Δ by maintaining repression over its targets (Figure 2.1). This regulation over Ume6 targets was maintained until addition of the hormone auxin in the presence of *OsTIR*, which facilitated rapid depletion of Ume6 protein levels (Figure 2.3A and 2.3B). Rapid depletion of Ume6 during mitotic growth conditions, when it acts as a repressor, resulted in the derepression of its targets (Figure 2.5). This depletion was specific to EMGs, particularly those under the control of Ume6 and avoid derepression of both MMGs and LMGs. This acute depletion of Ume6 also avoided many of the secondary effects associated with prolonged exposure to EMGs (Figure 2.11). In *ume6*Δ, where cells are exposed to EMG for an extended period, there were 1263 DEGs with a padj < 0.05 and log2FC > 0.6 (Table 1.3). This large number of DEGs is likely due to the severe

growth defect associated with *ume6*Δ and hence represents a combination of direct and indirect effects. Reducing background signal for many non-specific genes associated with *ume6*Δ allowed for more clarity in defining Ume6 targets. Indeed, by combining our RNAseq dataset with a previous Ume6 ChIP-Seq dataset acquired during starvation in the absence of Ime1, we identified 144 direct targets of Ume6. Of these, 86.1% (124/144) were also present in the *ume6*Δ mutant (Figure2.11). Thus, the AID system helped to

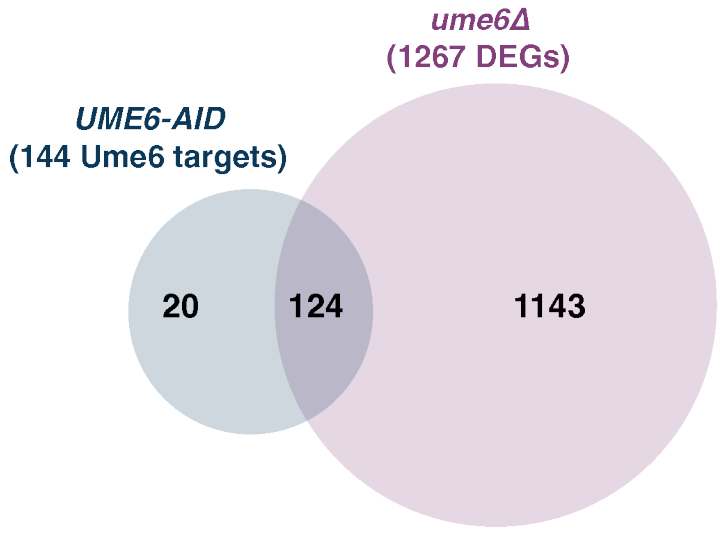

Figure 2.11: Venn diagram of overlapping and non-overlapping differentially expressed genes for Ume6-AID and *ume6*Δ. DESeq2 was used to compare WT and *ume6*Δ (padj < 0.05; Log2FC > 0.6) resulting in identification of 1267 DEGs. Venn diagram showing the 124 overlapping DEGs between Ume6 deplete (144 DEGs) and *ume6*Δ (1267 DEGs).

circumvent many of the pleiotropic secondary effects associated with the *ume6*Δ mutants, while also contributing heavily to our understanding of the Ume6 regulon.

Interestingly, GO enrichment revealed Ume6 regulates genes involved in metabolism and thus also helps coordinate the energy needs required by cells during early meiosis (Figure 2.10). However, not all of this regulation over metabolic genes appears to be direct. Instead, Ume6 regulates the expression of other TFs. One such target of Ume6 is the *CAT8* gene ("catabolite repression"), which is responsible for coordinating metabolic pathways such as the tricarboxylic acid (TCA) cycle and the respiratory chain that allows cells to utilize non-fermentative carbon sources (Bonander et al. 2008). Cat8 achieves this through recognition of the carbon source response element (CSRE), which it uses to bind and activate transcription of its target genes (Du et al. 2022). This CSRE exists in several genes associated with the reprogramming of cells to take advantage of non-fermentative carbon sources. These Cat8 targets include *ACS1*, *FBP1*, *ICL1*, *IDP2*, *JEN1*, *MLS1*, *PCK1*, *SFC1*, and *SIP4* (Haurie et al. 2001). Of these, four showed upregulation in response to Ume6 depletion (*ACS1*, *JEN1*, *SFC1*, and

SIP4). Whether the remaining five are subject to additional layers of regulation remains unclear. Furthermore, *SIP4* was strongly upregulated post-Ume6 depletion and encodes another CSRE recognizing transcriptional activator, which further contributes to regulation of gluconeogenic genes (Roth et al. 2004). *CAT8*, and consequently *SIP4*, are regulated by the TF Mig1 (De Vit et al. 1997). In response to drops in glucose levels, Mig1 becomes phosphorylated and displaced from the *CAT8* promoter thus depressing Cat8

Table 1.3: *ume6*Δ Responsive Genes During Mitotic Growth

Systematic Name	Gene	Present in Ume6 Depletion List
YMR056C	*AAC1*	No
YCR107W	*AAD3*	No
YNL141W	*AAH1*	No
YCR088W	*ABP1*	No
YER045C	*ACA1*	No
YBL015W	*ACH1*	Yes
YLR304C	*ACO1*	No
YAL054C	*ACS1*	Yes
YDR448W	*ADA2*	No
YAR015W	*ADE1*	No
YLR359W	*ADE13*	No
YMR120C	*ADE17*	No
YCL058W-A	*ADF1*	No
YBR145W	*ADH5*	No
YCR105W	*ADH7*	No
YCR011C	*ADP1*	No
YDR216W	*ADR1*	No
YCR010C	*ADY2*	Yes
YDL239C	*ADY3*	Yes
YLR040C	*AFB1*	No
YDR085C	*AFR1*	No
YGL032C	*AGA2*	No
YIL044C	*AGE2*	No
YCL025C	*AGP1*	No
YFL055W	*AGP3*	No
YFL030W	*AGX1*	No
YLR109W	*AHP1*	No
YER093C-A	*AIM11*	No
YIL087C	*AIM19*	No
YIL158W	*AIM20*	No

Table 1.3: *ume6*Δ Responsive Genes During Mitotic Growth (continued)

Systematic Name	Gene	Present in Ume6 Depletion List
YIR003W	*AIM21*	No
YML087C	*AIM33*	No
YMR003W	*AIM34*	No
YPL158C	*AIM44*	No
YOR374W	*ALD4*	Yes
YPL061W	*ALD6*	No
YNL148C	*ALF1*	Yes
YNL270C	*ALP1*	Yes
YDR111C	*ALT2*	No
YGR225W	*AMA1*	Yes
YDR242W	*AMD2*	No
YBR211C	*AME1*	No
YOR378W	*AMF1*	No
YBR158W	*AMN1*	No
YGL156W	*AMS1*	No
YKL047W	*ANR2*	No
YCL050C	*APA1*	No
YKL103C	*APE1*	No
YHL019C	*APM2*	No
YIL040W	*APQ12*	No
YDR441C	*APT2*	No
YNL065W	*AQR1*	No
YPR192W	*AQY1*	No
YFL054C	*AQY3*	No
YIL062C	*ARC15*	No
YCR048W	*ARE1*	No
YNR019W	*ARE2*	Yes
YOL058W	*ARG1*	No
YJL071W	*ARG2*	No
YJL088W	*ARG3*	No
YHR018C	*ARG4*	No
YER069W	*ARG5,6*	No
YMR062C	*ARG7*	No
YOL140W	*ARG8*	No
YHL040C	*ARN1*	No
YHL047C	*ARN2*	No

Table 1.3: *ume6*Δ Responsive Genes During Mitotic Growth (continued)

Systematic Name	Gene	Present in Ume6 Depletion List
YDR127W	*ARO1*	No
YDR035W	*ARO3*	No
YDR101C	*ARX1*	No
YKL185W	*ASH1*	No
YGR097W	*ASK10*	No
YOR377W	*ATF1*	No
YGR177C	*ATF2*	No
YGL180W	*ATG1*	Yes
YCR068W	*ATG15*	No
YCL038C	*ATG22*	No
YDR022C	*ATG31*	No
YIL146C	*ATG32*	No
YLR356W	*ATG33*	No
YOL083W	*ATG34*	No
YJL185C	*ATG36*	No
YLR312C	*ATG39*	No
YOR152C	*ATG40*	No
YPL250C	*ATG41*	No
YBL078C	*ATG8*	Yes
YNR002C	*ATO2*	No
YLR393W	*ATP10*	No
YPR020W	*ATP20*	No
YNR020C	*ATP23*	No
YMR279C	*ATR2*	No
YOR011W	*AUS1*	No
YIL088C	*AVT7*	No
YPR122W	*AXL1*	No
YIL140W	*AXL2*	No
YIL124W	*AYR1*	No
YGR224W	*AZR1*	No
YOR134W	*BAG7*	No
YIL015W	*BAR1*	No
YHR208W	*BAT1*	No
YIL033C	*BCY1*	No
YLR399C	*BDF1*	No
YAL061W	*BDH2*	No

Table 1.3: *ume6*Δ Responsive Genes During Mitotic Growth (continued)

Systematic Name	Gene	Present in Ume6 Depletion List
YNL039W	*BDP1*	No
YER155C	*BEM2*	No
YGR282C	*BGL2*	No
YCL029C	*BIK1*	No
YNR058W	*BIO3*	No
YNR057C	*BIO4*	No
YNR056C	*BIO5*	No
BIO6	*BIO6*	No
BIO6	*BIO6*	No
YIL096C	*BMT5*	No
YJR025C	*BNA1*	No
YJR078W	*BNA2*	No
YBL098W	*BNA4*	No
YLR231C	*BNA5*	No
YFR047C	*BNA6*	No
YNL166C	*BNI5*	No
YIL159W	*BNR1*	No
YBL085W	*BOI1*	No
YCR032W	*BPH1*	No
YDL074C	*BRE1*	No
YNR051C	*BRE5*	No
YHR036W	*BRL1*	No
YNR069C	*BSC5*	No
YGR142W	*BTN2*	Yes
YOR078W	*BUD21*	No
YCR047C	*BUD23*	No
YCR063W	*BUD31*	No
YCR038C	*BUD5*	No
YLR353W	*BUD8*	No
YGR041W	*BUD9*	No
YNL305C	*BXI1*	No
YIL083C	*CAB2*	No
YPL111W	*CAR1*	Yes
YLR438W	*CAR2*	Yes
YML042W	*CAT2*	Yes
YMR280C	*CAT8*	Yes

Table 1.3: *ume6*Δ Responsive Genes During Mitotic Growth (continued)

Systematic Name	Gene	Present in Ume6 Depletion List
YLR175W	*CBF5*	No
YIL043C	*CBR1*	No
YIL142W	*CCT2*	No
YLR390W-A	*CCW14*	No
YLR307W	*CDA1*	No
YCR002C	*CDC10*	No
YOR257W	*CDC31*	No
YCR093W	*CDC39*	No
YMR001C	*CDC5*	No
YCR094W	*CDC50*	No
YDL164C	*CDC9*	No
YIL003W	*CFD1*	No
YCL064C	*CHA1*	No
YJL049W	*CHM7*	No
YGR157W	*CHO2*	No
YNL192W	*CHS1*	No
YOR028C	*CIN5*	No
YNR001C	*CIT1*	No
YCR005C	*CIT2*	No
YPR001W	*CIT3*	No
YGR108W	*CLB1*	No
YPR119W	*CLB2*	No
YMR199W	*CLN1*	No
YPL256C	*CLN2*	No
YIL002W-A	*CMI7*	No
YLR433C	*CNA1*	No
YIL157C	*COA1*	No
YPL189C-A	*COA2*	No
YNR075W	*COS10*	No
YBR203W	*COS111*	No
YGL263W	*COS12*	No
YJR161C/YDL248W	*COS5*	No
YGR295C	*COS6*	Yes
YHL048W	*COS8*	Yes
YKL219W	*COS9*	Yes
YOR316C	*COT1*	No

Table 1.3: *ume6*Δ Responsive Genes During Mitotic Growth (continued)

Systematic Name	Gene	Present in Ume6 Depletion List
YLL018C-A	*COX19*	Yes
YHR116W	*COX23*	Yes
YDR119W-A	*COX26*	No
YNL052W	*COX5A*	No
YIL111W	*COX5B*	No
YLR395C	*COX8*	No
YOR303W	*CPA1*	No
YJR109C	*CPA2*	No
YCR069W	*CPR4*	No
YNR028W	*CPR8*	No
YOR100C	*CRC1*	Yes
YDR223W	*CRF1*	No
YHR209W	*CRG1*	No
YLR213C	*CRR1*	No
YBR161W	*CSH1*	No
YOL007C	*CSI2*	No
YCR086W	*CSM1*	No
YIL132C	*CSM2*	No
YIL169C	*CSS1*	No
YIL169C	*CSS1*	No
YOL159C	*CSS3*	No
YIL036W	*CST6*	No
YLR394W	*CST9*	No
YPL018W	*CTF19*	Yes
YMR180C	*CTL1*	No
YCR015C	*CTO1*	No
YCR054C	*CTR86*	No
YLR286C	*CTS1*	No
YGR088W	*CTT1*	No
YML101C	*CUE4*	No
YCR017C	*CWH43*	No
YKL096W	*CWP1*	No
YNL111C	*CYB5*	No
YJR048W	*CYC1*	No
YDL117W	*CYK3*	No
YKR083C	*DAD2*	No

Table 1.3: *ume6*Δ Responsive Genes During Mitotic Growth (continued)

Systematic Name	Gene	Present in Ume6 Depletion List
YBR233W-A	*DAD3*	No
YML070W	*DAK1*	No
YFL053W	*DAK2*	No
YIR027C	*DAL1*	No
YIR029W	*DAL2*	No
YIR032C	*DAL3*	No
YIR028W	*DAL4*	No
YIR031C	*DAL7*	No
YJR150C	*DAN1*	No
YJR151C	*DAN4*	No
YJL149W	*DAS1*	No
YPL119C	*DBP1*	No
YCL016C	*DCC1*	No
YIR030C	*DCG1*	No
YOL149W	*DCP1*	No
YOR173W	*DCS2*	No
YMR173W	*DDR48*	No
YIL049W	*DFG10*	No
YKL121W	*DGR2*	No
YDL024C	*DIA3*	No
YLR348C	*DIC1*	No
YPL049C	*DIG1*	No
YDR263C	*DIN7*	No
YDR403W	*DIT1*	No
YEL071W	*DLD3*	No
YNL116W	*DMA2*	No
YER179W	*DMC1*	Yes
YGL240W	*DOC1*	No
YHR044C	*DOG1*	No
YDR273W	*DON1*	Yes
YIL010W	*DOT5*	No
YLR307C-A	*DPA10*	No
YIL103W	*DPH1*	No
YJL133C-A	*DPI8*	No
YER124C	*DSE1*	No
YHR143W	*DSE2*	No

Table 1.3: *ume6*Δ Responsive Genes During Mitotic Growth (continued)

Systematic Name	Gene	Present in Ume6 Depletion List
YMR276W	*DSK2*	No
YBR180W	*DTR1*	No
YHL016C	*DUR3*	No
YLR405W	*DUS4*	No
YEL018W	*EAF5*	No
YGR146C	*ECL1*	No
YAL059W	*ECM1*	No
YDR446W	*ECM11*	Yes
YBL043W	*ECM13*	No
YBL101C	*ECM21*	No
YPL021W	*ECM23*	No
YJR106W	*ECM27*	No
YHL030W	*ECM29*	No
YLR299W	*ECM38*	No
YKR076W	*ECM4*	No
YGR271C-A	*EFG1*	No
YIL064W	*EFM4*	No
YIR007W	*EGH1*	No
YCR075W-A	*EGO2*	No
YNL327W	*EGT2*	No
YCR034W	*ELO2*	No
YCL045C	*EMC1*	No
YLR080W	*EMP46*	No
YOL158C	*ENB1*	No
YGR254W	*ENO1*	No
YDL161W	*ENT1*	No
YIL005W	*EPS1*	No
YMR049C	*ERB1*	No
YGR175C	*ERG1*	No
YHR007C	*ERG11*	No
YML126C	*ERG13*	No
YJL167W	*ERG20*	No
YER044C	*ERG28*	No
YLR056W	*ERG3*	No
YMR015C	*ERG5*	No
YMR220W	*ERG8*	No

Table 1.3: *ume6*Δ Responsive Genes During Mitotic Growth (continued)

Systematic Name	Gene	Present in Ume6 Depletion List
YCR075C	*ERS1*	No
YGL054C	*ERV14*	No
YIL151C	*ESL1*	No
YLR318W	*EST2*	No
YOR317W	*FAA1*	No
YER015W	*FAA2*	No
YFR019W	*FAB1*	No
YDL166C	*FAP7*	No
YJL157C	*FAR1*	No
YKL187C	*FAT3*	No
YLR377C	*FBP1*	No
YLR051C	*FCF2*	No
YOR388C	*FDH1*	Yes
YOR388C	*FDH1*	Yes
YCR028C	*FEN2*	No
YMR319C	*FET4*	No
YGR131W	*FHN1*	No
YCR089W	*FIG2*	No
YER032W	*FIR1*	No
YIL065C	*FIS1*	No
YDR534C	*FIT1*	No
YMR306W	*FKS3*	Yes
YKR102W	*FLO10*	No
YIR019C	*FLO11*	No
YHR211W	*FLO5*	No
YAL063C	*FLO9*	No
YIL134W	*FLX1*	No
YIL098C	*FMC1*	No
YHR176W	*FMO1*	No
YBR047W	*FMP23*	No
YDL222C	*FMP45*	No
YGR052W	*FMP48*	No
YER004W	*FMP52*	No
YBL013W	*FMT1*	No
YDR110W	*FOB1*	No
YKR009C	*FOX2*	Yes

Table 1.3: *ume6*Δ Responsive Genes During Mitotic Growth (continued)

Systematic Name	Gene	Present in Ume6 Depletion List
YLR449W	*FPR4*	No
YOR381W	*FRE3*	No
YNR060W	*FRE4*	No
YOL152W	*FRE7*	No
YPL141C	*FRK1*	No
YCL026C-A	*FRM2*	No
YOR324C	*FRT1*	No
YHR049W	*FSH1*	No
YCR076C	*FUB1*	No
YPL262W	*FUM1*	No
YAL034C	*FUN19*	No
YBR021W	*FUR4*	No
YCL027W	*FUS1*	No
YMR232W	*FUS2*	No
YBL016W	*FUS3*	No
YIL097W	*FYV10*	No
YLR068W	*FYV7*	No
YLR081W	*GAL2*	No
YPL248C	*GAL4*	No
YBR018C	*GAL7*	No
YKR039W	*GAP1*	No
YHR089C	*GAR1*	No
YLR343W	*GAS2*	No
YMR215W	*GAS3*	No
YOL132W	*GAS4*	No
YFL021W	*GAT1*	No
YCL011C	*GBP2*	No
YJL125C	*GCD14*	No
YDR019C	*GCV1*	No
YPR184W	*GDB1*	No
YPL110C	*GDE1*	No
YAL062W	*GDH3*	No
YOR355W	*GDS1*	No
YBR187W	*GDT1*	No
YCL073C	*GEX1*	No
YKR106W	*GEX2*	No

Table 1.3: *ume6*Δ Responsive Genes During Mitotic Growth (continued)

Systematic Name	Gene	Present in Ume6 Depletion List
YMR255W	*GFD1*	No
YDL198C	*GGC1*	No
YDR309C	*GIC2*	No
YGR066C	*GID10*	No
YCL039W	*GID7*	No
YDR507C	*GIN4*	No
YBR045C	*GIP1*	No
YER054C	*GIP2*	No
YNL255C	*GIS2*	No
YCL040W	*GLK1*	No
YDR272W	*GLO2*	No
YOR040W	*GLO4*	No
YDR506C	*GMC1*	Yes
YLR445W	*GMC2*	Yes
YGR256W	*GND2*	No
YNL274C	*GOR1*	No
YHR005C	*GPA1*	No
YOL059W	*GPD2*	No
YPR160W	*GPH1*	No
YPL076W	*GPI2*	No
YDL021W	*GPM2*	No
YIL053W	*GPP1*	No
YER062C	*GPP2*	No
YKL026C	*GPX1*	No
YBR244W	*GPX2*	No
YPL223C	*GRE1*	No
YCL035C	*GRX1*	No
YGR032W	*GSC2*	No
YJL103C	*GSM1*	Yes
YOR185C	*GSP2*	No
YFR015C	*GSY1*	No
YLR258W	*GSY2*	No
YMR251W	*GTO3*	No
YIR038C	*GTT1*	No
YDL238C	*GUD1*	No
YIL155C	*GUT2*	No

Table 1.3: *ume6*Δ Responsive Genes During Mitotic Growth (continued)

Systematic Name	Gene	Present in Ume6 Depletion List
YIL041W	*GVP36*	No
YFL027C	*GYP8*	No
YOR358W	*HAP5*	No
YCL026C-B	*HBN1*	No
YCR065W	*HCM1*	No
YDR014W-A	*HED1*	Yes
YNL014W	*HEF3*	No
YMR207C	*HFA1*	Yes
YGL251C	*HFM1*	Yes
YGR187C	*HGH1*	No
YNL031C	*HHT2*	No
YDR317W	*HIM1*	No
YCL030C	*HIS4*	No
YIL116W	*HIS5*	No
YDR528W	*HLR1*	No
YLR450W	*HMG2*	No
YCL066W	*HMLALPHA1*	No
YCL067C	*HMLALPHA2*	No
YLR205C	*HMX1*	No
YIL072W	*HOP1*	Yes
YGL033W	*HOP2*	Yes
YMR251W-A	*HOR7*	No
YIL112W	*HOS4*	No
YKL084W	*HOT13*	No
YPR193C	*HPA2*	No
YEL066W	*HPA3*	No
YOL155C	*HPF1*	No
YIL110W	*HPM1*	No
YDR399W	*HPT1*	No
YFL014W	*HSP12*	No
YJL159W	*HSP150*	No
YCR021C	*HSP30*	No
YDR533C	*HSP31*	No
YDR171W	*HSP42*	Yes
YDR258C	*HSP78*	No
YPL240C	*HSP82*	Yes

Table 1.3: *ume6*Δ Responsive Genes During Mitotic Growth (continued)

Systematic Name	Gene	Present in Ume6 Depletion List
YDR225W	*HTA1*	No
YDR224C	*HTB1*	No
YPL067C	*HTC1*	No
YCR020W-B	*HTL1*	No
YGR268C	*HUA1*	No
YOR284W	*HUA2*	No
YJR036C	*HUL4*	Yes
YHR094C	*HXT1*	No
YNL318C	*HXT14*	No
YMR011W	*HXT2*	No
YDR345C	*HXT3*	No
YHR092C	*HXT4*	No
YJL214W	*HXT8*	No
YIR037W	*HYR1*	No
YIL090W	*ICE2*	No
YER065C	*ICL1*	No
YPR006C	*ICL2*	No
YMR195W	*ICY1*	No
YNL037C	*IDH1*	No
YOR136W	*IDH2*	No
YPL117C	*IDI1*	No
YDL066W	*IDP1*	No
YLR174W	*IDP2*	No
YFR017C	*IGD1*	Yes
YMR108W	*ILV2*	No
YCL009C	*ILV6*	No
YGR287C	*IMA1*	No
YHR216W	*IMD2*	No
YJL106W	*IME2*	Yes
YGL192W	*IME4*	No
YCR046C	*IMG1*	No
YIL154C	*IMP2'*	No
YNL075W	*IMP4*	No
YLR413W	*INA1*	No
YIR024C	*INA22*	No
YDR287W	*INM2*	No

Table 1.3: *ume6*Δ Responsive Genes During Mitotic Growth (continued)

Systematic Name	Gene	Present in Ume6 Depletion List
YJL153C	*INO1*	Yes
YIL002C	*INP51*	No
YNL106C	*INP52*	Yes
YHR085W	*IPI1*	No
YOL015W	*IRC10*	No
YPL017C	*IRC15*	Yes
YIR036C	*IRC24*	No
YDR540C	*IRC4*	No
YIL026C	*IRR1*	No
YBR086C	*IST2*	No
YIR005W	*IST3*	No
YPL135W	*ISU1*	No
YOR226C	*ISU2*	No
YOL101C	*IZH4*	No
YKL217W	*JEN1*	Yes
YJR119C	*JHD2*	No
YLL057C	*JLP1*	No
YNL188W	*KAR1*	No
YKL161C	*KDX1*	No
YHR158C	*KEL1*	No
YIL125W	*KGD1*	No
KHR1	*KHR1*	No
YLR096W	*KIN2*	Yes
YCR091W	*KIN82*	No
YLL019C	*KNS1*	No
YCL059C	*KRR1*	No
YBL071W-A	*KTI11*	No
YIL085C	*KTR7*	No
YCL005W	*LDB16*	No
YMR148W	*LDO16*	No
YMR147W	*LDO45*	No
YPL054W	*LEE1*	Yes
YGL009C	*LEU1*	No
YCL018W	*LEU2*	No
YNL104C	*LEU4*	No
YJR070C	*LIA1*	No

Table 1.3: *ume6*Δ Responsive Genes During Mitotic Growth (continued)

Systematic Name	Gene	Present in Ume6 Depletion List
YJL038C	*LOH1*	No
YLR011W	*LOT6*	No
YDL240W	*LRG1*	No
YHR081W	*LRP1*	No
YCL034W	*LSB5*	No
YGR244C	*LSC2*	No
YBL026W	*LSM2*	No
YJR005C-A	*LSO1*	Yes
YDL087C	*LUC7*	No
YIR034C	*LYS1*	No
YIL094C	*LYS12*	No
YDL182W	*LYS20*	No
YDL131W	*LYS21*	No
YGL154C	*LYS5*	No
YKL029C	*MAE1*	No
YER142C	*MAG1*	No
YEL053C	*MAK10*	No
YCR020C-A	*MAK31*	No
YCR019W	*MAK32*	No
YBR298C	*MAL31*	No
YER106W	*MAM1*	No
YIL070C	*MAM33*	No
YNR073C	*MAN2*	No
YDL003W	*MCD1*	No
YDL054C	*MCH1*	No
YKL221W	*MCH2*	No
YOL119C	*MCH4*	No
YIL150C	*MCM10*	No
YGR053C	*MCO32*	Yes
YIL156W-B	*MCO8*	No
YNL173C	*MDG1*	No
YKL085W	*MDH1*	Yes
YBR136W	*MEC1*	Yes
YJL102W	*MEF2*	Yes
YER044C-A	*MEI4*	Yes
YPL121C	*MEI5*	Yes

Table 1.3: *ume6*Δ Responsive Genes During Mitotic Growth (continued)

Systematic Name	Gene	Present in Ume6 Depletion List
YOR351C	*MEK1*	Yes
YBR126W-A	*MEO1*	No
YGR121C	*MEP1*	No
YNL142W	*MEP2*	No
YNL210W	*MER1*	No
YKR069W	*MET1*	No
YFR030W	*MET10*	No
YGL125W	*MET13*	No
YKL001C	*MET14*	No
YPR167C	*MET16*	No
YLR303W	*MET17*	No
YIL128W	*MET18*	No
YNL277W	*MET2*	No
YOL064C	*MET22*	No
YIR017C	*MET28*	No
YJR010W	*MET3*	No
YIL046W	*MET30*	No
YPL038W	*MET31*	No
YJR137C	*MET5*	No
YBR213W	*MET8*	No
YPL187W	*MF(ALPHA)1*	No
YDL233W	*MFG1*	No
YML062C	*MFT1*	No
YIR033W	*MGA2*	Yes
YOR232W	*MGE1*	No
YCL044C	*MGR1*	No
YDL160C-A	*MHF2*	No
YCL057C-A	*MIC10*	No
YGL035C	*MIG1*	No
YER028C	*MIG3*	No
YHR015W	*MIP6*	No
YGL106W	*MLC1*	No
YPL164C	*MLH3*	No
YLR049C	*MLO50*	No
YNL117W	*MLS1*	No
YLL061W	*MMP1*	No

Table 1.3: *ume6*Δ Responsive Genes During Mitotic Growth (continued)

Systematic Name	Gene	Present in Ume6 Depletion List
YMR177W	*MMT1*	No
YGL183C	*MND1*	Yes
YIR025W	*MND2*	No
YOR350C	*MNE1*	No
YPL050C	*MNN9*	No
YIL014W	*MNT3*	No
YIL106W	*MOB1*	No
YFL034C-B	*MOB2*	No
YHR162W	*MPC2*	No
YOR177C	*MPC54*	Yes
YIR002C	*MPH1*	No
YDR033W	*MRH1*	No
YPL184C	*MRN1*	No
YDL045W-A	*MRP10*	No
YDR462W	*MRPL28*	No
YKL170W	*MRPL38*	No
YIR021W	*MRS1*	No
YKL009W	*MRT4*	No
YDL183C	*MRX19*	No
YGR014W	*MSB2*	No
YHR039C	*MSC7*	No
YCR092C	*MSH3*	No
YFL003C	*MSH4*	Yes
YDL154W	*MSH5*	Yes
YIR009W	*MSL1*	No
YOL116W	*MSN1*	No
YKL062W	*MSN4*	No
YDL107W	*MSS2*	No
YGR023W	*MTL1*	No
YAL034W-A	*MTW1*	No
YCL033C	*MXR2*	No
YER156C	*MYG1*	No
YNL240C	*NAR1*	No
YIL007C	*NAS2*	No
YMR069W	*NAT4*	No
YJL116C	*NCA3*	No

Table 1.3: *ume6*Δ Responsive Genes During Mitotic Growth (continued)

Systematic Name	Gene	Present in Ume6 Depletion List
YDR397C	*NCB2*	No
YNL036W	*NCE103*	No
YLR194C	*NCW2*	No
YIL144W	*NDC80*	Yes
YOR372C	*NDD1*	No
YDL085W	*NDE2*	No
YOL104C	*NDJ1*	Yes
YHR124W	*NDT80*	No
YLR265C	*NEJ1*	No
YIL048W	*NEO1*	No
YLR042C	*NFG1*	No
YOR156C	*NFI1*	No
YCL017C	*NFS1*	No
YML118W	*NGL3*	No
YBR212W	*NGR1*	No
YDL208W	*NHP2*	No
YNL078W	*NIS1*	No
YIL164C	*NIT1*	No
YLR315W	*NKP2*	No
YHR170W	*NMD3*	No
YNL200C	*NNR1*	No
YOR056C	*NOB1*	No
YNR053C	*NOG2*	No
YHR072W-A	*NOP10*	No
YOL041C	*NOP12*	No
YER002W	*NOP16*	No
YPL043W	*NOP4*	No
YPL146C	*NOP53*	No
YLR197W	*NOP56*	No
YOR310C	*NOP58*	No
YGR103W	*NOP7*	No
YIL038C	*NOT3*	No
YJR072C	*NPA3*	No
YCR026C	*NPP1*	No
YGR043C	*NQM1*	No
YIR035C	*NRE1*	No

Table 1.3: *ume6*Δ Responsive Genes During Mitotic Growth (continued)

Systematic Name	Gene	Present in Ume6 Depletion List
YBR066C	*NRG2*	No
YOR071C	*NRT1*	No
YER126C	*NSA2*	No
YNL091W	*NST1*	No
YBR001C	*NTH2*	No
YIL115C	*NUP159*	No
YKL120W	*OAC1*	No
YNL099C	*OCA1*	No
YCR095C	*OCA4*	No
YPL134C	*ODC1*	No
YBR230C	*OM14*	No
YIL136W	*OM45*	No
YOR130C	*ORT1*	No
YLR054C	*OSW2*	No
YFL044C	*OTU1*	No
YPL171C	*OYE3*	No
YDR488C	*PAC11*	No
YMR174C	*PAI3*	No
YHR097C	*PAL2*	No
YDR251W	*PAM1*	No
YIR006C	*PAN1*	No
YIL145C	*PAN6*	No
YCR077C	*PAT1*	No
YLL025W	*PAU17*	No
YEL049W	*PAU2*	No
YLR461W	*PAU4*	No
YNR076W	*PAU6*	No
YPL272C	*PBI1*	No
YCL052C	*PBN1*	No
YBR233W	*PBP2*	No
YBR295W	*PCA1*	Yes
YLR151C	*PCD1*	No
YDR228C	*PCF11*	No
YBR186W	*PCH2*	Yes
YIL071C	*PCI8*	No
YKR097W	*PCK1*	No

Table 1.3: *ume6*Δ Responsive Genes During Mitotic Growth (continued)

Systematic Name	Gene	Present in Ume6 Depletion List
YNL289W	*PCL1*	No
YDL127W	*PCL2*	No
YHR071W	*PCL5*	No
YER059W	*PCL6*	No
YDL179W	*PCL9*	No
YEL058W	*PCM1*	No
YBR222C	*PCS60*	No
YGR087C	*PDC6*	No
YGL248W	*PDE1*	No
YPR002W	*PDH1*	No
YCL043C	*PDI1*	No
YOR328W	*PDR10*	No
YIL013C	*PDR11*	No
YNR070W	*PDR18*	No
YBR035C	*PDX3*	No
YPL154C	*PEP4*	No
YFR023W	*PES4*	No
YER153C	*PET122*	No
YCR020C	*PET18*	No
YJR034W	*PET191*	No
YBL030C	*PET9*	No
YHR160C	*PEX18*	No
YGR239C	*PEX21*	No
YMR018W	*PEX9*	Yes
YIL107C	*PFK26*	No
YOL136C	*PFK27*	No
YCR012W	*PGK1*	No
YMR105C	*PGM2*	No
YCL004W	*PGS1*	No
YKL043W	*PHD1*	No
YOL084W	*PHM7*	Yes
YDR481C	*PHO8*	No
YML123C	*PHO84*	No
YNR013C	*PHO91*	No
YDR374C	*PHO92*	Yes
YER053C	*PIC2*	No

Table 1.3: *ume6*Δ Responsive Genes During Mitotic Growth (continued)

Systematic Name	Gene	Present in Ume6 Depletion List
YLR273C	*PIG1*	Yes
YIL045W	*PIG2*	No
YKL163W	*PIR3*	No
YJL160C	*PIR5*	No
YOL100W	*PKH2*	Yes
YIL042C	*PKP1*	No
YGL059W	*PKP2*	No
YMR008C	*PLB1*	No
YMR006C	*PLB2*	No
YPL036W	*PMA2*	No
YIL122W	*POG1*	No
YBR088C	*POL30*	No
YGR030C	*POP6*	No
YNL055C	*POR1*	No
YIL114C	*POR2*	No
YIL160C	*POT1*	No
YGL205W	*POX1*	Yes
YDR075W	*PPH3*	No
YNL217W	*PPN2*	No
YPL148C	*PPT2*	No
YHR201C	*PPX1*	No
YEL060C	*PRB1*	No
YMR297W	*PRC1*	No
YCL057W	*PRD1*	Yes
YIR008C	*PRI1*	No
YIL095W	*PRK1*	No
YMR278W	*PRM15*	No
YIL037C	*PRM2*	No
YIL117C	*PRM5*	No
YAR031W	*PRM9*	No
YKL116C	*PRR1*	No
YBL064C	*PRX1*	Yes
YJL079C	*PRY1*	No
YKR013W	*PRY2*	No
YJL078C	*PRY3*	No
YDR055W	*PST1*	Yes

Table 1.3: *ume6*Δ Responsive Genes During Mitotic Growth (continued)

Systematic Name	Gene	Present in Ume6 Depletion List
YCR079W	*PTC6*	No
YOR208W	*PTP2*	No
YER075C	*PTP3*	No
YLR414C	*PUN1*	Yes
YGL063W	*PUS2*	No
YLR142W	*PUT1*	No
YKL015W	*PUT3*	Yes
YOR348C	*PUT4*	No
YLR196W	*PWP1*	No
YPL147W	*PXA1*	Yes
YKL188C	*PXA2*	No
YGL062W	*PYC1*	Yes
YOR347C	*PYK2*	No
YIL120W	*QDR1*	No
YIL121W	*QDR2*	Yes
YBR043C	*QDR3*	No
YBR114W	*RAD16*	No
YCR066W	*RAD18*	No
YKL113C	*RAD27*	No
YER095W	*RAD51*	No
YDR217C	*RAD9*	No
YOR101W	*RAS1*	No
YNL098C	*RAS2*	No
YLR084C	*RAX2*	No
YCR036W	*RBK1*	No
YMR034C	*RCH1*	No
YIL077C	*RCI37*	No
YGL158W	*RCK1*	No
YBR073W	*RDH54*	No
YOR285W	*RDL1*	No
YCR106W	*RDS1*	No
YLR329W	*REC102*	Yes
YHR157W	*REC104*	Yes
YPR007C	*REC8*	Yes
YLR263W	*RED1*	Yes
YBR267W	*REI1*	No

Table 1.3: *ume6*Δ Responsive Genes During Mitotic Growth (continued)

Systematic Name	Gene	Present in Ume6 Depletion List
YOR346W	*REV1*	No
YIL139C	*REV7*	No
YMR182C	*RGM1*	No
YPR165W	*RHO1*	No
YOL143C	*RIB4*	No
YBR256C	*RIB5*	No
YCR028C-A	*RIM1*	No
YHL024W	*RIM4*	Yes
YGL045W	*RIM8*	No
YHR197W	*RIX1*	No
YOR095C	*RKI1*	No
YLR009W	*RLP24*	No
YNL002C	*RLP7*	No
YEL072W	*RMD6*	No
YGR044C	*RME1*	No
YPL024W	*RMI1*	No
YGL250W	*RMR1*	Yes
YLL046C	*RNP1*	Yes
YCL028W	*RNQ1*	No
YIL066C	*RNR3*	No
YFR022W	*ROG3*	No
YOR340C	*RPA43*	No
YBR154C	*RPB5*	No
YGL070C	*RPB9*	No
YHR143W-A	*RPC10*	No
YHR088W	*RPF1*	No
YKR081C	*RPF2*	No
YIL119C	*RPI1*	No
YNL301C	*RPL18B*	No
YLR344W	*RPL26A*	No
YFR032C-A	*RPL29*	No
YIL018W	*RPL2B*	No
YDL191W	*RPL35A*	No
YDL136W	*RPL35B*	No
YLR185W	*RPL37A*	No
YNL162W	*RPL42A*	No

Table 1.3: *ume6*Δ Responsive Genes During Mitotic Growth (continued)

Systematic Name	Gene	Present in Ume6 Depletion List
YML091C	*RPM2*	Yes
YIL075C	*RPN2*	No
YPR187W	*RPO26*	No
YDL081C	*RPP1A*	No
YIR015W	*RPR2*	No
YOR293W	*RPS10A*	No
YKR057W	*RPS21A*	No
YIL069C	*RPS24B*	No
YLR333C	*RPS25B*	No
YKL156W	*RPS27A*	No
YLR388W	*RPS29A*	No
YDL061C	*RPS29B*	No
YPL081W	*RPS9A*	No
YIL153W	*RRD1*	No
YPR116W	*RRG8*	No
YNL213C	*RRG9*	No
YLR141W	*RRN5*	No
YPL012W	*RRP12*	No
YDR412W	*RRP17*	No
YDR280W	*RRP45*	No
YDR083W	*RRP8*	No
YPR137W	*RRP9*	No
YOR294W	*RRS1*	No
YCR045C	*RRT12*	No
YFR032C	*RRT5*	No
YOL048C	*RRT8*	No
YLR221C	*RSA3*	No
YCR052W	*RSC6*	No
YJR127C	*RSF2*	No
YIL093C	*RSM25*	No
YGR215W	*RSM27*	No
YMR266W	*RSN1*	No
YLR281C	*RSO55*	No
YGR152C	*RSR1*	No
YBR147W	*RTC2*	No
YDL204W	*RTN2*	No

Table 1.3: *ume6*Δ Responsive Genes During Mitotic Growth (continued)

Systematic Name	Gene	Present in Ume6 Depletion List
YOR077W	*RTS2*	Yes
YGR161C	*RTS3*	No
YHR154W	*RTT107*	No
YCR009C	*RVS161*	No
YDR389W	*SAC7*	No
YHR079C-A	*SAE3*	Yes
YBR280C	*SAF1*	No
YJR004C	*SAG1*	No
YPL274W	*SAM3*	No
YJL098W	*SAP185*	No
YGL229C	*SAP4*	No
YDR180W	*SCC2*	Yes
YBL091C-A	*SCS22*	No
YGL126W	*SCS3*	No
YGL028C	*SCW11*	No
YEL057C	*SDD1*	No
YKL148C	*SDH1*	No
YDR178W	*SDH4*	No
YJL045W	*SDH9*	No
YBR214W	*SDS24*	No
YIL084C	*SDS3*	No
YGL224C	*SDT1*	No
YIR022W	*SEC11*	No
YIL109C	*SEC24*	No
YIL076W	*SEC28*	No
YFL045C	*SEC53*	No
YDR077W	*SED1*	No
YCR067C	*SED4*	No
YAR008W	*SEN34*	No
YAL067C	*SEO1*	No
YER081W	*SER3*	No
YIL074C	*SER33*	No
YJL105W	*SET4*	No
YJR095W	*SFC1*	Yes
YOR315W	*SFG1*	No
YLR321C	*SFH1*	No

Table 1.3: *ume6*Δ Responsive Genes During Mitotic Growth (continued)

Systematic Name	Gene	Present in Ume6 Depletion List
YIL099W	*SGA1*	No
YIR001C	*SGN1*	No
YER096W	*SHC1*	No
YER118C	*SHO1*	No
YIL104C	*SHQ1*	No
YOL110W	*SHR5*	No
YOR137C	*SIA1*	No
YLR079W	*SIC1*	No
YIL123W	*SIM1*	No
YJL089W	*SIP4*	Yes
YEL065W	*SIT1*	No
YHR149C	*SKG6*	No
YPL026C	*SKS1*	No
YKL108W	*SLD2*	No
YOR008C	*SLG1*	No
YNL047C	*SLM2*	No
YCR024C	*SLM5*	No
YIL147C	*SLN1*	No
YHR030C	*SLT2*	No
YDR088C	*SLU7*	No
YGR081C	*SLX9*	No
YNL196C	*SLZ1*	Yes
YPL027W	*SMA1*	No
YOR159C	*SME1*	No
YDL194W	*SNF3*	No
YGR197C	*SNG1*	No
YMR095C	*SNO1*	No
YIL061C	*SNP1*	No
YDR011W	*SNQ2*	No
YMR096W	*SNZ1*	No
YIL166C	*SOA1*	No
YCR073W-A	*SOL2*	No
YGR248W	*SOL4*	No
YDL246C	*SOR2*	No
YLL021W	*SPA2*	No
YMR191W	*SPG5*	No

Table 1.3: *ume6*Δ Responsive Genes During Mitotic Growth (continued)

Systematic Name	Gene	Present in Ume6 Depletion List
YNL012W	*SPO1*	Yes
YHL022C	*SPO11*	Yes
YHR014W	*SPO13*	Yes
YHR153C	*SPO16*	Yes
YPL130W	*SPO19*	No
YMR017W	*SPO20*	No
YOL091W	*SPO21*	No
YIL073C	*SPO22*	Yes
YBR250W	*SPO23*	No
YPR036W-A	*SPO24*	No
YGL170C	*SPO74*	No
YLR341W	*SPO77*	No
YOR190W	*SPR1*	No
YDR218C	*SPR28*	No
YGR059W	*SPR3*	No
YHR139C	*SPS100*	No
YDR522C	*SPS2*	No
YCL048W	*SPS22*	No
YOR313C	*SPS4*	No
YMR179W	*SPT21*	No
YIR012W	*SQT1*	No
YCR081W	*SRB8*	No
YOR247W	*SRL1*	No
YPL033C	*SRL4*	No
YDL092W	*SRP14*	No
YMR101C	*SRT1*	Yes
YKL086W	*SRX1*	Yes
YKL218C	*SRY1*	No
YAL005C	*SSA1*	Yes
YER103W	*SSA4*	No
YBR169C	*SSE2*	Yes
YCR073C	*SSK22*	No
YIL143C	*SSL2*	No
YIL030C	*SSM4*	No
YMR183C	*SSO2*	No
YHR184W	*SSP1*	No

Table 1.3: *ume6*Δ Responsive Genes During Mitotic Growth (continued)

Systematic Name	Gene	Present in Ume6 Depletion List
YLR452C	*SST2*	No
YPL092W	*SSU1*	No
YOR047C	*STD1*	No
YHR084W	*STE12*	No
YDR410C	*STE14*	No
YJR086W	*STE18*	No
YFL026W	*STE2*	No
YKL178C	*STE3*	No
YOR212W	*STE4*	No
YDR103W	*STE5*	No
YCL032W	*STE50*	No
YKL209C	*STE6*	No
YDL130W-A	*STF1*	No
YIL126W	*STH1*	No
YDR536W	*STL1*	No
YCL008C	*STP22*	No
YDL048C	*STP4*	No
YJR130C	*STR2*	No
YGL184C	*STR3*	Yes
YIL162W	*SUC2*	No
YPR151C	*SUE1*	Yes
YNL244C	*SUI1*	No
YBR294W	*SUL1*	No
YLR092W	*SUL2*	No
YNL066W	*SUN4*	No
YBR143C	*SUP45*	No
YML052W	*SUR7*	No
YPR009W	*SUT2*	No
YPL163C	*SVS1*	No
YDR146C	*SWI5*	No
YNL187W	*SWT21*	No
YIL047C	*SYG1*	No
YPL105C	*SYH1*	No
YCR042C	*TAF2*	No
YCR060W	*TAH1*	No
YIL129C	*TAO3*	No

Table 1.3: *ume6*Δ Responsive Genes During Mitotic Growth (continued)

Systematic Name	Gene	Present in Ume6 Depletion List
YBR069C	*TAT1*	No
YJL083W	*TAX4*	No
YNL087W	*TCB2*	No
YPR157W	*TDA6*	No
YJL052W	*TDH1*	No
YJR009C	*TDH2*	No
YBR083W	*TEC1*	No
YIL039W	*TED1*	No
YNL128W	*TEP1*	No
YJR019C	*TES1*	No
YPL157W	*TGS1*	No
YGR144W	*THI4*	No
YPL214C	*THI6*	No
YOR192C	*THI72*	No
YLR004C	*THI73*	No
YDR438W	*THI74*	No
YPR045C	*THP3*	No
YHR025W	*THR1*	No
YCR053W	*THR4*	No
YIL078W	*THS1*	No
YHR005C-A	*TIM10*	No
YIL022W	*TIM44*	No
YER011W	*TIR1*	No
YIL011W	*TIR3*	No
YLR136C	*TIS11*	No
YBR117C	*TKL2*	No
YDR468C	*TLG1*	No
YLR327C	*TMA10*	No
YIL137C	*TMA108*	No
YOR252W	*TMA16*	No
YDR107C	*TMN2*	No
YER184C	*TOG1*	No
YBR162C	*TOS1*	No
YGR221C	*TOS2*	No
YGL179C	*TOS3*	No
YGR096W	*TPC1*	No

Table 1.3: *ume6*Δ Responsive Genes During Mitotic Growth (continued)

Systematic Name	Gene	Present in Ume6 Depletion List
YKL166C	*TPK3*	No
YIL138C	*TPM2*	No
YLL028W	*TPO1*	No
YGR138C	*TPO2*	No
YOR273C	*TPO4*	No
YHR099W	*TRA1*	No
YOL093W	*TRM10*	Yes
YDR007W	*TRP1*	No
YKL211C	*TRP3*	No
YGL026C	*TRP5*	No
YCR083W	*TRX3*	No
YDR453C	*TSA2*	No
YML100W	*TSL1*	Yes
YDL060W	*TSR1*	No
YLR435W	*TSR2*	No
YCR084C	*TUP1*	No
YDR100W	*TVP15*	No
YOR344C	*TYE7*	No
YOR339C	*UBC11*	No
YDR059C	*UBC5*	No
YLL039C	*UBI4*	Yes
YKR098C	*UBP11*	No
YIL156W	*UBP7*	No
YLR024C	*UBR2*	Yes
YGR019W	*UGA1*	No
YBR006W	*UGA2*	No
YDL210W	*UGA4*	No
YDL169C	*UGX2*	No
YAR027W	*UIP3*	No
YPL186C	*UIP4*	No
YFR026C	*ULI1*	No
YIL031W	*ULP2*	Yes
YDR207C	*UME6*	Yes
YMR271C	*URA10*	No
YJR103W	*URA8*	No
YIL008W	*URM1*	No

Table 1.3: *ume6*Δ Responsive Genes During Mitotic Growth (continued)

Systematic Name	Gene	Present in Ume6 Depletion List
YLR132C	*USB1*	Yes
YPL230W	*USV1*	No
YKR042W	*UTH1*	No
YIL091C	*UTP25*	No
YDR398W	*UTP5*	No
YDR449C	*UTP6*	No
YHR196W	*UTP9*	No
YOR106W	*VAM3*	No
YML115C	*VAN1*	No
YBR293W	*VBA2*	No
YKR105C	*VBA5*	No
YDL128W	*VCX1*	No
YGL258W	*VEL1*	No
YIL056W	*VHR1*	No
YER064C	*VHR2*	No
YIL135C	*VHS2*	No
YOR054C	*VHS3*	No
YBR105C	*VID24*	No
YNL321W	*VNX1*	No
YOR089C	*VPS21*	No
YGL104C	*VPS73*	Yes
YLR337C	*VRP1*	No
YER072W	*VTC1*	No
YDR089W	*VTC5*	No
YIL173W	*VTH1*	No
YDR374W-A	*WIP1*	Yes
YOR230W	*WTM1*	No
YFL010C	*WWM1*	No
YIL101C	*XBP1*	No
YGR194C	*XKS1*	Yes
YLR070C	*XYL2*	No
YIR018W	*YAP5*	No
YAR071W/YHR215W	*YAR071W/YHR215W*	No
YAR035W	*YAT1*	No
YER024W	*YAT2*	No
YBL028C	*YBL028C*	No

Table 1.3: *ume6*Δ Responsive Genes During Mitotic Growth (continued)

Systematic Name	Gene	Present in Ume6 Depletion List
YBR062C	*YBR062C*	No
YBR085C-A	*YBR085C-A*	No
YBR184W	*YBR184W*	Yes
YBR197C	*YBR197C*	No
YBR238C	*YBR238C*	No
YBR241C	*YBR241C*	No
YBR284W	*YBR284W*	Yes
YBR285W	*YBR285W*	No
YBR299W/YGR292W	*YBR299W/YGR292W*	No
YBR299W/YGR292W	*YBR299W/YGR292W*	No
YGR203W	*YCH1*	No
YCL001W-A	*YCL001W-A*	No
YCL002C	*YCL002C*	No
YCL012C	*YCL012C*	No
YCL021W-A	*YCL021W-A*	No
YCL048W-A	*YCL048W-A*	No
YCL049C	*YCL049C*	No
YCR004C	*YCP4*	No
YCR007C	*YCR007C*	No
YCR023C	*YCR023C*	No
YCR061W	*YCR061W*	Yes
YCR090C	*YCR090C*	No
YCR099C	*YCR099C*	No
YCR102C	*YCR102C*	No
YCR102C	*YCR102C*	No
YLL055W	*YCT1*	No
YDL114W	*YDL114W*	No
YDL129W	*YDL129W*	No
YDL199C	*YDL199C*	No
YDR018C	*YDR018C*	Yes
YDR042C	*YDR042C*	No
YDR222W	*YDR222W*	Yes
YDR391C	*YDR391C*	Yes
YDR476C	*YDR476C*	No
YDR541C	*YDR541C*	No
YER010C	*YER010C*	No

Table 1.3: *ume6*Δ Responsive Genes During Mitotic Growth (continued)

Systematic Name	Gene	Present in Ume6 Depletion List
YER034W	*YER034W*	No
YER152C	*YER152C*	No
YMR040W	*YET2*	No
YFL040W	*YFL040W*	No
YFR018C	*YFR018C*	Yes
YGL101W	*YGK1*	No
YGL036W	*YGL036W*	Yes
YGL039W	*YGL039W*	No
YGL081W	*YGL081W*	Yes
YGL117W	*YGL117W*	No
YGL185C	*YGL185C*	No
YGL262W	*YGL262W*	No
YNL160W	*YGP1*	No
YGR035C	*YGR035C*	No
YGR067C	*YGR067C*	No
YGR201C	*YGR201C*	No
YGR234W	*YHB1*	No
YHR029C	*YHI9*	No
YHL012W	*YHL012W*	No
YHL044W	*YHL044W*	Yes
YHR022C	*YHR022C*	No
YHR033W	*YHR033W*	No
YHR138C	*YHR138C*	No
YHR180W	*YHR180W*	No
YHR202W	*YHR202W*	Yes
YHR213W	*YHR213W*	No
YHR214W/YAR066W	*YHR214W/YAR066W*	No
YIL006W	*YIA6*	No
YPL201C	*YIG1*	No
YCR059C	*YIH1*	No
YIL001W	*YIL001W*	No
YIL014C-A	*YIL014C-A*	No
YIL024C	*YIL024C*	Yes
YIL059C	*YIL059C*	No
YIL067C	*YIL067C*	No
YIL092W	*YIL092W*	No

Table 1.3: *ume6*Δ Responsive Genes During Mitotic Growth (continued)

Systematic Name	Gene	Present in Ume6 Depletion List
YIL102C-A	*YIL102C-A*	No
YIL108W	*YIL108W*	No
YIL152W	*YIL152W*	No
YIL161W	*YIL161W*	No
YIL172C/YOL157C/YJL221C	*YIL172C/YOL157C/YJL221C*	No
YIR016W	*YIR016W*	No
YIR042C	*YIR042C*	No
YJL043W	*YJL043W*	No
YJL132W	*YJL132W*	No
YJL213W	*YJL213W*	No
YJL218W	*YJL218W*	No
YJR096W	*YJR096W*	No
YJR149W	*YJR149W*	No
YJR158W/YDL245C	*YJR158W/YDL245C*	No
YJR160C/YDL247W	*YJR160C/YDL247W*	No
YIL023C	*YKE4*	No
YKL068W-A	*YKL068W-A*	No
YKR005C	*YKR005C*	Yes
YKR015C	*YKR015C*	No
YKR041W	*YKR041W*	No
YLL056C	*YLL056C*	No
YLL058W	*YLL058W*	No
YLR030W	*YLR030W*	No
YLR149C	*YLR149C*	No
YLR152C	*YLR152C*	No
YLR257W	*YLR257W*	No
YLR363W-A	*YLR363W-A*	No
YLR446W	*YLR446W*	No
YLR460C	*YLR460C*	No
YML002W	*YML002W*	No
YML083C	*YML083C*	No
YML131W	*YML131W*	No
YMR085W	*YMR085W*	Yes
YMR196W	*YMR196W*	No
YMR206W	*YMR206W*	No
YMR244W	*YMR244W*	No

Table 1.3: *ume6*Δ Responsive Genes During Mitotic Growth (continued)

Systematic Name	Gene	Present in Ume6 Depletion List
YFR049W	*YMR31*	No
YNL019C	*YNL019C*	No
YNL092W	*YNL092W*	No
YNL134C	*YNL134C*	No
YNL146W	*YNL146W*	No
YNL194C	*YNL194C*	No
YNL195C	*YNL195C*	No
YNL320W	*YNL320W*	No
YNL332W/YFL058W	*YNL332W/YFL058W*	No
YNL332W/YFL058W	*YNL332W/YFL058W*	No
YNR014W	*YNR014W*	No
YNR066C	*YNR066C*	No
YNR071C	*YNR071C*	No
YOL019W	*YOL019W*	No
YOL131W	*YOL131W*	Yes
YOL156W/YJL219W	*YOL156W/YJL219W*	No
YOL156W/YJL219W	*YOL156W/YJL219W*	No
YOR296W	*YOR296W*	No
YOR338W	*YOR338W*	Yes
YOR365C	*YOR365C*	No
YOR387C	*YOR387C*	No
YOR389W	*YOR389W*	Yes
YOR389W	*YOR389W*	Yes
YMR104C	*YPK2*	No
YPL088W	*YPL088W*	No
YPL090C/YBR181C	*YPL090C/YBR181C*	No
YPL245W	*YPL245W*	No
YPL264C	*YPL264C*	No
YPL280W/YOR391C	*YPL280W/YOR391C*	No
YPL280W/YOR391C	*YPL280W/YOR391C*	No
YPL281C/YOR393W	*YPL281C/YOR393W*	No
YPL281C/YOR393W	*YPL281C/YOR393W*	No
YPR071W	*YPR071W*	No
YPR145C-A	*YPR145C-A*	Yes
YPR196W	*YPR196W*	No
YLR120C	*YPS1*	No

Table 1.3: *ume6*∆ Responsive Genes During Mitotic Growth (continued)

Systematic Name	Gene	Present in Ume6 Depletion List
YLR121C	*YPS3*	No
YIR039C	*YPS6*	No
YNL093W	*YPT53*	No
YIL063C	*YRB2*	No
YOR003W	*YSP3*	Yes
YBR148W	*YSW1*	No
YIR026C	*YVH1*	No
YOL109W	*ZEO1*	No
YDR285W	*ZIP1*	Yes
YGL249W	*ZIP2*	Yes
YBR046C	*ZTA1*	No
YNL241C	*ZWF1*	No

targets. However, no role for Ume6 in the regulation of *CAT8* has been asserted. Not surprisingly, in work utilizing a *ume6*∆, *CAT8* derepression was dismissed as a side effect of general strain differences between SK1 and W303 (Williams et al. 2002). How strain differences could affect the target list of our Ume6 depletion system is interesting and worth following up on. Despite this, our Ume6 depletion system has afforded greater clarity in designating Ume6 targets and allowed the identification of 144 direct Ume6 targets involved in diverse cellular pathways. Another interesting addition to the Ume6 regulon is *UME6* itself. However, if Ume6 regulates its own promoter, then formation of the Ume6-Sin3-Rpd3 complex in mitotic cells would be expected to repress *UME6* expression during vegetative growth. Excessive repression of Ume6 would only serve to dysregulate Ume6 targets contributing to cell sickness. However, Ume6 is expressed during vegetative growth, albeit at low levels (Figure 2.5). Furthermore, mitotic depletion of Ume6 leads to a modest upregulation of *UME6* transcripts (Figure 2.5). Thus, Ume6 appears to repress its own transcription during mitotic growth but to a much lesser extent than the EMGs, many of which are essentially quiescent in mitotically dividing cells. It has been shown that in addition to Sin3-Rpd3, Ume6 also associates with the chromatin remodeler Isw2 for full repression of EMGs (Goldmark et al. 2000; Donovan et al. 2021). Whether Ume6, Sin3-Rpd3, and Isw2 work together at the *UME6* promoter and how they simultaneously achieve silencing of the EMGs requires further investigation.

Conclusions

In summary, here we develop a more versatile allele of *UME6* that can be conditionally and acutely depleted. By not terminally removing Ume6, we allowed Ume6

to maintain repression over its targets. Maintaining this repression prevented expression of the meiotic machinery during mitotic growth. This strategy also suppressed accumulation of secondary effects associated with *ume6*Δ where misregulation of Ume6 targets causes sickness, limiting cell's ability to grow. Additionally, maintaining repression of Ume6 targets reduced expression of direct and indirect genes that can contribute to background signal, which could impede definition of Ume6 targets. Furthermore, because depletion of a repressor leads to derepression of its targets, our system has the added advantage of derepressing Ume6 targets specifically for subsequent identification. Recognizing this, we have reviewed a previously acquired ChIP-Seq dataset that indicates direct Ume6 binding. By combining this ChIP-seq dataset with our RNAseq depletion dataset, we identified direct targets of Ume6 that, upon depletion, became derepressed. Looking over the transcriptome we found 144 Ume6 direct targets and further inspection indicated these genes in a broad set of different cellular programs.

Surprisingly, our dataset also revealed that Ume6 regulates its own promoter which, during mitotic growth when Ume6 acts as a repressor. Because EMGs represent a diverse class of genes whose functions are unique to meiosis, their proper regulation is critical to cellular health. Indeed, loss in regulation over these genes, such as with *ume6*Δ, results reduced growth kinetics and pleiotropy. Thus, having Ume6 autoregulate its own promoter at a time when Ume6 acts as a repressor would threaten to derepress EMG. Despite this, cells are able to achieve an equilibrium where enough Ume6 is present to maintain EMG repression. How this is achieved remains unclear and likely depends on the interplay between Ume6, Sin3-Rpd3, and the chromatin remodeler, Isw2.

Chapter 3

Ume6's Conversion to an Activator Complex Through Ime1 Binding is Critical to EMG Expression

Introduction

Gametogenesis culminates in the formation of reproductive cells via a series of highly coordinated processes driven by a dynamic and tightly controlled gene expression program. One key process in gametogenesis is meiosis, a specialized form of cell division that involves recombination between homologous chromosomes and reduction of chromosome number by half. Faithful execution of meiosis is crucial, as most human miscarriages and congenital birth defects arise from meiotic errors (Hassold and Hunt 2001; Nagaoka et al. 2012). Moreover, inappropriate activation of meiotic genes has been implicated in a range of cancer types, underscoring the significance of proper meiotic gene regulation (Lingg et al. 2022; McFarlane and Wakeman 2017; Hanahan and Weinberg 2011; Feichtinger and McFarlane 2019). Therefore, understanding the mechanisms that regulate gene expression and meiotic execution during gametogenesis is of utmost importance.

Entry into meiosis occurs in respirationally-competent diploid cells, where the *IME1* promoter is derepressed in response to nitrogen and glucose starvation (reviewed in van Werven and Amon 2011). Once translated, Ime1 is phosphorylated by the kinases Rim11 and Rim15 to promote its nuclear localization and interaction with the DNA binding TF, Ume6 (Malathi et al. 1999, 1997; Pnueli et al. 2004; Vidan and Mitchell 1997). However, as was previously shown, Ume6 acts as a transcriptional repressor during mitosis due to its association with Sin3-Rpd3. How the binding of Ime1 to Ume6 alleviates this repression and influences EMG expression was not clear. Previous experiments that

make use of the aforementioned Ume6 null mutant have made it difficult to assess the meiosis-specific functions of *UME6* and to understand how the interaction between Ume6 and Ime1 influences EMG expression. Consequently, two distinct models have been proposed to explain the impact of Ime1 on Ume6 during meiosis. The first model suggests that Ime1, which possesses an activation domain, binds to Ume6 and transforms the complex from a transcriptional repressor into an activator, thereby resulting in EMG expression (Figure 1.1, top panel; Rubin-Bejerano et al. 1996; Smith et al. 1993; Washburn and Esposito 2001; Bowdish et al. 1995). Consistent with this model, Raithatha et al. found that Ume6 remains bound to EMG promoters when these genes are activated (Raithatha et al. 2021). The second model posits that binding of Ime1 to Ume6 serves as a signal that leads to the subsequent degradation of Ume6, thereby releasing EMG repression (Figure 1.1, bottom panel; Mallory et al. 2007; Law et al. 2014; Mallory et al. 2012). While the basis of these discordant observations regarding Ume6 stability is not clear, the difference may stem from the asynchrony with which sporulating cultures of *S. cerevisiae* proceed through meiosis.

By using two different meiotic synchronization methods, here we describe a thorough mechanistic characterization of Ume6's role in meiotic gene expression. We surprisingly find that Ume6 is upregulated early in meiosis, downstream of Ime1, and is degraded only after prophase I, downstream of the transcriptional regulator Ndt80. The expression of the same gene set is hindered when Ume6 is depleted during the transition from mitotic to meiotic cell fate. Thus, we provide conclusive evidence that Ume6 plays a critical role in EMG expression and gamete production, consistent with the co-activator model. This is in contrast with the role of Ume6 during mitotic growth, where our data confirm that it acts primarily as part of a repressive complex. Finally, by using a nanobody-based trap, we found that tethering of a heterologous transactivation domain to Ume6 is sufficient to induce EMGs and produce viable gametes in the absence of Ime1, demonstrating that Ume6 is the primary determinant of EMG targeting. Altogether, our findings highlight Ume6 as an essential meiotic transcription factor, working in concert with Ime1, rather than a mitotic repressor that is simply an antagonist of meiotic gene expression.

Results

Diametric regulation of *UME6* expression by the meiotic transcription factors Ime1 and Ndt80

The two models for Ume6-dependent control of EMG expression were postulated based on different conclusions about the levels and timing of Ume6 degradation during meiosis.

These differences may have stemmed from the asynchronous nature of meiotic entry and/or the use of *UME6* null allele, which causes significant growth defects during mitotic

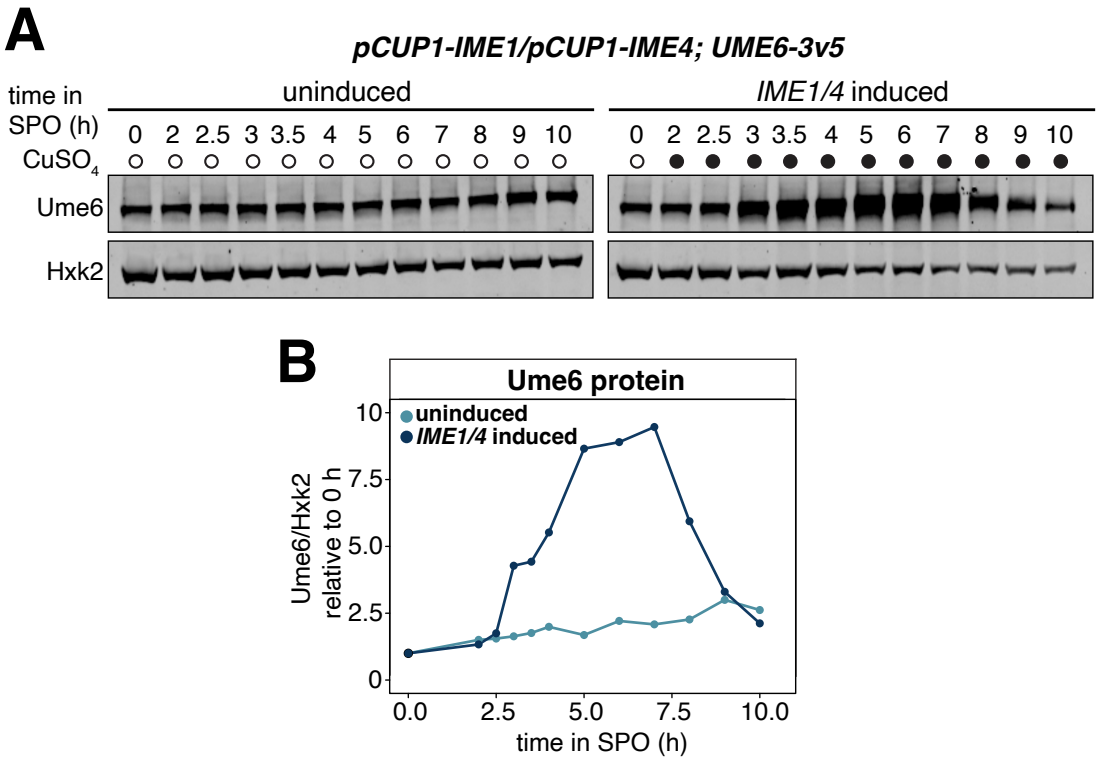

Figure 3.1: Immunoblotting for Ume6 protein levels during *pCUP1-IME1 pCUP1-IME4* induction. (A) Ume6 protein abundance in response to withholding (uninduced) or inducing (induced) *IME1/4* during synchronous meiotic progression. The strain carrying *pCUP1-IME1* and *pCUP1-IME4* along with a 3v5-tagged allele of *UME6* (UB3301) was transferred to sporulation medium (SPO) at 0 h and cells were arrested at meiotic entry. After 2h, the meiotic culture was split in two. The vehicle control (water) was added to the first flask preventing meiotic entry. $CuSO_4$ (50 μM) was added to the other flask to induce meiosis. Cells were collected at the indicated times for protein extraction and Ume6 levels were determined using anti-V5 immunoblotting and Hxk2 as a loading control. Representative blots from one of three biological replicates are shown. (B) Quantification of immunoblotting in A

growth due to EMG derepression (Strich et al. 1994; Nachman et al. 2007). To investigate the role of *UME6* in the expression of early meiotic genes (EMGs), we first followed Ume6 protein levels in a population of cells undergoing highly synchronized meiotic progression. Synchronization of meiotic progression was achieved by using an established method that utilizes a copper-inducible promoter (*pCUP1*) to control the expression of two key regulators of meiotic entry: *IME1*, which encodes an early meiotic transcription factor, and *IME4*, which encodes an mRNA N6-adenosine methyltransferase (Berchowitz et al. 2013; Chia and van Werven 2016). We then monitored the abundance of an endogenously *3V5* tagged allele of *UME6* in these cells. Under the uninduced condition, Ume6 protein levels

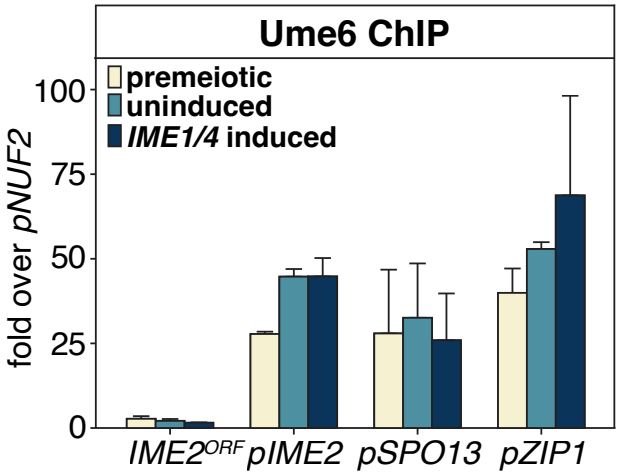

Figure 3.2: Ume6 ChIP-qPCR at meiotic promoters during *pCUP1-IME1* and *pCUP1-IME4* induction. Changes in *UME6* expression in response to *IME1/4* and *NDT80* induction. Ume6 occupancy at the *IME2*, *SPO13*, and *ZIP1* promoters, as well as the *IME2 ORF* where binding is not expected was analyzed by chromatin immunoprecipitation followed by qPCR (ChIP-qPCR) in strain UB3301. Cells were transferred to SPO and arrested at meiotic entry by withholding *IME1/4* for 2h (premeiotic). At this time, a sample of OD_{600} = 50 was collected. *IME1/4* was then either induced by addition of $CuSO_4$ (50 μM; *IME1/4* induced) or withheld (uninduced). Cells were allowed to continue in SPO for 2 h after this and samples of OD_{600} = 50 for uninduced and *IME1/4* induced were collected. Mean enrichment for three biological replicates is presented with the standard error of each primer pair used. Ume6 signal at target sites was normalized over *NUF2* promoter enrichment.

remained largely unchanged (Figure 3.1A and 3.1B, uninduced). In contrast, induction of *IME1* and *IME4* (t = 2 h) resulted in a substantial increase in Ume6 protein levels, up to 8-fold, which was already evident 1 h following *pCUP1* induction (t = 3 h) and remained elevated until 7 h post-induction (Figure 3.1A and 3.1B, *IME1/4* induced). Thus, Ume6 protein levels actually increase following *IME1/4* induction and remain elevated until around 7 h when cells transition out of prophase I.

To test whether Ume6 remained bound to EMG promoters following *IME1/4* induction, we performed chromatin immunoprecipitation followed by quantitative polymerase chain reaction (ChIP-qPCR). Ume6 enrichment was monitored at the promoters of three well-characterized EMGs, *IME2*, *SPO13*, and *ZIP1,* as well as the open reading frame (ORF) of *IME2* where Ume6 is not expected to bind. In the three EMGs analyzed, Ume6 remained bound at these promoters at levels similar to premeiotic conditions, irrespective of *IME1/IME4* induction. Thus, Ume6 is not displaced from EMG promoters during meiotic entry, suggesting that it plays a role in EMG activation during meiosis (Figure 3.2).

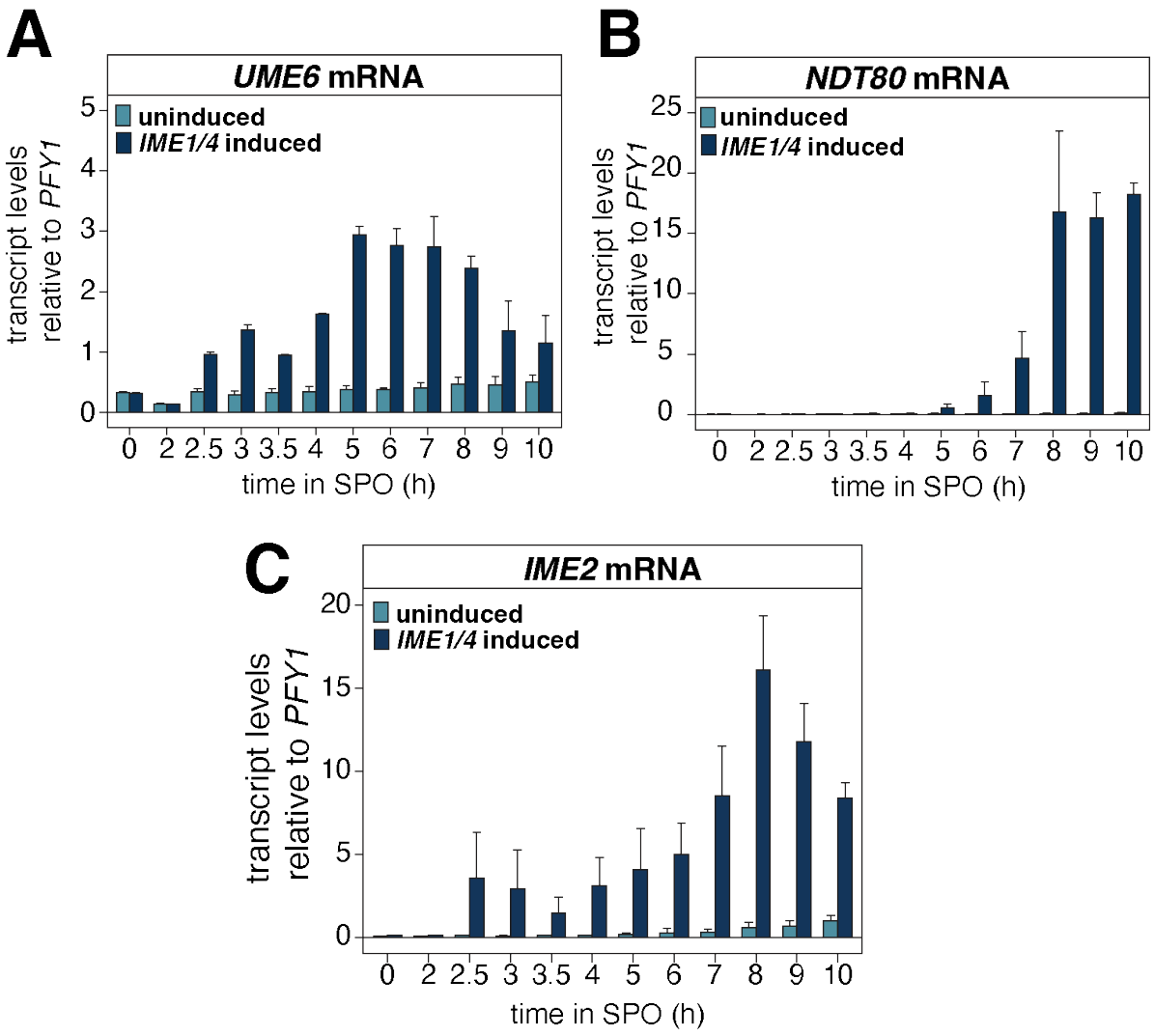

Figure 3.3: Quantitative measurements of transcript abundance during *pCUP1-IME1 pCUP1-IME4* induction. Changes in *UME6* expression in response to *IME1/4* and *NDT80* induction. RNA samples were collected at the indicated times to monitor expression patterns for (A) *UME6,* (B) *NDT80*, and (C) *IME2* in response to *IME1/4* induction. RNA was extracted from samples and transcript levels for *UME6* and *NDT80* were determined using RT-qPCR. The CT mean for two biological replicates is presented along with the range for uninduced and *IME1/4* induced samples at the specified time points. To control for technical variation, we normalized expression of *UME6* and *NDT80* relative to *PFY1*.

Given that *IME1* and *IME4* are involved in transcriptional and posttranscriptional gene regulation, respectively (Shah and Clancy 1992; Hongay et al. 2006; reviewed in van Werven and Amon 2011), we reasoned that the elevated Ume6 protein levels in meiosis could be due to an increase in *UME6* mRNA abundance and hence Ume6 synthesis. To investigate this further, we analyzed *UME6* transcripts by reverse transcription and qPCR (RT-qPCR). In the absence of *IME1/4* induction, *UME6* transcript levels were largely

unchanged (Figure 3.3A, *IME1/4* uninduced). However, in response to *IME1/4* induction, we observed ~7-fold increase in *UME6* transcript levels going from pre- to post-induction. This coincided with increased expression of the EMG *IME2* (Figure 3.3C). Furthermore, *UME6* transcript levels peaked after 5 h and remained high until 8 h, consistent with the immunoblotting data (Figure 3.1A and 3.3A). Together, these findings demonstrate that *IME1/4* induces the expression of both EMG and *UME6* and leads to elevated Ume6 protein levels during meiotic entry.

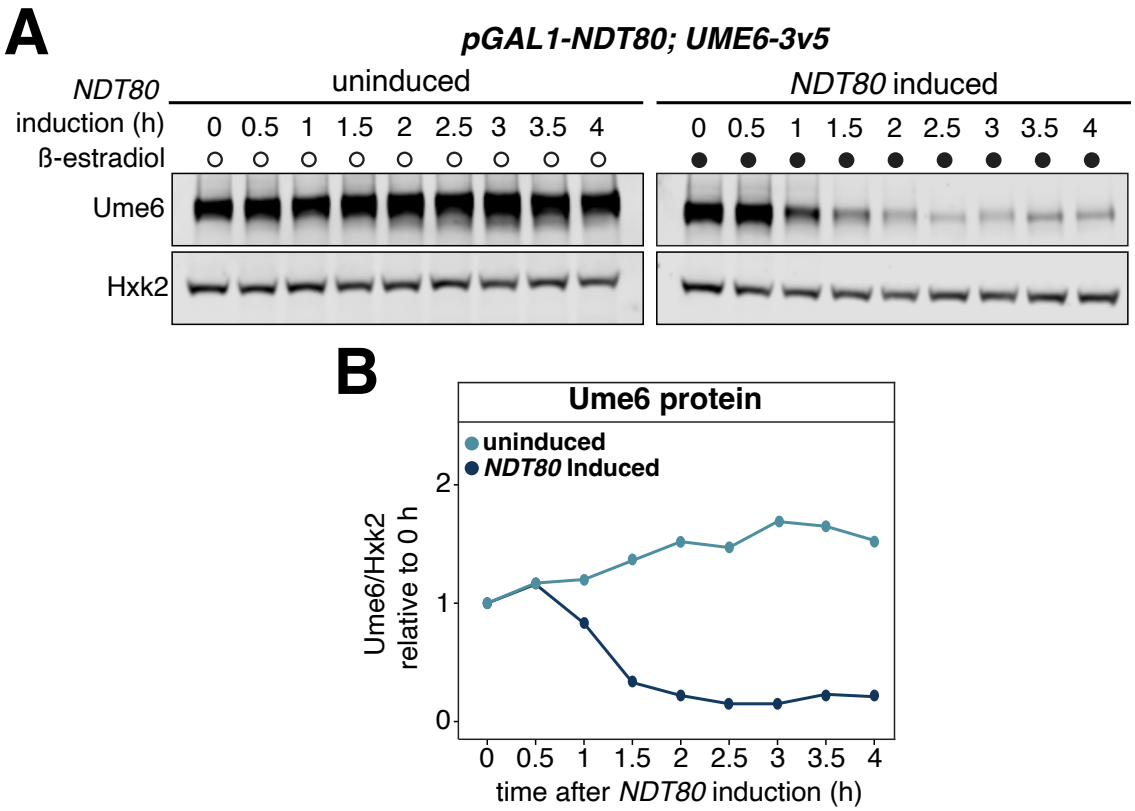

Figure 3.4: Immunoblotting for Ume6 protein levels in *NDT80* inducible background. Changes in *UME6* expression in response to *IME1/4* and *NDT80* induction. Ume6 protein levels in monitored in response to *NDT80* induction. The strain harboring the *pGAL1-NDT80* and *GAL4-ER* in combination with 3v5-tagged Ume6 (UB21877) was transferred to SPO. Cells were allowed to progress through meiosis for 5 h before arresting at pachytene of prophase I (t=0 h). A sample for protein and RNA was collected and cultures were split into two flasks. The first flask received the vehicle control (EtOH) to withhold *NDT80* expression (uninduced) while the other flask received ß-estradiol (1µM) to induce *NDT80* expression allowing exit from prophase (*NDT80* induced). Samples were collected at the designated time points. (A) Ume6 levels were determined using anti-V5 immunoblotting and Hxk2 for a loading control as before. Representative blots from one of three biological replicates are shown. (B) Quantification of immunoblots in A.

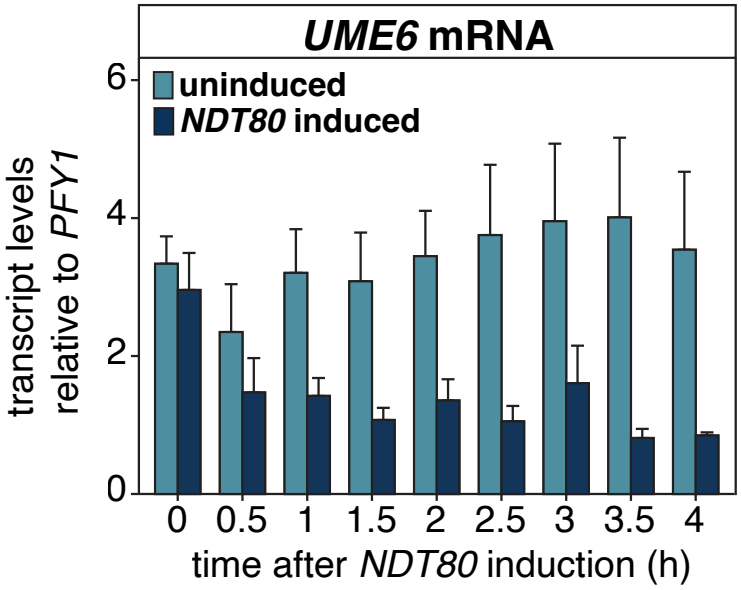

Figure 3.5: Analysis of *UME6* transcript level response to *NDT80* induction. Changes in *UME6* expression in response to *IME1/4* and *NDT80* induction. *UME6* transcripts in the presence and absence of *NDT80* were monitored by RT-qPCR after RNA extraction. The CT mean of three biological replicates is presented along with the standard error. Technical variation was controlled for by normalization to *PFY1*.

Following an initial increase, Ume6 protein levels began to decline after ~7 h in SPO. This timing coincided with the expression of *NDT80* (Figure 3.3B), which encodes a transcription factor necessary for exit from meiotic prophase I, initiation of meiotic divisions, and gamete maturation (Xu et al. 1995). To directly test how Ndt80 influences Ume6, we took advantage of an inducible *NDT80* system whereby *NDT80* mRNA expression is triggered by a β-estradiol-activatable transcription factor (Benjamin et al. 2003; Carlile and Amon 2008). Cells were incubated in SPO for 5 h to achieve prophase I arrest, and then β-estradiol was withheld or added to the media, thereby either preventing or allowing for *NDT80* expression and progression through the meiotic divisions, respectively. In the absence of *NDT80* induction, Ume6 protein levels remained unchanged (Figure 3.4A and 3.4B, uninduced). However, after 1.5 h following *NDT80* induction, Ume6 abundance was reduced to 32% of the initial levels and reached 15% after 4 h (Figure 3.4A and 3.4B, *NDT80* induced). To assess whether *NDT80* induction also influenced *UME6* transcript levels, RNA samples were collected for RT-qPCR. Withholding *NDT80* induction resulted in *UME6* transcript levels remaining largely unchanged (Figure 3.5; uninduced). In contrast, *NDT80* induction led to a ~32% drop in *UME6* transcript levels as early as 1.5 h (Figure 3.5; *NDT80* induced). We conclude that Ume6 protein levels decrease in response to Ndt80, not Ime1, and this downregulation is

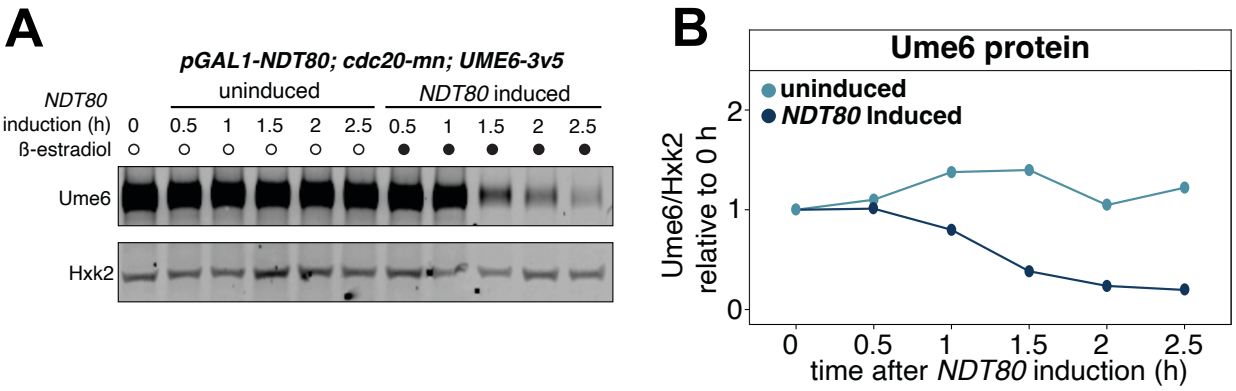

Figure 3.6: Immunoblotting of Ume6 protein levels to determine Cdc20 involvement in *NDT80*-mediated downregulation of Ume6. (A) A strain harboring the *pGAL1-NDT80* and *GAL4-ER* system was combined with the *cdc20-mn* allele (UB22674) and grown as in Figure 3F and 3G. Protein samples were collected at the designated time points and Ume6 levels were determined by anti-V5 immunoblotting using Hxk2 as a loading control. (B) Quantification of western blot.

due in part to a reduction in *UME6* transcript levels. Downregulation of *UME6* following *NDT80* expression thus restricts the timing of Ume6 removal to when meiotic cells are transitioning from early to mid-meiotic gene expression.

Cdc20, which serves as an activator for the APC E3 ligase, has been previously implicated in Ume6 degradation based on the use of a temperature-sensitive *CDC20* allele. (Mallory et al. 2007). Exposing cells to high temperatures is known to disrupt meiotic progression in a variety of organisms. Thus, the use a *cdc20-ts* allele may have confounding effects beyond *CDC20* inactivation. To circumvent this limitation, we utilized a meiotic-null allele of *CDC20*, *cdc20-mn*, and combined it with the inducible *NDT80* system *(pGAL-NDT80; GAL4-ER; pCLB2-CDC20*). However, Ume6 protein levels still declined in the *cdc20-mn* mutant following *NDT80* induction (Figure 3.6A and 3.6B). This finding is consistent with a previous report, which also found no evidence of Cdc20 involvement in Ume6 turnover during meiosis (Raithatha et al. 2021).

Our data thus far help differentiate Ume6's meiotic role in EMG activation through three key insights: (1) *IME1* expression results in the upregulation of *UME6* itself, leading to increased Ume6 protein levels; (2) Ume6 remains bound to the EMG promoters in the presence of Ime1; and (3) *NDT80* expression triggers events that lead to the downregulation of *UME6*, and thus reduced Ume6 protein levels, following exit from prophase I. These results are consistent with a model whereby Ime1 and Ume6 form an activator complex and once the early meiotic events are completed, *UME6* is downregulated in an Ndt80-dependent manner.

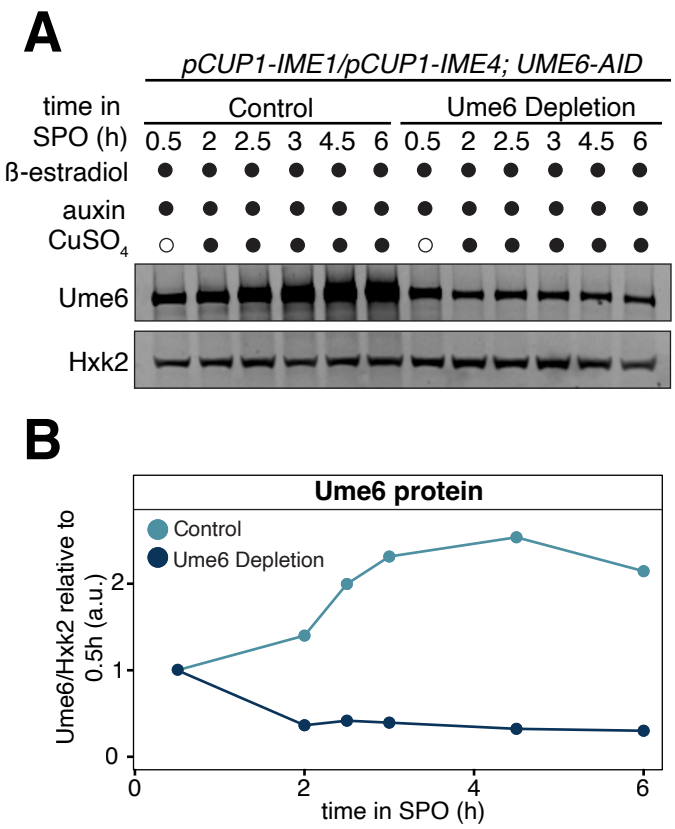

Figure 3.7: Monitoring Ume6-AID depletion by immunoblotting during meiosis. Ume6 depletion shortly before meiotic entry disrupts gamete formation and EMG expression. Cultures from control (UB25688) and Ume6 depletion (UB25092) strains were transferred to SPO at 0 h. ß-estradiol (5 nM) and auxin (200 μM) were added at 0.5 h. Then, $CuSO_4$ (50μM) was added at 2 h to induce meiosis. Samples for protein and RNA were collected at designated times. (A) Ume6 protein abundance was analyzed using anti-V5 immunoblotting and Hxk2 as a loading control. Representative blots from one of three biological replicates are shown. (B) Quantification of the immunoblots in A.

Meiotic depletion of Ume6 inhibits gamete formation and prevents proper activation of EMGs.

Our findings support the notion that the Ime1-Ume6 activator complex drives the expression of EMGs; however, it remains unclear how loss of *UME6* function, specifically during gametogenesis, impacts meiotic progression and gene expression. To address this question, we combined *UME6-AID* with the inducible *IME1/4* system, thus allowing us to rapidly deplete Ume6 shortly before meiotic entry. Our data thus far indicate that the

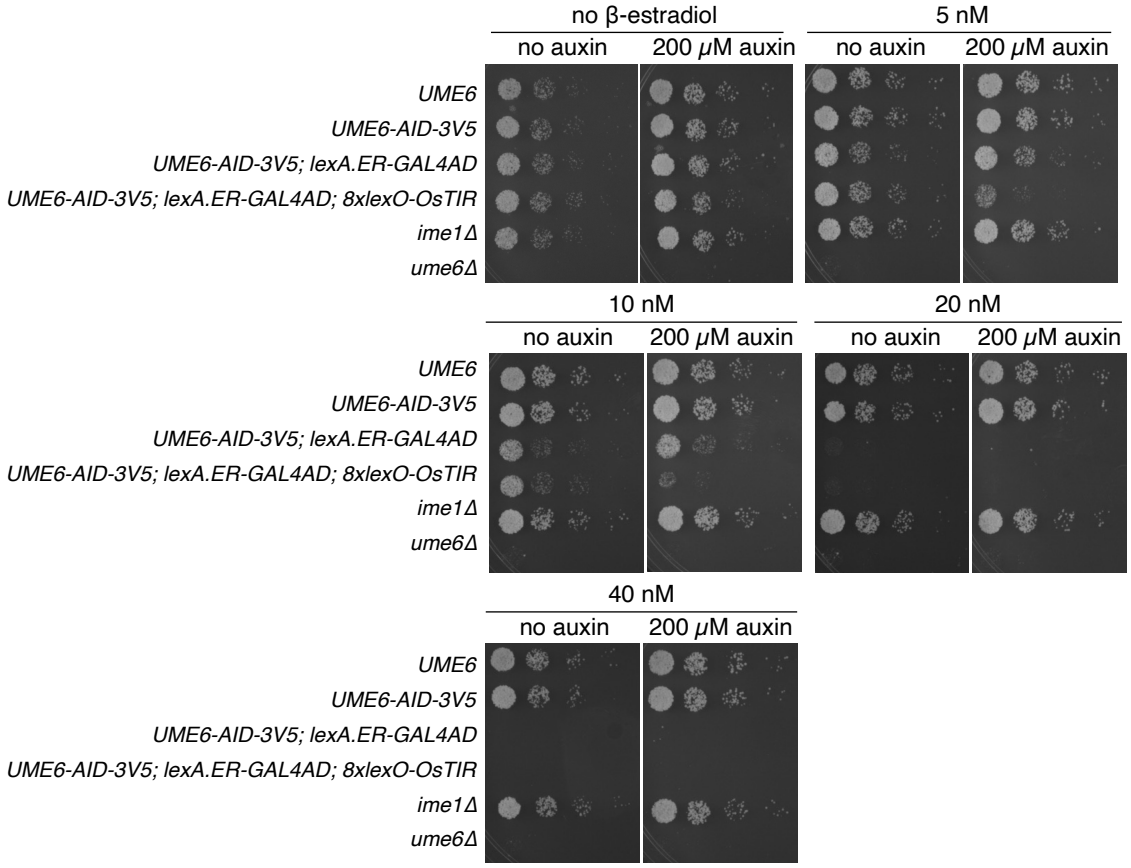

Figure 3.8: Growth phenotype associated LexA-Gal4.AD nuclear localization at differing ß-estradiol concentration. (Related to Figure 4) Increased levels of ß-estradiol in the presence of LexA-ER-Gal4.AD is toxic. Growth phenotype associated various concentrations of auxin and/or ß-estradiol. Genotype of diploid strains are *UME6* (UB19103), *UME6-AID-3V5* (UB19101), *UME6-AID-3V5; lexA-ER-GAL4.AD* (UB25688), *UME6-AID-3V5; lexA-ER-GAL4.AD; 8xlexO-OsTIR* (UB25092), *ime1*Δ (UB19105), and *ume6*Δ (UB22812). Strains were serially diluted onto plates containing nutrient-rich media with agar (YPD) and allowed to grow at 30˚C for 48 h before images were acquired.

Ume6 regulon contains at least 144 direct targets and that Ume6 is highly expressed during early meiosis, remaining bound to the EMG promoters. Thus, we predicted that depletion of Ume6 during meiosis would lead to a failure in EMG expression, disrupting gamete formation. To test the consequences of Ume6 depletion on meiosis, cells were cultured as before using the inducible *IME1/4* system and were allowed to acclimate to SPO for 30 min. Ume6 depletion took place over the next 1.5 h at which point *IME1/4 was* induced. Samples for protein and RNA were collected prior to and following Ume6 depletion and *IME1/4* induction. Consistent with our previous observations, in control cells, Ume6 protein levels increased by 58% as early as 30 min following *IME1/4* induction and doubled by 4.5 h (Figure 3.7A and 3.7B). In contrast, cells that were depleted for

Ume6 experienced a noticeable drop in Ume6 protein levels, down to 30.6% of starting levels at 6 h (Figure 3.7A and 3.7B; Figure 3.8, please refer to materials and methods for a detailed description of the differences between mitotic and meiotic depletion strains and conditions).

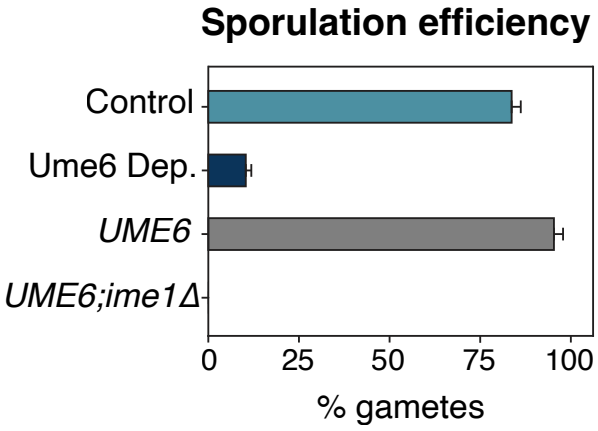

Figure 3.9: Monitoring spore formation defect associated with removal of Ume6 prior to *pCUP1-IME1 pCUP1-IME4* induction. Ume6 depletion shortly before meiotic entry disrupts gamete formation and EMG expression. Sporulation efficiency data for control (UB25688) and Ume6 depletion strains (UB25092) along with two additional controls, a *pCUP1-IME1*; *pCUP1-IME4*; *UME6* (*UME6*) strain (UB19103) and *ime1*Δ (UB19105) strain. Cells were allowed to complete meiosis for 24 h before calculating sporulation efficiency. For this, 100 cells were counted and percentage of cells that formed tetrads were noted as % gametes. Data from average of three biological replicates is presented for control, Ume6 depletion, *UME6*, and *ime1*Δ (black). Error bars indicate standard error.

To determine the impact of Ume6 depletion on meiosis, we next analyzed the cells' ability to produce gametes, known as spores in yeast. For comparison, a strain containing only the inducible *IME1/4* system (*pCUP1-IME1; pCUP1-IME4; UME6)* as well as an *IME1* null mutant (*ime1*Δ) where meiosis cannot occur was included (Figure 3.9). *ume6*Δ cells were too sick to process for the meiotic experiments. Sporulation efficiency was 95.3% for the *pCUP1-IME1/4* strain and 0% for the *ime1*Δ mutant (Figure 3.9). In the control strain where Ume6 was not depleted, sporulation efficiency was 84%, indicating that our system experiences only minor deficiencies (Figure 3.9). In contrast, the Ume6 depletion strain displayed a severe reduction in sporulation efficiency (10%; Figure 3.9), indicating that acute removal of Ume6 inhibits cells' ability to complete the meiotic program.

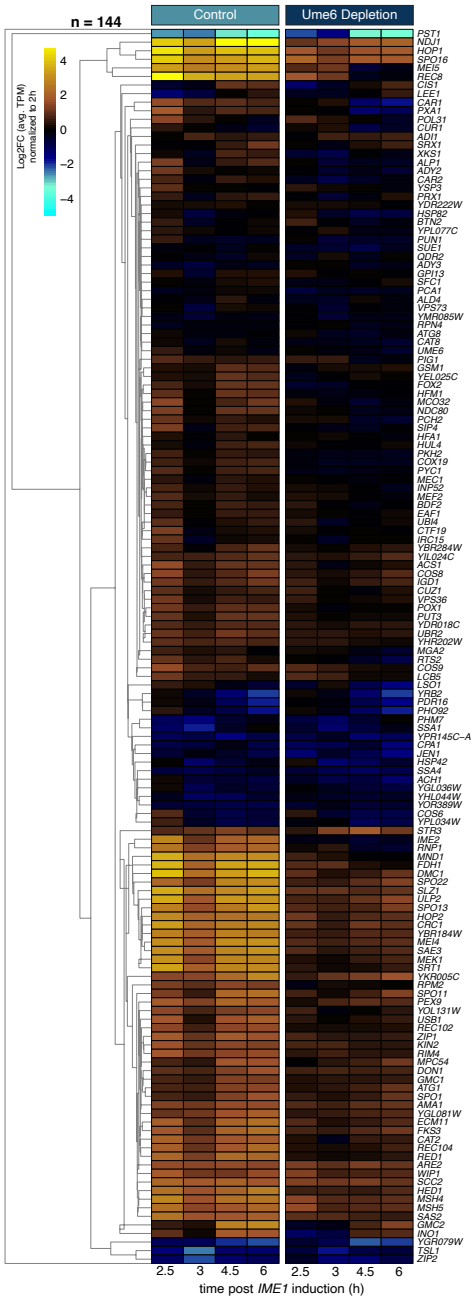

Figure 3.10: Heatmap of transcript levels for Ume6 targets in response to Ume6 depletion at meiotic entry. The gene set derived from mitotic depletion of Ume6 was observed by heatmap for the indicated meiotic samples. The log2 of mean TPMs across three biological replicates are shown for the 144 DEGs and normalized to t = 2 h just before *IME1*/4 induction. Expression ranges from decreased expression to increased expression or no expression change. DEGs were clustered by Euclidian distance (centroid) and partitioned vertically by strain background.

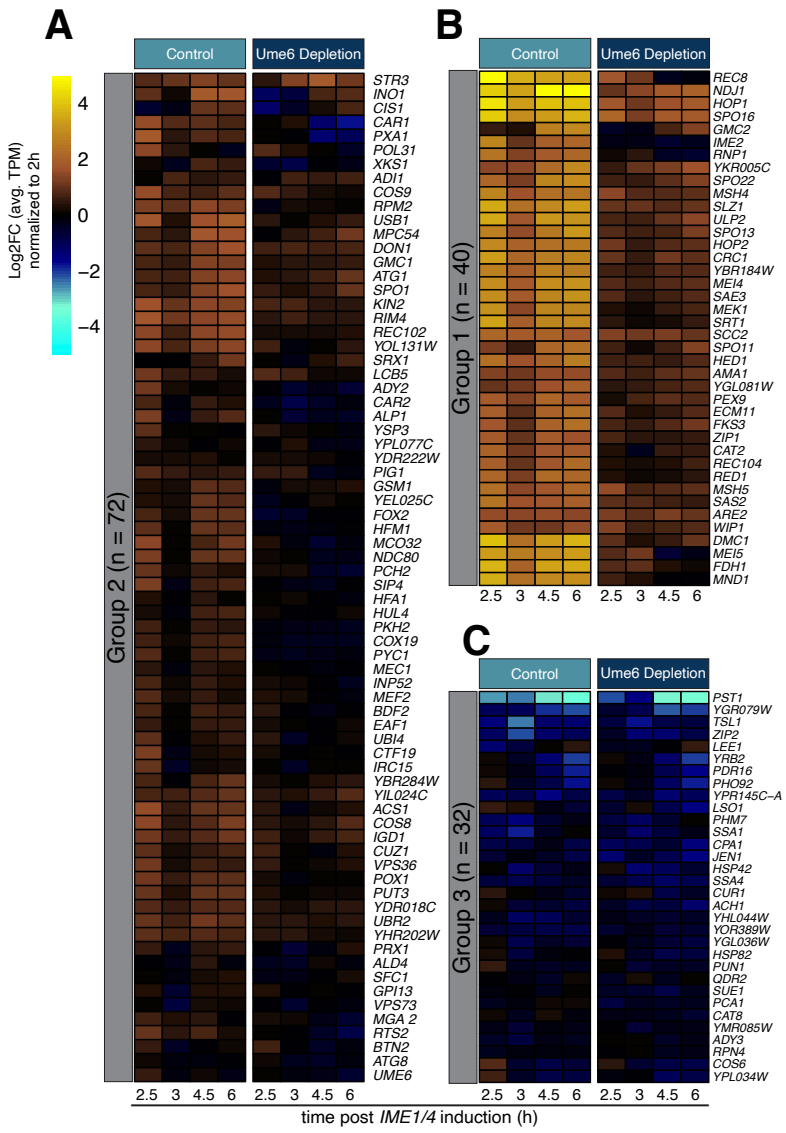

Figure 3.11: K-means clustered heatmap for Ume6 targets in response to Ume6 depletion. Ume6 depletion shortly before meiotic entry disrupts gamete formation and EMG expression. The log2FC of average TPM for three biological replicates is shown for the 144 Ume6 targets identified from mitotic cells. To evaluate EMG response to Ume6 degradation following *IME1/4* induction, TPM were normalized to the 2 h time point just before *IME1/4* induction. Those Ume6 targets with no change in expression after *IME1/4* induction are colored black. Targets whose expression decreases are colored blue/cyan. Targets whose expression increases are colored sienna/yellow. A heatmap of the 144 Ume6 targets shown in Figure 3.10 was split using k-means clustering based on their Euclidean distance and application of the "elbow test" to identify an optimal k of 3 (k-means = 3). This produced three distinct groupings of genes based on their response to *IME1/4* induction: group 1 (B), group 2 (A), and group 3 (C).

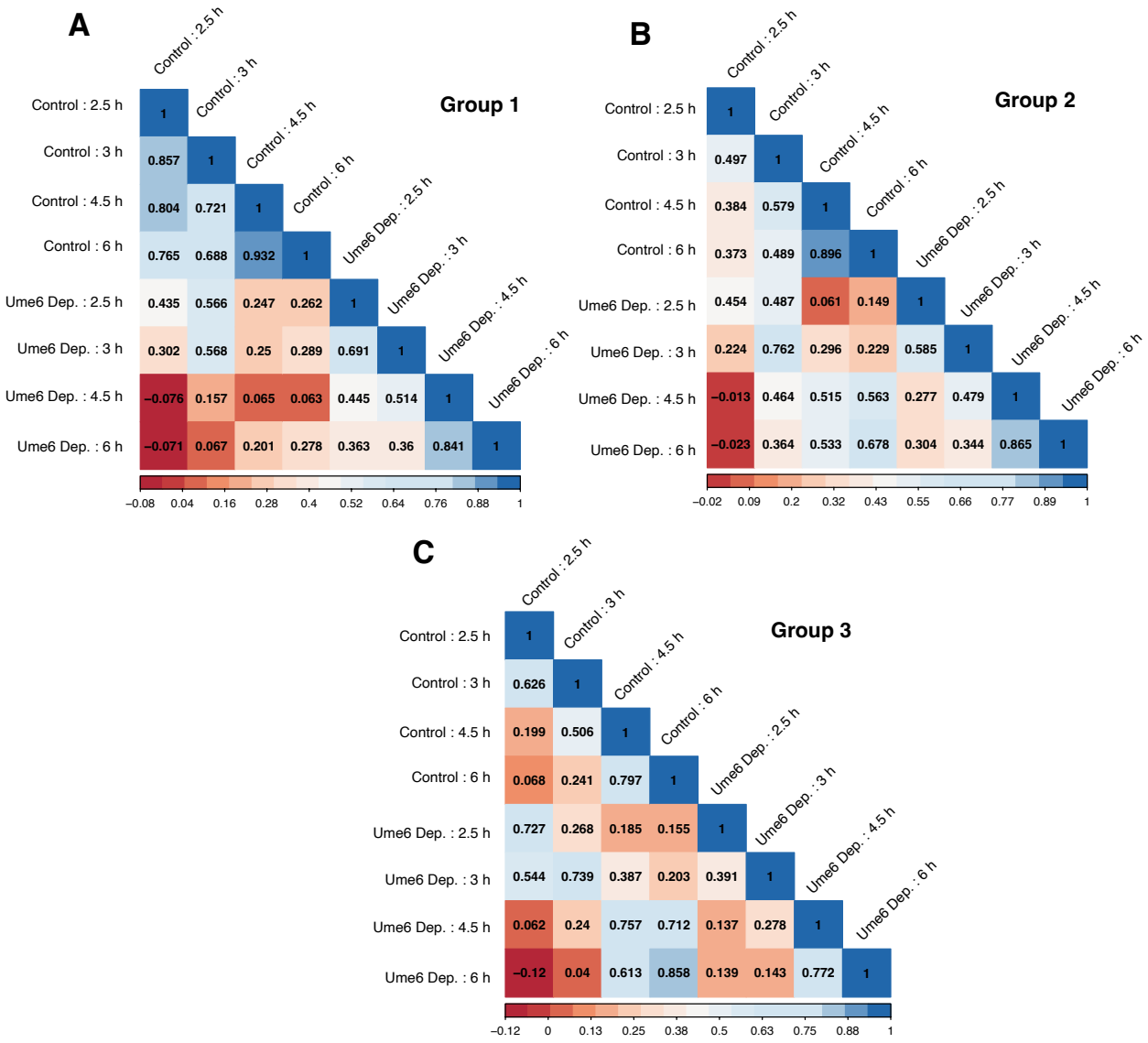

Figure 3.12: Spearman analysis of differential impacts on subsets of the Ume6 regulon. Heatmap for Spearman correlation between samples was generated using the corrplot package in R for group 1 (Figure 3.12A), group 2 (Figure 3.12B), and group 3 (Figure 3.12C). Red boxes signify poor sample relatedness while blue boxes signify high sample relatedness.

To monitor how Ume6 depletion impacts the transcript levels of EMGs, we performed RNA-seq and analyzed our previously generated list of 144 mitotically repressed Ume6 targets to assess whether Ume6 was necessary for their meiotic expression. We monitored the Log2FC of average transcripts per million (TPM), which represent reads normalized to gene length, relative to the 2 h time point just before *IME1/4* induction and found that the majority (112/144; 78%) of the mitotically repressed Ume6

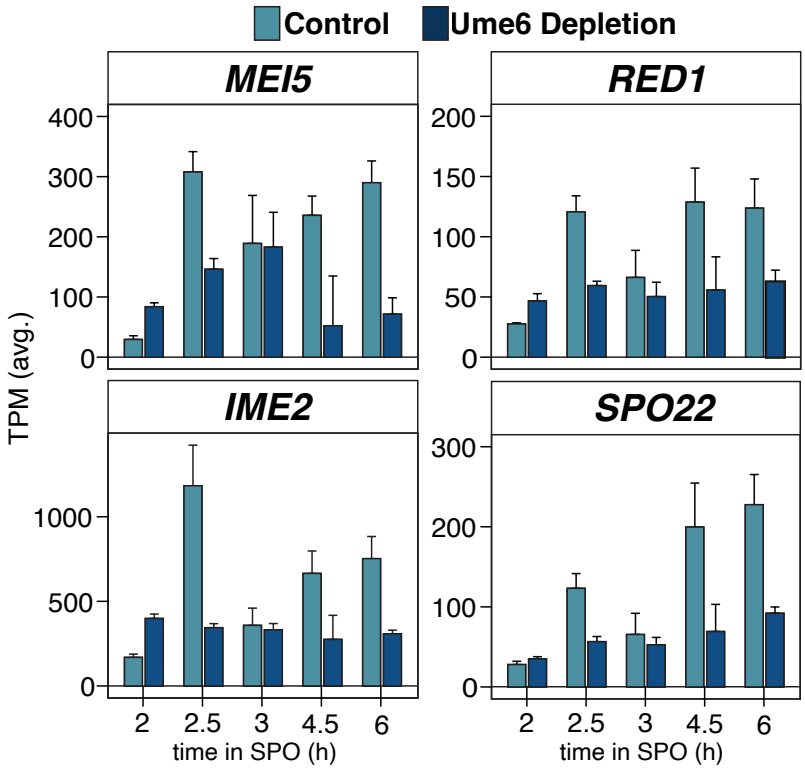

Figure 3.13: Inspecting transcript levels for the key meiotic genes *MEI5*, *RED1*, *IME2*, and *SPO22*. Ume6 depletion shortly before meiotic entry disrupts gamete formation and EMG expression. Four genes from group 1 were selected for closer inspection. This included *MEI5*, *IME2*, *RED1*, and *SPO22*, which are presented as a bar plot showing mean of TPM including the standard error for three biological replicates. This bar plot compares control and Ume6 depletion conditions at the designated times.

targets now showed reduced expression upon Ume6 depletion relative to the control sample (Figure 3.10; Figure 3.11A-C; Figure 3.12A-C).

To better highlight the genes that are most impacted by Ume6 depletion, we applied k-means clustering, which groups genes by their Euclidian distance while minimizing variation. Using the "elbow method," we found k = 3 to be optimal for subdividing our 144 genes in the Ume6 regulon (Thorndike 1953; Fritz et al. 2020). Group 1 contained 40 genes that were important for meiotic recombination and chromosome pairing, while group 2 had a combination of 72 meiotic and metabolic genes. Inspecting these subgroups, we found that genes in group 1 and 2 showed an average of ~43% and ~20% decrease in expression, respectively, in response to Ume6 depletion (Figure 3.11A and 3.11B, comparing TPM for Ume6 depletion and control at 2.5 h). Indeed, Spearman analysis at 2.5 h for group 1 and 2 showed high dissimilarity between control

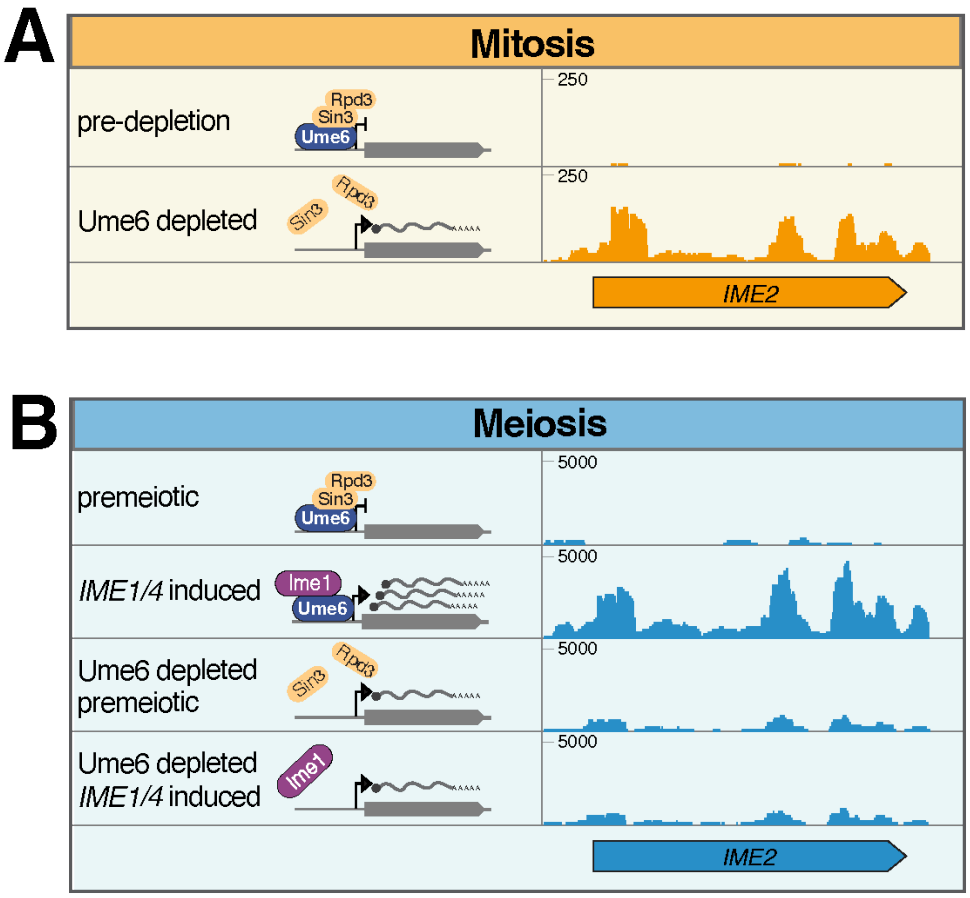

Figure 3.14: Impacts of Ume6 disruption on *IME2* during mitotic and meiotic programs using genome browser tracks. Ume6 depletion shortly before meiotic entry disrupts gamete formation and EMG expression. Genome browser views of mRNA tracks highlighting consequential differences between depleting Ume6 during mitotic growth compared to meiosis for the EMG *IME2*. (A) During mitotic growth, prior to Ume6 depletion (pre-depletion) *IME2* signal is mostly undetectable (top). Then, in response to Ume6 depletion (Ume6 depleted) *IME2* signal appears indicating a loss of repression. (B) Conversely, in the presence of Ume6 without Ime1 (premeiotic), signal for *IME2* is mostly undetectable, similar to mitotic conditions, and after *IME1/4* induction (*IME1/4* induced) *IME2* becomes strongly expressed as indicated by the mapped reads. However, in the absence of Ume6, before or after *IME1/4* induction (Ume6 depleted + premeiotic and Ume6 depleted + *IME1/4* induced, respectively), *IME2* signal remains slightly stronger than premeiotic but much weaker than *IME1/4* induced. Scales for the genome browser under each condition, mitosis and meiosis, are indicated and an illustration for Ume6's presence and interaction with its cofactors is provided. Scales on the y-axis show relative track heights between mitosis and meiosis.

and Ume6 depletion (ρ = 0.435 and 0.454, respectively; Figure 3.12A and 3.12B). This reduced expression and dissimilarity between conditions persisted until 6 h. Conversely, group 3 contained several different genes involved in meiosis, metabolism, and cell wall maintenance. Expression profiles for group 3 were overall more similar between control

and Ume6 depletion (~3% increase in expression of the Ume6 depletion sample compared to control at 2.5 h). Consistently, Spearman analysis showed increased sample relatedness from 2.5 h until 6 h (ρ = 0.74, 0.71, 0.86, and 0.88, at 2.5, 3, 4.5, and 6 h respectively; Figure 3.11C and Figure 3.12C). Thus, depletion of Ume6 prior to *IME1/4* induction disrupted 112 of our 144 Ume6 targets (78%), highlighting Ume6's importance in EMG activation during meiosis.

Focusing on four representative EMGs from group 1, *IME2*, *MEI5*, *SPO22*, and *RED1*, we found that differences in transcript levels were already detectable early on, since strains retaining a functional Ume6 (control) had lower basal expression levels, consistent with Ume6 acting repressively prior to *IME1* expression (Figure 3.11B and 3.13). Furthermore, in the control strain, gene expression spiked going from pre-*IME1/4* induction at 2 h to post-*IME1/4* induction at 2.5 h reaching 7-, 11-, 5-, and 4-fold, for *IME2*, *MEI5*, *SPO22*, and *RED1*, respectively (Figure3.13). However, depletion of Ume6 resulted in largely unchanged expression for *IME2*, *MEI5*, *SPO22*, and *RED1* (Figure 3.13, Ume6 Depletion). Taken together, the failure to form gametes combined with reduced transcript levels of meiotic genes in response to Ume6 depletion emphasizes the critical involvement of Ume6 in the expression of EMG*s.*

These findings demonstrate Ume6's dual role both as a repressor and an activator. By acutely depleting Ume6 under distinct developmental programs, we arrived at two very different outcomes. Mitotic depletion of Ume6 resulted in the derepression of its target genes, illustrating Ume6's role in ensuring EMG quiescence during the mitotic gene expression program (Figure 3.14A). Consistently, depletion of Ume6 under nutrient-deprived conditions (i.e., in the absence of *IME1*) also led to derepression of EMGs (Figure 3.14B; premeiotic). However, this level of EMG derepression was not sufficient to initiate meiosis. On the other hand, depletion of Ume6 shortly before *IME1/4* induction prevented the proper activation of EMGs, thereby exemplifying Ume6's second role as an activator of EMGs during the meiotic program (Figure 3.14B). Thus, Ume6 serves as a primary determinant as to whether cells silence or induce the meiotic gene expression program depending on the cellular state and the associated cofactors.

Tethering of Ume6^{T99N} to Ime1 using the GFP nanobody trap system rescues meiotic defects associated with *UME6^{T99N}*.

Previous studies have demonstrated that the meiotic kinase Rim11 phosphorylates both Ime1 and Ume6 to promote their interaction (Mitchell and Bowdish 1992; Rubin-Bejerano et al. 1996; Malathi et al. 1997). One key phosphorylation residue in Ume6 is Threonine 99 (T99). Indeed, a particular mutation at this position, T99N (Ume6^{T99N}), was found to

severely reduce Rim11's ability to phosphorylate Ume6 (Bowdish et al. 1995; Malathi et al. 1997), thereby preventing binding of Ume6 to Ime1. To restore the interaction between Ime1 and Ume6^{T99N}, we utilized a GFP nanobody trap approach where Ume6^{T99N} carrying

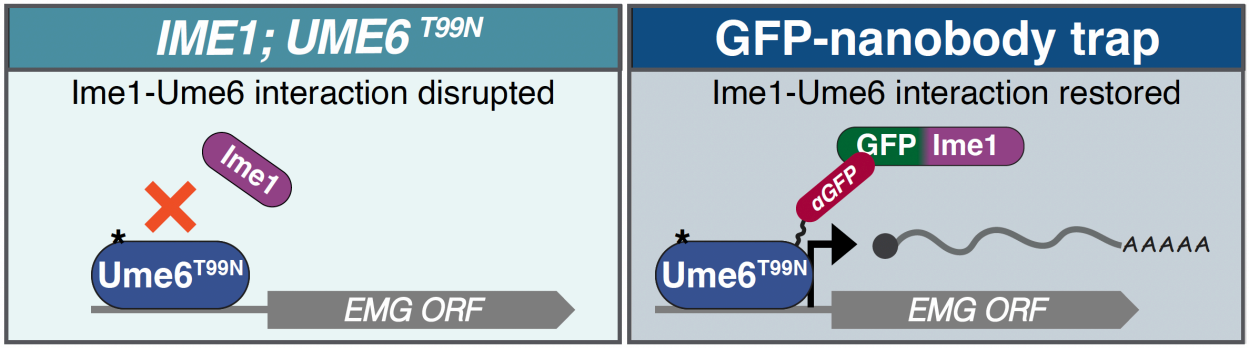

Figure 3.15: Schematic of GFP Nanobody tethering strategy. Tethering of Ime1 and Ume6 using the GFP nanobody rescues the *UME6^{T99N}* meiotic defects. Illustration of the GFP-nanobody trap approach. The star on Ume6^{T99N} represents the T99N mutation within Ume6 that obstructs Ime1 from binding within this domain.

a *3V5* epitope was fused to the VH16 anti-GFP nanobody (*UME6^{T99N}-3V5-αGFP*; Figure 3.15; Fridy et al. 2014). For controls, we included *UME6*, *UME6-3V5*, and *UME6^{T99N}-3V5*. We then combined the *UME6* alleles with either *IME1* or an N-terminally GFP-tagged *IME1* at the endogenous locus (*GFP-IME1*; Moretto et al. 2018). If the interaction between Ime1 and Ume6 is sufficient to drive EMG expression, then in the *UME6^{T99N}-3V5-αGFP GFP-IME1* strain, where tethering occurs, sporulation should be rescued.

We first examined sporulation efficiency in the strains possessing different allelic combinations of *IME1* and *UME6*. For untagged *UME6*, the sporulation efficiency was >90% when combined with either untagged or GFP-tagged *IME1* (94.3% and 97.0%, respectively; Figure 3.16). *UME6-3V5* had a small drop in sporulation efficiency (92.7% and 89% for *IME1* and *GFP-IME1*, respectively; Figure 3.17), suggesting the tag mildly impairs *UME6* function. However, strains with *UME6^{T99N}-3V5* had a severe defect in sporulation efficiency (27% and 18.7% for *IME1* and *GFP-IME1*, respectively). Addition of the GFP Nanobody to *UME6^{T99N}-3V5* (*UME6^{T99N}-3V5-αGFP*) in cells containing untagged *IME1* further reduced the cell's sporulation efficiency to 9.0%. Despite this substantial drop in sporulation efficiency, when *UME6^{T99N}-3V5-αGFP* was paired with *GFP-IME1*, the sporulation efficiency was dramatically improved to 93.7% (Figures 3.17). Thus, restoring the interaction between Ume6 and Ime1 is sufficient to complete the meiotic program and produce gametes.

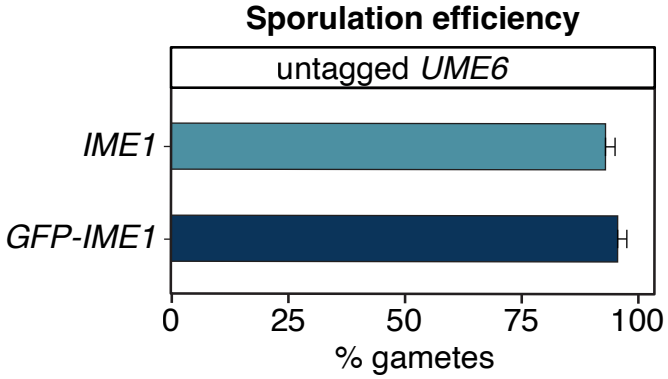

Figure 3.16: Sporulation results for *GFP* tagging of *IME1*. As in Figure 3.17, sporulation results are reported for the control strain containing untagged *UME6* with either *IME1* (light blue; UB26621) or *GFP-IME1* (dark blue; UB26637). Briefly, Cells were grown in presporulation media, then transferred to SPO, and allowed 24 h to complete the meiotic program before 100 cells were counted. The average of three biological replicates is presented with the standard error.

To investigate the extent to which the nanobody-based tethering of Ume6^{T99N} to Ime1 rescues the meiotic program, we collected RNA samples for various allelic combinations of *UME6* and *IME1* relative to their introduction to SPO media at 0, 2, 4, and 6 h, to monitor EMG transcript abundance. First, we inspected 263 genes that are associated with driving early meiotic events based on previous studies (Mao-Draayer et al. 1996; Pâques and Haber 1999; Williams et al. 2002; Brar et al. 2012; Tresenrider et al. 2021). 89 of these genes were present in the Ume6 direct target list (Table 1.1). In *UME6-3V5* carrying either untagged or GFP-tagged *IME1*, many of these genes were upregulated after transfer to SPO (Figure 3.18A and 3.18B, compare 0 vs 2, 4, 6 h). Introduction of *UME6^{T99N}-3V5* resulted in a moderate disruption of EMG expression (Figure 3.19). Consistent with the sporulation data, *UME6^{T99N}-3V5-αGFP* had a more severe defect in EMG expression than *UME6^{T99N}-3V5* (Figure 3.19). However, tethering of Ume6^{T99N} to Ime1 restored EMG expression back to wild type (Figure 3.19). This rescue was further supported by PCA, where points associated with *GFP-IME1; UME6-3V5 or GFP-IME1; UME6^{T99N}-αGFP* separated from untagged *IME1; UME6^{T99N}-αGFP* along PC1 (Figure 3.20).

To globally identify the functional classes of genes expressed by tethering of Ime1 to Ume6, we performed DESeq2. Comparing *IME1* to *GFP-IME1* in the *UME6^{T99N}-3V5-αGFP* background, we identified 316 DEGs (padj < 0.05; log2FC > 1.5; 2h in SPO; Figure 3.21). Of these 316 DEGs, 137 were present in the EMG list and 70 were present in the Ume6 direct target list. GO enrichment revealed a number of early meiotic terms such as

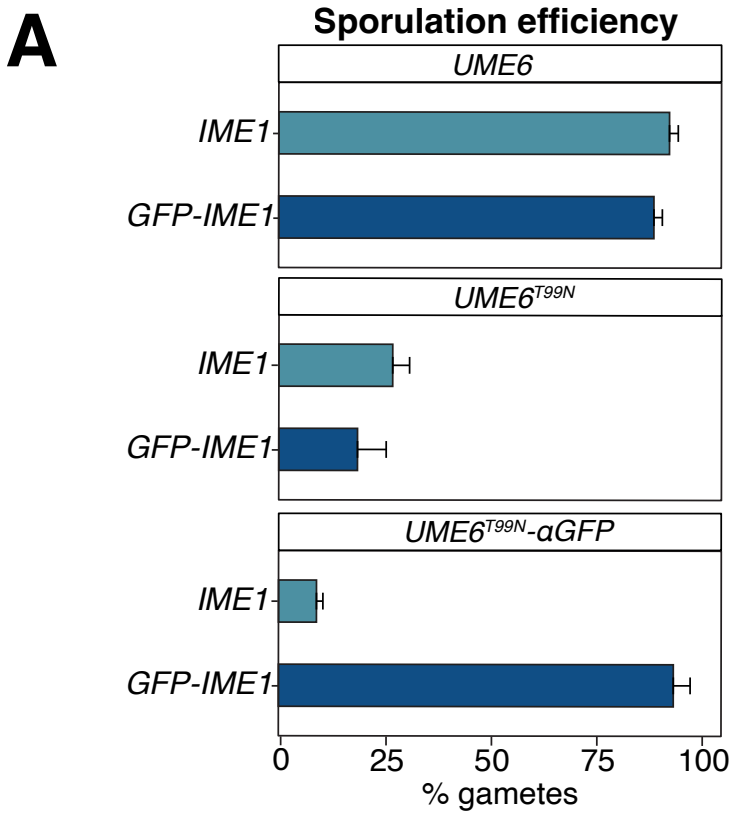

Figure 3.17: Resulting sporulation from both tagged Ume6 and Ume6^{T99N} and how this compares to tethering of Ime1 to Ume6^{T99N}. Sporulation efficiency measured for strains containing either wild-type *IME1* and *UME6-3V5* (UB26625), *UME6^{T99N}-3V5* (UB26629), and *UME6^{T99N}-3V5-αGFP(VH16)* (UB27313), or *GFP-IME1* and *UME6-3V5* (UB26641), *UME6^{T99N}-3V5* (UB26645), and *UME6^{T99N}-3V5-αGFP(VH16)* (UB27243). *3V5* is not annotated in the figure labels for simplicity. Cells were grown in presporulation media before being transferred to SPO and allowed 24 h to complete the meiotic program before sporulation efficiency was measured. As before, 100 cells were counted and percentage of cells that formed tetrads were noted as % gametes for each allele combination and the average of three biological replicates is presented with the standard error.

homologous recombination and SC formation, indicating that the tethering strategy restored early meiotic functions (Figure 3.22). Additionally, inspecting tethering results for our mitotic Ume6 target list showed a similar rescue in expression (Figure 3.23 and 3.24). Finally, key EMGs including *IME2*, *ZIP1* and *SPO13* displayed a strong rescue in their expression when Ume6^{T99N} was tethered to Ime1 (Figure 3.18B). We note that at 0 h, use of the GFP nanobody trap resulted in unusually high expression for many EMGs (Figure 3.18A and 3.18B). This is likely due to the high affinity between GFP and the αGFP

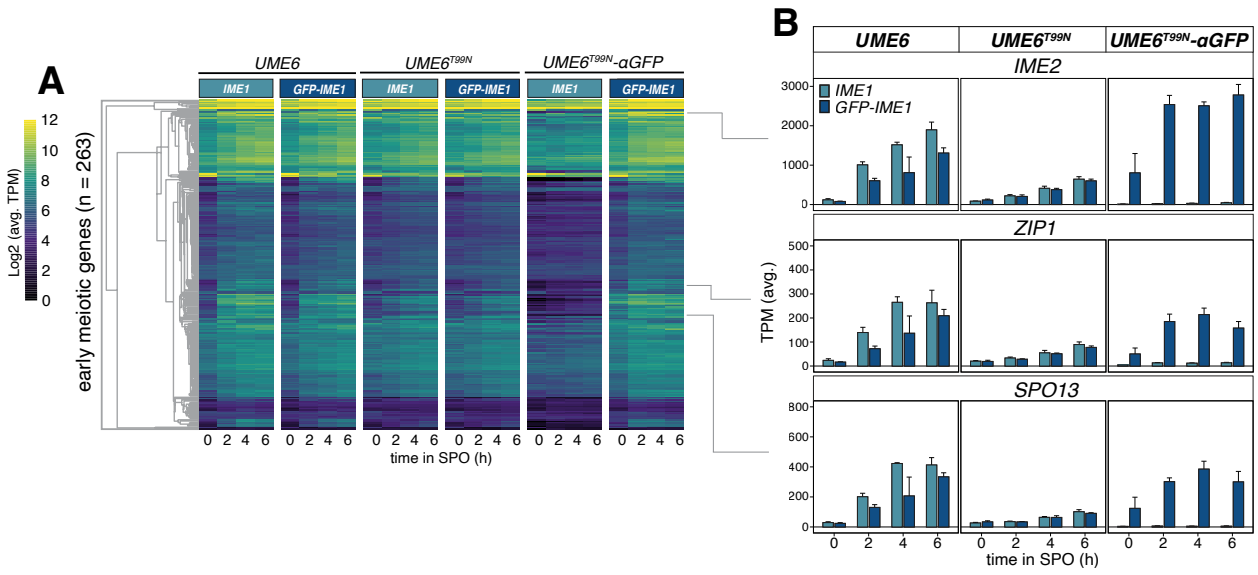

Figure 3.18: Expression of the early meiotic regulon visualized by heatmap with accompanying subset of genes. Tethering of Ime1 and Ume6 using the GFP nanobody rescues the *UME6^{T99N}* meiotic defects. Strains used in Figure 3.17 were transferred to SPO (t = 0 h) and RNA samples were collected at the designated times. RNA samples were processed as described in Figure 3.10 and TPM tables were generated from three biological replicates. To examine early gene response, a set of genes identified as early expressed by Williams et al. and Brar et al. and identified as *IME1* responsive by Tresenrider et al. were termed Early Meiotic Genes and monitored in our dataset. (A) Heatmap representing Log2 of the mean TPM across three biological replicates for Early Meiotic Genes. Strains harboring distinct *UME6* alleles in combination with either untagged *IME1* (light blue) or *GFP-IME1* (dark blue) are presented on top of the heatmap. (B) Barplot representation for mean of TPM at a designated time point is shown for *IME2*, *ZIP1*, and SPO13. Standard error from three biological replicates is included. *UME6* alleles for each representative gene plot are shown at the top of their respective barplot. The gene represented by the barplot is shown at the top of each group and *IME1* allele is shown as either untagged (*IME1*) or GFP tagged (*GFP-IME1*).

antibody, which can bypass post-translational regulations that control Ime1-Ume6 interaction and nuclear localization, thereby resulting in earlier meiotic initiation. Regardless, these data further corroborate the significance of Ime1-Ume6 interaction in establishing the meiotic program.

We also checked the magnitude and timing of *NDT80* expression along with its targets (Figure 3.25). In the *UME6-3V5* control strain, *NDT80* expression remained low from 0 to 4 h at which point *NDT80* expression increased ~6.5 fold (Figure 3.25B; from t = 4h to 6h). Conversely, *NDT80* transcripts were largely unchanged in strains with

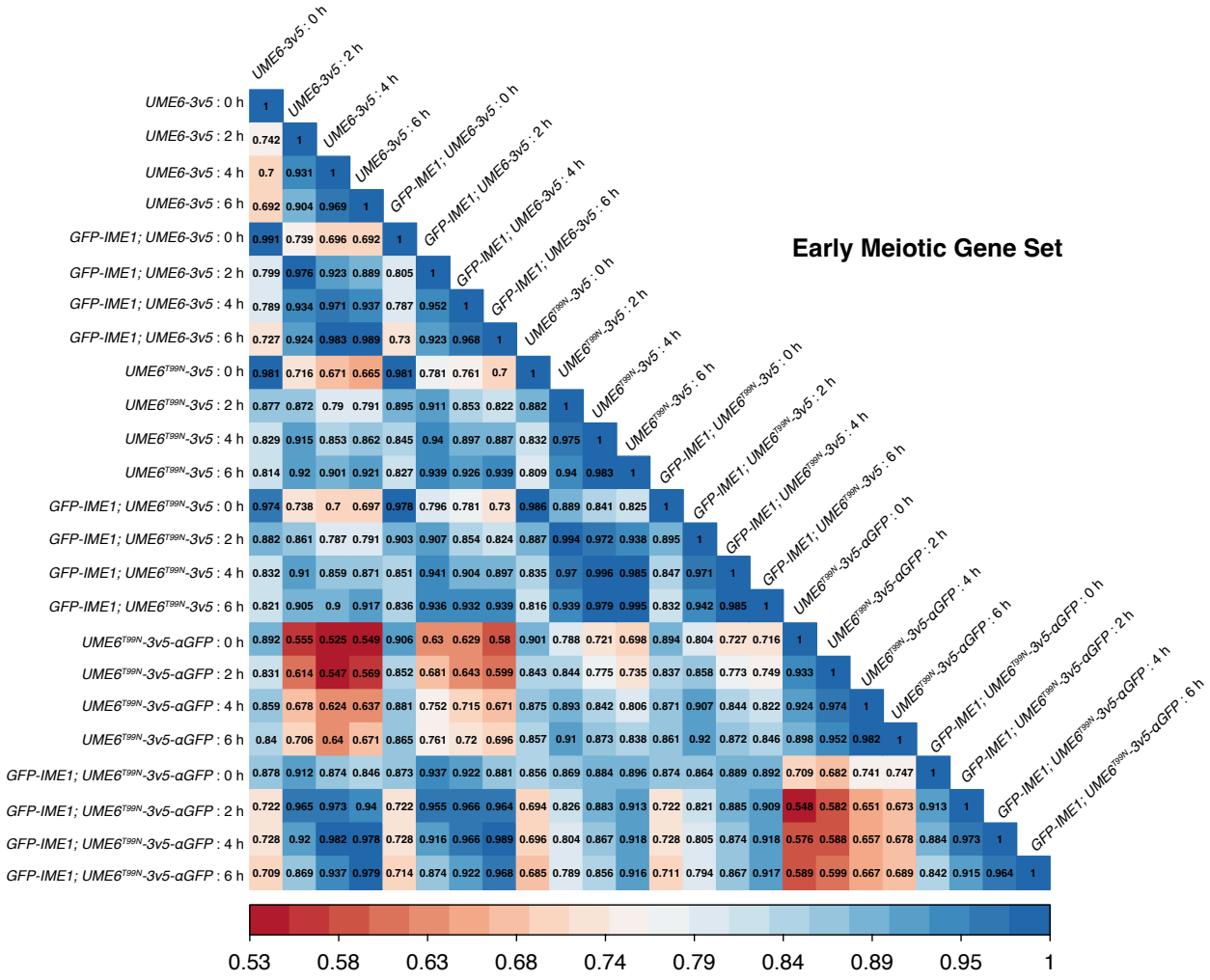

Figure 3.19: Spearman analysis for sample relatedness between different *UME6* and *IME1* alleles. For B and D, Corrplot package was used in R to generate heatmaps for Spearman correlation between samples. Red boxes show samples with poor correlation and blue shows samples with high correlation. Heatmap showing sample relatedness for the early meiotic gene set derived from Brar et al. 2012, Cheng et al. 2018, and Tresenrider et al. 2021.

UME6^{T99N}-3V5 or *UME6^{T99N}-3V5-αGFP.* However, tethering of Ume6^{T99N} to Ime1 led to upregulation of *NDT80* (Figure 3.25B ~11.3-fold increase from t = 4 to 6 h in the *UME6^{T99N}-3V5-αGFP; GFP-IME1* strain). Expression of *NDT80* is indicative of chromosome segregation and gamete maturation and several genes have been identified as upregulated during these events (Winter 2012; Cheng et al. 2018). Many of the Ndt80 target genes responded to formation of the Ime1-Ume6 complex, or lack thereof (Figure 3.25A and 3.25B). Indeed, cells possessing *UME6^{T99N}-3V5* or *UME6^{T99N}-3V5-αGFP* failed to activate these genes or did so at a reduced level (Figure 3.25A and Figure 3.26).

In contrast, tethering of Ume6^{T99N} to Ime1 resulted in the timely activation of Ndt80 targets (Figure 3.25A and 3.25B). Altogether, these findings further emphasize the importance of Ime1-Ume6 interaction while also demonstrating that bringing Ime1 in proximity of Ume6 is sufficient to drive meiotic initiation and gamete production.

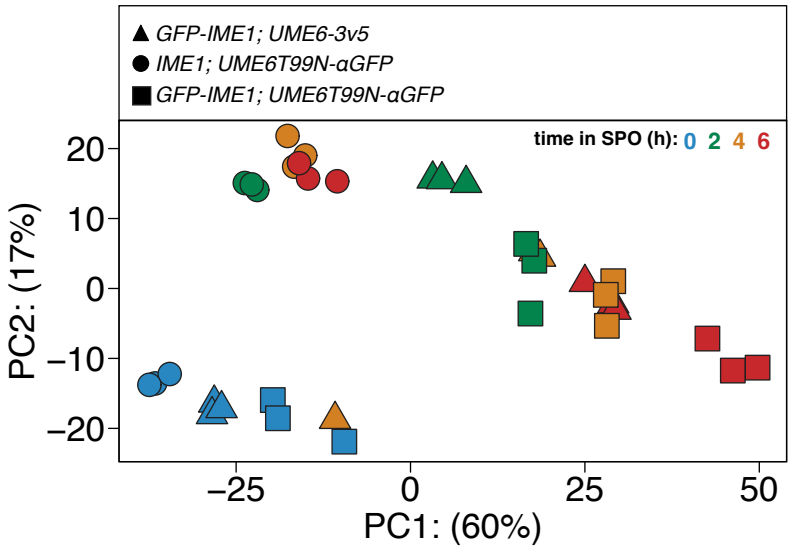

Figure 3.20: Assessment of sample relatedness using PCA. Results of PCA visualized using the ggplot2 package and observing PC1 (x-axis) and PC2 (y-axis). Sample-to-sample variation by PCA was monitored for *GFP-IME1; UME6-3V5* (UB26641), *IME1; UME6^{T99N}-3V5*-αGFP (UB27313), and *GFP-IME1; UME6^{T99N}-3V5*-αGFP (UB27243) and strains were distinguished by shapes. Time points were assigned a unique color. Note that due to poor read depth, one replicate for *GFP-IME1; UME6-3V5* is isolated from the rest (4 h).

Tethering of a heterologous activation domain to Ume6^{T99N} restores EMG expression, gamete formation, and viability.

Since its initial discovery, Ime1 has been regarded as the master transcription factor in the activation of EMGs (Kassir et al. 1988). Strains lacking *IME1* (*ime1*Δ) fail to initiate meiosis and genetic screens have identified several mutations in *IME1* that disrupt meiotic initiation (Smith et al. 1993). Furthermore, mutations like *UME6^{T99N}* or depletion of Ume6, which block Ime1's ability to dock with Ume6 and localize to EMG promoters, also result in meiotic failure (this study; Mitchell and Bowdish 1992). Thus, Ime1 is an essential factor in launching the meiotic transcriptional program.

On the other hand, the modularity of transcription factors has long been appreciated (Hahn and Young 2011). In fact, Ime1 itself can be broken into three distinct subdomains: an activation domain (AD), a nutrient-responsive domain, and a Ume6 interaction domain (Smith et al. 1993). Here, we found that tethering of Ime1 to Ume6^{T99N} is sufficient to

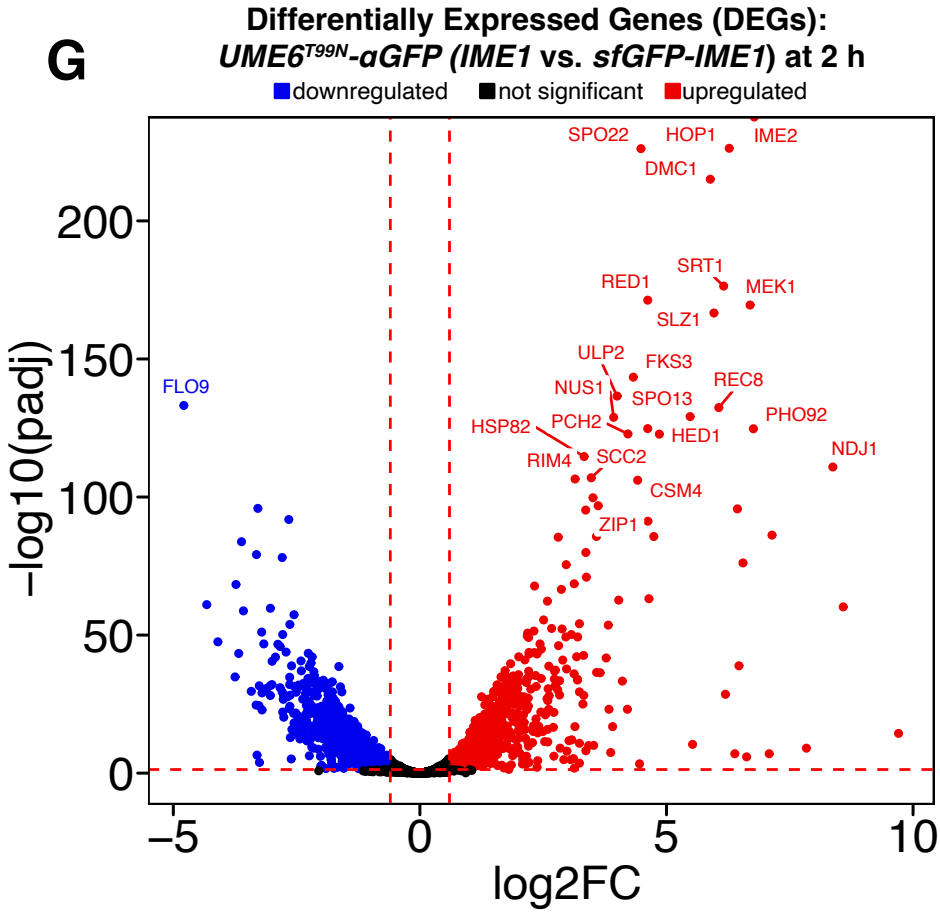

Figure 3.21: Differential expression using DESeq2 comparing tethered and untethered *IME1* 2h post-SPO induction. (G) Volcano plot representing DESeq2 analysis between *IME1; UME6*^{T99N}*-3V5*-αGFP (UB27313), and *GFP-IME1; UME6*^{T99N}*-3V5*-αGFP (UB27243) at 2 h that showed DEGs (padj < 0.05) either up- or downregulated or showing no overall change.

initiate the meiotic program. We reasoned that this may occur because: (1) Ume6 needs to associate with an AD in order to function as a coactivator or (2) Ime1 has additional functions besides serving as a transactivator, which are restored upon recruitment to Ume6. To distinguish between these possibilities, we employed a heterologous AD from *E. coli*, known as B112 (Ottoz et al. 2014), and kept it either untagged or fused to GFP (Figure 3.27). As controls, we used Ime1 or GFP-Ime1 (Figure 3.27). Each transgene was integrated at the *HIS3* locus and was tested for its ability to suppress *ime1*Δ in the *UME6*^{T99N}*-3V5-αGFP* background. All constructs were placed under the control of the *IME1* promoter to maintain physiological regulation and transgene expression was confirmed by immunoblotting (Figure 3.28). Meiotic initiation through

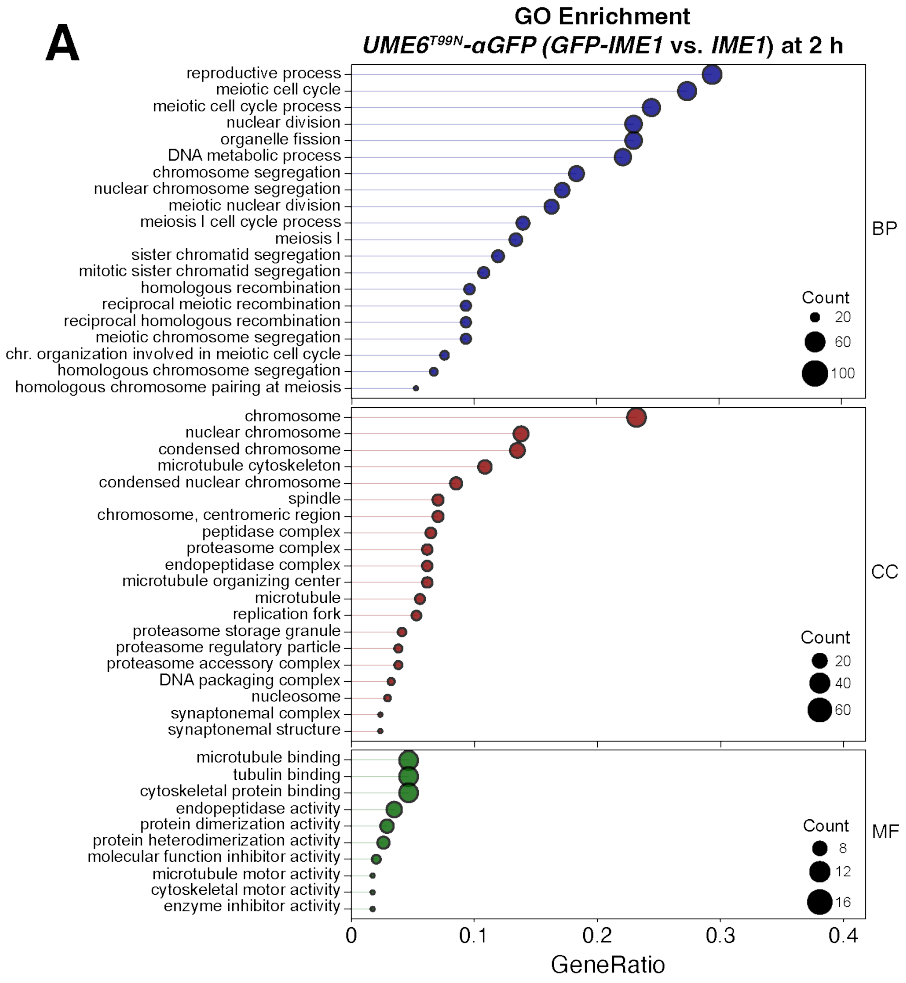

Figure 3.22: GO enrichment for genes called differentially expressed at 2h post-SPO induction. Tethering of Ime1 and Ume6 using the GFP nanobody rescues the *UME6^{T99N}* meiotic defects. DESeq2 analysis between *IME1; UME6^{T99N}-3V5*-αGFP (UB27313), and *GFP-IME1; UME6^{T99N}-3V5*-αGFP (UB27243) at 2 h identified 316 DEGs (padj < 0.05). (A) Barplot representation for mean of TPM at a designated time point is shown for *IME2*, *ZIP1*, and SPO13. Standard error from three biological replicates is included. *UME6* alleles for each representative gene plot are shown at the top of their respective barplot. The gene represented by the barplot is shown at the top of each group and *IME1* allele is shown as either light blue (*IME1*) or dark blue (*GFP-IME1*). DESeq2 analysis between *IME1; UME6^{T99N}-3V5*-αGFP (UB27313), and *GFP-IME1; UME6^{T99N}-3V5*-αGFP (UB27243) at 2 h identified 316 DEGs (padj < 0.05). GO enrichment was used on the 316 DEGs that were upregulated (log2FC > 1.5). The gene ratio is shown on the x-axis and is the percent of genes in a given GO term out of the total 316 genes total. As before, the point size corresponds to the number of genes in that GO term while color signifies category: BP, biological process; CC, cellular component; MF, molecular function.

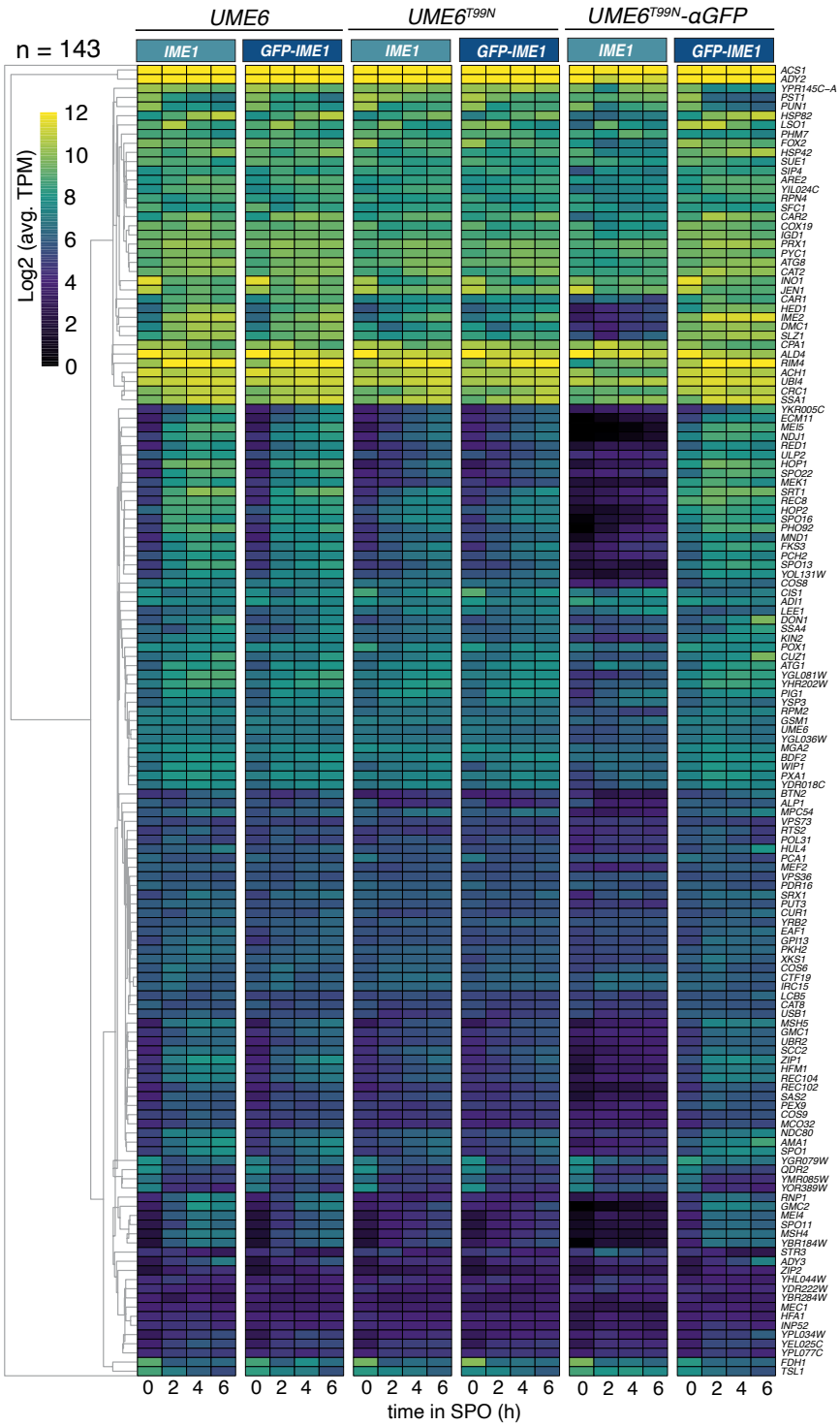

Figure 3.23: Heatmap showing expression of Ume6 targets for different *IME1* and *UME6* allelic combinations. Heatmap for the log2 of average TPM across three biological replicates of the 143 Ume6 targets.

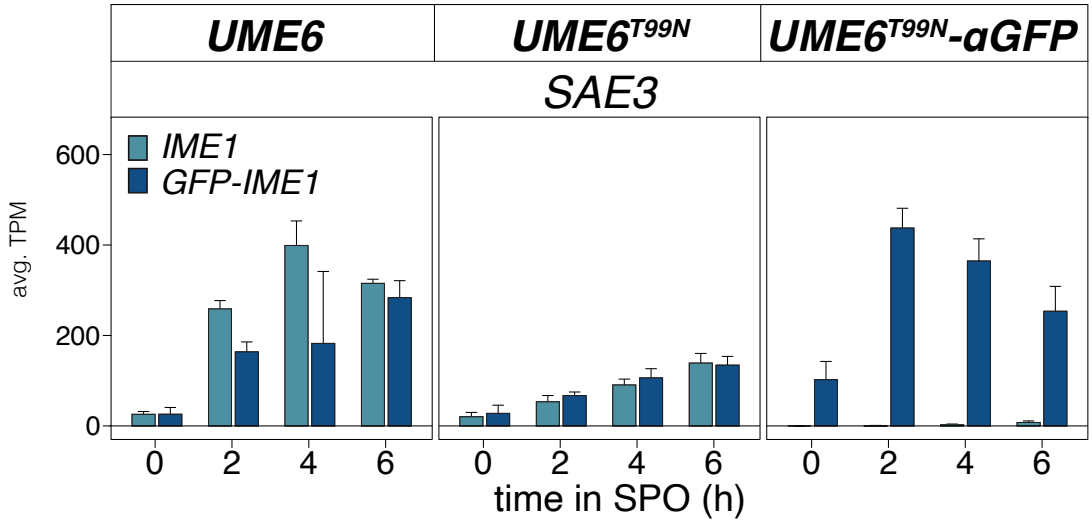

Figure 3.24: Barplot showing *SAE3* expression. We note that *SAE3* was dropped while constructing our heatmap due to low expression and instead is presented as a barplot here.

tethering of a heterologous AD to Ume6 would suggest that Ume6 is the primary determinant of EMG activation through its association with a transactivator. Conversely, failure to initiate meiosis would indicate a unique role for Ime1 in conducting the meiotic program.

To test whether B112 could rescue the defects associated with *ime1*Δ, we first measured sporulation efficiency in the *UME6^{T99N}-3V5-αGFP* background. As expected, in strains carrying an untagged *B112* or *IME1* allele, no spores were formed (Figure 3.29A). *GFP-IME1* strain mostly produced tetrads (92%) and a few dyads (4%). Interestingly, *GFP-B112* also produced several tetrads (71.7%) and some dyads (10.3%) (Figure 3.29B). We next examined gamete viability for the strains that underwent sporulation. We found that 92.6% of the gametes from *GFP-IME1* were viable (Figure 3.29CC and 3.29D). Notably, the *GFP-B112* strain also had high gamete viability of 93.2%, though colonies were marginally smaller (Figure 3.29C and 3.29D). These results demonstrate that tethering of either Ime1 or a heterologous AD to Ume6 is sufficient to induce meiosis and generate viable gametes.

Next, we performed RNA-seq to gain insights into the underlying response from the transcriptome. First, we analyzed global differences between samples using Spearman's rank correlation. We find that differences between strains carrying untagged *IME1* or *B112* transgenes were minimal (Figure 3.30A). However, comparison between untagged and GFP-fused transgenes showed a stark difference (Figure 3.30A). Interestingly, comparison of *GFP-IME1* to *GFP-B112* revealed high correlation at earlier

time points (ρ = 0.960, 0.912 at 0 and 2 h, respectively), but divergence at later time points (ρ = 0.757, and 0.848 at 4 and 6 h, respectively). We observed similar patterns using PCA (Figure 3.30B). These results indicate that the gene expression profiles of *GFP-IME1* and *GFP-B112* start similarly but diverge from one another later in meiosis.

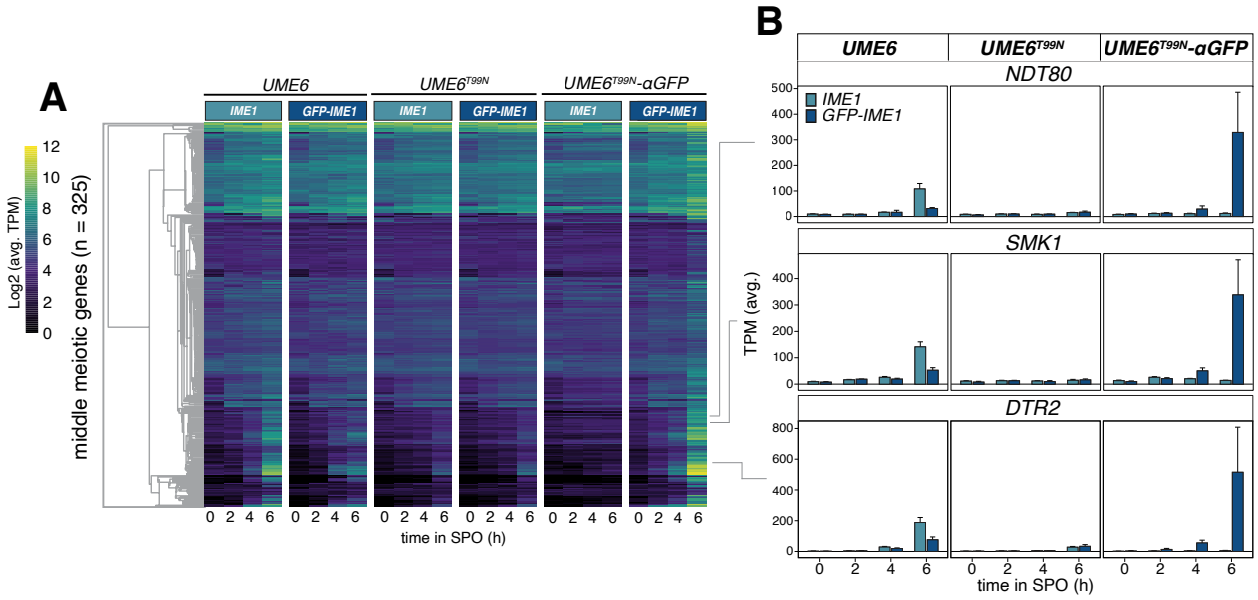

Figure 3.25: Heatmap of middle meiotic gene transcript levels. Tethering of Ime1 and Ume6 using the GFP nanobody rescues the *UME6*^{T99N} meiotic defects. (A) Heatmap prepared as described in Figure 3.18A representing a set of genes identified in Cheng et al. as responding to *NDT80* induction (Cheng et al. 2018). (B) Barplots as prepared as described in Figure 3.18B representing *NDT80*, *SMK1*, and *DTR2*.

Next, we focused on the EMGs previously shown to respond to *IME1* induction (Tresenrider et al. 2021) and visualized them on a heatmap (Figure 3.31A). *GFP-IME1* and *GFP-B112* resulted in higher EMG expression compared to their untagged counterparts. However, while EMG expression in *GFP-IME1* began to decrease at 4 and 6 h, EMGs remain elevated in *GFP-B112*. Looking more closely at *IME2*, *SPO13*, and *ZIP1*, we observed a pattern where these transcripts in *GFP-IME1* and *GFP-B112* were at their highest at 0 h (Figure 3.31B). In the *GFP-IME1* strain, *IME2*, *SPO13*, and *ZIP1* transcript levels were reduced by nearly half every two hours. Conversely, in the *GFP-B112* strain, *IME2*, *SPO13*, and *ZIP1* transcript levels increased subtly after 2 h in SPO (Figure 3.31B). Furthermore, the Ume6 mitotic targets identified in this study were expressed in both *GFP-IME1* and *GFP-B112* (Figure 3.32A and 3.32B). To identify when peak expression of EMGs occurred in *GFP-IME1* and *GFP-B112*, we applied gene set enrichment analysis (GSEA; GSEA Subramanian et al. 2005; Mootha et al. 2003). GSEA revealed that EMG enrichment was highest at 2 h for *GFP-IME1* (Normalized Enrichment

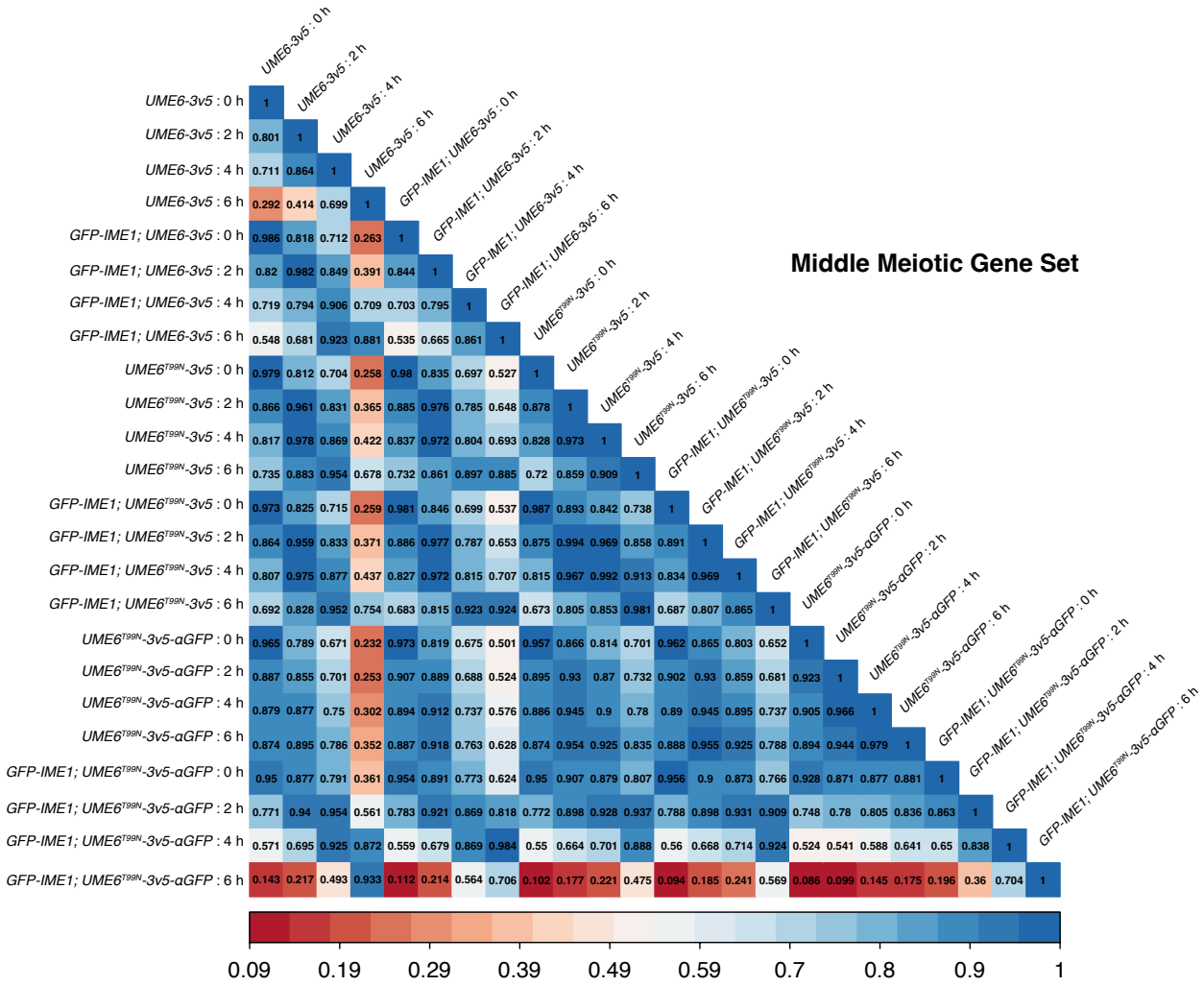

Figure 3.26: Heatmap showing sample relatedness for the middle meiotic gene set found in Cheng et al. 2018. Rescue of Ume6^{T99N} using GFP Nanobody decreases variation with wild-type strains. DESeq2 results were processed using the VST and plotPCA functions associated with DESeq2.

Score (NES) = 3.93; Figure 3.33). Conversely, in *GFP-B112*, EMGs were most enriched at 6h (NES = 4.21). Thus, when both Ime1 and B112 are recruited to Ume6 through artificial tethering, cells are able to trigger EMG expression, albeit with different dynamics.

To understand the differences between *GFP-IME1* and *GFP-B112* at t = 6 h that may cause these discrepancies in EMG expression, we performed DESeq2. DESeq2 identified 543 DEGs enriched in *GFP-IME1* compared to *GFP-B112*, several of which were middle meiotic genes (MMGs) including *NDT80* (padj < 0.05; log2FC > 1.5; Figure 3.34A). Consistent with this, GO enrichment terms were largely involved in ascospore wall development, a process controlled by *NDT80* (Figure 3.34B). Thus, the prolonged

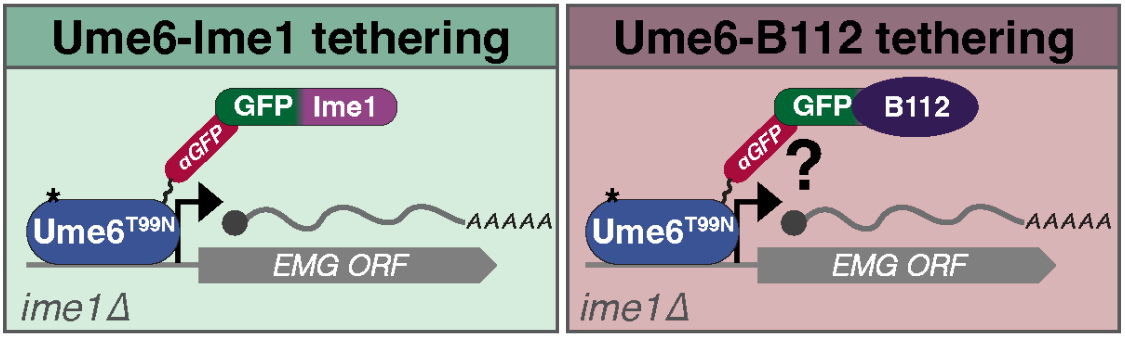

Figure 3.27: Schematic representation of tethering with heterologous activation domain. Artificial tethering of the heterologous B112 activation domain to Ume6^{T99N} is sufficient to induce meiosis and produce viable gametes. Illustration of the GFP-Nanobody trap approach using *IME1* and the heterologous activation domain *B112* to suppress *ime1*Δ in a *UME6^{T99N}-3V5-αGFP(VH16)*. The star present on Ume6^{T99N} represents the point mutation T99N that prevents Ime1 from associating normally with Ume6 within this region. Sporulation efficiency was measured for strains harboring *ime1*Δ and *UME6^{T99N}-3V5-αGFP(VH16)* with either untagged *IME1* (UB32574), *GFP-IME1* (UB32572), untagged *B112* (UB33048), or *GFP-B112* (UB30295). 100 cells were counted to determine the percentage of unsporulated cells, dyads or tetrads. Data from three biological replicates along with standard error are displayed.

expression of EMGs in *GFP-B112* may relate to a delay in meiotic progression. The downregulation of EMGs and exit from meiotic prophase is largely dependent on activation of *NDT80* and its targets (Xu et al. 1995; Brar et al. 2012; Okaz et al. 2012; Chia et al. 2021). To determine whether *GFP-B112* also delays *NDT80* expression, we monitored *NDT80* transcript levels in our dataset along with many of its downstream targets (Cheng et al. 2018). We first visualized *NDT80* and its targets by heatmap (Figure 3.35A). During early time points (t = 0-2 h) *NDT80* expression was low in both *GFP-B112* and *GFP-IME1* along with two of its targets *SMK1* and *DTR2* (Figure 3.35B). *NDT80* transcript level increased in *GFP-IME1* by ~5.7 fold going from 2 to 4 h, whereas *NDT80* levels in *GFP-B112* only began increasing going from 4 to 6 h (~4.5 fold). Similar results were observed for the Ndt80-targets *SMK1* and *DTR2*. To determine whether the delay in *NDT80* expression extended to *NDT80* targets in the *GFP-B112* strain, we analyzed these genes in our dataset (*NDT80* target list was obtained from Cheng et al 2018). Using GSEA, we observed that the highest enrichment of *NDT80* targets occurred around 4 and 6 h for *GFP-IME1* (NES = 3.74 and 3.75, respectively; Figure 3.36). Conversely, enrichment of *NDT80* targets in *GFP-B112* did not occur until 6 h (NES = 3.16) and was not as strong compared to *GFP-IME1* (Figure 3.36). Taken together, our results indicate that *GFP-IME1* and *GFP-B112* are able to initiate the meiotic program and produce viable gametes in the *UME6^{T99N}-3V5-αGFP* background. However, while *GFP-IME1* appears to achieve this in a timely manner, *GFP-B112* appears to have an extended meiotic prophase and subsequent delay in *NDT80* expression.

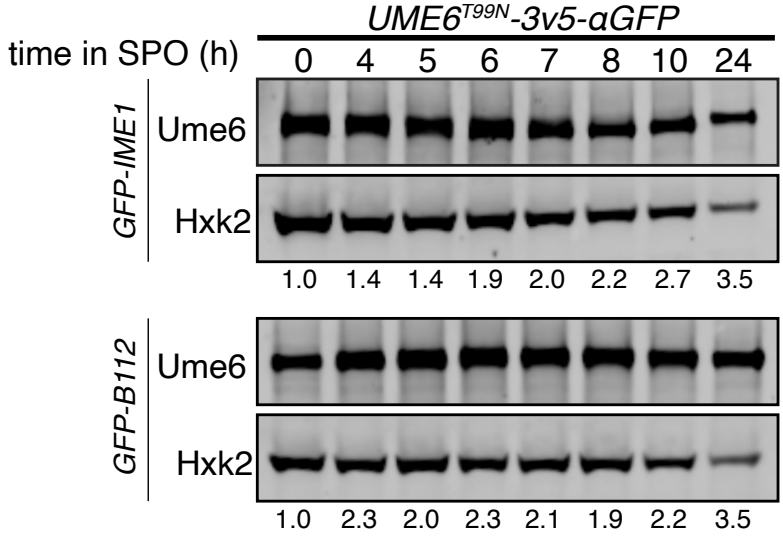

Figure 3.28: Monitoring Ume6 abundance during meiosis in *GFP-IME1* and *GFP-B112* backgrounds. A heterologous activation domain (AD) rescues Ume6^{T99N} and ime1Δ triggering meiosis using the GFP Nanobody system. Ume6 levels were measured in *GFP-IME1* (UB32572) and *GFP-B112* (UB30295) strains by collecting time points at the designated times and performing anti-V5 immunoblotting using Hxk2 as a loading control. Values below blots were calculated by first normalizing Ume6 levels to Hxk2 in each lane, and then dividing that ratio by the initial (0 h) time point.

To further confirm a delay in meiotic progression, we used an endogenously fluorescent tagged histone H2B (*HTB1-mCherry*) and performed time-lapse microscopy. We observed a delay in the onset of anaphase I in the *GFP-B112* strain (Figure 3.37A and 3.37B). While *GFP-IME1* cells took ~6.2 h (n = 191, SD = 1.9 h) to initiate anaphase I, *GFP-B112* cells took 12.5 h (n = 162, SD = 3.4 h) to reach anaphase I ($p < 0.00001$; one-tailed T-test). We find that this slowdown of meiotic progression is consistent with the delayed activation of the *NDT80* regulon in *GFP-B112*. However, despite the delay in *GFP-B112* cells, once initiated the divisions are completed with similar timing compared to *GFP-IME1* (Figure 3.37A).

Taken altogether, these data support a model where Ime1's association with Ume6 generates an activator complex to induce EMG*s*. Removal or disruption of the interaction between Ime1 and Ume6 hinders meiotic entry. Furthermore, EMGs can be activated when a heterologous AD is tethered to Ume6 indicating that generic transcriptional activators are able to initiate the meiotic program and even produce viable gametes when targeted to the correct genomic locations. This suggests that Ime1 serves chiefly as transactivator for Ume6 and that Ime1 has been evolutionarily tuned to allow timely expression of EMGs and execution of the meiotic program.

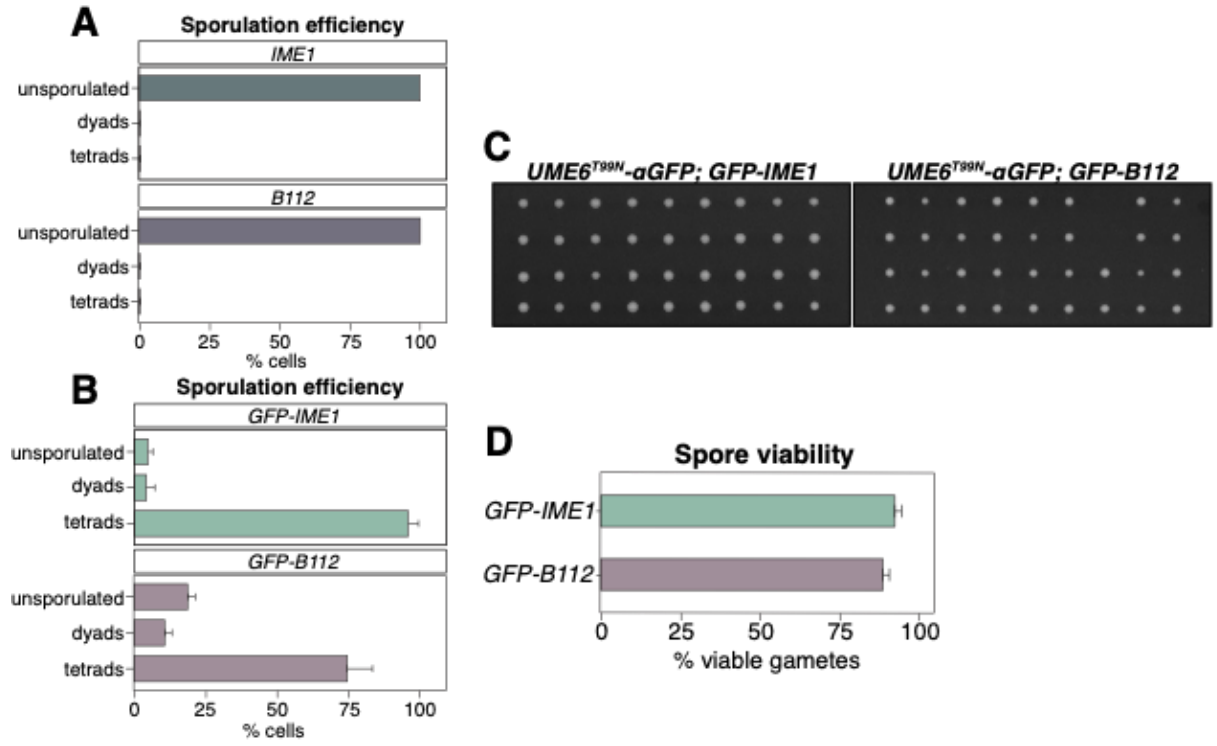

Figure 3.29: Measuring sporulation efficiency and viability in the absence of activation domain tethering. Sporulation efficiency was measured for strains harboring *ime1*Δ and *UME6^{T99N}-3V5-αGFP(VH16)* with either (A) untagged *IME1* (UB32574) and untagged *B112* (UB33048) or (B) *GFP-IME1* (UB32572) and *GFP-B112* (UB30295).100 cells were counted and their ability to produce dyads or tetrads as well as those that remained unsporulated is presented for three biological replicates along with the standard error. Data from three biological replicates along with standard error are displayed. Strains harboring both *ime1*Δ and *UME6T99N-3V5-αGFP(VH16)* with *GFP-IME1* (UB32572) or *GFP-B112* (UB30295) were transferred to SPO and allowed to complete the meiotic program for 48 h. Spore viability was tested by digesting tetrads in zymolase 100T (1mg/ml) for 12 min before dissecting them onto nutrient rich YPD agar plates. (C) Representative plates from the dissections are shown for *GFP-IME1*(UB32572) and *GFP-B112* (UB30295). (D) Quantification of spore viability. Spore viability was defined as the percent of spores that formed colonies after being transferred to nutrient rich plates out of the total 296. Note that untagged activation domains failed to produce spores and were therefore not included in the analysis.

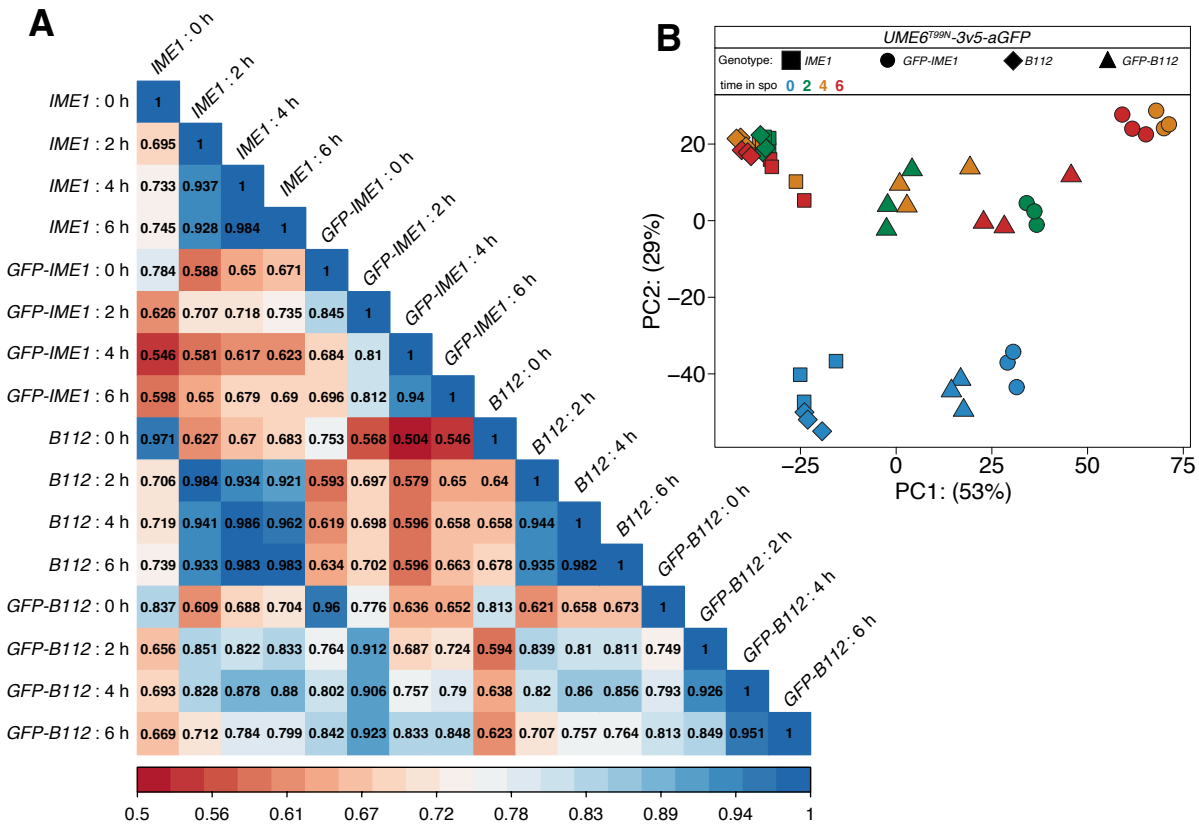

Figure 3.30: Statistical analysis of global transcriptional differences by Spearman analysis and PCA. (A) Corrplot package was used in R to generate heatmaps comparing sample relatedness between *GFP*-tagged and untagged alleles of *IME1* and *B112*. Red denotes poor correlation and blue is high correlation. (B) DESeq2 results between untagged- and GFP-tagged ADs were processed by using VST and plotPCA functions associated with DESeq2. A PCA plot that highlights PC1 (x-axis) and PC2 (y-axis) was built using ggplot2 and is presented here. Shapes denote distinct genotypes while colors denote time points. We note that differences exist between samples at 0 h for untagged and tagged *IME1* and *B112*. This is most likely caused by the affinity GFP has for the nanobody trap, resulting in strong recruitment of the activation domain to Ume6 and earlier than normal meiotic initiation.

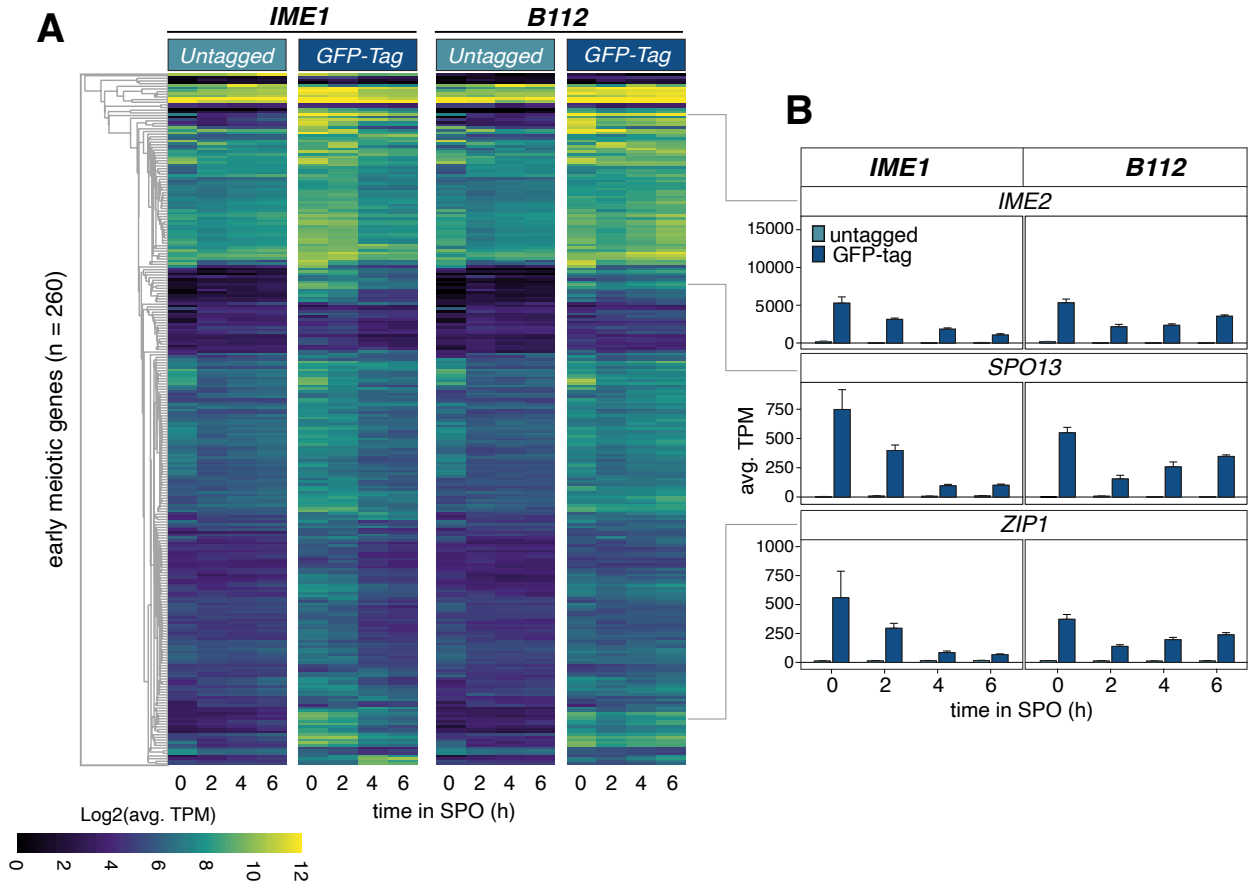

Figure 3.31: Heatmap of early meiotic gene expression for tethered and untethered activation domains. Artificial tethering of the heterologous B112 activation domain to Ume6^{T99N} is sufficient to induce meiosis and produce viable gametes. Strains containing both *ime1*Δ and *UME6^{T99N}-3V5-αGFP(VH16)* with either untagged *IME1* (UB32574), *GFP-IME1* (UB32572), untagged *B112* (UB33048), or *GFP-B112* (UB30295) were transferred to SPO (t = 0h) and RNA samples were collected at the specified times. Heatmaps for EMGs were generated as described previously and represent log2 of the mean for three biological replicates. (A) *UME6^{T99N}-3V5-αGFP(VH16)* is present in combination with *IME1* (left) or *B112* (right) either untagged (light blue) or GFP-tagged (dark blue) in both heatmaps. (B) Barplot showing mean TPM for the indicated genes for either untagged (light blue) or GFP-tagged (dark blue) *IME1* (left column) or *B112* (right column).

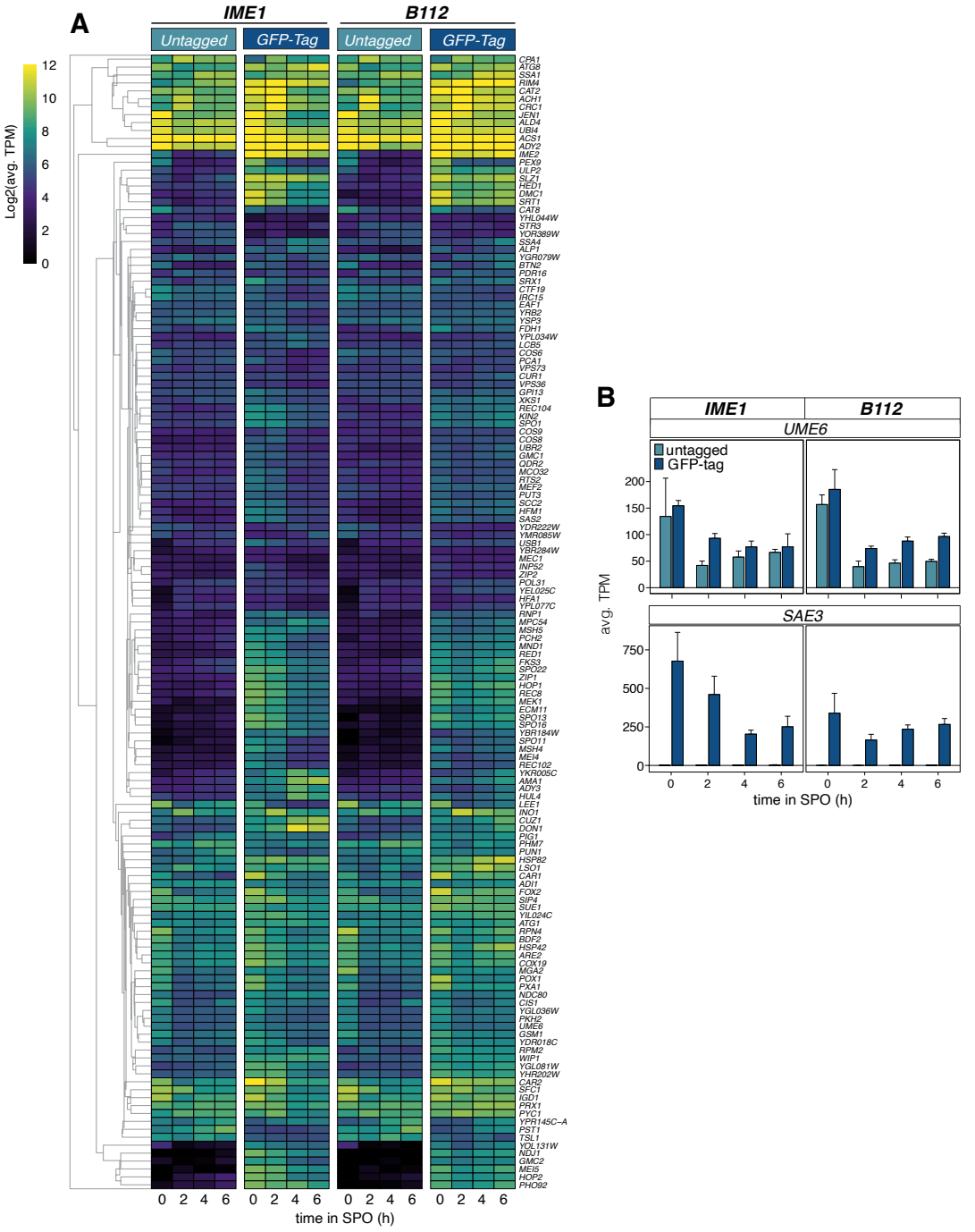

Figure 3.32: Expression levels for the Ume6 regulon in tethered and untethered activation domain backgrounds. (A) Heatmap showing log2 of mean TPM across three biological replicates for 143 Ume6 targets. Transcript levels for *SAE3* in response to tethering of *B112* compared to *IME1*. (B) We note that *SAE3* again was dropped while constructing our heatmap due to low expression present and instead is presented as a barplot.

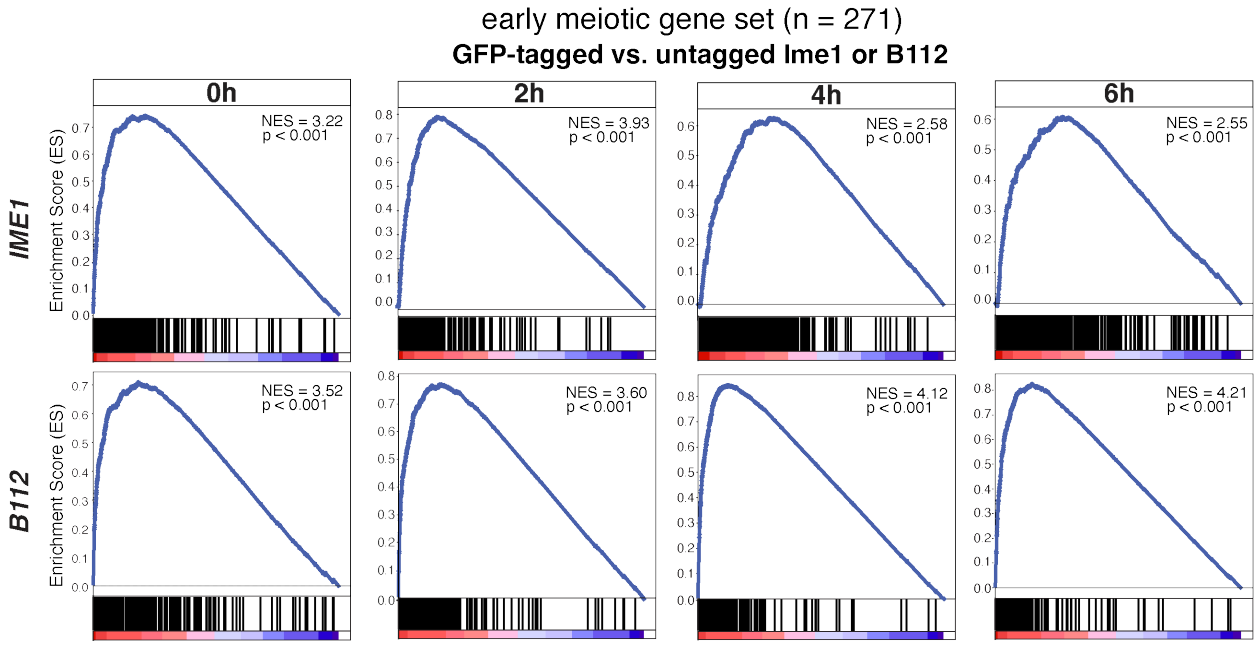

Figure 3.33: Enrichment of the early meiotic regulon across time for both activation domains. Artificial tethering of the heterologous B112 activation domain to Ume6^{T99N} is sufficient to induce meiosis and produce viable gametes. Gene set enrichment analysis (GSEA) comparing untagged and sfGFP-tagged *IME1* (top) or *B112* (bottom) for "Early Meiotic Genes" at designated time points. The ES line represents enrichment for a set of genes in a given sample and the peak position denotes the degree to which that set is over- or underrepresented. The enrichment score was then normalized to account for gene set variation and is presented as normalized enrichment score (NES). Vertical bars represent a gene and its position along the heatmap (bottom) shows how enriched that gene is in either *GFP-AD* (left-side) or untagged *AD* (right-side).

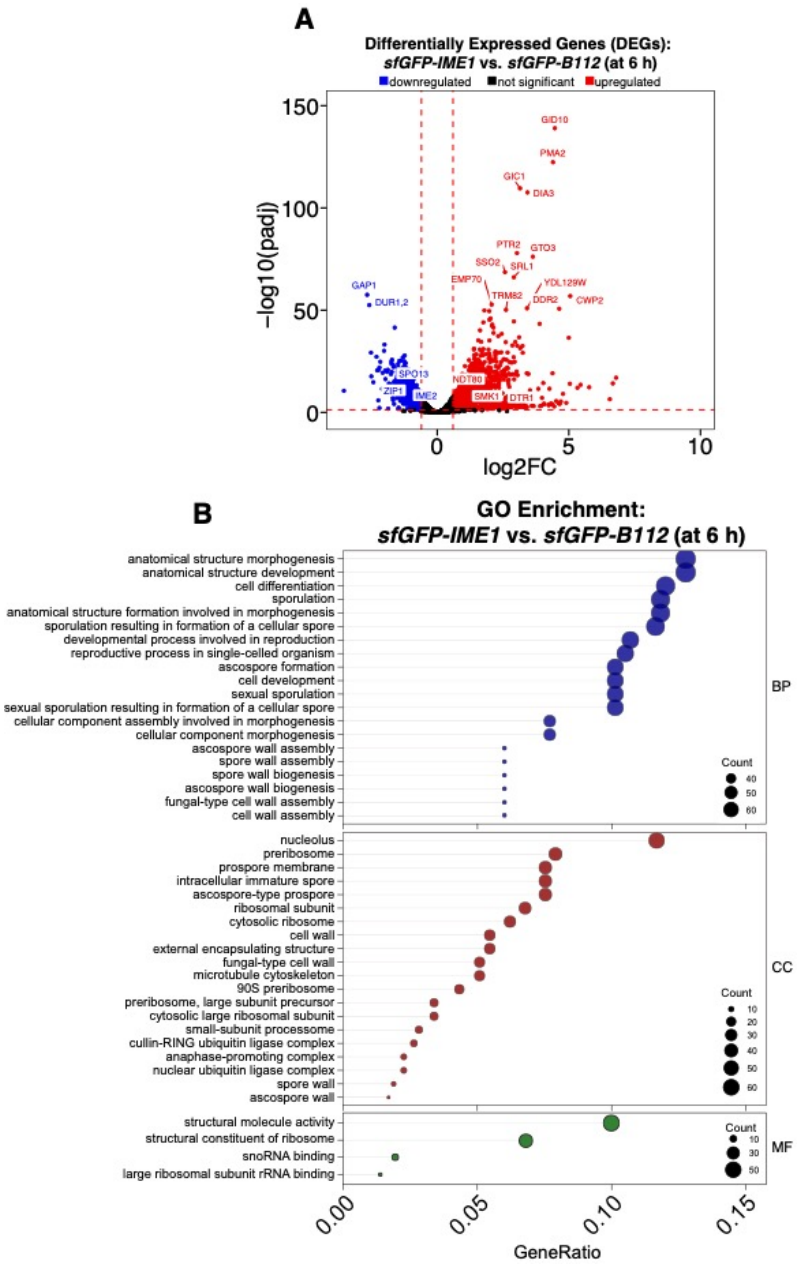

Figure 3.34: Differential gene expression patterns between *GFP-IME1* and *GFP-B112* at 6h using DESeq2 and GO enrichment. (A) Volcano plot highlighting DEG found using DESeq2 analysis between *GFP-IME1* (UB32625) and *GFP-B112* (UB31729) at 6 h that showed 543 DEGs (padj < 0.05; log2FC > 1.5) either up- (red) or downregulated (blue) or showing no overall change (black). (B) GO enrichment applied to the 543 DEGs identified by DESeq2. Gene ratio is presented on the x-axis and is the percent of genes in a given GO term out of the total 543 genes total. Again, point size signifies the number of genes in that GO term while color signifies category: BP, biological process; CC, cellular component; MF, molecular function.

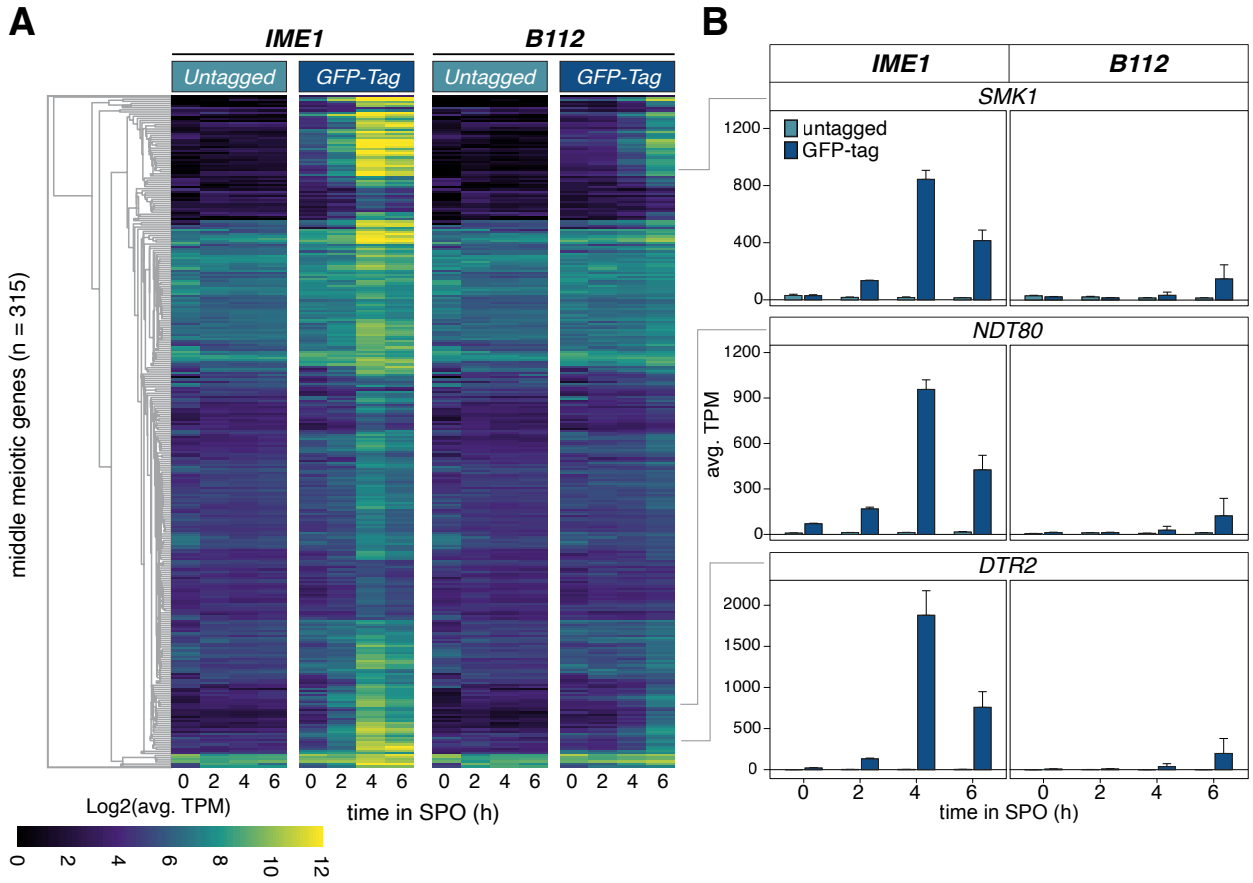

Figure 3.35: Expression levels for middle meiotic genes in tethered and untethered activation domains by heatmap. Middle meiotic gene expression is delayed with the B112 activation domain. (A and B) Cells were prepared as in Figure 3.31. Heatmaps for Middle Meiotic Genes (A and B) were made as previously described and represent log2 of the mean for three biological replicates. *UME6^{T99N}-3V5-αGFP(VH16)* was combined with either *IME1* (left) or *B112* (right) lacking (light blue) or possessing (dark blue) the GFP-tagged, respectively. (B) Barplot showing mean TPM for the indicated genes for either untagged or GFP-tagged *IME1* (left column) or *B112* (right column).

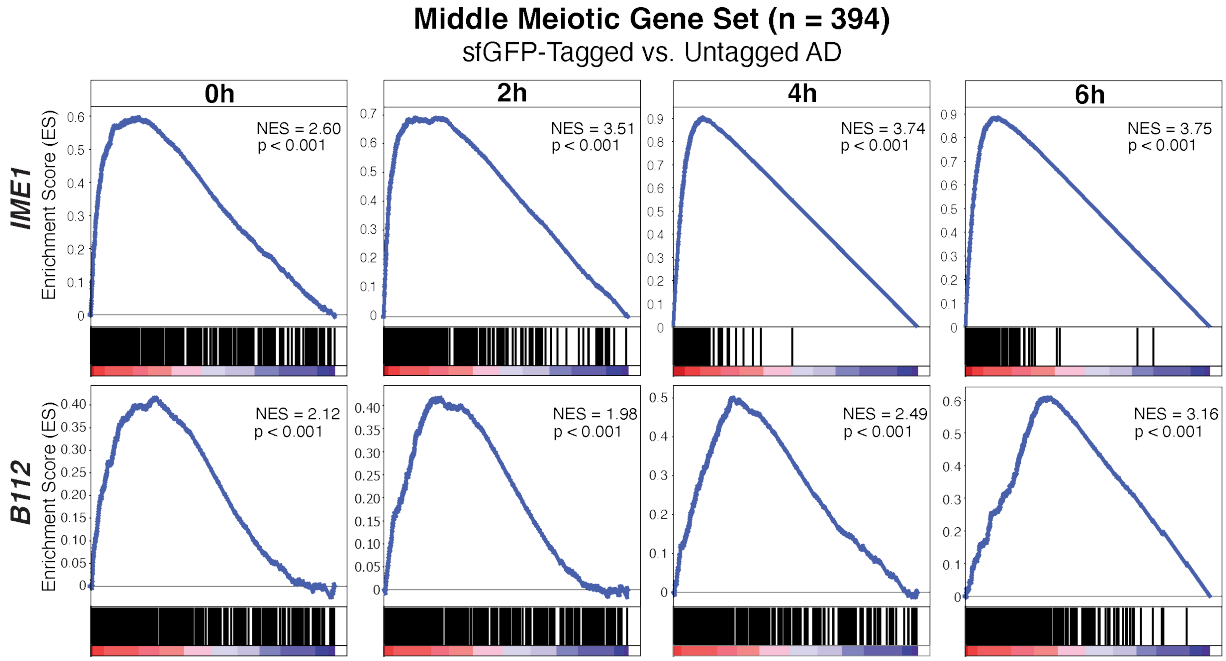

Figure 3.36: GSEA analysis of middle meiotic genes across time in *GFP-IME1* and *GFP-B112* backgrounds. Middle meiotic gene expression is delayed with the B112 activation domain. GSEA was applied as in Figure 3.33. This time using the NDT80 cluster from Cheng et al. 2018 to observe enrichment of *NDT80* and its downstream targets, here called "middle meiotic genes."

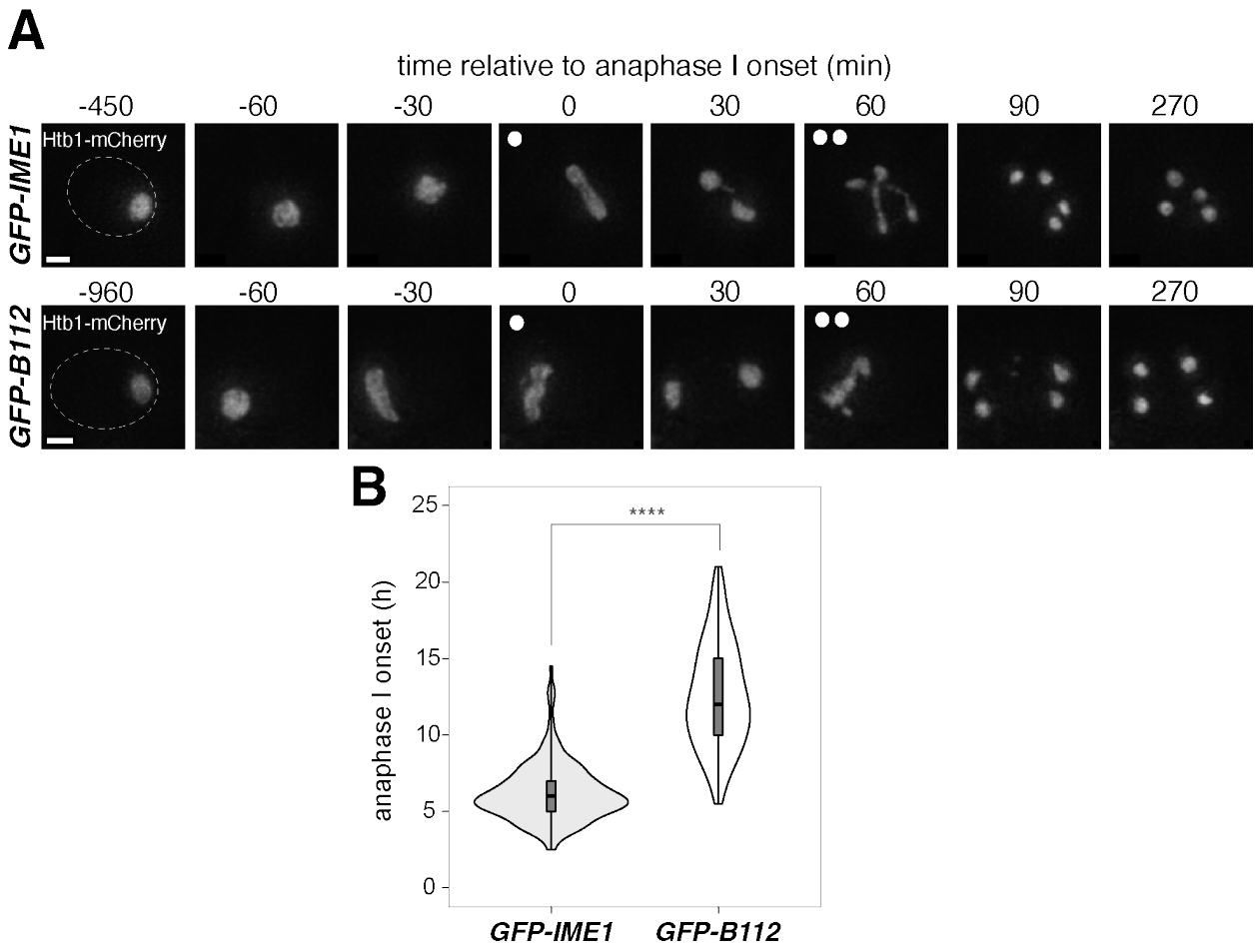

Figure 3.37: Timing in anaphase I onset determined by time-lapse microscopy. Middle meiotic gene expression is delayed with the B112 activation domain. Cells were transferred to SPO after brief sonication and using the CellASIC Platform in an environmentally controlled chamber at 30˚C, pictures were acquired at 30 min intervals for over 21 h. (A) Representative images for Z-projected cells carrying either *GFP-IME1* (UB32625) or *GFP-B112* (UB31729) at the specified times. Using HTB1-mCherry, a histone marker, we labeled chromatin to identify anaphase I onset. Anaphase I is defined as the start of chromatin bifurcating into two distinct foci. Onset of anaphases I and II are denoted by either one or two white circles. Scale bar, 2 µm. Dashed lines represent cell boundary. (B) Quantification of anaphase I onset in cells containing *GFP-IME1* or *GFP-B112* are presented as a violin plot containing a box plot. For *GFP-IME1*, 191 cells were counted and average time to anaphase I onset was 6.2 h. For *GFP-B112*, 162 cells were counted and average time to anaphase I onset was 12.5 h. t-test results are presented on the graph and show differences in the population $t(352) = -21.8$, $p < 0.00001$ (****) in a one-tailed test.

Discussion

Ume6 and Ime1 are upregulated through a feed-forward mechanism

Ume6 protein levels remain constant in the absence of *IME1* expression. However, induction of *IME1* and *IME4* leads to a dramatic increase in *UME6* transcript levels, resulting in an upsurge in Ume6 protein abundance (Figure 3.1A and 3.1B). These findings indicate that Ume6 is not degraded in response to *IME1* expression, as previously postulated (Mallory et al. 2007; Law et al. 2014; Mallory et al. 2012), but is rather upregulated. Consistently, published datasets (Tresenrider et al. 2021; Chia et al. 2021) indicate a URS1 site proximal to the *UME6* transcriptional start site (TSS). The URS1 is located -147 bp upstream of the *UME6* TSS, suggesting that Ume6 regulates its own promoter. We further observed meiotic upregulation of *UME6* through tethering of Ume6 to a heterologous activation domain (Figure 3.32B). Taken altogether, Ume6 appears to stimulate its own expression during meiotic entry through a URS1 motif. Interestingly, *IME1* is also known to regulate its promoter through a URS1 motif (van Werven et al. 2012; Moretto et al. 2021). This indicates that cells have evolved feed-forward mechanisms that ensure both Ime1 and Ume6 are present at sufficient levels during meiotic entry. In addition to the feed-forward regulation by Ime1-Ume6, *IME1* mRNA is further stabilized by Ime4, which functions as an N6-adenosine methyltransferase (Shah and Clancy 1992; Hongay et al. 2006). However, it is currently unknown whether *UME6* mRNA is also regulated by Ime4. Future work could reveal more commonality between transcriptional and post-transcriptional control of *IME1* and *UME6*.

Ume6 and Ime1 form an activator complex to drive EMG expression during gametogenesis.

Our findings indicate that Ume6 and Ime1 form an activator complex to drive EMG expression. Besides upregulation of *UME6* following meiotic entry, four lines of evidence are consistent with this interpretation: First, depletion of Ume6 shortly before *IME1* activation disrupts EMG expression and gamete formation (Figure 3.7-3.13). Second, Ume6's association with EMG promoters is unaffected by *IME1* expression (Figure 3.2). Third, rescuing the interaction between Ume6^{T99N} and Ime1 using a nanobody trap approach leads to an increase in Ume6 levels, rather than promoting its degradation, and enables activation of EMGs as well as meiotic execution (Figure 3.16-3.26). Finally, substitution of Ime1 with a heterologous activation domain from bacteria is sufficient to induce EMG expression and production of viable gametes in a Ume6-dependent manner,

albeit the kinetics of this were reduced (Figure 3.28-3.37). This finding also suggests that Ime1 is unlikely to possess an additional function beyond serving as a finely tuned transactivator for Ume6.

The transcription factor Ndt80 downregulates Ume6 following exit from meiotic prophase.

Ume6 protein levels decrease during mid, rather than early, meiosis in response to *NDT80* expression. Ndt80's involvement in *UME6* downregulation comes at a time when many early meiotic events must be terminated. Although Ime1 remains bound to Ume6 during meiosis, it has been shown that Ime1 is unable to fully initiate EMG expression mitotically while Sin3-Rpd3 is bound to Ume6 (Smith et al. 1990). Thus, Ndt80 could influence Sin3-Rpd3 in the downregulation of both EMGs and *UME6*. Whether Rpd3 is bound to EMG promoters during meiosis is ambiguous. Some studies suggest that Rpd3 is enriched at the *IME2* promoter during meiosis (Inai et al. 2007; Raithatha et al. 2021) while others have found Rpd3 signal to be transiently lost (Pnueli et al. 2004). It is unclear where the discrepancy arises and has left Sin3-Rpd3's involvement largely unresolved. However, the list of genes responsive to Ndt80 activation is quite expansive (Cheng et al. 2018). A target of Ndt80 may function to reduce or reverse the effects of Ume6 phosphorylation by Rim11 and/or Rim15 permitting Sin3-Rpd3 to reestablish a repressive state for EMGs. Further investigation is required to understand the mechanism by which Ndt80 mediates *UME6* downregulation and the biological significance of such regulation.

Chapter 4

Conclusions and Future of the Field

4.1 The Road to a Unified Model of Meiotic Initiation

TFs are central to coordinating production of machinery involved in cellular programs. In the context of meiotic differentiation in *Saccharomyces cerevisiae*, TFs are critical in proper and timely execution of the different developmental stages. Since their identification as regulators of meiotic entry, *IME1* (or “Inducer of MEiosis I”) and *UME6* (or “Unscheduled Meiotic gene Expression 6”), have been regarded as the primary determinants in the decisions of cells to enter meiosis (Kassir et al. 1988; Park et al. 1992; Strich et al. 1994). For *IME1*, further investigations identified its functional domains. Of importance were the tyrosine-rich activation and the starvation response domains near the C-terminus of Ime1 (Smith et al. 1993). Subsequent investigation into *IME1* found that it coordinates meiotic entry through its interaction with Ume6 and that mutations in the N-terminus of Ume6 obstructed Ime1 binding (Bowdish et al. 1995; Rubin-Bejerano et al. 1996; Malathi et al. 1997). Additionally, there were hints that tethering of an activation domain to Ume6 was sufficient to drive EMG expression under meiotic conditions (Rubin-Bejerano et al. 1996). This led many researchers to conclude that Ime1 and Ume6 form an activator complex to drive EMG expression and initiate meiosis. However, previous work had already implicated Ume6 as a repressor of these meiotic genes during mitosis and an alternative explanation was being developed. This explanation took into account that failures to properly regulate meiotic factors like *IME2* and *SPO13* during mitosis frequently resulted in meiotic arrest (Strich et al. 1989, 1994). This arrest likely stemmed from an inability to properly downregulate EMGs around the time of chromosome segregation. The degradation model was fully actualized during a time series experiment. Using immunoblotting to monitor Ume6 levels and how this coincided with *SPO13* expression, researchers found that upon shifting cells to meiotic conditions a drop in Ume6 protein levels preceded the upregulation of *SPO13* transcripts (Mallory et al. 2007). In the same report, the group drew a link between Ume6 downregulation and Cdc20 using a temperature sensitive allele of *CDC20* (*cdc20-ts*). Doing so, they found that disruption of *CDC20*, brought on by shifting cells to a higher temperature, prevented both Ume6 downregulation and meiotic gene expression (Mallory et al. 2007). Since, the group has identified key residues in Ume6 that, when acetylated, promote Ume6’s dissociation from promoters of EMG (Mallory et al. 2012; Law et al. 2014). More recently, evidence rejecting Cdc20’s involvement in the downregulation of Ume6 has been presented (Raithatha et al. 2021). Additionally, ChIP-PCR has been used to show Ume6, instead of being

removed, functions as the scaffold that recruits an assortment of factors responsible in gene activation. These models, and the data surrounding them, have led to conflicting roles for both Ime1 and Ume6 in meiotic initiation.

Challenges in differentiating between these two models have stemmed largely from the asynchronicity with which cells enter meiosis. Meiotic differentiation is a tightly controlled and sequentially executed developmental program. The sequential nature of meiosis manifests as gene expression clusters associated with a specific developmental needs (Chu et al. 1998; Brar et al. 2012; Chia et al. 2021). For example, early genes are associated with events like recombination and synaptonemal complexing and their expression is prevented from overlapping with middle genes, which are largely involved in chromosome segregation. This controlled expression creates waves of transcription that denote how far a cell has progressed through the meiotic program. However, heterogeneity in a population of cells can blur developmental boundaries and obfuscate when events are occurring. Furthermore, *IME1* expression is a primary driver of meiotic entry. However, the *IME1* promoter itself is highly regulated and receives input from several pathways including carbon source, nitrogen levels, and mating type (Reviewed in van Werven and Amon 2011). The complexity of the *IME1* promoter leads to highly variable expression of *IME1* and contributes heavily to the asynchronicity with which cells enter the meiotic program. Additionally, use of strain backgrounds other than the meiotically optimized strain SK1 can result in increased time to completion of the meiotic program. This prolonged meiosis can further exacerbate the heterogeneity found in cell populations and further blur developmental boundaries. Taken together, in the absence of a system that increases synchronicity of meiotic initiation, defining the timings with which Ume6 is downregulated and how this coincides with EMG expression would prove challenging.

Technological advances in biological tools have afforded more options with which to approach this question. Here we employ a variety these tools to definitively resolve which model best explains the role of Ime1 and Ume6 in the expression of EMGs. Utilization of the auxin-inducible degron (AID) system allowed the construction of a more versatile allele of *UME6*. Using this allele during mitosis, we find that Ume6 regulates a diverse set of genes including its own promoter (Chapter 2). Next, using inducible alleles of *IME1* and *IME4*, we were able to better synchronize cells and define the timing of Ume6 degradation and whether it coincided with *IME1/4* expression (Chapter 3). We find that expression of *IME1/4* does not lead to downregulation of Ume6. Instead, consistent with the coactivator model and the observation that Ume6 autoregulates its own promoter, we observe *IME1/4* expression leads to *UME6* upregulation. Furthermore, we reconcile observations within the degradation model by identifying *NDT80* as the driver of *UME6* downregulation. Because *NDT80* expression is restricted to after completion of meiotic

prophase, we assert that the timing of Ume6 downregulation must also be after these events. We next combine our Ume6-AID and inducible *IME1/4* system to demonstrate the removal of Ume6 prior to *IME1/4* expression disrupts meiotic initiation and formation of the gametic products. This failure to initiate meiosis suggests that Ume6 must be available for Ime1 to influence EMG expression and is more consistent with a coactivator model. Finally, using a GFP nanobody tethering strategy, we show that recruitment of the heterologous activation domain B112 from *E.coli* is sufficient to drive meiotic initiation. Contrary to this, if Ime1 binding to Ume6 promoted Ume6's displacement from EMG promoters and subsequent degradation, B112 would not be able to fulfill this function and thus cells could not initiate meiosis. Thus, based on the data, the degradation model makes the incorrect prediction.

Our data resolves the discrepancy between many observations found in the field and highlights Ime1 and Ume6 as a coactivator complex. Additionally, our findings introduce many more avenues of inquiry. Firstly, some of these discrepancies between each model have arisen due to strain differences and it's unclear if our system could be adapted to better understand Ime1 and Ume6's interaction in other strain backgrounds like W303 and S288C. Furthermore, preliminary work has shown that depletion of Ume6 post-*IME1/4* induction has a less severe reduction in gamete formation. Thus, it's unclear how long Ime1 and Ume6 need to maintain EMG expression before being dispensable. Next, our work has implicated *NDT80* as being involved in *UME6* downregulation. How this is achieved is unknown, but the *NDT80* regulon has been shown to be expansive (Cheng et al. 2018). The most appealing explanation is that *NDT80* regulates a phosphatase that serves to reverse the effects of the kinases Rim11 and Rim15 to displace Ime1 from Ume6 and facilitate reassociation of Sin3-Rpd3. Five phosphatases exist that either are known or unknown to have a meiotic phenotype including *CDC14*, *MSG5*, *PTC5*, *PTP3*, and *YMR1*. However, more work is required to determine if this is the mechanism employed by *NDT80* to facilitate *UME6* downregulation. Additionally, it is unclear if Ume6 protein experiences active turnover since *NDT80* also regulates meiosis specific Fbox proteins like *DAS1*, *GRR1*, *MFB1,* and *MDM30*. Taken together, our results open the road to more areas of research.

4.2 The Future of the Ume6 Ime1 Activator Complex

Our findings implicate Ume6 as a major determinant of EMG expression and successful meiotic execution. Through binding to a transcriptional activator, like Ime1, Ume6 is converted from a repressor to an activator. As part of the Ime1-Ume6 co-activator complex, both *IME1* and *UME6* appear to engage in a feed-forward mechanism by harboring a URS1-motif in their promoters. This mechanism ensures adequate protein levels and proper EMG expression through promoting their own mRNA production.

Removal of Ume6 prior to *IME1* and *IME4* induction is deleterious for meiotic success and EMG expression. Furthermore, mutants that prevent proper Ime1 and Ume6 interaction also disrupt meiotic initiation. However, through reuniting Ume6 with even a heterologous activation domain, EMG expression and the meiotic program can be rescued.

This reliance on formation of an activator complex is functionally analogous to mammalian systems, where MEIOSIN and STRA8 form a complex to drive meiotic initiation. MEIOSIN, like Ume6, has been shown to bind to promoters of EMGs and recruit STRA8 to those sites (Ishiguro et al. 2020). Additionally, like Ime1, STRA8 has been shown to carry the activation domain necessary for EMG activation (Tedesco et al. 2009; Ishiguro et al. 2020). *Meiosin* KO strains fail to initiate meiosis even in the presence of STRA8 (Ishiguro et al. 2020). The functional similarities between STRA8-MEIOSIN and Ime1-Ume6 are striking. Therefore, our study could shed light into the transcriptional regulation of meiotic entry in more complex systems and provide a lens to investigate the associated meiotic defects.

4.3 Final Thoughts

Altogether, this work unifies decades worth of observations relating to the interaction between Ime1 and Ume6 and how to these two factors facilitate meiotic initiation, together. We've also introduced a feedback mechanism present within *UME6* regulation during mitosis. But more importantly, this mechanism shifts to a feed forward mechanism for *UME6* during meiosis, aligning it more with *NDT80* and *IME1*, and elevating it to the level of a true meiotic TF and not just a dispensable mitotic repressor. Through the development of a depletable allele of *UME6*, we have both expanded and also refined the Ume6 regulon and largely eliminated the need to use *ume6*Δ.

Ume6's role as the docking site for Ime1 to promote meiotic initiation places the Ime1/Ume6 activator complex more in line with other mechanisms of eukaryotic gene regulation like those in mammalian systems. Thus, insights gleamed about Ime1/Ume6's regulation of its target genes could have functional paralogs in mammalian systems. Of particular interest is the regulation of a newly identified form of cis-regulation called long undecoded transcript isoforms (LUTIs). Our work served to functionally validate Ume6 regulation over 61 LUTIs during meiosis. With the presence of LUTIs in human cell lines, as is the case with the MDM2 locus (Hollerer et al. 2019), it will be interesting to see if Stra8/Meiosin regulate meiotic LUTIs as well.

Chapter 5

Appendix A

5.1 Sum1-AID depletion during mitotic growth

Introduction

As discussed in Chapter 3, mid-meiotic *UME6* downregulation occurs in an Ndt80-dependent manner. Despite Ndt80's involvement in *UME6* transcriptional downregulation, no obvious MSE is detectable. Thus, Ndt80 likely influences *UME6* through one of its many downstream targets. However, as was demonstrated by Cheng et al. 2018, the Ndt80 regulon is large and spans at least 394 genes. Compound this with the highly dynamic nature of meiosis and identifying candidates could prove challenging. However, Ndt80 shares its promoter with another transcription factor, Sum1, which is critical for repressing expression of middle meiotic genes during mitotic growth (Pierce et al. 2003). As with Ume6, much of what is known about Sum1 comes from use of Sum1 null (*sum1*Δ) strains. And, as with *ume6*Δ, *sum1*Δ strains suffer from many pleiotropic effects leaving them sick (Reviewed in Winter 2012). Using the AID system proved effective in circumventing many of the pleiotropic effects for *ume6*Δ allowing better resolution of the Ume6 regulon. Thus, using Sum1-AID could prove invaluable in defining the Sum1, and by extension, Ndt80 regulons. Additionally, Sum1-AID's ability to recapitulate *UME6* downregulation during mitosis could allow a less dynamic context under which to study the phenomenon. Taken together, Sum1-AID could aid in answering many relevant biological questions about *UME6* regulation and middle meiotic genes.

Results

To determine the degree of Sum1-AID depletion, we monitored Sum1 levels by immunoblotting in the absence and presence of the F-box receptor *OsTIR1* as before (henceforth termed "control" and "Sum1 depletion," respectively). Here, *OsTIR1* expression is driven by $CuSO_4$ addition (See Methods). In control cells, addition of $CuSO_4$ and auxin had no detectable impact on Sum1 levels (Figure 5.1A and 6.1B; See Control). Conversely, introduction of $CuSO_4$ and auxin to Sum1 depletion strains resulted in sharp

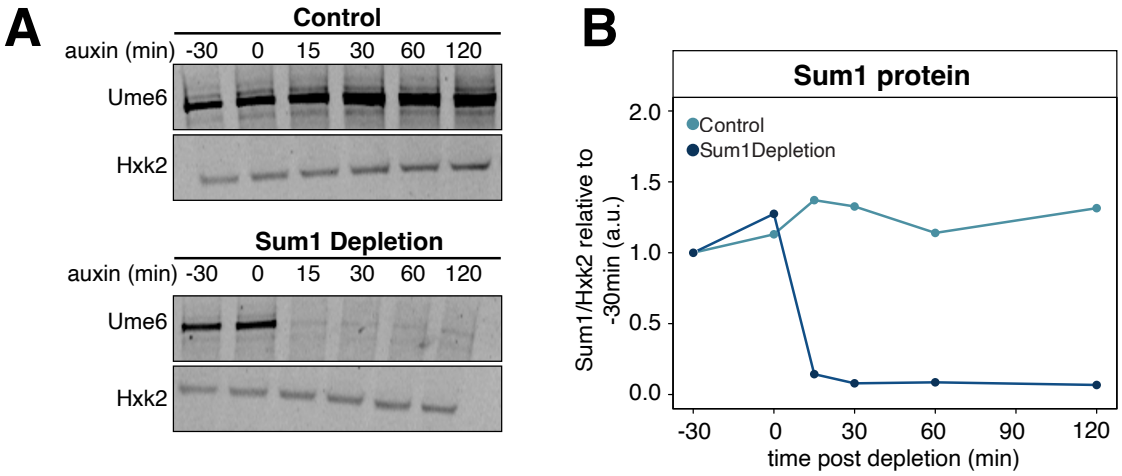

Figure 5.1: Measuring Sum1 protein levels by immunoblotting. (A) Monitoring of Sum1 protein levels in response to addition of auxin and beta-estradiol in the presence or absence of *osTIR* (Ume6 depletion or control, respectively) was performed using immunoblotting. Strains with (UB24885) or without (UB24883) the *osTIR* construct or strains with wild-type *SUM1* (WT; UB17716) or *SUM1* null (*sum1*Δ; UB25684) were inoculated in YPD. Cultures were grown overnight to OD_{600} > 10 and then back diluted to OD_{600} = 0.25. Once cells reached log phase (OD_{600} = 0.5) $CuSO_4$ (50 µM final) was added to all cultures (t_{auxin} = -30 min) to induce Os*TIR*. Cells were allowed to continue shaking for 30 min at which point auxin (200 µM) was added, initiating Sum1-AID degradation only in the *osTIR* containing strains (t_{auxin} = 0 min). Protein and RNA samples were collected at the designated time points. Note, cultures for wild-type *SUM1* and *sum1*Δ were collected at t_{auxin} = -30 min prior to chemical treatments. (A) Sum1 protein levels were monitored by anti-V5 immunoblotting and using Hxk2 as a loading control. Representative blots from one of three biological replicates are shown. (B) Quantification of immunoblots in A.

declines to Sum1 levels. Upon treatment, Sum1 levels were reduced to ~14% of the initial levels by 15min and remained below 10% for the duration of the time series (Figure 5.1A and 6.1B; See Sum1 Depletion). Thus, our AID system was able to trigger an acute decline in overall Sum1 levels.

To gauge the transcriptome's response to Sum1 depletion, we performed RNA-seq. First, using Spearman's rank correlation coefficient (ρ), we determined global changes in gene expression between conditions (Figure 5.2A). Initially, control and Sum1 depletion samples were highly similar (-30 min; ρ = 0.993). Then, upon depleting Sum1 the sample relatedness slightly diverged (ρ = 0.955, 0.955, 0.967, and 0.971 for 15, 30, 60, and 120min, respectively). Additionally, we used principal component analysis (PCA; Figure 5.2B) to monitor sample-to-sample variability across time. Together, PC1 (71%) and PC2 (14%) accounted for 85% of the variation we observed between samples. Prior to addition of $CuSO_4$ for *OsTIR* induction, both control and Sum1 depletion strains showed little variation. Addition of $CuSO_4$ resulted in control samples shifting largely along PC2. Furthermore, Sum1 depletion samples shifted along PC1 and PC2 in response to $CuSO_4$ treatment, indicating $CuSO_4$ had an influence on sample-to-sample variation. Addition of auxin in the control however, had little effect as indicated by points clustering together for

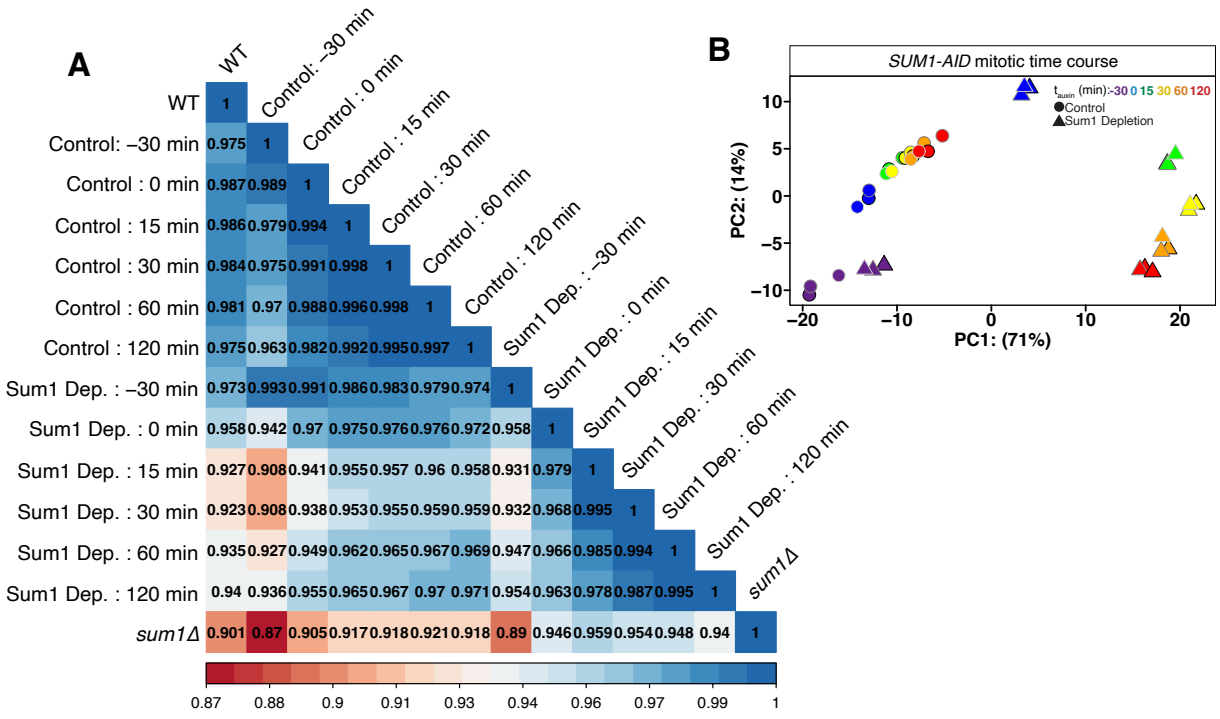

Figure 5.2: Spearman correlation and PCA analysis of sample-to-sample variation (A) and (B). Normalized counts data generated from DESeq2 were analyzed for the control and Sum1 deplete time course data. Measuring the impact of Sum1 depletion using Spearman correlation and PCA (A and B) Sample-to-sample variation was analyzed using Spearman rank order correlation (ρ) with the corrplot package and the variance stabilizing transformation (VST) and plotPCA function associated with DESeq2. (A) Results of Spearman analysis. Red boxes are samples with low relatedness and blue boxes are samples with increased relatedness. (B) A PCA plot was then generated from these data using the ggplot2 package to visualize the influence of PC1 (x-axis) and PC2 (y-axis) on samples. To distinguish between samples, control (UB24883) and Sum1 deplete (UB24885) conditions were differentiated by shapes while specific time points were assigned colors.

the remaining time points. In contrast, Sum1 depletion as a result of auxin addition shifted samples strongly along PC1 and PC2 away from other samples. Taken together, Sum1 depletion appears to trigger strong changes to the patterns of gene expression.

Next, we turned our attention to a subset of meiotic genes. First, we monitored the transcript levels for *SMK1* and *DTR1*, two middle meiotic genes known to be regulated by Sum1 (Xie et al. 1999). For both *SMK1* and *DTR1* in the control strain, transcript levels remained largely unchanged (Figure 5.3A; See Control). However, depletion of Sum1 resulted in a nearly 2.8- and 10-fold increase in transcript abundance for *SMK1* and *DTR1*, respectively (Figure 5.3A; comparing 0 min and 15 min for Sum1 Depletion).

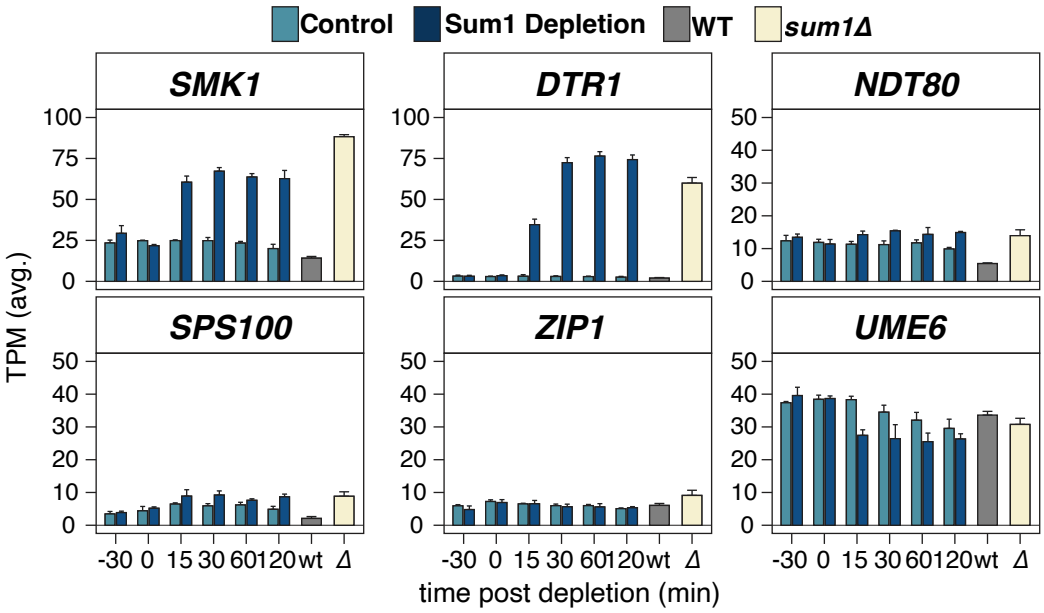

Figure 5.3: Expression levels for a subset of key meiotic genes. To investigate the response of different meiotic genes to Sum1 degradation, RNA was extracted, and cDNA libraries were generated, sequenced, and analyzed as described in materials and methods. (A) Time series data for control (light blue) and Sum1 depletion (dark blue) are shown as well as for *SUM1* (grey) and *sum1*Δ (ivory). The average TPM for *SMK1*, *DTR1*, *NDT80*, *SPS100*, *ZIP1*, and *UME6* are presented with standard error for three biological replicates.

Additionally, the *NDT80* promoter contains an MSE site that is recognized by Sum1 and contributes to repression of *NDT80* during mitotic growth. Thus we checked whether Sum1 depletion derepresses the *NDT80* promoter. Interestingly, *NDT80* transcripts were only upregulated marginally (1.3-fold; Figure 5.3A; See Sum1 depletion). This limited upregulation of *NDT80* is potentially due to the dual regulation of *NDT80* by both Ume6 and Sum1. Thus, removal of Sum1 alone is not sufficient to derepress *NDT80* to nearly the levels of other Sum1 targets like *SMK1* and *DTR1*. Next, we inspected whether other meiotic gene clusters were upregulated in response to Sum1 depletion. For this, we analyzed *SPS100* and *ZIP1*, which belong to the late and early meiotic gene clusters, respectively. Both genes were largely unaffected by Sum1 depletion, indicating these gene families remained mostly repressed in our system. Finally, we noticed that *UME6* transcripts experienced a Sum1 depletion-dependent drop (~30%; Figure 5.3; Comparing 0 min and 15 min for Sum1 Depletion). This suggests that *UME6* transcript levels respond to derepression of Sum1 targets. Thus, Ndt80 and Sum1 both regulate a factor associated with the control of *UME6* transcript levels.

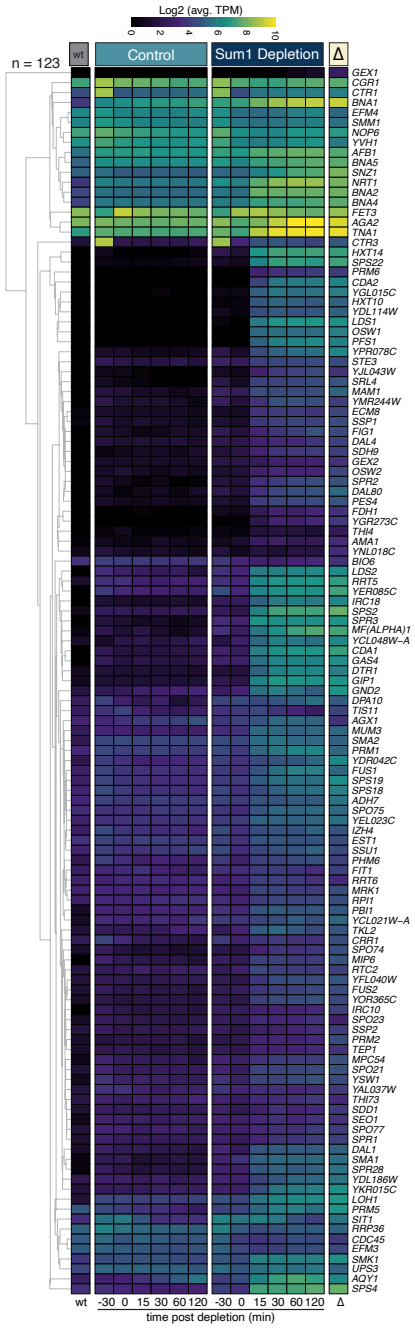

Figure 5.4: Heatmap of genes responsive to Sum1-AID depletion as determined by DESeq2. Differentially expressed genes (DEGs) between Sum1 depletion and control as well as WT and *sum1*Δ conditions were identified with the R package DESeq2 using Kallisto generated counts tables. The log2 of mean TPMs across three biological replicates are shown for the 124 DEGs identified ranging from no expression (black) to high expression (yellow). DEGs were clustered by Euclidian distance (centroid) and partitioned vertically by strain background. We note that one gene, *YFL012W*, was dropped from the list due to low expression.

Table 2.1: Sum1 Depletion Responsive Gene Targets

Systematic ID	Gene	ChIP Peak	log2FC_15min	log2FC_30min
YHR185C	*PFS1*	Yes	8.36571007	7.1549631
YAL018C	*LDS1*	Yes	7.74330347	8.46398493
YNL318C	*HXT14*	Yes	7.10954801	7.29750622
YOR255W	*OSW1*	Yes	6.96771944	6.83022686
YLR308W	*CDA2*	Yes	6.73977733	9.03014437
YCL048W	*SPS22*	Yes	5.87846754	6.84514553
YGL015C	*YGL015C*	Yes	5.80868867	5.70052717
YGR059W	*SPR3*	Yes	5.73699728	5.63787001
YFL011W	*HXT10*	Yes	5.49832694	6.58282514
YDL114W	*YDL114W*	Yes	4.88554014	5.16585212
YML047C	*PRM6*	No	4.8810314	4.52515555
YBR045C	*GIP1*	Yes	4.81376051	5.2999236
YLR307W	*CDA1*	Yes	4.15176184	4.71509079
YOR313C	*SPS4*	Yes	4.04012792	4.20217362
YJL037W	*IRC18*	Yes	4.00644634	4.59991583
YDR522C	*SPS2*	Yes	3.90337152	4.95521104
YPL187W	*MF(ALPHA)1*	No	3.89994762	5.34728765
YPL027W	*SMA1*	No	3.86103574	3.70694517
YPL033C	*SRL4*	Yes	3.79549523	4.41343906
YPR078C	*YPR078C*	Yes	3.70313031	4.57547267
YOL132W	*GAS4*	No	3.67255654	4.49589877
YBR180W	*DTR1*	Yes	3.66183771	4.81769853
YER106W	*MAM1*	No	3.51045684	3.37818082
YFR023W	*PES4*	Yes	3.4563884	3.48055028
YOR214C	*SPR2*	Yes	3.37589629	3.60789419
YFR032C	*RRT5*	Yes	3.35813196	3.8801637

Table 2.1: Sum1 Depletion Responsive Gene Targets (continued)

Systematic ID	Gene	ChIP Peak	log2FC_15min	log2FC_30min
YOL047C	*LDS2*	Yes	3.25526908	3.73409999
YDR218C	*SPR28*	Yes	3.25410646	3.28706436
YER085C	*YER085C*	No	3.18950305	3.63658352
YCL048W-A	*YCL048W-A*	Yes	3.18616127	4.33763693
YKR034W	*DAL80*	No	2.958498	3.44676378
YJL043W	*YJL043W*	Yes	2.90825637	4.02517829
YBR040W	*FIG1*	No	2.85728979	3.09676285
YLR411W	*CTR3*	Yes	2.76341175	2.75984486
YBR076W	*ECM8*	Yes	2.75994554	3.11630223
YGR256W	*GND2*	Yes	2.73877926	3.1261751
YHR184W	*SSP1*	Yes	2.60875572	3.01591154
YJR078W	*BNA2*	Yes	2.59953099	2.70511308
YBR117C	*TKL2*	No	2.57171601	2.85867399
YPR192W	*AQY1*	Yes	2.55459849	2.97945115
YIR027C	*DAL1*	Yes	2.48666829	2.9671148
YKL178C	*STE3*	Yes	2.46108617	2.69226002
YMR244W	*YMR244W*	Yes	2.45299604	3.47808862
YOR298W	*MUM3*	Yes	2.44840277	2.35163346
YGR273C	*YGR273C*	No	2.44832806	4.64492893
YGR225W	*AMA1*	No	2.41908522	1.89108197
YOR365C	*YOR365C*	Yes	2.33602428	2.61824844
YOR388C	*FDH1*	No	2.3232204	3.49382412
YJL045W	*SDH9*	Yes	2.29131751	2.77334459
YFL012W	*YFL012W*	No	2.29063223	3.30760855
YLR307C-A	*DPA10*	Yes	2.28650926	2.16065887
YHR015W	*MIP6*	Yes	2.23859112	2.26158312
YOR071C	*NRT1*	Yes	2.08242435	2.70341417
YKR015C	*YKR015C*	Yes	2.06188506	3.03255066
YLR054C	*OSW2*	No	2.00248888	2.61300037
YGL170C	*SPO74*	Yes	1.95117149	2.28989925
YDL186W	*YDL186W*	Yes	1.89875819	2.14712719
YMR232W	*FUS2*	Yes	1.86139667	2.33866923
YOL091W	*SPO21*	No	1.84188438	1.91534477
YFL040W	*YFL040W*	No	1.80557285	2.36706973
YGR260W	*TNA1*	Yes	1.75225062	2.52170156
YIL117C	*PRM5*	Yes	1.72491302	2.49517832

Table 2.1: Sum1 Depletion Responsive Gene Targets (continued)

Systematic ID	Gene	ChIP Peak	log2FC_15min	log2FC_30min
YPL272C	*PBI1*	Yes	1.70867372	1.72945804
YKR106W	*GEX2*	Yes	1.67384935	2.04926673
YBL098W	*BNA4*	No	1.6726407	1.73588256
YJL038C	*LOH1*	Yes	1.66492064	2.06605223
YIR028W	*DAL4*	Yes	1.63096436	2.15757218
YCL073C	*GEX1*	No	1.61381861	2.43215767
YBR147W	*RTC2*	Yes	1.61188337	1.66978868
YGR144W	*THI4*	No	1.52681094	1.83440884
YBR148W	*YSW1*	Yes	1.47198359	1.64080231
YEL023C	*YEL023C*	Yes	1.45009287	1.56833096
YDR042C	*YDR042C*	No	1.44214176	1.49550593
YPR054W	*SMK1*	Yes	1.44148089	1.61912828
YEL065W	*SIT1*	No	1.38803999	2.11029566
YIL037C	*PRM2*	No	1.36098036	1.50129314
YLR213C	*CRR1*	Yes	1.3476099	1.77716142
YNL202W	*SPS19*	Yes	1.33934153	2.11230671
YJR025C	*BNA1*	Yes	1.33834663	1.90084693
YLR136C	*TIS11*	Yes	1.32985095	1.31032393
YOR177C	*MPC54*	No	1.32208598	1.89543595
YBR250W	*SPO23*	No	1.31801066	1.48313186
YNL128W	*TEP1*	No	1.2909779	1.46974052
YNL279W	*PRM1*	No	1.27686011	1.72549238
YDR281C	*PHM6*	Yes	1.27594393	1.10238604
YML066C	*SMA2*	Yes	1.26332144	1.48072854
YOL015W	*IRC10*	Yes	1.2590172	1.44298034
YMR096W	*SNZ1*	Yes	1.22797336	1.88340716
YCL027W	*FUS1*	No	1.20395397	2.11354805
YLL005C	*SPO75*	Yes	1.09791193	1.48080493
YNL204C	*SPS18*	Yes	1.07038598	1.51642447
YOL101C	*IZH4*	Yes	1.02971529	1.37062972
YCL021W-A	*YCL021W-A*	No	1.02525878	1.05953777
YEL057C	*SDD1*	Yes	0.97683677	1.13972161
YOR190W	*SPR1*	Yes	0.95061882	1.45825059
YDL079C	*MRK1*	No	0.93892368	1.12767396
YNL018C	*YNL018C*	Yes	0.91243221	0.43840105

Table 2.1: Sum1 Depletion Responsive Gene Targets (continued)

Systematic ID	Gene	ChIP Peak	log2FC_15min	log2FC_30min
YLR341W	*SPO77*	Yes	0.90821863	0.87648286
YGL146C	*RRT6*	Yes	0.88097279	0.82878194
YFL030W	*AGX1*	Yes	0.84147753	1.47786562
YLR231C	*BNA5*	Yes	0.79851572	1.09092999
YOR242C	*SSP2*	No	0.76090302	0.92876112
YAL067C	*SEO1*	No	0.74848519	1.09416433
YLR040C	*AFB1*	No	0.73519801	1.11768216
YIL119C	*RPI1*	Yes	0.68843905	0.98770665
YLR233C	*EST1*	Yes	0.67562672	0.72494321
YCR105W	*ADH7*	Yes	0.66231273	0.78797328
YDR185C	*UPS3*	Yes	0.6586062	0.89265611
YLR004C	*THI73*	No	0.65014341	0.83351595
YPR124W	*CTR1*	Yes	0.62755004	0.79054184
YAL037W	*YAL037W*	No	0.62498373	1.04187006
YPL092W	*SSU1*	No	0.6234826	0.86643353
YDR534C	*FIT1*	Yes	0.54248018	1.00415654
YGL032C	*AGA2*	No	0.53308761	1.55589186
YMR058W	*FET3*	No	0.53280883	0.59054265
YNR015W	*SMM1*	Yes	-0.5135012	-0.2869013
YGL029W	*CGR1*	No	-0.5250006	-0.3407487
YOR287C	*RRP36*	No	-0.6557722	-0.292088
YJR129C	*EFM3*	No	-0.67573	-0.2638374
YDL213C	*NOP6*	No	-0.6843482	-0.3999018
YIL064W	*EFM4*	Yes	-0.6849325	-0.2688118
YIR026C	*YVH1*	No	-0.6923913	-0.2705133
BIO6	*BIO6*	No	-0.7622129	-0.7052729
YLR103C	*CDC45*	No	-1.0228811	-0.6806373

To identify potential candidates involved in regulating *UME6* transcript levels we sought to better define the Sum1 regulon. For this we looked at differentially expressed genes (DEGs; see Materials and Methods for details). Our analysis resulted in a list of 124 Sum1-responsive genes (Figure 5.4A; Table 2.1). Analysis of these 124 Sum1-responsive genes by ChIP-Seq showed 64.5% (80/124) contained a detectable Sum1 ChIP peak representing bona fide Sum1 targets (Table 2.1). Further inspection of these 124 Sum1-responsive genes showed many were derepressed rapidly, within 15 min

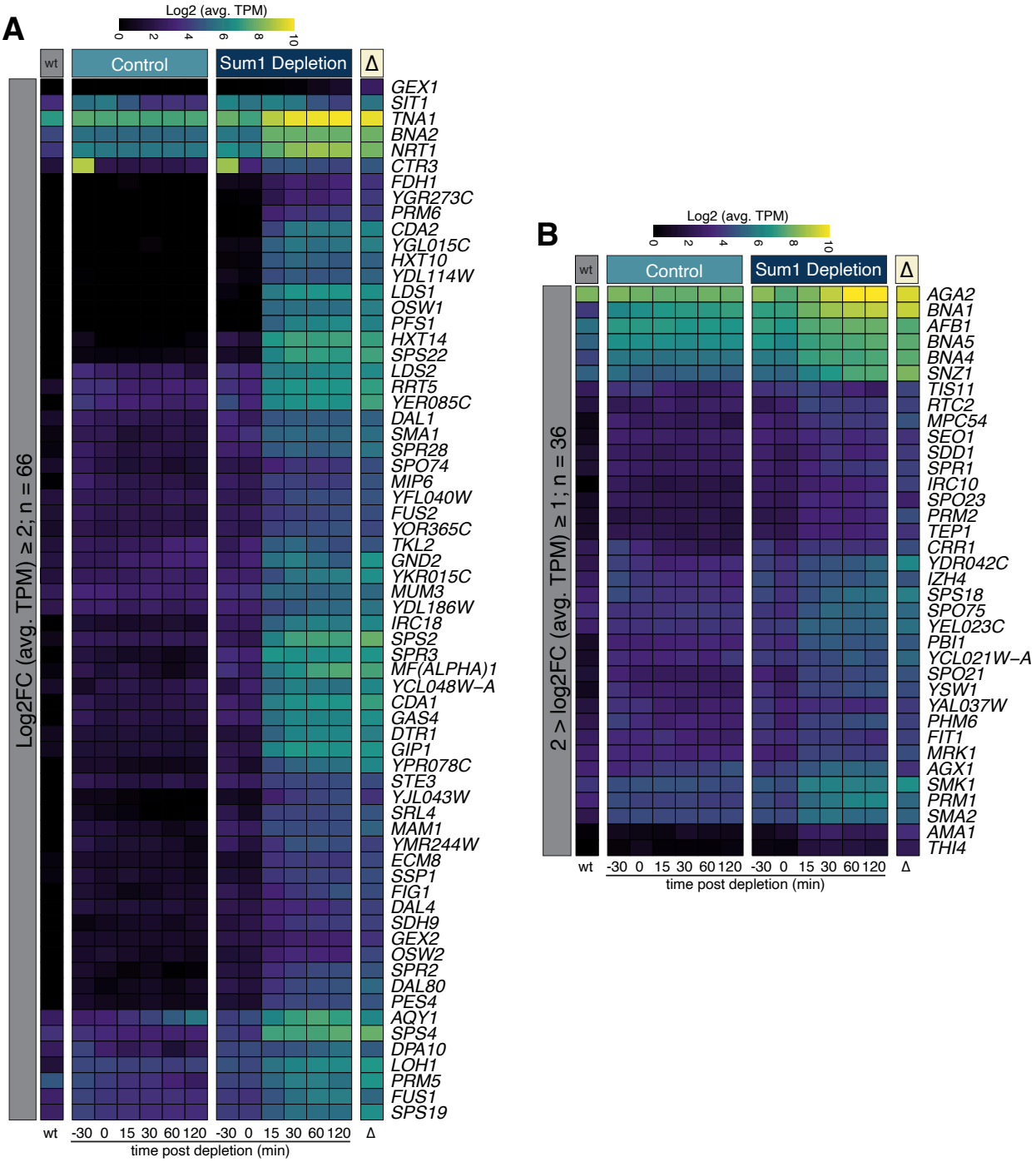

Figure 5.5: Subset of Sum1-AID depletion responsive genes that show greater log2FC. A heatmap as in Figure 5.4 highlighting a subset of DEGs that showed the greatest response to Sum1 depletion at t = 30min. This resulted in (A) 66 DEGs with a log2FC ≥ 2 (avg. TPM) and (B) 36 DEGs with a log2FC ≥ 1 and < 2.

following auxin administration, with 102/124 (82.3%%) having a log2FC ≥ 1. Indeed, this heightened expression was maintained in all 102 Sum1-responsive genes even at 30 min

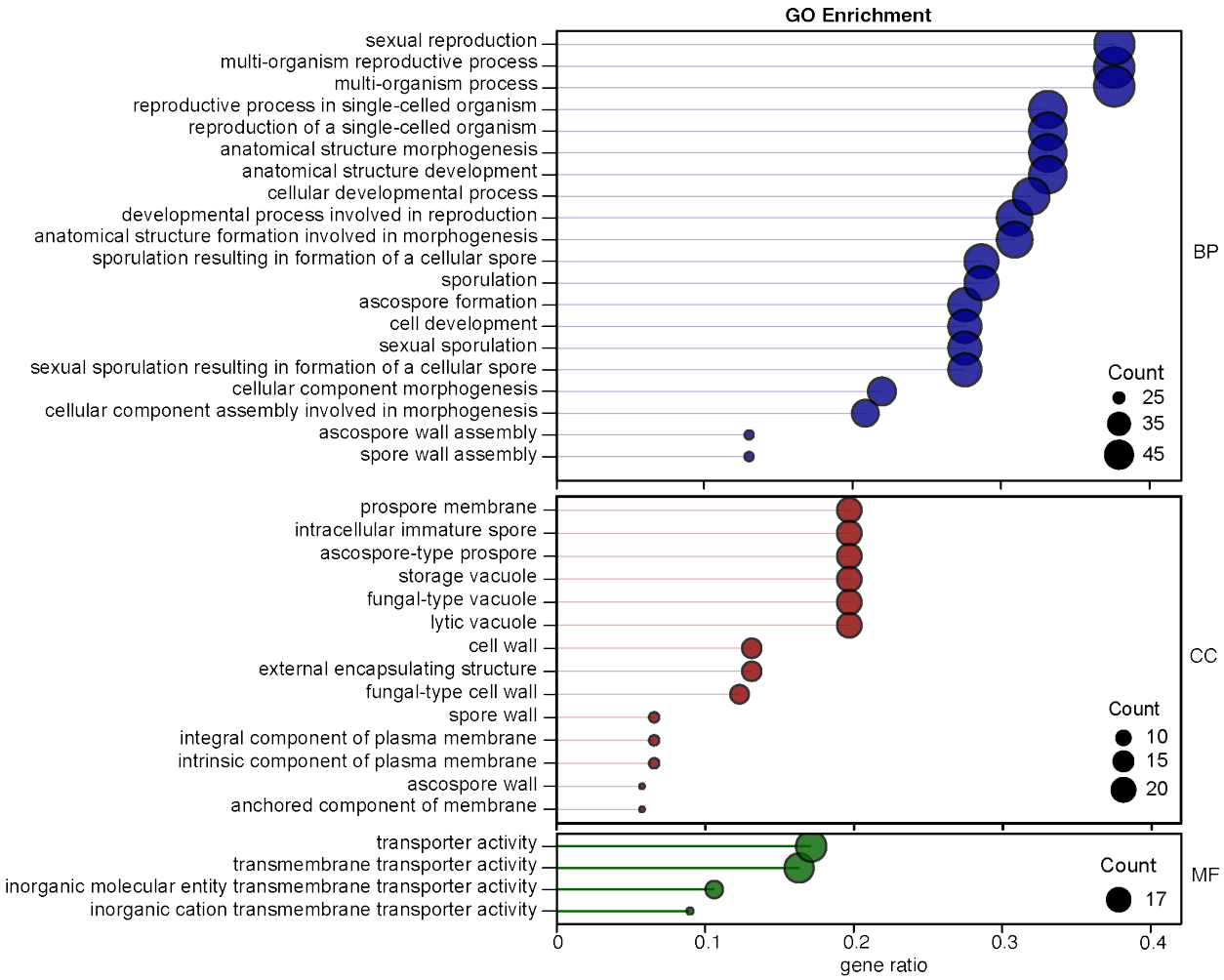

Figure 5.6: GO enrichment plot for Sum1-AID depletion responsive genes during mitotic growth. GO enrichment analysis of the 124 DEGs that responded to Sum1 depletion. The gene ratio is shown on the x-axis and is the percent of genes in a given GO term out of the total 124 genes total. Point size denotes the number of genes in that GO term and color signifies category: KEGG, KEGG pathway database; BP, biological process; CC, cellular component; MF, molecular function.

(Figure 5.5A and 6.5B). Analysis of these 124 Sum1-responsive genes by GO enrichment analysis showed several terms associated with spore wall formation and cellular morphogenesis (Figure 5.6A). This is consistent with Sum1's regulation of middle meiotic genes, which themselves coordinate large scale changes to cellular architecture.

Finally, we compared our list of Sum1-AID responsive genes to both the Ndt80 targets list from Cheng et al. 2018 and our own *sum1*Δ list derived from RNA-seq and differential expression analysis (Figure 5.7A; Table 2.2). We find that 50.8% (63/124) of our Sum1-AID responsive genes are present in both the Ndt80 target and *sum1*Δ lists,

Table 2.2: *sum1*Δ Responsive Genes During Mitotic Growth

Systematic Name	Gene	log2FoldChange
YFL012W	*YFL012W*	9.835749
YGL138C	*YGL138C*	9.092121
YLR308W	*CDA2*	8.835346
YJL037W	*IRC18*	8.421257
YNL318C	*HXT14*	8.342127
YHR185C	*PFS1*	8.305230
YCL048W	*SPS22*	7.690892
YDL007C-A	*YDL007C-A*	7.513718
YFL014W	*HSP12*	7.442100
YPL033C	*SRL4*	7.303449
YFL011W	*HXT10*	7.089335
YER085C	*YER085C*	7.063595
YLR307W	*CDA1*	7.002766
YGL015C	*YGL015C*	6.985166
YGR059W	*SPR3*	6.952356
YPL187W	*MF(ALPHA)1*	6.713385
YML047C	*PRM6*	6.565917
YDL114W	*YDL114W*	6.488742
YDR523C	*SPS1*	6.003551
YBR040W	*FIG1*	5.664922
YFR032C	*RRT5*	5.448345
YOR214C	*SPR2*	5.341461
YCL073C	*GEX1*	5.220872
YCL048W-A	*YCL048W-A*	5.188708
YLR054C	*OSW2*	5.060174
YJL045W	*SDH9*	4.986696
YGR294W/YBR301W	*YGR294W/YBR301W*	4.923790
YGR273C	*YGR273C*	4.818829
YBR180W	*DTR1*	4.793870
YKR015C	*YKR015C*	4.570697
YHR126C	*ANS1*	4.514358
YGL158W	*RCK1*	4.473098
YPL280W/YOR391C	*YPL280W/YOR391C*	4.396115
YPL280W/YOR391C	*YPL280W/YOR391C*	4.396115
YOR388C	*FDH1*	4.366542
YHR015W	*MIP6*	4.330636

Table 2.2: *sum1*Δ Responsive Genes During Mitotic Growth (continued)

Systematic Name	Gene	log2FoldChange
YLR327C	*TMA10*	4.265563
YGR043C	*NQM1*	4.167032
YGL230C	*YGL230C*	4.122333
YIR028W	*DAL4*	4.093127
YHR184W	*SSP1*	4.075236
YCL021W-A	*YCL021W-A*	4.069816
YOR071C	*NRT1*	4.037655
YNL195C	*YNL195C*	3.931426
YOR313C	*SPS4*	3.912557
YDL223C	*HBT1*	3.910780
YDR042C	*YDR042C*	3.910053
YOR177C	*MPC54*	3.787491
YIR039C	*YPS6*	3.751834
YEL039C	*CYC7*	3.675667
YIR027C	*DAL1*	3.651148
YDR070C	*FMP16*	3.627895
YNL202W	*SPS19*	3.479696
YHR087W	*RTC3*	3.444822
YNL160W	*YGP1*	3.417321
YPR192W	*AQY1*	3.408870
YML128C	*MSC1*	3.401150
YBR148W	*YSW1*	3.358264
YDL186W	*YDL186W*	3.330836
YGL205W	*POX1*	3.306405
YPR145C-A	*YPR145C-A*	3.290559
YOR134W	*BAG7*	3.289425
YPL281C/YOR393W	*YPL281C/YOR393W*	3.248084
YPL281C/YOR393W	*YPL281C/YOR393W*	3.248084
YGR225W	*AMA1*	3.228398
YJL144W	*ROQ1*	3.187905
YGL170C	*SPO74*	3.184007
YOR120W	*GCY1*	3.150451
YML100W	*TSL1*	3.136106
YGR087C	*PDC6*	3.096199
YGR234W	*YHB1*	3.090065
YNL093W	*YPT53*	3.085040
YOR365C	*YOR365C*	3.081685

Table 2.2: *sum1*Δ Responsive Genes During Mitotic Growth (continued)

Systematic Name	Gene	log2FoldChange
YPR160W	*GPH1*	3.074241
YOR289W	*YOR289W*	3.056209
YGL121C	*GPG1*	3.031686
YFR047C	*BNA6*	2.955008
YER121W	*YER121W*	2.948427
YMR090W	*YMR090W*	2.933263
YPL186C	*UIP4*	2.930254
YFL040W	*YFL040W*	2.909234
YGR248W	*SOL4*	2.883410
YJL089W	*SIP4*	2.819587
YML066C	*SMA2*	2.783818
YOR298W	*MUM3*	2.778085
YAL067C	*SEO1*	2.774843
YHR140W	*YHR140W*	2.762420
YML058W-A	*HUG1*	2.697571
YGR260W	*TNA1*	2.697485
YDL130W-A	*STF1*	2.689991
YER142C	*MAG1*	2.655968
YLR178C	*TFS1*	2.648790
YJL052W	*TDH1*	2.629013
YHL044W	*YHL044W*	2.624346
YNL335W/YFL061W	*YNL335W/YFL061W*	2.607997
YIL113W	*SDP1*	2.598452
YGR052W	*FMP48*	2.594370
YNL204C	*SPS18*	2.591293
YER037W	*PHM8*	2.588134
YGL261C/YIL176C	*YGL261C/YIL176C*	2.551686
YDR403W	*DIT1*	2.547136
YPR054W	*SMK1*	2.536914
YFL060C/YNL334C	*YFL060C/YNL334C*	2.476675
YEL023C	*YEL023C*	2.469181
YIL160C	*POT1*	2.464269
YNL128W	*TEP1*	2.454058
YNL274C	*GOR1*	2.442240
YAL061W	*BDH2*	2.423740
YFL054C	*AQY3*	2.388998
YEL057C	*SDD1*	2.329969

Table 2.2: *sum1*Δ Responsive Genes During Mitotic Growth (continued)

Systematic Name	Gene	log2FoldChange
YHR138C	*YHR138C*	2.313343
YLR231C	*BNA5*	2.310824
YLL039C	*UBI4*	2.296056
YPL282C/YOR394W	*YPL282C/YOR394W*	2.295741
YPL282C/YOR394W	*YPL282C/YOR394W*	2.295741
YDR461C-A	*CMI8*	2.281769
YBR054W	*YRO2*	2.260001
YMR169C	*ALD3*	2.245955
YOL159C	*CSS3*	2.220624
YLR081W	*GAL2*	2.209053
YCL027W	*FUS1*	2.207019
YJR161C/YDL248W	*YJR161C/YDL248W*	2.199638
YBR147W	*RTC2*	2.176930
YDR216W	*ADR1*	2.174293
YPR151C	*SUE1*	2.154718
YCR005C	*CIT2*	2.138226
YGR008C	*STF2*	2.136015
YOR062C	*YOR062C*	2.113555
YNR014W	*YNR014W*	2.105990
YNR071C	*YNR071C*	2.073144
YDR248C	*YDR248C*	2.059690
YFR017C	*IGD1*	2.010799
YEL065W	*SIT1*	2.009887
YOL154W	*ZPS1*	2.004822
YKL163W	*PIR3*	2.002744
YBR132C	*AGP2*	1.972264
YHR139C	*SPS100*	1.947105
YBR183W	*YPC1*	1.923806
YNL270C	*ALP1*	1.888311
YAL037W	*YAL037W*	1.861546
YJL079C	*PRY1*	1.812282
YNL279W	*PRM1*	1.806554
YPL230W	*USV1*	1.801358
YDR281C	*PHM6*	1.783351
YIR032C	*DAL3*	1.782638
YLL005C	*SPO75*	1.762433
YLL055W	*YCT1*	1.752814

Table 2.2: *sum1*Δ Responsive Genes During Mitotic Growth (continued)

Systematic Name	Gene	log2FoldChange
YKL086W	*SRX1*	1.742966
YPR002W	*PDH1*	1.738227
YER045C	*ACA1*	1.734096
YIL087C	*AIM19*	1.731087
YOR317W	*FAA1*	1.722659
YLR408C	*BLS1*	1.721062
YLR036C/YIL089W	*YLR036C/YIL089W*	1.692521
YHR160C	*PEX18*	1.662499
YMR251W	*GTO3*	1.646731
YDR059C	*UBC5*	1.642517
YAR031W	*PRM9*	1.640777
YKL151C	*NNR2*	1.620810
YIL097W	*FYV10*	1.609409
YEL060C	*PRB1*	1.601584
YNL012W	*SPO1*	1.581272
YMR253C	*YMR253C*	1.579449
YNR064C	*YNR064C*	1.571766
YLR136C	*TIS11*	1.563696
YDR171W	*HSP42*	1.555022
YGL154C	*LYS5*	1.551913
YER079W	*YER079W*	1.526726
YDR273W	*DON1*	1.524709
YPL223C	*GRE1*	1.511103
YGR174C	*CBP4*	1.495596
YHL022C	*SPO11*	1.494427
YJL170C	*ASG7*	1.477349
YOR215C	*AIM41*	1.474110
YHR016C	*YSC84*	1.466271
YLR345W	*YLR345W*	1.460849
YJL132W	*YJL132W*	1.453663
YOR003W	*YSP3*	1.438382
YDR453C	*TSA2*	1.438126
YBR269C	*SDH8*	1.423108
YOL059W	*GPD2*	1.410409
YOL104C	*NDJ1*	1.399290
YMR195W	*ICY1*	1.396758
YJR109C	*CPA2*	1.395948

Table 2.2: *sum1*Δ Responsive Genes During Mitotic Growth (continued)

Systematic Name	Gene	log2FoldChange
YPR006C	*ICL2*	1.393706
YDR506C	*GMC1*	1.361992
YOL152W	*FRE7*	1.345721
YMR280C	*CAT8*	1.336564
YCR091W	*KIN82*	1.335322
YPR026W	*ATH1*	1.330504
YBR126W-A	*MEO1*	1.323710
YBL049W	*MOH1*	1.312133
YKL062W	*MSN4*	1.306264
YGL096W	*TOS8*	1.306245
YAL055W	*PEX22*	1.292825
YNR002C	*ATO2*	1.288886
YLR152C	*YLR152C*	1.287196
YBR063C	*CNM1*	1.286441
YIR031C	*DAL7*	1.261639
YMR244C-A	*COA6*	1.259126
YOR020W-A	*MCO10*	1.257794
YPL154C	*PEP4*	1.257121
YHR124W	*NDT80*	1.256012
YLR329W	*REC102*	1.233354
YKR098C	*UBP11*	1.224900
YOR044W	*IRC23*	1.221103
YPL258C	*THI21*	1.205142
YIR005W	*IST3*	1.198488
YGL062W	*PYC1*	1.184398
YPL092W	*SSU1*	1.182668
YPL265W	*DIP5*	1.176751
YKL096W	*CWP1*	1.176686
YKL103C	*APE1*	1.176570
YGR067C	*YGR067C*	1.171633
YIR029W	*DAL2*	1.158173
YCR020C	*PET18*	1.150496
YBR056W	*MRX18*	1.144524
YJL164C	*TPK1*	1.143882
YOL156W/YJL219W	*YOL156W/YJL219W*	1.138959
YOR036W	*PEP12*	1.137717
YJR094C	*IME1*	1.128625

Table 2.2: *sum1*Δ Responsive Genes During Mitotic Growth (continued)

Systematic Name	Gene	log2FoldChange
YPL087W	*YDC1*	1.126286
YML030W	*RCF1*	1.121803
YOR161C	*PNS1*	1.120529
YLR177W	*YLR177W*	1.117510
YJR008W	*MHO1*	1.117385
YJL213W	*YJL213W*	1.111599
YLR023C	*IZH3*	1.107482
YMR077C	*VPS20*	1.099546
YIL073C	*SPO22*	1.085832
YPL004C	*LSP1*	1.084774
YDR371W	*CTS2*	1.084706
YLR423C	*ATG17*	1.084167
YLR284C	*ECI1*	1.083144
YDL200C	*MGT1*	1.080925
YLR142W	*PUT1*	1.079286
YDL238C	*GUD1*	1.078040
YBR150C	*TBS1*	1.063275
YMR020W	*FMS1*	1.059222
YLR165C	*PUS5*	1.057628
YML129C	*COX14*	1.056324
YBR072W	*HSP26*	1.049271
YBR006W	*UGA2*	1.047484
YMR317W	*YMR317W*	1.046962
YIL156W-B	*MCO8*	1.042673
YIR025W	*MND2*	1.040156
YDR040C	*ENA1*	1.033431
YGR032W	*GSC2*	1.032023
YOR338W	*YOR338W*	1.025329
YKL053C-A	*MDM35*	1.025167
YDL115C	*IWR1*	1.021101
YCL067C	*HMLALPHA2*	1.016178
YBR026C	*ETR1*	1.012712
YOR226C	*ISU2*	1.011123
YMR188C	*MRPS17*	1.005344
YFR057W	*YFR057W*	1.003996
YMR252C	*MLO1*	1.002173
YGL134W	*PCL10*	1.000101

Table 2.2: *sum1*Δ Responsive Genes During Mitotic Growth (continued)

Systematic Name	Gene	log2FoldChange
YGR194C	*XKS1*	0.999493
YIL066C	*RNR3*	0.999236
YKL217W	*JEN1*	0.994891
YIR007W	*EGH1*	0.994221
YBR149W	*ARA1*	0.986941
YBR230C	*OM14*	0.977050
YDL139C	*SCM3*	0.975920
YEL005C	*VAB2*	0.974115
YDR540C	*IRC4*	0.970412
YBL059W	*IAI11*	0.966882
YHR210C	*YHR210C*	0.959512
YOL016C	*CMK2*	0.954009
YOR148C	*SPP2*	0.952979
YLR270W	*DCS1*	0.952743
YKL133C	*RCI50*	0.951706
YDL072C	*YET3*	0.950391
YDR223W	*CRF1*	0.948289
YBR145W	*ADH5*	0.946126
YPR168W	*NUT2*	0.943725
YLR356W	*ATG33*	0.942607
YER028C	*MIG3*	0.941138
YHR055C	*CUP1-2*	0.940185
YCR045C	*RRT12*	0.937910
YBR258C	*SHG1*	0.937583
YLR306W	*UBC12*	0.934651
YPR157W	*TDA6*	0.932919
YDL107W	*MSS2*	0.928102
YIL120W	*QDR1*	0.924949
YNL328C	*MDJ2*	0.920047
YEL059C-A	*SOM1*	0.918619
YGR129W	*SYF2*	0.918575
YLL057C	*JLP1*	0.917946
YAR033W	*MST28*	0.914327
YDL174C	*DLD1*	0.913694
YDR173C	*ARG82*	0.910073
YFR045W	*MRX20*	0.908711

Table 2.2: *sum1*Δ Responsive Genes During Mitotic Growth (continued)

Systematic Name	Gene	log2FoldChange
YDR032C	*PST2*	0.906317
YLL015W	*BPT1*	0.905878
YDR079C-A	*TFB5*	0.896090
YDR078C	*SHU2*	0.895719
YLR309C	*IMH1*	0.892985
YAL039C	*CYC3*	0.884390
YJR107W	*LIH1*	0.884060
YKL189W	*HYM1*	0.877811
YPL024W	*RMI1*	0.875795
YDR191W	*HST4*	0.872048
YCR097W	*HMRA1*	0.871666
YLR170C	*APS1*	0.868198
YMR114C	*YMR114C*	0.864302
YMR204C	*INP1*	0.863288
YPL206C	*PGC1*	0.858922
YDL183C	*MRX19*	0.857465
YDR263C	*DIN7*	0.856211
YBR137W	*YBR137W*	0.855053
YOL096C	*COQ3*	0.852574
YHR116W	*COX23*	0.851246
YMR263W	*SAP30*	0.849985
YDL194W	*SNF3*	0.848781
YMR137C	*PSO2*	0.847659
YOR077W	*RTS2*	0.845107
YER050C	*RSM18*	0.841466
YKR101W	*SIR1*	0.834806
YGR138C	*TPO2*	0.826561
YCL058W-A	*ADF1*	0.823841
YKL023W	*SKA1*	0.821922
YAL027W	*SAW1*	0.821762
YKL150W	*MCR1*	0.819028
YOR059C	*LPL1*	0.818287
YGL249W	*ZIP2*	0.810589
YER162C	*RAD4*	0.810402
YJL031C	*BET4*	0.802490
YHR038W	*RRF1*	0.798923

Table 2.2: *sum1*Δ Responsive Genes During Mitotic Growth (continued)

Systematic Name	Gene	log2FoldChange
YLR151C	*PCD1*	0.797772
YKL121W	*DGR2*	0.797572
YDL239C	*ADY3*	0.791697
YKL129C	*MYO3*	0.789008
YOR389W	*YOR389W*	0.785436
YDL199C	*YDL199C*	0.785266
YJL155C	*FBP26*	0.783146
YDL046W	*NPC2*	0.781077
YHR096C	*HXT5*	0.778465
YIR038C	*GTT1*	0.776767
YFL044C	*OTU1*	0.772582
YHR011W	*DIA4*	0.769671
YIR036C	*IRC24*	0.768469
YGR169C-A	*LSO2*	0.767257
YIL169C	*CSS1*	0.763812
YNL146W	*YNL146W*	0.763313
YDR244W	*PEX5*	0.761248
YGR097W	*ASK10*	0.758527
YER041W	*YEN1*	0.754802
YPR121W	*THI22*	0.753462
YOL009C	*MDM12*	0.752907
YLL063C	*AYT1*	0.750975
YLR119W	*SRN2*	0.744508
YDR479C	*PEX29*	0.743558
YFR055W	*IRC7*	0.740946
YDR286C	*MGP12*	0.740652
YOL155C	*HPF1*	0.739574
YCR014C	*POL4*	0.738614
YIR014W	*VLD1*	0.731973
YGL164C	*YRB30*	0.730017
YBL038W	*MRPL16*	0.724392
YGR127W	*YGR127W*	0.722253
YPL013C	*MRPS16*	0.718054
YPR047W	*MSF1*	0.717465
YLL056C	*YLL056C*	0.716163
YML050W	*AIM32*	0.711005
YLR453C	*RIF2*	0.709256

Table 2.2: *sum1*Δ Responsive Genes During Mitotic Growth (continued)

Systematic Name	Gene	log2FoldChange
YBR014C	*GRX7*	0.708116
YPL214C	*THI6*	0.707676
YDR079W	*PET100*	0.705492
YOR265W	*RBL2*	0.703408
YKL087C	*CYT2*	0.699217
YBR111C	*YSA1*	0.697370
YKR066C	*CCP1*	0.696982
YNL142W	*MEP2*	0.694869
YKL188C	*PXA2*	0.692977
YDR350C	*ATP22*	0.692913
YOL126C	*MDH2*	0.689722
YCR004C	*YCP4*	0.688977
YBR282W	*MRPL27*	0.688862
YLL029W	*FRA1*	0.687827
YER116C	*SLX8*	0.686291
YBR280C	*SAF1*	0.681761
YJR148W	*BAT2*	0.678806
YMR052W	*FAR3*	0.675283
YGL227W	*VID30*	0.675231
YKL039W	*PTM1*	0.670589
YJL068C	*YJL068C*	0.662866
YGR179C	*OKP1*	0.661938
YDR525W-A	*SNA2*	0.657469
YDR231C	*COX20*	0.657378
YBR043C	*QDR3*	0.654106
YDR316W	*OMS1*	0.652108
YIR042C	*YIR042C*	0.650538
YLR247C	*IRC20*	0.647916
YIL072W	*HOP1*	0.647079
YGR048W	*UFD1*	0.646428
YJR012C	*YJR012C*	0.644065
YOR357C	*SNX3*	0.642859
YGR197C	*SNG1*	0.639409
YAR023C	*YAR023C*	0.637577
YPL257W	*YPL257W*	0.637136
YDL086W	*YDL086W*	0.635011
YMR314W	*PRE5*	0.634706

Table 2.2: *sum1*Δ Responsive Genes During Mitotic Growth (continued)

Systematic Name	Gene	log2FoldChange
YDL099W	*BUG1*	0.631908
YLR286C	*CTS1*	0.631086
YOR158W	*PET123*	0.630609
YDR323C	*PEP7*	0.630247
YGL045W	*RIM8*	0.628144
YDR122W	*KIN1*	0.626639
YDR168W	*CDC37*	0.626427
YNL122C	*MRP35*	0.620260
YMR136W	*GAT2*	0.619695
YML110C	*COQ5*	0.613710
YER093C-A	*AIM11*	0.611903
YLR376C	*PSY3*	0.611829
YOR163W	*DDP1*	0.608725
YDR185C	*UPS3*	0.608447
YPR107C	*YTH1*	0.606589
YPR066W	*UBA3*	0.606296
YJR039W	*MLO127*	0.604184
YPL250C	*ATG41*	0.604043
YMR278W	*PRM15*	0.603631

while 40.3% (50/124) were uniquely overlapping with the *sum1*Δ, and 8.9% (11/124) were only identified in the Sum1-AID system. Interestingly, 17% (67/394) of the Ndt80 targets uniquely overlapped with *sum1*Δ. Upon closer inspection of these 67 genes, only *SPS1* and *HIM1* were found to be responsive to Sum1 depletion and were overlooked based on our criteria. Additionally, *SPO19* responded to Sum1 depletion, but its expression was delayed thus excluding it from our list. Overall, despite these few oversights, many of the remaining 64 genes found overlapping between the Ndt80 targets and *sum1*Δ list did not respond to Sum1 depletion. Finally, we note that 82.1% (823/1003) of the remaining genes responsive to *sum1*Δ were uniquely found in the *sum1*Δ list and likely represent the many pleiotropic effects that cells experience due to prolonged Sum1 removal.

Discussion:

Adapting the AID system to temporally deplete Sum1-AID was allow for conditional depletion of Sum1 during mitosis. Implementing this strategy yielded insights into both Sum1 targets and *UME6* regulation. Firstly, depletion of Sum1 during mitotic conditions dropped Sum1 levels to 14% after 15 min and specifically upregulated the middle meiotic

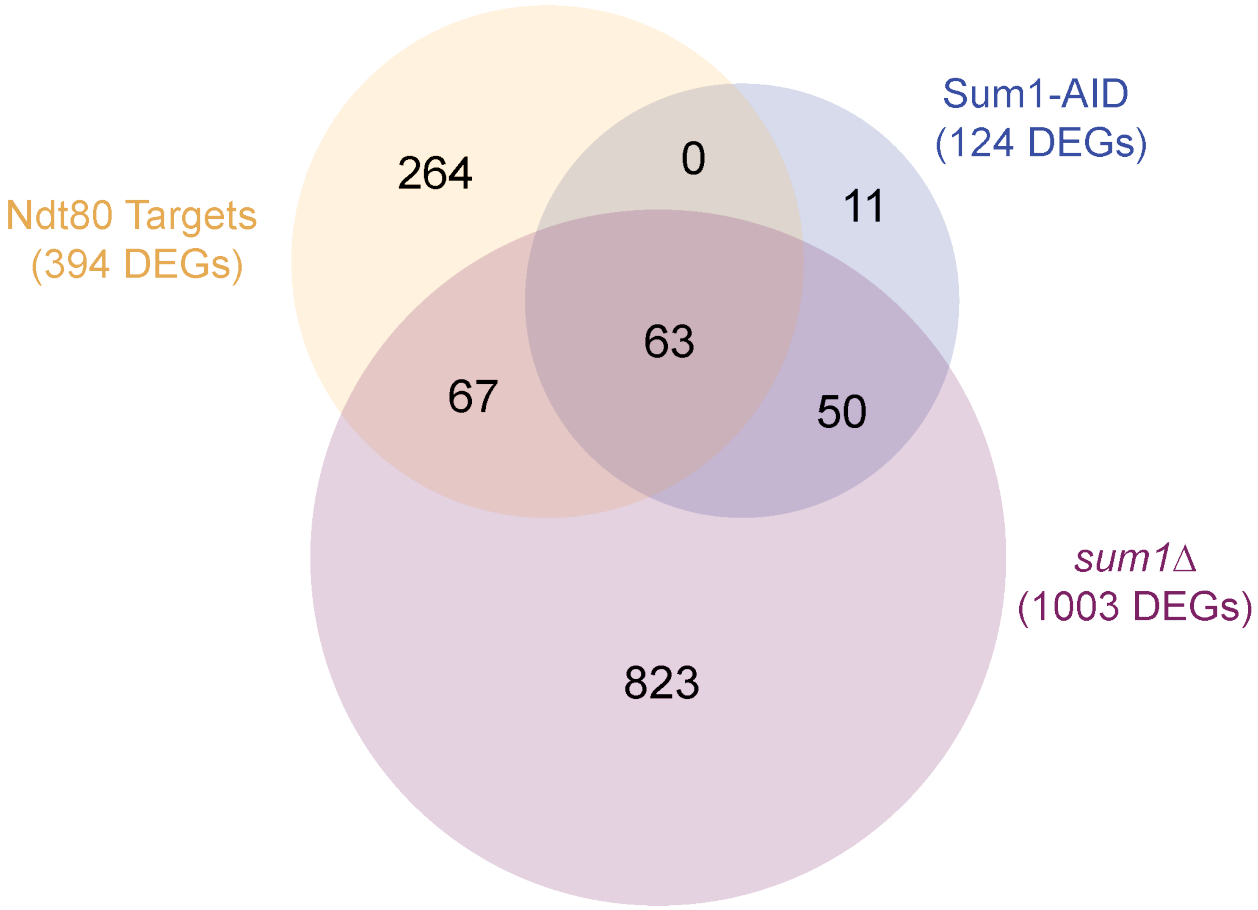

Figure 5.7: Overlap in Ndt80, Sum1-AID, and *sum1*Δ target lists by VennDiagram. Venn diagram of overlapping and non-overlapping differentially expressed genes for between Ndt80 targets (394 genes), Sum1-AID (124 genes), and *sum1*Δ (1003 genes). DESeq2 was used to compare WT and *sum1*Δ (padj < 0.05; Log2FC > 0.6) resulting in identification of 1003 DEGs.

genes *SMK1* and *DTR1*, which have been shown to be under Sum1 control (Hickman and Rusche 2007; Whinston et al. 2013). This depletion of Sum1 resulted in the concurrent downregulation of *UME6* transcripts. Despite *UME6* downregulation, repression over the early meiotic genes was still maintained presumably because the effect was minimal or Ume6 protein stability. Regardless, the drop in *UME6* transcripts was detectable allowing interrogation of *UME6* transcription regulation during mitotic growth. Furthermore, analysis of our Sum1-AID depletion dataset revealed 124 genes responded to Sum1 depletion and a ChIP peak was able to be identified in 80 of these genes indicating direct regulation. Comparison of this Sum1-AID list to an Ndt80 target list and *sum1*Δ list revealed 91.1% (113/124) were captured in these other lists. Strikingly, the *sum1*Δ list contained an additional 823 genes not found in either Sum1-AID or the Ndt80 targets. Many of these 823 genes unique to the *sum1*Δ list are metabolic or stress related in nature further justifying why *sum1*Δ strains are sick. Interestingly, the Ndt80 targets list contained an additional 264 genes. Whether these are unique to Ndt80, merely

meiosis specific, or a combination of both is unclear. However, our Sum1-AID system was able to recapitulate the effect of *UME6* downregulation observed during meiosis while also providing a shorter list of candidates that may be involved in this regulation. Thus, we believe our Sum1-AID system could prove useful in studying the middle meiotic downregulation of *UME6* transcripts.

Chapter 6

Appendix B: Materials and Methods

6.1 Strains and Plasmids

The strains for this study, listed in Table 6.1, are derivatives of the sporulation proficient SK1 strain background (Padmore et al. 1991). The following alleles for were derived from other studies: *pCUP-IME1* and *pCUP-IME4* (Berchowitz et al. 2013), *pGAL-NDT80* and *GAL4-ER* (Benjamin et al. 2003), *HTB1-mCherry* (Matos et al. 2008), *GFP-IME1* (Moretto et al. 2018), and LexA/*lexO* (Ottoz et al. 2014).

Gene tagging or deletion was carried out using a PCR-mediate one-step integration protocol described previously (Longtine et al. 1998; Janke et al. 2004) and the PCR products generated from plasmids in Table 6.2 using primers from Table 6.3.1.

Endogenous Ume6 was C-terminally tagged with three V5 epitopes (3V5) using plasmid pUB81 and Ume6 C-terminal tagging primers. A *UME6* degron allele was generated by C-terminally tagging endogenous Ume6 with an auxin-inducible degron (IAA7) and a 3V5 epitope from plasmid pUB763 using C-terminal tagging primers. To delete the *UME6* gene, the ORF was replaced by a HygBMX6 marker from plasmid pUB217 using *ume6*Δ primers. A plasmid containing *3V5-αGFP* for Ume6 tagging was generated as follows: a 3v5 PCR product from pUB84 was generated using 3v5 fragment primers. Along with this fragment, pUB1707 (gifted from Laura Lackner's Lab) was subjected to *HindIII* and *Sal1* digestion at 37˚ for 1h. Enzymatic inactivation was then carried out at 80˚C for 20min. Digested products were separated by gel electrophoresis on a 1% agarose gel in 1xTBE for 25min. Fragments were then excised and transferred from the gel to a 1.5ml Eppendorf tube where they were subjected to clean up using the QIAquick Gel Extraction Kit (QIAGEN) according to protocol. Plasmid was then constructed using an NEB T4 Ligase protocol (NEB – m0202L) and transformed into competent bacteria (DH5α) for amplification. Plasmid was collected using QIAquick Plasmid Kit (QIAGEN) and named pUB2441 (*3V5-αGFP*). To C-terminally tag endogenous Ume6, a *3V5-αGFP* fragment from pUB2441 was generated using Ume6 C-terminal tagging primers.

The LexA/*lexO* system, described previously (Ottoz et al. 2014), was exploited to control *OsTIR* expression (*4xlexO-osTIR*). Additionally, to increase *OsTIR* output during meiosis, an *8xlexO-osTIR* was cloned into a *HIS3* single integration vector by Gibson Assembly (Gibson et al. 2009). Fragments were generated using pUB817, pUB99, and pUB925, with primers for *OsTIR* Fragment, *HIS* Vector, and *8x-lexO* Fragment. Fragments were

then ligated according to the Gibson protocol outlined by New England BioLabs (NEB) to generate plasmid pUB2442. pUB1052 and pUB2442 were digested using *PmeI* at 37˚C for 1 h. Fragments for *lexA-GAL4AD* and 8x*lexO-osTIR* were then integrated at the *TRP1* and *HIS3* locus, respectively.

Table 6.1. Strains used in this study.

Strain	*Genotype*
UB13	*ho::LYS2 lys2 ura3 leu2::hisG his3::hisG trp1::hisG* ***(SK1 wild-type)***
UB95	*MAT***a***/MATalpha* *ndt80::pGAL-NDT80::TRP1/ndt80::pGAL-NDT80::TRP1;* *ura3::pGPD1-GAL4(848).ER::URA3/ura3::pGPD1-GAL4(848).ER::URA3*
UB3301	*MAT***a***;MATalpha;* *ime1::pCUP-IME1::HphMX/ime1::pCUP-IME1::HphMX;* *ime4::pCUP-IME4::NAT/ime4::pCUP-IME4::NAT;* *ume6::UME6-3V5::His3MX/ume6::UME6-3V5::His3MX*
UB17716	*MAT***a***; trp1::TRP1; his3::HIS3*
UB18216	*MAT***a***;* *ume6::UME6-IAA7-3V5::KanMX; trp1::TRP1; his3::HIS3*
UB18287	*MATa;* *ume6::UME6-IAA7-3V5::KanMX;* *trp1::pGPD1-LexA-ER-HA-B112::TRP1;* *his3::HIS3*
UB17646	*MAT***a***;* *ume6::UME6-IAA7-3V5::KanMX;* *trp1::pGPD1-LexA-ER-HA-B112::TRP1;* *his3::4xplexO-OsTIR1(ScOP)::HIS3*
UB17718	*MAT***a***;* *ume6::hygBMX ; trp1::TRP1; his3::HIS3*
UB19103	*MAT***a***/alpha;* *ime1::pCUP-IME1::NATMX/ime1::pCUP-IME1::NATMX;* *ime4::pCUP-IME4::NATMX/ime4::pCUP-IME4::NATMX;* *trp1::TRP1/trp1::TRP1;* *his3::HIS3/his3::HIS3*
UB19101	*MAT***a***/alpha;* *ime1::pCUP-IME1::NATMX/ime1::pCUP-IME1::NATMX;* *ime4::pCUP-IME4::NATMX/ime4::pCUP-IME4::NATMX;* *ume6::Ume6-AID-3v5::KanMX/ume6::Ume6-AID-3v5::KanMX;* *trp1::TRP1/trp1::TRP1;* *his3::HIS3/his3::HIS3*

UB19105	*MAT**a**/alpha;* *ime1::HygBMX/ime1::HygBMX;* *trp1::TRP1/trp1::TRP1; his3::HIS3/his3::HIS3*
UB24883	*MAT**a**;* *sum1::Sum1-3V5-IAA7-KanMX* *trp1::TRP1 (C. glabrata)* *his3::HIS3 (C. glabrata)*
UB24885	*MAT**a**;* *sum1::Sum1-3V5-IAA7-KanMX* *his3::pCup1-OsTIR1(codon optimized)::HIS3* *trp1::TRP1 (C. glabrata)*
UB25684	*MAT**a**;* *sum1::HygB* *trp1::TRP1 (C. glabrata)* *his3::HIS3 (C. glabrata)*
UB25688	*MAT**a**/alpha;* *ime1::pCUP-IME1::NATMX/ime1::pCUP-IME1::NATMX;* *ime4::pCUP-IME4::NATMX/ime4::pCUP-IME4::NATMX;* *ume6::UME6-IAA7-3V5::KanMX/ume6::UME6-IAA7-3V5::KanMX;* *trp1::pGPD1-LexA-ER-HA-GAL4(770-881)::TRP1/trp1::pGPD1-LexA-ER-HA-GAL4(770-881)::TRP1;* *his3::HIS3/his3::HIS3*
UB25092	*MAT**a**/alpha;* *ime1::pCUP-IME1::NATMX/ime1::pCUP-IME1::NATMX;* *ime4::pCUP-IME4::NATMX/ime4::pCUP-IME4::NATMX;* *ume6::UME6-IAA7-3V5::KanMX/ume6::UME6-IAA7-3V5::KanMX;* *trp1::pGPD1-LexA-ER-HA-GAL4(770-881)::TRP1/trp1::pGPD1-LexA-ER-HA-GAL4(770-881)::TRP1; his3::8xplexO-OSTIR1(ScOP)::HIS3/his3::8xplexO-OSTIR1(ScOP)::HIS3*
UB26621	*MAT**a**/alpha; ura3::URA3/ura3::URA3*
UB26637	*MAT**a**/alpha;* *ime1::sfGFP-IME1/ime1::sfGFP-IME1;* *ura3::URA3/ura3::URA3*
UB26625	*MAT**a**/alpha;* *ume6::UME6-3v5::KanMX/ume6::UME6-3v5::KanMX;* *ura3::URA3/ura3::URA3*
UB26641	*MAT**a**/alpha;* *ime1::sfGFP-IME1/ime1::sfGFP-IME1;* *ume6::UME6-3v5::KanMX/ume6::UME6-3v5::KanMX;* *ura3::URA3/ura3::URA3*

UB26629	*MAT**a**/alpha;* *ume6::UME6(T99N)-3v5::KanMX/ume6::UME6(T99N)-3v5::KanMX;* *ura3::URA3/ura3::URA3*
UB26645	*MAT**a**/alpha;* *ime1::sfGFP-IME1/ime1::sfGFP-IME1;* *ume6::UME6(T99N)-3v5::KanMX/ume6::UME6(T99N)-3v5::KanMX;* *ura3::URA3/ura3::URA3*
UB27313	*MAT**a**/alpha;* *ume6::UME6(T99N)-antiGFP(VH16)::URA3/ume6::UME6(T99N)-antiGFP(VH16)::URA3*
UB27243	*MAT**a**/alpha;* *ime1::sfGFP-IME1/ime1::sfGFP-IME1;* *ume6::UME6(T99N)-antiGFP(VH16)::URA3/ume6::UME6(T99N)-antiGFP(VH16)::URA3*
UB32574	*MAT**a**/alpha;* *ime1::HygBMX/ime1::HygBMX;* *his3::pIME1-IME1::HIS3/his3::pIME1-IME1::HIS3;* *ume6::UME6(T99N)-antiGFP(VH16)::URA3/ume6::UME6(T99N)-antiGFP(VH16)::URA3*
UB32572	*MAT**a**/alpha;* *ime1::HygBMX/ime1::HygBMX;* *his3::pIME1-sfGFP-IME1::HIS3/his3::pIME1-sfGFP-IME1::HIS3;* *ume6::UME6(T99N)-antiGFP(VH16)::URA3/ume6::UME6(T99N)-antiGFP(VH16)::URA3*
UB33044	*MAT**a**/alpha;* *ime1::HygBMX/ime1::HygBMX;* *his3::pIME1-SV40-GAL4(75-881)::HIS3/his3::pIME1-SV40-GAL4(75-881)::HIS3;* *ume6::UME6(T99N)-antiGFP(VH16)::URA3/ume6::UME6(T99N)-antiGFP(VH16)::URA3*
UB30293	*MAT**a**/alpha;* *ime1::HygBMX/ime1::HygBMX;* *his3::pIME1-sfGFP-SV40-GAL4(75-881)::HIS3/his3::pIME1-sfGFP-SV40-GAL4(75-881)::HIS3;* *ume6::UME6(T99N)-antiGFP(VH16)::URA3/ume6::UME6(T99N)-antiGFP(VH16)::URA3*

UB33048	*MAT**a**/alpha;* *ime1::HygBMX/ime1::HygBMX;* *his3::pIME1-SV40-B112::HIS3/his3::pIME1-SV40-B112::HIS3;* *ume6::UME6(T99N)-antiGFP(VH16)::URA3/ume6::UME6(T99N)-antiGFP(VH16)::URA3*
UB30295	*MAT**a**/alpha;* *ime1::HygBMX/ime1::HygBMX;* *his3::pIME1-sfGFP-SV40-B112::HIS3/his3::pIME1-sfGFP-SV40-B112::HIS3;* *ume6::UME6(T99N)-antiGFP(VH16)::URA3/ume6::UME6(T99N)-antiGFP(VH16)::URA3*
UB31727	*MAT**a**/alpha;* *ime1::HygBMX/ime1::HygBMX;* *his3::pIME1-sfGFP-SV40-GAL4(75-881)::HIS3/his3::pIME1-sfGFP-SV40-GAL4(75-881)::HIS3;* *ume6::UME6(T99N)-antiGFP(VH16)::URA3/ume6::UME6(T99N)-antiGFP(VH16)::URA3;* *htb1::HTB1-mCherry::HISMX6/htb1::HTB1-mCherry::HISMX6*
UB31729	*MAT**a**/alpha;* *ime1::HygBMX/ime1::HygBMX;* *his3::pIME1-sfGFP-SV40-B112::HIS3/his3::pIME1-sfGFP-SV40-B112::HIS3;* *ume6::UME6(T99N)-antiGFP(VH16)::URA3/ume6::UME6(T99N)-antiGFP(VH16)::URA3;* *htb1::HTB1-mCherry::HISMX6/htb1::HTB1-mCherry::HISMX6*
UB33625	*MAT**a**/alpha;* *ime1::HygBMX/ime1::HygBMX;* *his3::pIME1-sfGFP-IME1::HIS3/his3::pIME1-sfGFP-IME1::HIS3;* *ume6::UME6(T99N)-antiGFP(VH16)::URA3/ume6::UME6(T99N)-antiGFP(VH16)::URA3;* *htb1::HTB1-mCherry::HISMX6/htb1::HTB1-mCherry::HISMX6*
UB19103	*MAT**a**, ho::LYS2, lys2, ura3, leu2::hisG, his3::hisG, trp1::hisG* *MATalpha, ho::LYS2, lys2?, leu2::hisG, ura3, his3::hisG, trp1::hisG* *trp1::TRP1 (C. glabrata)/trp1::TRP1 (C. glabrata)* *his3::HIS3 (C. glabrata)/his3::HIS3 (C. glabrata)* *pCUP-IME1::NAT/pCUP-IME1::NAT* *pCUP-IME4::NAT/pCUP-IME4::NAT*

UB19101	*MAT**a**, ho::LYS2, lys2, ura3, leu2::hisG, his3::hisG, trp1::hisG* *MATalpha, ho::LYS2, lys2?, leu2::hisG, ura3, his3::hisG, trp1::hisG* *UME6-IAA7-3V5::KanMX/UME6-IAA7-3V5::KanMX* *trp1::TRP1 (C. glabrata)/trp1::TRP1 (C. glabrata)* *his3::HIS3 (C. glabrata)/his3::HIS3 (C. glabrata)* *pCUP-IME1::NAT/pCUP-IME1::NAT* *pCUP-IME4::NAT/pCUP-IME4::NAT*
UB19105	*MAT**a**, ho::LYS2, lys2, ura3, leu2::hisG, his3::hisG, trp1::hisG* *MATalpha, ho::LYS2, lys2?, leu2::hisG, ura3, his3::hisG, trp1::hisG* *ime1Δ::Hyg/ime1Δ::Hyg* *trp1::TRP1 (C. glabrata)/trp1::TRP1 (C. glabrata)* *his3::HIS3 (C. glabrata)/his3::HIS3 (C. glabrata)*
UB22812	*MAT**a**, ho::LYS2, lys2, ura3, leu2::hisG, his3::hisG, trp1::hisG* *MATalpha, ho::LYS2, lys2, ura3, leu2::hisG, his3::hisG, trp1::hisG* *ume6Δ::Hyg/ume6Δ::Hyg* *trp1::TRP1 (C. glabrata)/trp1::TRP1 (C. glabrata)* *his3::HIS3 (C. glabrata)/his3::HIS3 (C. glabrata)*
UB21877	*MAT**a**/MATalpha;* *ndt80::pGAL-NDT80::TRP1/ndt80::pGAL-NDT80::TRP1;* *ura3::pGPD1-GAL4(848).ER::URA3/ura3::pGPD1-GAL4(848).ER::URA3;* *ume6::UME6-3V5::HISMX/ume6::UME6-3V5::HISMX;* *htb1::HTB1-mCherry::HISMX6/htb1::HTB1-mCherry::HISMX6*
UB22674	*MAT**a**/MATalpha;* *ndt80::pGAL-NDT80::TRP1/ndt80::pGAL-NDT80::TRP1;* *ura3::pGPD1-GAL4(848).ER::URA3/ura3::pGPD1-GAL4(848).ER::URA3;* *ume6::UME6-3V5::HISMX/ume6::UME6-3V5::HISMX;* *cdc20:pCLB2-CDC20::KanMX/cdc20:pCLB2-CDC20::KanMX* *htb1::HTB1-mCherry::HISMX6/htb1::HTB1-mCherry::HISMX6*
UB11118	*MAT**a**/MATalpha;* *ndt80::pGAL-NDT80::TRP1/ndt80::pGAL-NDT80::TRP1;* *ura3::pGPD1-GAL4(848).ER::URA3/ura3::pGPD1-GAL4(848).ER::URA3;* *htb1::HTB1-mCherry::HISMX6/htb1::HTB1-mCherry::HISMX6*

Table 6.2. Plasmids used in this study.

Plasmid Name	Description
pUB1305	pL245-3V5-IAA17
pUB84	pFA6a-3V5(SCop)-kanMX6
pUB99	pNH603-pGPD1

pUB217	pFA6a-hphNT1
pUB763	pFA6a-IAA7-3V5-KanMx6
pUB817	pMJ983
pUB925	pL399
pUB2441	3v5-GFP NanoBody (VH16)–CaURA3
pUB2442	8xLexO-osTIR(ScOP)-HIS3
pUB2443	pIME1-sfGFP-SV40-B112-HIS3
pUB2444	pIME1-sfGFP-linker-IME1-HIS3
pUB2445	pIME1-IME1-HIS3
pUB2446	pIME1-SV40-B112-HIS3
pUB2448	UME6(T99N)-294-314-gRNA2

Table 6.3. Primers.

Table 6.3.1: Deletion and C-terminal tagging		
Construct name	**Forward primer**	**Reverse primer**
Ume6 C-terminal Tagging: Ume6-3v5 Ume6-IAA7-3v5 Ume6^{T99N}-3v5 Ume6^{T99N}-3v5-aGFP UB2849/ UB2850:	5’AAAAACAAAAGAGGCCAAAAGAAGAGCAATGAAAAAAAAA**CGGATCCCCGGGTTAATTAA**3’	5’ATAATAATAATAACAATATCTCTTTTTTTTTTTTTCAGTGGAATT**CGAGCTCGTTTAAAC**3’
ume6Δ UB5676/ UB5677:	5’ACCGCACTCAAACCATTTGCATGGACCTTAACTCACG**CGGATCCCCGGGTTAATTAA**3’	5’ATAGTAACAATATCTCTTTTTTTTTTTTTCAGTGAGCTT**CACTAGTGGATCTGATATCATCG**3’
UME6^{T99N} Repair Template pUB6001/ pUB6002	5’CTATTATGAAATCGACATGTGCGCCCAACAACAATCCTGTGCATACTCCGTCTGGTTCGC3’	5’TTTGGACTTTCAAACTCGGCGAACCAGACGGAGTATGCACAGGATTGTTGTTGGGCGCAC3’

UME6^{T99N} gRNA pUB5999/ pUB6000	5'AAACTGCATACTCCGTCTGGTTCG3'	5'GACTCGAACCAGACGGAGTATGCA3'
3V5 Fragment pUB10419/ pUB10420:	5'AGAACGCGGCCGCCAGCTGAAGCTTCGTACCGGATCCCCGGGTTAATTAA3'	5'AGCACCGTCACCGATCCGTCGACCTGCAGCAGCGGTTGAATCTAAACCTA3'
pUB969 Vector Amplification pUB10421/ pUB3699:	5'CCCTCCATCCGCGGCCGCTACAAAGCCGAATCCACCACGG3'	5'GCCACCGCGGTGGAGCTCTAAGC3'
pIME1 Fragment pUB10422/ pUB10423	5'TTCGGCTTTGTAGCGGCCGCGGATGGAGGGTTGGCATAAAAATG3'	5'CCTGCAGCGTACGCATCCCGGGTTTGTTTGTGGGGAGAGGAATAG3'
sfGFP Fragment pUB10424/ pUB10425:	5'CTATTCCTCTCCCCACAAACAAACCCGGGATGCGTACGCTGCAGGTC3'	5'TCCACCGCGGTGGCTCGAGTCCCTTATAAAGCTCGTCCAT3'
SV40-NLS-B112 (sfGFP) Fragment pUB10428/ pUB10429	5'AAGGGACTCGAGATGCCCAAGAAAAAGCGCAAGGTAGAATTTCCAGGTATTACTTTGAG3'	5'TATTTGCTTAGAGCTCCACCGCGGTGGTTAAAGCTTGAAACACAAATCAG3'
SV40-NLS-B112 Fragment pUB10430/ pUB523	5'CCACAAACAAACCCGGGATGCCCAAGAAAAAGCGC3'	5'CGCACTCACGTAAACACTTAATC3'
sfGFP-IME1 Fragment pUB10425/ pUB10432	5'TCCACCGCGGTGGCTCGAGTCCCTTATAAAGCTCGTCCAT3'	5'AGAGCTCCACCCTCGAGTTAAGAATAGGTTTTACTAAACTTGTAGGATATTTCTTG3'
IME1 Fragment pUB10431/	5'CAAACAAACCCGGGATGCAAGCGGATATGCATGG3'	5'AGAGCTCCACCCTCGAGTTAAGAATAGGTTTTACTAAACTTGTAGGATATTTCTTG3'

pUB10432		
OsTIR Fragment pUB3870/ pUB4098	5'TATCAAGCTTATGACTTATTTTCCTGAAGAAG3'	5'GAGCTCCACCTCATAAAATCTTGACGAAGTTAGG3'
HIS Vector pUB10421/ pUB4099	5'CAAAGCCGAATCCACCACGG3'	5'GATTTTATGAGGTGGAGCTCTAAGCAAATAGC3'
8x-LexO Fragment pUB3915/ pUB3869	5'CCGTGGTGGATTCGGCTTTGAATAATATATAAACCTGTATAATATAACCTTG3'	5'AATAAGTCATAAGCTTGATATCGAATTCC3'

Table 6.3.2: qPCR Primers		
UME6 ORF pUB7051/ pUB7052	5'CGCGGTGAAGACCCGTTTGC3'	5'CGGTGGAGGTGGTGGGATGT3'
NDT80 ORF pUB172/ pUB173	5'TCTATACAACCGCCCAGCTC3'	5'GACACAAAATGGAGGGCAAT 3'
IME2 ORF pUB415/ pUB416	5'TGCCTCTTTAGGCGATTCGT3'	5'GCTCGAACTTTTCCCGTGATT3'
PFY1 ORF pUB3301/ pUB3302	5'ACGGTAGACATGATGCTGAGG3'	5'ACGGTTGGTGGATAATGAGC3'
pZIP1 pUB10433/ pUB10434	5'ACTGCAAGTCTCTGAAAGTTTTAGCTG3'	5'TTCTCTAAAAATTTAGCCGCCGAGG3'
pSPO13 pUB10435/ pUB10436	5'GAGAAATAGCCGCCGACAAAAAGG3'	5'GTGCCATAATTATTCTCGACTCAACTTCAATC3'

pIME2 pUB1217/ pUB1218	5'CCAAATACGCTTTTTAAACTTGG3'	5'CTCAAATAGCCGCCGTAAC3'
pNUF2 pUB140/ pUB462	5'GAACGCTGATATACTCGACTAAC3'	5'GTCGCTGCGTATTCAGCGTA3'

Rescuing of *ime1*Δ using the heterologous activation domain (AD) B112 was achieved by constructing integration plasmids containing the full *IME1* promoter and either tagged or untagged B112. As a vector, pUB969 was amplified with pUB969 Vector Amplification primers. The fragment for *pIME1* was amplified with *pIME1* Fragment primers. Length of the *IME1* promoter was decided using Moretto et al. 2018 and ensuring both *IRT1* and *IRT2* (-2314 bp from *IME1* AUG) were included. This was done to recapitulate *IME1* transcriptional regulation and restrict AD expression to meiotic conditions. The fragment for *GFP* was amplified using *GFP* Fragment primers. A fragment for B112 with homology to *GFP* and containing the *SV40 NLS* sequence was amplified using *SV40-NLS-B112 (GFP)* Fragment primers from pUB1054. Plasmids were digested, ligated, and collected as described by the NEB protocol. Sequences were validated by PCR and sequencing and named pUB2443. The plasmid for B112 lacking *GFP* were produced using pUB2443 by first amplifying B112 using primer *SV40-NLS-B112* Fragment primers. Then, parent plasmids and fragments were digested using *XmaI* and *SacI* at 37˚C for 1h before enzymes were heat inactivated at 80˚C for 20min. Vector and inserts were then ligated according to the NEB protocol for the T4 ligase reaction before being named pUB2446. Single integration vectors for *IME1* were constructed in a similar way. *IME1* and *GFP-IME1* fragments were amplified from genomic DNA using primer *GFP-IME1* or *IME1* Fragment primers, respectively. Plasmid pUB2443, along with *IME1* and *GFP-IME1* fragments were digested using *XmaI* and *SacI* at 37˚C for 1h before heat inactivation at 80˚C for 20min. Fragments were then ligated using T4 Ligase according to the NEB protocol before being named pUB2444 (*pIME1-GFP-linker-IME1-HIS3*) or 2446 (*pIME1-IME1-HIS3*). All plasmids were sequence verified.

Ume6^{T99N} was created using a similar Cas9-based method to a previously published protocol (Sawyer et al. 2019). gRNA primers detailed in Table 6.3.1 were inserted into a centromeric plasmid (pUB1305) carrying a *URA3* marker and *pPGK1-dCas9* to generate pUB2447 and pUB2448. These plasmids were co-transformed into yeast with Ume6^{T99N} Repair Template primers to introduce the missense mutation, T99N (ACT to AAT). The plasmid was sustained on SC-ura plate for selection and successful transformants were then transferred to nutrient rich plates to lose the plasmid.

6.2 Growth Conditions

Mitotic Ume6 Depletion: For mitotic depletion assays, cells with wild-type *UME6* (WT), *UME6* null allele (*ume6*Δ), and *UME6-AID-3V5; lexA-ER-B112* strains with and without *p4xlexO-OsTIR*, were first grown in YPD (1% yeast extract, 2% peptone, 2% glucose, 22.4 mg/L uracil, and 80 mg/L tryptophan) for ~24 h to reach saturation (OD_{600} ≥10). YPD cultures were then used to inoculate fresh YPD to OD_{600} = 0.2 and grown for ~3 h to log phase (OD_{600} ≥0.5). During log phase, a sample for WT and *ume6*Δ was taken. Then, induction of *TIR* was initiated as follows. *UME6-AID*; *lexA-ER-B112* cells with and without the *p4xlexO-OsTIR* allele had *ß*-estradiol added (40 nM). Cells were incubated for 30 min before 3-indoleacetic acid (auxin) was added (200 µM). However, Ume6-AID-3v5 depletion only occurred in TIR+ strains. During the time course, samples were collected for RNA and protein extraction at -30 (ß-estradiol addition), 0 (auxin addition), 15, 30, 60, and 120 min.

Mitotic Sum1 Depletion: For mitotic depletion assays, cells carrying wild-type *SUM1* (WT), *SUM1* null allele (*sum1*Δ), *SUM1-AID-3V5,* and *SUM1-AID-3V5; pCUP1-osTIR* strains, were grown in YPD overnight for ~24 h to reach saturation (OD_{600} ≥10). Saturated YPD cultures were then used to inoculate fresh YPD to OD_{600} = 0.2. These cultures were grown for ~3 h to log phase (OD_{600} ≥0.5). Samples for WT and *sum1*Δ were collected at the start of log phase. Then, induction of *TIR* was initiated as follows. *SUM1-AID-3V5* cells with and without *pCUP1-osTIR* were inoculated with CuSO4 (50 nM). Then, cells were incubated for 30 min before 3-indoleacetic acid (auxin) was added (200 µM). Only in cells containing the *pCUP1-osTIR* was Sum1-AID-3v5 depleted. During the time course, samples were collected for RNA and protein extraction at -30 (CuSO4 addition), 0 (auxin addition), 15, 30, 60, and 120 min.

Meiotic Synchronization: A general starvation-based method was used to sporulate cells. Briefly, cells were grown in YPD for ~24 h shaking at 275 rpm to reach saturation (OD_{600} ≥ 10). The YPD culture was then used to inoculate BYTA (1% yeast extract, 2% bacto tryptone, 1% potassium acetate, and 50 mM potassium phthalate) to OD_{600} = 0.25 and grown for 16-18 h at 30˚C to OD_{600} ≥ 5. These cells were then pelleted, washed with sterile water, and resuspended in sporulation (SPO) media (40mg Adenine Hemisulfate, 40 mg Uracil, 20 mg Histidine, 20 mg Leucine, 20 mg Tryptophan, 20g KOAc (2%) 0.02% raffinose, pH 7 in 1 L Arrowhead H_2O) to a density of OD_{600} = 1.85 and shaken at 30˚ C at 275 rpm for the remainder of the experiment. Sporulation efficiency was always checked under a light microscope ~24 h after shifting to SPO to determine the percentage of tetrads formed. For Figure 3.1-3.3 and 3.7-3.13, *pCUP1-IME1* and *pCUP1-IME4* system was used to synchronize meiotic entry as described previously (Berchowitz et al. 2013; Chia and van Werven 2016). The induction timing and expression levels of *IME1*

and *IME4* in this context have been previously characterized (Chia and van Werven 2016; Chia et al. 2021). Note that the use of *pCUP-IME1 pCUP-IME4* causes a reproducible increase in total expression for many EMGs analyzed at 2.5 h before dropping at 3 h (observable in the heatmaps and individual plots). Cells appear to then equilibrate. The cause of this fluctuation is unclear but has also been observed by other researchers in the lab.

For Figure 3.4-3.6, *NDT80* Block-Release system was used to synchronize progression into the meiotic divisions as described previously (Benjamin et al. 2003; Carlile and Amon 2008). The induction timing and expression level of *NDT80* in this context have been previously characterized (Benjamin et al. 2003). After 5 h in SPO, *ß*-estradiol (1µM final) was added to induce *NDT80* expression. During the time course, samples were collected for RNA and protein extraction just prior to *NDT80* induction (0 h), and 0.5, 1.0, 1.5, 2.0, 2.5, 3, 3.5, and 4 h following induction.

Meiotic Depletion: Strains carrying both *UME6-AID-3V5; lexA-ER-GAL4$^{770-881}$* with and without the *p8xlexO-OsTIR* allele were processed as described in "Meiotic Synchronization" with the following modifications. After 0.5 h in SPO, *ß*-estradiol (5nM final) and auxin (200 µM final) were added simultaneously. Ume6-AID-3v5 depletion occurred only in the strain carrying *p8xlexO-OsTIR*. After additional 1.5h (2h in SPO), copper (II) sulphate (50 µM final) was added to trigger *IME1* and *IME4* expression from *pCUP1* promoter to release cells into meiotic prophase. Throughout the time course, samples were collected for RNA and protein extraction: after transition to SPO (0.5 h), post Ume6-AID depletion (2 h), and post *IME1* and *IME4* induction (2.5, 3, 4.5, and 6 h). Note that the TIR+ strain used for the meiotic depletion experiments carries 8 *lexO* sites within the osTIR1 promoter and that both TIR+ (Ume6 depletion) and TIR- (control) strains contain the chimeric transcription factor LexA-ER-GAL4$^{770-881}$, instead of LexA-ER-B112, for triggering *osTIR1* expression in the presence of ß-estradiol. Furthermore, lower concentration of ß-estradiol (5 nM vs 40nM) was used to induce *osTIR* expression. These adjustments were necessary in order to avoid growth and sporulation defects in cells carrying *lexA-ER-GAL4$^{770-881}$*. As a result of these modifications, the extent of Ume6 depletion was less dramatic in meiotic cells compared to mitotic cells. Nevertheless, we still observed significant defects in EMG expression and sporulation efficiency, indicating that meiotic cells are highly sensitive to Ume6 levels.

6.3 Immunoblotting

For protein extraction from meiotic cultures, ~3.7 OD_{600} of cells were collected and resuspended in 5% TCA (w/v) . For mitotic cultures, ~ 1 OD_{600} of cells were collected. Samples were processed by centrifugation (1900 x g, 3 m, room temperature) and washed in TE50, pH 7.5 (50 mM Tris and 1 mM EDTA) and acetone before being dried

overnight at room temperature. Pellets were resuspended in protein breakage buffer (TE50, 2.75 mM dithiothreitol (DTT) supplemented with 1x cOmplete EDTA-free protease inhibitor cocktail [Roche]) and disrupted using a Mini-Beadbeater-96 (BioSpec). Lysates were then mixed with 50 µL of 3xSDS loading buffer (187.5 mM Tris, pH 6.8, 6% 2-mercaptoethanol, 30% glycerol, 9% SDS, and 0.05% bromophenol blue), incubated at 95˚C for 5 min to denature, and allowed to cool for at least 5 min before centrifugation at full speed for 5 min.

Proteins were separated by SDS-PAGE electrophoresis on a Bolt 4-12% Bis-Tris Plus Gel (Thermo Fisher Scientific) and then transferred onto a 0.45-µm nitrocellulose membrane in a Mini Trans-Blot Cell (Bio-Rad) containing 25 mM Tris, 192 mM glycine, and 7.5% methanol. Protein transfer was carried out using a Mini Trans-Blot Cell at a constant 180 mA (maximum, 70 V) for 3 h. Membranes were blocked at room temperature for 30 m using Odyssey Blocking Buffer (PBS; LI-COR Biosciences) before being incubated at 4˚C in Odyssey Blocking Buffer (PBS) containing mouse anti-V5 antibody (RRID: AB 2556564, R960-25; Thermo Fisher Scientific) at a 1:3000 dilution for detection of 3v5 tagged alleles of Ume6. Additionally, hexokinase Hxk2 was used as a loading control and detected using a rabbit anti-Hxk2 antibody (RRID: AB 219918, 1004159; Rockland) at a 1:10,000 dilution. Membranes were incubated at 4˚C for 16-18 h and primary antibody was removed. Membranes were then washed three times in 1x PBS (+0.01% Tween) shaking gently for 5 min at room temperature before being placed in the Odyssey Blocking Buffer (PBS) containing anti-mouse secondary antibody conjugated to IRDye 800CW at a 1:15,000 dilution (RRID: AB 621847, 926-32212; LI-COR Biosciences) and an anti-rabbit antibody conjugated to IRDye 680RD at a 1:15,000 dilution (RRID: AB 10956166, 926-68071; LI-COR Biosciences). Blots were washed again in PBS (+0.01% Tween-20) as before and imaged with an Odyssey CLx scanner (LI-COR Biosciences). Band intensities were quantified with the Image Studio software associated with the scanner.

6.4 Live-cell imaging

Using CellASIC ONIX Microfluidic Platform (EMD Millipore), SPO cultures (OD_{600} = 1.85) were sonicated briefly to avoid clumping and transferred to a microfluidic Y04D plate and loaded into chambers using a pressure of 8 psi for 5 sec. Subsequently, fresh conditioned sporulation media (filter-sterilized SPO from a meiotic culture at 30˚C 5 h into sporulation) was fed at a flow rate pressure of 2 psi for 24 h (King et al. 2019, 2022). The microfluidic Y04E plate was then loaded into an environmental chamber heated to 30˚C mounted on a DeltaVision Elite wide-field fluorescence microscope (GE Healthcare) with a PCO Edge sCMOS camera and operated by the associated softWoRx software. Images were acquired at 60x/1.5116n oil immersion Plan Apochromat objective at 30min intervals across 21.5 h. An image stack of 4 Z positions at a 1µm step size were acquired using

mCherry (10% Intensity; 25-ms exposure) and FITC (10% Intensity; 25-ms exposure) filter sets. These images were deconvolved in softWoRx software (GE Healthcare) with a 3D iterative constrained deconvolution algorithm (enhanced ratio) with 15 iterations. Once images were collected, Fiji was used to adjust brightness and contrast after images were stabilized with the Image Stabilizer plugin (Schindelin et al. 2012; Li 2008).

6.5 RT-qPCR

For meiotic cultures, OD_{600} ~3.7 of cells were collected. These samples were processed for total RNA first by centrifugation (2 m, 1900 g, 4˚ C). Supernatant was removed and cells were washed in nuclease-free water before being centrifuged again (1 min, 21000 g, 4˚ C). Water was removed from cell pellet and total RNA was isolated by combining acid-washed glass beads (Sigma Aldrich – G8772), 400 µL TES buffer (10 mM Tris pH 7.5, 10 mM EDTA, 0.5% SDS), and 400 µL acid phenol (0.1% w/v 8-hydroxyquinoline). The solution was shaken in a thermo mixer for 30 m at 65 ˚C at 1400 rpm and centrifuged (10 min, 21000 g, 4˚C). Roughly 325 µL of aqueous layer was transferred to 300 µL of chloroform and centrifuged (5 min, 21000 g, room temperature). Next, 250 µL of the aqueous layer was transferred to 400 µL of 100% isopropanol (supplemented w/ 50 µL 3M NaOAc), inverted ~10 times, and incubated for 16-18 h at 4˚C. RNA was then pelleted by centrifugation (20 min, 21000 g, 4 ˚C) and washed in 80% EtOH. The EtOH was removed, and pellets were dried for 30-40 min before being resuspended in nuclease-free water. 5 µg of purified total RNA was then treated with DNase (TURBO DNA-free kit, Thermo Fisher (MA, USA) according to manufacturer, and 4 µL (<1 µg) of DNase treated total RNA was then reverse transcribed into cDNA with the use of random hexamers (Superscript III Supermix, Thermo Fisher) according to manufacturer's instructions. cDNA was then quantified using the SYBR green mix (Life Technologies (CA, USA)) and measured using the Applied Biosystem StepOnePlus™ Real-Time PCR system (Thermofisher – 4376600). Signal for *IME2*, *NDT80*, *SPO13*, and *UME6* was measured using oligonucleotides outlined in Table 6.3.2. Signal was then normalized to *PFY1* for meiotic cultures.

6.6 Chromatin Immunoprecipitation

For chromatin immunoprecipitation (ChIP), meiotic culture (OD_{600} = ~ 50) was fixed in 1.0% v/v formaldehyde for ~20min at room temperature before quenching the reaction with 100mM glycine. Cell pellets were collected by centrifugation (3000 x g, 5min, 4˚C) and washed in cold PBS. Cell pellets were then resuspended in 1 ml FA lysis buffer (50 mM Hepes pH 7.5, 150 mM NaCl, 1 mM EDTA, 1% Triton, 0.1% sodium deoxycholate) with 0.1% sodium dodecyl sulfate (SDS) and 10% w/v cOmplete™ protease inhibitor pellet. Cells were broken using a mini beadbeater (BioSpec) and lysate was transferred

to a 1.5 mL low adhesion Eppendorf tube and debris was cleared by centrifugation (2000 x g, 3min, 4˚C). Supernatant was transferred to a new 1.5 mL low adhesion Eppendorf tube and lysate was centrifuged (20000 x g, 15min, 4˚C). Supernatant was discarded, leaving a cloudy pellet behind. Pellets were resuspended in 1ml lysis buffer + 0.1% SDS + cOmplete protease inhibitor and chromatin was sheared by sonication using a Bioruptor (Diagenode (Seraing, Belgium), 8 cycles of 30sec ON/45sec OFF). From sonicated samples, 50 µL of input was transferred for a 1.5 mL Eppendorf tube. Remaining extracts were incubated overnight at 4˚C in agarose beads conjugated to anti-V5 antibody (Millipore Sigma – A7345). Bead bound chromatin was then washed twice in 1ml lysis buffer, buffer 1 (250mM NaCl in lysis buffer + 0.1% SDS), and finally buffer 2 (10 mM Tris pH 8, 250 mM LiCl, 0.5% NP-40, 0.5% deoxycholate sodium, 1 mM EDTA) before reverse crosslinking was done in Tris-EDTA buffer (100 mM Tris pH 8.0, 10 mM EDTA, 1.0% v/v SDS) at 65˚C overnight. Previously collected inputs were also incubated overnight at 65˚C in Tris-EDTA. After 1h of proteinase K treatment at 65˚C, samples were cleaned using QiaQuick PCR cleanup (Qiagen – 28106) and enrichment of Ume6 at *IME2*, *SPO13*, and *ZIP1*, promoters as well as the *IME2 ORF* was measured by real-time PCR using SYBR green mix. RT-qPCR was carried out as follows: each IP was run alongside a dilution series of its sample matched input. This was done using primers that target the promoter of *NUF2* (*pNUF2*) as well as the above-mentioned sites. Using the input data, a dilution curve was used to normalize for fragment abundance. Then, Ume6 binding enrichment was assessed looking at the ratio of *pIME2*, *pSPO13*, *pZIP1*, and *IME2 ORF* fragments, over *pNUF2* fragments where Ume6 is not expected to bind. Oligonucleotide sequences used for ChIP are outlined in Table 6.3.2.

6.7 RNA-seq

RNA samples were collected and processed as described in RT-qPCR section. To prepare mRNA-seq libraries, 10 µg of total RNA was polyA-selected and processed using the NEXTFLEX Rapid Direction RNA-seq Kit (NOVA-5138-10 and NOVA-5138-11; PerkinElmer) according to the provided manual. Quantification of resulting cDNA yields was performed using a Qubit 3 (ThermoFisher Scientific) using the high sensitivity DNA assay kit. AMPure XP beads (A63881; Beckman Coulter) were using during size selection (200-500bp) and fragment quality and quantity was analyzed using high sensitivity D1000 ScreenTapes on the Agilent 4200 TapeStation (Agilent Technologies, Inc.). Samples were sequenced through the Vincent J. Coates QB3 Genomics Sequencing Facility at the University of California, Berkeley using 100 bp single-end sequencing on an Illumina Novaseq 6000. Alignment of sequenced reads was carried out using either HISAT2 or Kallisto. For HISAT2, the protocol outlined by Pertea et al. 2016 was used with SK1 reference genome, sourced from the Saccharomyces Genome Resequencing Project at the Sanger Institute to visualize transcript isoforms (Pertea et al. 2016). For Kallisto, pseudoalignments were carried out according to a manual developed by Bray et al. to

generate TPM and raw counts tables (Bray et al. 2016). Kallisto quant settings were adjusted to -b 5 -l 160 -s 20 - -single - -threads 4 based on fragment lengths determined by the Agilent 4200 TapeStation (Agilent Technologies, Inc.)

6.8 Heatmaps and Plots

R was further used for Spearman's correlation and with the packages pheatmap (ver. 1.0.12) and ggplot2 (ver. 3.4.0) to generate heatmaps and plots used in this manuscript, respectively (Wickham et al. 2019).

6.9 Differential Gene Expression Analysis

Ume6 Target Identification

Identification of differentially expressed genes (DEGs) responsive to Ume6 mitotic depletion was performed using two complementary approaches in R (R: ver. 4.1.3; RStudio: ver. 2022.07.1 Build 554). First, raw counts generated from Kallisto were exported to R. Then, using the DESeq2 package (ver. 1.34.0), differences in expression between control and Ume6 depletion samples across time (t = 0, 15, 30, 60, 120 min) were determined using an FDR of 5% (R Core Team; Love et al. 2014). To set up time series analysis, the DESeq2 "test" parameter was set to "Likelihood Ratio Test (LRT)" that, by default, uses the Wald test to generate results tables. Time series analysis between control and Ume6 depletion conditions using DESeq2 identified 177 Ume6-responsive genes (Table 1.1). Depletion of Ume6 during mitotic growth should derepress its targets, therefore we inspected the list of 177 Ume6-responsive genes looking for sustained derepression from 15 min to 120 min (post-Ume6 depletion). We noted some genes that were largely unchanged post-Ume6 depletion (i.e. *ERO1* and *BOI1*, ~1% and ~3% increase, respectively, comparing Ume6 depletion to control at t = 15 min) that were counted significant by DESeq2. Thus, to control for any false positives in our list of 177, we generated a custom R script to filter out these transcripts. In brief, to avoid transcripts that displayed a response independent of Ume6 depletion, we performed pairwise analysis using DESeq2 at t = -30 min and 0 min. Those genes with differential expression at these times (padj < 0.05; abs(log2FC) > 1) were removed. Next, we looked transcripts that displayed an acute response to Ume6 depletion at 15 min (padj < 0.05; abs(log2FC) > 0.3), as would be expected of direct regulation by Ume6. Filtering of transcripts using this script reduced the list from 177 to 135.

Second, we noted that some genes previously identified in Williams et al. 2002 as being derepressed in *ume6*∆ were not present in the list of 177 (i.e. *PIG1*). Further inspection in our TPM table revealed *PIG1* did experience a ~34% increase in expression post-Ume6 depletion (t = 15 min, comparing Ume6 depletion to control). Thus, to identify any genes missed by DESeq2, we performed additional analysis using TPM data and a custom R script. Briefly, we took the ratio between Ume6 depletion and control samples at each

time point (t = 15, 30, 60, and 120 min). This was done for the TPM of all genes. Next, we took the average (avg.) of these ratios across all time points. We then looked for genes whose avg. TPM ratio between Ume6 depletion and control across time was ≥ 1.4 or ≤ 0.6. Doing so, we identified 128 genes, 98 that were previously called significant by DESeq2. The 30 additional genes were inspected before being added to the list of 135 DESeq2 targets resulting in a total list of 165. Thus, between DESeq2 and TPM analysis we identified 165 distinct genes that responded to Ume6 depletion, referred to herein as our "composite list" (Table 1.1).

Sum1 Target Identification

Differential analysis was carried out as outlined in "Ume6 Target Identification" with the following modifications. Firstly, TPM data and the custom R script were not used in filtering. DEGs identified using DESeq2 at t = -30 min and 0 min removed if they showed padj < 0.05 and a log2FC > 2. Furthermore, DEGs identified by DESeq2 at t = 15 min were only considered significant if padj < 0.05 and log2FC > 0.5. Finally, DEGs identified across the time series (t = 0, 15, 30, 60, and 120 min) comparing control and Sum1 Deplete were only considered significant if padj < 0.05 and log2FC > 0.6. This resulted in 124 DEGs identified as being acutely responsive to Sum1 depletion (Table 2.1).

6.10 ChIP Peak Curation

Using a previously published dataset from Tresenrider et al. (2021) we analyzed ChIP peak scores for our composite list of 165 Ume6 targets. We divided the average ChIP peak score (n = 3 biological replicates) for each of the 165 Ume6-responsive genes by the ChIP peak score of *IME2*, a well-characterized Ume6 target and selected those with ratios ≥ 0.5. This analysis resulted in 144 Ume6-responsive genes that were also enriched for a Ume6 ChIP peak, indicating direct targets (Figure 2.7, Table 1.1).

Sum1-ChIP Peak Calling

Samples for ChIP were generated as outlined in "Chromatin Immunoprecipitation" and processed as outlined in "RNA-Seq" with the following modifications. The NEXTFLEX® Rapid DNA-Seq Kit 2.0 (NOVA-5188-02) was used to generate libraries according to protocol, before being sequenced through the Vincent J. Coates QB3 Genomics Sequencing Facility at the University of California, Berkeley using 100 bp single-end sequencing on an Illumina Novaseq 6000. Reads were aligned using HISAT2 as outlined. Peak calling was done visually in the Integrative Genomics Viewer (IGV; Robinson et al. 2011).

6.11 GO Enrichment

Go enrichment was performed in R using the clusterProfiler package (Yu et al. 2012) together with the org.Sc.sgd.db (ver. 3.14.0; Carlson 2021).

6.12 Motif Discovery

Motif enrichment analysis for Ume6 targets was performed using MEME (ver. 5.5.1 (Bailey et al. 2015). Sequences for 1,000 bp up- or downstream as well as the ORF were obtained using YeastMine (Balakrishnan et al. 2012) and exported to MEME as Fasta files for analysis with restricting the motif length's upper limit to 15 nucleotides, but otherwise using default settings. A $p < 0.05$ for a motif in a given gene was considered significant. These motifs were also validated using ChIP-Seq data from Tresenrider et al. 2021.

6.13 Gene Set Enrichment Analysis (GSEA)

Normalized counts generated from DESeq2 were compared between samples using GSEA v4.3.2 [build: 13] to assess enrichment of gene sets (Mootha et al. 2003; Subramanian et al. 2005). The "Early Meiotic Gene" set was generated by analyzing previously established data (Brar et al. 2012; Chia et al. 2021; Tresenrider et al. 2021). First, genes whose TPM changed in response to *pCUP1-IME1 pCUP1-IME4* induction by a log2FC > 1.0 were taken from Tresenrider et al (609 genes). Next, using a list of *NDT80* targets generated in Cheng and Otto et al, we removed MMGs from this list. The remaining 518 genes were then curated using Brar et al. and Chia et al., limiting expression timing to between meiotic entry and prior to metaphase I. Finally, genes with high TPM levels during mitotic growth were also excluded. This resulted in a list of 272 early expressed meiotic genes termed "Early Meiotic Genes". As mentioned, the second set of genes termed "Middle Meiotic Genes" were defined in Cheng and Otto et al. as a set of 394 genes responsive to *NDT80* induction (*NDT80* cluster, Cheng et al. 2018). The desktop version of GSEA was used to load in data and determine enrichment with the following modifications: "Collapse/Remap to gene symbols" was set to "No Collapse" and "Permutation Type" was set to "Gene Set", other settings were unchanged.

Bibliography:

Amon A. 1996. Mother and daughter are doing fine: asymmetric cell division in yeast. *Cell* **84**: 651–654.

Andersson SG, Zomorodipour A, Andersson JO, Sicheritz-Pontén T, Alsmark UC, Podowski RM, Näslund AK, Eriksson AS, Winkler HH, Kurland CG. 1998. The genome sequence of Rickettsia prowazekii and the origin of mitochondria. *Nature* **396**: 133–140.

Ayer DE, Kretzner L, Eisenman RN. 1993. Mad: A heterodimeric partner for Max that antagonizes Myc transcriptional activity. *Cell* **72**: 211–222.

Bailey TL, Elkan C. 1994. Fitting a mixture model by expectation maximization to discover motifs in biopolymers. *Proc Int Conf Intell Syst Mol Biol* **2**: 28–36.

Bailey TL, Johnson J, Grant CE, Noble WS. 2015. The MEME Suite. *Nucleic Acids Res* **43**: W39–W49.

Balakrishnan R, Park J, Karra K, Hitz BC, Binkley G, Hong EL, Sullivan J, Micklem G, Michael Cherry J. 2012. YeastMine—an integrated data warehouse for Saccharomyces cerevisiae data as a multipurpose tool-kit. *Database* **2012**: bar062.

Banani SF, Lee HO, Hyman AA, Rosen MK. 2017. Biomolecular condensates: organizers of cellular biochemistry. *Nat Rev Mol Cell Biol* **18**: 285–298.

Benjamin KR, Zhang C, Shokat KM, Herskowitz I. 2003. Control of landmark events in meiosis by the CDK Cdc28 and the meiosis-specific kinase Ime2. *Genes Dev* **17**: 1524–1539.

Berchowitz LE, Gajadhar AS, Werven FJ van, Rosa AAD, Samoylova ML, Brar GA, Xu Y, Xiao C, Futcher B, Weissman JS, et al. 2013. A developmentally regulated translational control pathway establishes the meiotic chromosome segregation pattern. *Genes Dev* **27**: 2147–2163.

Boija A, Klein IA, Sabari BR, Dall'Agnese A, Coffey EL, Zamudio AV, Li CH, Shrinivas K, Manteiga JC, Hannett NM, et al. 2018. Transcription Factors Activate Genes through the Phase-Separation Capacity of Their Activation Domains. *Cell* **175**: 1842-1855.e16.

Bonander N, Ferndahl C, Mostad P, Wilks MDB, Chang C, Showe L, Gustafsson L, Larsson C, Bill RM. 2008. Transcriptome analysis of a respiratory Saccharomyces cerevisiae strain suggests the expression of its phenotype is glucose insensitive and predominantly controlled by Hap4, Cat8 and Mig1. *BMC Genomics* **9**: 365.

Bowdish KS, Mitchell AP. 1993. Bipartite structure of an early meiotic upstream activation sequence from Saccharomyces cerevisiae. *Mol Cell Biol* **13**: 2172–2181.

Bowdish KS, Yuan HE, Mitchell AP. 1995. Positive control of yeast meiotic genes by the negative regulator UME6. *Mol Cell Biol* **15**: 2955–2961.

Bowles J, Knight D, Smith C, Wilhelm D, Richman J, Mamiya S, Yashiro K, Chawengsaksophak K, Wilson MJ, Rossant J, et al. 2006. Retinoid Signaling Determines Germ Cell Fate in Mice. *Science* **312**: 596–600.

Bram RJ, Lue NF, Kornberg RD. 1986. A GAL family of upstream activating sequences in yeast: roles in both induction and repression of transcription. *EMBO J* **5**: 603–608.

Brar GA, Yassour M, Friedman N, Regev A, Ingolia NT, Weissman JS. 2012. High-Resolution View of the Yeast Meiotic Program Revealed by Ribosome Profiling. *Science* **335**: 552–557.

Bray NL, Pimentel H, Melsted P, Pachter L. 2016. Near-optimal probabilistic RNA-seq quantification. *Nat Biotechnol* **34**: 525–527.

Brückner A, Polge C, Lentze N, Auerbach D, Schlattner U. 2009. Yeast two-hybrid, a powerful tool for systems biology. *Int J Mol Sci* **10**: 2763–2788.

Brzovic PS, Heikaus CC, Kisselev L, Vernon R, Herbig E, Pacheco D, Warfield L, Littlefield P, Baker D, Klevit RE, et al. 2011. The acidic transcription activator Gcn4 binds the Mediator subunit Gal11/Med15 using a simple protein interface forming a fuzzy complex. *Mol Cell* **44**: 942–953.

Carlile TM, Amon A. 2008. Meiosis I Is Established through Division-Specific Translational Control of a Cyclin. *Cell* **133**: 280–291.

Carlson M. 2021. org.Sc.sgd.db: Genome wide annotation for Yeast.

Chargaff E. 1950. Chemical specificity of nucleic acids and mechanism of their enzymatic degradation. *Experientia* **6**: 201–209.

Chaubal A, Pile LA. 2018. Same agent, different messages: insight into transcriptional regulation by SIN3 isoforms. *Epigenetics Chromatin* **11**: 17.

Chen J, Tresenrider A, Chia M, McSwiggen DT, Spedale G, Jorgensen V, Liao H, van Werven FJ, Ünal E. 2017. Kinetochore inactivation by expression of a repressive mRNA. *eLife* **6**.

Cheng Z, Otto GM, Powers EN, Keskin A, Mertins P, Carr SA, Jovanovic M, Brar GA. 2018. Pervasive, Coordinated Protein-Level Changes Driven by Transcript Isoform Switching during Meiosis. *Cell* **172**: 910-923.e16.

Chia M, Li C, Marques S, Pelechano V, Luscombe NM, van Werven FJ. 2021. High-resolution analysis of cell-state transitions in yeast suggests widespread transcriptional tuning by alternative starts. *Genome Biol* **22**: 34.

Chia M, Tresenrider A, Chen J, Spedale G, Jorgensen V, Ünal E, Werven FJ van. 2017. Transcription of a 5' extended mRNA isoform directs dynamic chromatin changes and interference of a downstream promoter. *eLife* **6**: e27420.

Chia M, van Werven FJ. 2016. Temporal Expression of a Master Regulator Drives Synchronous Sporulation in Budding Yeast. *G3 Bethesda Md* **6**: 3553–3560.

Chu S, DeRisi J, Eisen M, Mulholland J, Botstein D, Brown PO, Herskowitz I. 1998. The transcriptional program of sporulation in budding yeast. *Science* **282**: 699–705.

Clapier CR, Cairns BR. 2009. The biology of chromatin remodeling complexes. *Annu Rev Biochem* **78**: 273–304.

Colomina N, Garí E, Gallego C, Herrero E, Aldea M. 1999. G1 cyclins block the Ime1 pathway to make mitosis and meiosis incompatible in budding yeast. *EMBO J* **18**: 320–329.

Colomina N, Liu Y, Aldea M, Garí E. 2003. TOR Regulates the Subcellular Localization of Ime1, a Transcriptional Activator of Meiotic Development in Budding Yeast. *Mol Cell Biol* **23**: 7415–7424.

Cutter AR, Hayes JJ. 2015. A brief review of nucleosome structure. *FEBS Lett* **589**: 2914–2922.

De Vit MJ, Waddle JA, Johnston M. 1997. Regulated nuclear translocation of the Mig1 glucose repressor. *Mol Biol Cell* **8**: 1603–1618.

Donovan DA, Crandall JG, Truong VN, Vaaler AL, Bailey TB, Dinwiddie D, Banks OG, McKnight LE, McKnight JN. 2021. Basis of specificity for a conserved and promiscuous chromatin remodeling protein eds. J.L. Workman, K. Struhl, J.L. Workman, and B. Bartholomew. *eLife* **10**: e64061.

Du Z, Deng H, Cheng Y, Zhai Z, Guo X, Wang Z, He X. 2022. Cat8 Response to Nutritional Changes and Interaction With Ehrlich Pathway Related Factors. *Front Microbiol* **13**. https://www.frontiersin.org/articles/10.3389/fmicb.2022.898938 (Accessed August 2, 2023).

Duina AA, Miller ME, Keeney JB. 2014. Budding yeast for budding geneticists: a primer on the Saccharomyces cerevisiae model system. *Genetics* **197**: 33–48.

Dynan WS, Tjian R. 1983. Isolation of transcription factors that discriminate between different promoters recognized by RNA polymerase II. *Cell* **32**: 669–680.

Feichtinger J, McFarlane RJ. 2019. Meiotic gene activation in somatic and germ cell tumours. *Andrology* **7**: 415–427.

Ferder IC, Fung L, Ohguchi Y, Zhang X, Lassen KG, Capen D, Brown D, Xavier RJ, Wang N. 2019. Meiotic gatekeeper STRA8 suppresses autophagy by repressing Nr1d1 expression during spermatogenesis in mice. *PLoS Genet* **15**: e1008084.

Fields S, Song O. 1989. A novel genetic system to detect protein-protein interactions. *Nature* **340**: 245–246.

Fischer JA, Giniger E, Maniatis T, Ptashne M. 1988. GAL4 activates transcription in Drosophila. *Nature* **332**: 853–856.

Fridy PC, Li Y, Keegan S, Thompson MK, Nudelman I, Scheid JF, Oeffinger M, Nussenzweig MC, Fenyö D, Chait BT, et al. 2014. A robust pipeline for rapid production of versatile nanobody repertoires. *Nat Methods* **11**: 1253–1260.

Fritz M, Behringer M, Schwarz H. 2020. LOG-Means: efficiently estimating the number of clusters in large datasets. *Proc VLDB Endow* **13**: 2118–2131.

Gibson DG, Young L, Chuang R-Y, Venter JC, Hutchison CA, Smith HO. 2009. Enzymatic assembly of DNA molecules up to several hundred kilobases. *Nat Methods* **6**: 343–345.

Goldmark JP, Fazzio TG, Estep PW, Church GM, Tsukiyama T. 2000. The Isw2 Chromatin Remodeling Complex Represses Early Meiotic Genes upon Recruitment by Ume6p. *Cell* **103**: 423–433.

Grandori C, Cowley SM, James LP, Eisenman RN. 2000. The Myc/Max/Mad network and the transcriptional control of cell behavior. *Annu Rev Cell Dev Biol* **16**: 653–699.

Haber JE. 2012. Mating-type genes and MAT switching in Saccharomyces cerevisiae. *Genetics* **191**: 33–64.

Hahn S, Young ET. 2011. Transcriptional Regulation in Saccharomyces cerevisiae: Transcription Factor Regulation and Function, Mechanisms of Initiation, and Roles of Activators and Coactivators. *Genetics* **189**: 705–736.

Hanahan D, Weinberg RA. 2011. Hallmarks of cancer: the next generation. *Cell* **144**: 646–674.

Hassold T, Hunt P. 2001. To err (meiotically) is human: the genesis of human aneuploidy. *Nat Rev Genet* **2**: 280–291.

Haurie V, Perrot M, Mini T, Jenö P, Sagliocco F, Boucherie H. 2001. The Transcriptional Activator Cat8p Provides a Major Contribution to the Reprogramming of Carbon Metabolism during the Diauxic Shift in Saccharomyces cerevisiae *. *J Biol Chem* **276**: 76–85.

Henikoff S. 2000. Heterochromatin function in complex genomes. *Biochim Biophys Acta* **1470**: O1-8.

Herbig E, Warfield L, Fish L, Fishburn J, Knutson BA, Moorefield B, Pacheco D, Hahn S. 2010. Mechanism of Mediator recruitment by tandem Gcn4 activation domains and three Gal11 activator-binding domains. *Mol Cell Biol* **30**: 2376–2390.

Hickman MA, Rusche LN. 2007. Substitution as a Mechanism for Genetic Robustness: The Duplicated Deacetylases Hst1p and Sir2p in Saccharomyces cerevisiae. *PLOS Genet* **3**: e126.

Hollerer I, Barker JC, Jorgensen V, Tresenrider A, Dugast-Darzacq C, Chan LY, Darzacq X, Tjian R, Ünal E, Brar GA. 2019. Evidence for an Integrated Gene Repression Mechanism Based on mRNA Isoform Toggling in Human Cells. *G3 Bethesda Md* **9**: 1045–1053.

Hondele M, Sachdev R, Heinrich S, Wang J, Vallotton P, Fontoura BMA, Weis K. 2019. DEAD-box ATPases are global regulators of phase-separated organelles. *Nature* **573**: 144–148.

Hongay CF, Grisafi PL, Galitski T, Fink GR. 2006. Antisense Transcription Controls Cell Fate in Saccharomyces cerevisiae. *Cell* **127**: 735–745.

Inai T, Yukawa M, Tsuchiya E. 2007. Interplay between Chromatin and trans-Acting Factors on the IME2 Promoter upon Induction of the Gene at the Onset of Meiosis. *Mol Cell Biol* **27**: 1254–1263.

Ishiguro K. 2023. Chapter One - Mechanism of initiation of meiosis in mouse germ cells. In *Current Topics in Developmental Biology* (ed. F. Cole), Vol. 151 of *Meiosis in Development and Disease*, pp. 1–26, Academic Press https://www.sciencedirect.com/science/article/pii/S0070215322000680 (Accessed August 1, 2023).

Ishiguro K, Matsuura K, Tani N, Takeda N, Usuki S, Yamane M, Sugimoto M, Fujimura S, Hosokawa M, Chuma S, et al. 2020. MEIOSIN Directs the Switch from Mitosis to Meiosis in Mammalian Germ Cells. *Dev Cell* **52**: 429-445.e10.

Janke C, Magiera MM, Rathfelder N, Taxis C, Reber S, Maekawa H, Moreno-Borchart A, Doenges G, Schwob E, Schiebel E, et al. 2004. A versatile toolbox for PCR-based tagging of yeast genes: new fluorescent proteins, more markers and promoter substitution cassettes. *Yeast* **21**: 947–962.

Jäschke Y, Schwarz J, Clausnitzer D, Müller C, Schüller H-J. 2011. Pleiotropic corepressors Sin3 and Ssn6 interact with repressor Opi1 and negatively regulate transcription of genes required for phospholipid biosynthesis in the yeast Saccharomyces cerevisiae. *Mol Genet Genomics MGG* **285**: 91–100.

Jedidi I, Zhang F, Qiu H, Stahl SJ, Palmer I, Kaufman JD, Nadaud PS, Mukherjee S, Wingfield PT, Jaroniec CP, et al. 2010. Activator Gcn4 Employs Multiple Segments of Med15/Gal11, Including the KIX Domain, to Recruit Mediator to Target Genes in Vivo♦. *J Biol Chem* **285**: 2438–2455.

Johnston M. 1987. A model fungal gene regulatory mechanism: the GAL genes of Saccharomyces cerevisiae. *Microbiol Rev* **51**: 458–476.

Kadamb R, Mittal S, Bansal N, Batra H, Saluja D. 2013. Sin3: insight into its transcription regulatory functions. *Eur J Cell Biol* **92**: 237–246.

Kakidani H, Ptashne M. 1988. GAL4 activates gene expression in mammalian cells. *Cell* **52**: 161–167.

Kassir Y, Granot D, Simchen G. 1988. IME1, a positive regulator gene of meiosis in S. cerevisiae. *Cell* **52**: 853–862.

Keegan L, Gill G, Ptashne M. 1986. Separation of DNA binding from the transcription-activating function of a eukaryotic regulatory protein. *Science* **231**: 699–704.

Kimble J, Crittenden SL. 2007. Controls of germline stem cells, entry into meiosis, and the sperm/oocyte decision in Caenorhabditis elegans. *Annu Rev Cell Dev Biol* **23**: 405–433.

King GA, Goodman JS, Schick JG, Chetlapalli K, Jorgens DM, McDonald KL, Ünal E. 2019. Meiotic cellular rejuvenation is coupled to nuclear remodeling in budding yeast eds. N. Mizushima, V. Malhotra, N. Mizushima, T. Haraguchi, and C.P. Lusk. *eLife* **8**: e47156.

King GA, Wettstein R, Varberg JM, Chetlapalli K, Walsh ME, Gillet LCJ, Hernández-Armenta C, Beltrao P, Aebersold R, Jaspersen SL, et al. 2022. Meiotic nuclear pore complex remodeling provides key insights into nuclear basket organization. *J Cell Biol* **222**: e202204039.

Kojima ML, de Rooij DG, Page DC. 2019. Amplification of a broad transcriptional program by a common factor triggers the meiotic cell cycle in mice. *eLife* **8**: e43738.

Kouzarides T. 2007. Chromatin modifications and their function. *Cell* **128**: 693–705.

Kribelbauer JF, Rastogi C, Bussemaker HJ, Mann RS. 2019. Low-Affinity Binding Sites and the Transcription Factor Specificity Paradox in Eukaryotes. *Annu Rev Cell Dev Biol* **35**: 357–379.

Lambert SA, Jolma A, Campitelli LF, Das PK, Yin Y, Albu M, Chen X, Taipale J, Hughes TR, Weirauch MT. 2018. The Human Transcription Factors. *Cell* **172**: 650–665.

Lamont LB, Crittenden SL, Bernstein D, Wickens M, Kimble J. 2004. FBF-1 and FBF-2 regulate the size of the mitotic region in the C. elegans germline. *Dev Cell* **7**: 697–707.

Law MJ, Mallory MJ, Dunbrack RL, Strich R. 2014. Acetylation of the Transcriptional Repressor Ume6p Allows Efficient Promoter Release and Timely Induction of the Meiotic Transient Transcription Program in Yeast. *Mol Cell Biol* **34**: 631–642.

Li K. 2008. The image stabilizer plugin for ImageJ. *http://www.cs.cmu.edu/~kangli/code/Image_Stabilizer.html*.

Lim CY, Santoso B, Boulay T, Dong E, Ohler U, Kadonaga JT. 2004. The MTE, a new core promoter element for transcription by RNA polymerase II. *Genes Dev* **18**: 1606–1617.

Lingg L, Rottenberg S, Francica P. 2022. Meiotic Genes and DNA Double Strand Break Repair in Cancer. *Front Genet* **13**: 831620.

Liu X, Liu X, Wang H, Dou Z, Ruan K, Hill DL, Li L, Shi Y, Yao X. 2020. Phase separation drives decision making in cell division. *J Biol Chem* **295**: 13419–13431.

Longtine MS, McKenzie A, Demarini DJ, Shah NG, Wach A, Brachat A, Philippsen P, Pringle JR. 1998. Additional modules for versatile and economical PCR-based gene deletion and modification in Saccharomyces cerevisiae. *Yeast Chichester Engl* **14**: 953–961.

Love MI, Huber W, Anders S. 2014. Moderated estimation of fold change and dispersion for RNA-seq data with DESeq2. *Genome Biol* **15**: 550.

Ma J, Przibilla E, Hu J, Bogorad L, Ptashne M. 1988. Yeast activators stimulate plant gene expression. *Nature* **334**: 631–633.

Majmudar CY, Wang B, Lum JK, Håkansson K, Mapp AK. 2009. A high-resolution interaction map of three transcriptional activation domains with a key coactivator from photo-cross-linking and multiplexed mass spectrometry. *Angew Chem Int Ed Engl* **48**: 7021–7024.

Malathi K, Xiao Y, Mitchell AP. 1999. Catalytic Roles of Yeast GSK3β/Shaggy Homolog Rim11p in Meiotic Activation. *Genetics* **153**: 1145–1152.

Malathi K, Xiao Y, Mitchell AP. 1997. Interaction of yeast repressor-activator protein Ume6p with glycogen synthase kinase 3 homolog Rim11p. *Mol Cell Biol* **17**: 7230–7236.

Mallory MJ, Cooper KF, Strich R. 2007. Meiosis-specific destruction of the Ume6p repressor by the Cdc20-directed APC/C. *Mol Cell* **27**: 951–961.

Mallory MJ, Law MJ, Sterner DE, Berger SL, Strich R. 2012. Gcn5p-dependent acetylation induces degradation of the meiotic transcriptional repressor Ume6p. *Mol Biol Cell* **23**: 1609–1617.

Mao-Draayer Y, Galbraith AM, Pittman DL, Cool M, Malone RE. 1996. Analysis of Meiotic Recombination Pathways in the Yeast Saccharomyces Cerevisiae. *Genetics* **144**: 71–86.

Marston AL, Amon A. 2004. Meiosis: cell-cycle controls shuffle and deal. *Nat Rev Mol Cell Biol* **5**: 983–997.

Maston GA, Evans SK, Green MR. 2006. Transcriptional regulatory elements in the human genome. *Annu Rev Genomics Hum Genet* **7**: 29–59.

Matos J, Lipp JJ, Bogdanova A, Guillot S, Okaz E, Junqueira M, Shevchenko A, Zachariae W. 2008. Dbf4-Dependent Cdc7 Kinase Links DNA Replication to the Segregation of Homologous Chromosomes in Meiosis I. *Cell* **135**: 662–678.

McFarlane RJ, Wakeman JA. 2017. Meiosis-like Functions in Oncogenesis: A New View of Cancer. *Cancer Res* **77**: 5712–5716.

Mitchell AP. 1994. Control of meiotic gene expression in Saccharomyces cerevisiae. *Microbiol Rev* **58**: 56–70.

Mitchell AP, Bowdish KS. 1992. Selection for early meiotic mutants in yeast. *Genetics* **131**: 65–72.

Mitrea DM, Cika JA, Guy CS, Ban D, Banerjee PR, Stanley CB, Nourse A, Deniz AA, Kriwacki RW. 2016. Nucleophosmin integrates within the nucleolus via multi-modal interactions with proteins displaying R-rich linear motifs and rRNA. *eLife* **5**: e13571.

Monteiro PT, Oliveira J, Pais P, Antunes M, Palma M, Cavalheiro M, Galocha M, Godinho CP, Martins LC, Bourbon N, et al. 2020. YEASTRACT+: a portal for cross-species comparative genomics of transcription regulation in yeasts. *Nucleic Acids Res* **48**: D642–D649.

Mootha VK, Lindgren CM, Eriksson K-F, Subramanian A, Sihag S, Lehar J, Puigserver P, Carlsson E, Ridderstråle M, Laurila E, et al. 2003. PGC-1α-responsive genes involved in oxidative phosphorylation are coordinately downregulated in human diabetes. *Nat Genet* **34**: 267–273.

Moreno-Campuzano S, Janga SC, Pérez-Rueda E. 2006. Identification and analysis of DNA-binding transcription factors in Bacillus subtilis and other Firmicutes--a genomic approach. *BMC Genomics* **7**: 147.

Moretto F, Wood NE, Chia M, Li C, Luscombe NM, van Werven FJ. 2021. Transcription levels of a noncoding RNA orchestrate opposing regulatory and cell fate outcomes in yeast. *Cell Rep* **34**: 108643.

Moretto F, Wood NE, Kelly G, Doncic A, Werven FJ van. 2018. A regulatory circuit of two lncRNAs and a master regulator directs cell fate in yeast. *Nat Commun* **9**: 780.

Nachman I, Regev A, Ramanathan S. 2007. Dissecting Timing Variability in Yeast Meiosis. *Cell* **131**: 544–556.

Nagaoka SI, Hassold TJ, Hunt PA. 2012. Human aneuploidy: mechanisms and new insights into an age-old problem. *Nat Rev Genet* **13**: 493–504.

Nasmyth K, Stillman D, Kipling D. 1987. Both positive and negative regulators of HO transcription are required for mother-cell-specific mating-type switching in yeast. *Cell* **48**: 579–587.

Neiman AM. 2011. Sporulation in the budding yeast Saccharomyces cerevisiae. *Genetics* **189**: 737–765.

Nishimura K, Fukagawa T, Takisawa H, Kakimoto T, Kanemaki M. 2009. An auxin-based degron system for the rapid depletion of proteins in nonplant cells. *Nat Methods* **6**: 917–922.

Okaz E, Argüello-Miranda O, Bogdanova A, Vinod PK, Lipp JJ, Markova Z, Zagoriy I, Novak B, Zachariae W. 2012. Meiotic Prophase Requires Proteolysis of M Phase Regulators Mediated by the Meiosis-Specific APC/CAma1. *Cell* **151**: 603–618.

Ottoz DSM, Rudolf F, Stelling J. 2014. Inducible, tightly regulated and growth condition-independent transcription factor in Saccharomyces cerevisiae. *Nucleic Acids Res* **42**: e130.

Pabo CO, Sauer RT. 1984. Protein-DNA recognition. *Annu Rev Biochem* **53**: 293–321.

Padmore R, Cao L, Kleckner N. 1991. Temporal comparison of recombination and synaptonemal complex formation during meiosis in S. cerevisiae. *Cell* **66**: 1239–1256.

Pâques F, Haber JE. 1999. Multiple Pathways of Recombination Induced by Double-Strand Breaks in Saccharomyces cerevisiae. *Microbiol Mol Biol Rev* **63**: 349–404.

Park H-D, Luche RM, Cooper TG. 1992. The yeast UME6 gene product is required for transcriptional repression mediated by the CAR1URS1 repressor binding site. *Nucleic Acids Res* **20**: 1909–1915.

Park JM, Kim H-S, Han SJ, Hwang M-S, Lee YC, Kim Y-J. 2000. In Vivo Requirement of Activator-Specific Binding Targets of Mediator. *Mol Cell Biol* **20**: 8709–8719.

Pertea M, Kim D, Pertea GM, Leek JT, Salzberg SL. 2016. Transcript-level expression analysis of RNA-seq experiments with HISAT, StringTie and Ballgown. *Nat Protoc* **11**: 1650–1667.

Pierce M, Benjamin KR, Montano SP, Georgiadis MM, Winter E, Vershon AK. 2003. Sum1 and Ndt80 proteins compete for binding to middle sporulation element sequences that control meiotic gene expression. *Mol Cell Biol* **23**: 4814–4825.

Pnueli L, Edry I, Cohen M, Kassir Y. 2004. Glucose and nitrogen regulate the switch from histone deacetylation to acetylation for expression of early meiosis-specific genes in budding yeast. *Mol Cell Biol* **24**: 5197–5208.

Quintero MJ, Maya D, Arévalo-Rodríguez M, Cebolla Á, Chávez S. 2007. An improved system for estradiol-dependent regulation of gene expression in yeast. *Microb Cell Factories* **6**: 10.

R Core Team. R: A language and environment for statistical computing. *R Found Stat Comput Vienna*. https://www.R-project.org.

Raithatha SA, Vaza S, Islam MT, Greenwood B, Stuart DT. 2021. Ume6 Acts as a Stable Platform To Coordinate Repression and Activation of Early Meiosis-Specific Genes in Saccharomyces cerevisiae. *Mol Cell Biol* **41**: e00378-20.

Rog O, Köhler S, Dernburg AF. 2017. The synaptonemal complex has liquid crystalline properties and spatially regulates meiotic recombination factors. *eLife* **6**: e21455.

Roth S, Kumme J, Schüller H-J. 2004. Transcriptional activators Cat8 and Sip4 discriminate between sequence variants of the carbon source-responsive promoter element in the yeast Saccharomyces cerevisiae. *Curr Genet* **45**: 121–128.

Rubin-Bejerano I, Mandel S, Robzyk K, Kassir Y. 1996. Induction of meiosis in Saccharomyces cerevisiae depends on conversion of the transcriptional represssor Ume6 to a positive regulator by its regulated association with the transcriptional activator Ime1. *Mol Cell Biol* **16**: 2518–2526.

Rundlett SE, Carmen AA, Suka N, Turner BM, Grunstein M. 1998. Transcriptional repression by UME6 involves deacetylation of lysine 5 of histone H4 by RPD3. *Nature* **392**: 831–835.

Sainsbury S, Bernecky C, Cramer P. 2015. Structural basis of transcription initiation by RNA polymerase II. *Nat Rev Mol Cell Biol* **16**: 129–143.

Sawyer EM, Joshi PR, Jorgensen V, Yunus J, Berchowitz LE, Ünal E. 2019. Developmental regulation of an organelle tether coordinates mitochondrial remodeling in meiosis. *J Cell Biol* **218**: 559–579.

Schindelin J, Arganda-Carreras I, Frise E, Kaynig V, Longair M, Pietzsch T, Preibisch S, Rueden C, Saalfeld S, Schmid B, et al. 2012. Fiji: an open-source platform for biological-image analysis. *Nat Methods* **9**: 676–682.

Shah JC, Clancy MJ. 1992. IME4, a gene that mediates MAT and nutritional control of meiosis in Saccharomyces cerevisiae. *Mol Cell Biol* **12**: 1078–1086.

Smith HE, Driscoll SE, Sia RAL, Yuan HE, Mitchell AP. 1993. Genetic Evidence for Transcriptional Activation by the Yeast Ime1 Gene Product. *Genetics* **133**: 775–784.

Smith HE, Su SS, Neigeborn L, Driscoll SE, Mitchell AP. 1990. Role of IME1 expression in regulation of meiosis in Saccharomyces cerevisiae. *Mol Cell Biol* **10**: 6103–6113.

Soutourina J. 2018. Transcription regulation by the Mediator complex. *Nat Rev Mol Cell Biol* **19**: 262–274.

Spiller C, Koopman P, Bowles J. 2017. Sex Determination in the Mammalian Germline. *Annu Rev Genet* **51**: 265–285.

Sternberg PW, Stern MJ, Clark I, Herskowitz I. 1987. Activation of the yeast HO gene by release from multiple negative controls. *Cell* **48**: 567–577.

Stormo GD. 2013. Modeling the specificity of protein-DNA interactions. *Quant Biol Beijing China* **1**: 115–130.

Strich R, Slater MR, Esposito RE. 1989. Identification of negative regulatory genes that govern the expression of early meiotic genes in yeast. *Proc Natl Acad Sci U S A* **86**: 10018–10022.

Strich R, Surosky RT, Steber C, Dubois E, Messenguy F, Esposito RE. 1994. UME6 is a key regulator of nitrogen repression and meiotic development. *Genes Dev* **8**: 796–810.

Su X, Ditlev JA, Hui E, Xing W, Banjade S, Okrut J, King DS, Taunton J, Rosen MK, Vale RD. 2016. Phase separation of signaling molecules promotes T cell receptor signal transduction. *Science* **352**: 595–599.

Subramanian A, Tamayo P, Mootha VK, Mukherjee S, Ebert BL, Gillette MA, Paulovich A, Pomeroy SL, Golub TR, Lander ES, et al. 2005. Gene set enrichment analysis: A knowledge-based approach for interpreting genome-wide expression profiles. *Proc Natl Acad Sci* **102**: 15545–15550.

Suzuki A, Hirasaki M, Hishida T, Wu J, Okamura D, Ueda A, Nishimoto M, Nakachi Y, Mizuno Y, Okazaki Y, et al. 2016. Loss of MAX results in meiotic entry in mouse embryonic and germline stem cells. *Nat Commun* **7**: 11056.

Tedesco M, Desimio MG, Klinger FG, De Felici M, Farini D. 2013. Minimal concentrations of retinoic acid induce stimulation by retinoic acid 8 and promote entry into meiosis in isolated pregonadal and gonadal mouse primordial germ cells. *Biol Reprod* **88**: 145.

Tedesco M, La Sala G, Barbagallo F, De Felici M, Farini D. 2009. STRA8 Shuttles between Nucleus and Cytoplasm and Displays Transcriptional Activity. *J Biol Chem* **284**: 35781–35793.

Thorndike RL. 1953. Who belongs in the family? *Psychometrika* **18**: 267–276.

Tresenrider A, Morse K, Jorgensen V, Chia M, Liao H, van Werven FJ, Ünal E. 2021. Integrated genomic analysis reveals key features of long undecoded transcript isoform-based gene repression. *Mol Cell* **81**: 2231-2245.e11.

Tsuchiya D, Yang Y, Lacefield S. 2014. Positive Feedback of NDT80 Expression Ensures Irreversible Meiotic Commitment in Budding Yeast. *PLOS Genet* **10**: e1004398.

Turjanski AG, Gutkind JS, Best RB, Hummer G. 2008. Binding-induced folding of a natively unstructured transcription factor. *PLoS Comput Biol* **4**: e1000060.

van Werven FJ, Amon A. 2011. Regulation of entry into gametogenesis. *Philos Trans R Soc Lond B Biol Sci* **366**: 3521–3531.

van Werven FJ, Neuert G, Hendrick N, Lardenois A, Buratowski S, van Oudenaarden A, Primig M, Amon A. 2012. Transcription of two long non-coding RNAs mediates mating type control of gametogenesis in budding yeast. *Cell* **150**: 1170–1181.

Vidal M, Strich R, Esposito RE, Gaber RF. 1991. RPD1 (SIN3/UME4) is required for maximal activation and repression of diverse yeast genes. *Mol Cell Biol* **11**: 6306–6316.

Vidan S, Mitchell AP. 1997. Stimulation of yeast meiotic gene expression by the glucose-repressible protein kinase Rim15p. *Mol Cell Biol* **17**: 2688–2697.

Wang H, Clark I, Nicholson PR, Herskowitz I, Stillman DJ. 1990. The Saccharomyces cerevisiae SIN3 gene, a negative regulator of HO, contains four paired amphipathic helix motifs. *Mol Cell Biol* **10**: 5927–5936.

Washburn BK, Esposito RE. 2001. Identification of the Sin3-binding site in Ume6 defines a two-step process for conversion of Ume6 from a transcriptional repressor to an activator in yeast. *Mol Cell Biol* **21**: 2057–2069.

Watson JD, Crick FH. 1953. Molecular structure of nucleic acids; a structure for deoxyribose nucleic acid. *Nature* **171**: 737–738.

Webster N, Jin JR, Green S, Hollis M, Chambon P. 1988. The yeast UASG is a transcriptional enhancer in human hela cells in the presence of the GAL4 trans-activator. *Cell* **52**: 169–178.

Weidberg H, Moretto F, Spedale G, Amon A, Werven FJ van. 2016. Nutrient Control of Yeast Gametogenesis Is Mediated by TORC1, PKA and Energy Availability. *PLOS Genet* **12**: e1006075.

Weinhandl K, Winkler M, Glieder A, Camattari A. 2014. Carbon source dependent promoters in yeasts. *Microb Cell Factories* **13**: 5.

Whinston E, Omerza G, Singh A, Tio CW, Winter E. 2013. Activation of the Smk1 Mitogen-Activated Protein Kinase by Developmentally Regulated Autophosphorylation. *Mol Cell Biol* **33**: 688–700.

Wickham H, Averick M, Bryan J, Chang W, McGowan LD, François R, Grolemund G, Hayes A, Henry L, Hester J, et al. 2019. Welcome to the Tidyverse. *J Open Source Softw* **4**: 1686.

Williams RM, Primig M, Washburn BK, Winzeler EA, Bellis M, Menthière CS de, Davis RW, Esposito RE. 2002. The Ume6 regulon coordinates metabolic and meiotic gene expression in yeast. *Proc Natl Acad Sci* **99**: 13431–13436.

Williamson I, Lettice LA, Hill RE, Bickmore WA. 2016. Shh and ZRS enhancer colocalisation is specific to the zone of polarising activity. *Dev Camb Engl* **143**: 2994–3001.

Winter E. 2012. The Sum1/Ndt80 transcriptional switch and commitment to meiosis in Saccharomyces cerevisiae. *Microbiol Mol Biol Rev MMBR* **76**: 1–15.

Woznica A, Gerdt JP, Hulett RE, Clardy J, King N. 2017. Mating in the Closest Living Relatives of Animals Is Induced by a Bacterial Chondroitinase. *Cell* **170**: 1175-1183.e11.

Xie J, Pierce M, Gailus-Durner V, Wagner M, Winter E, Vershon AK. 1999. Sum1 and Hst1 repress middle sporulation-specific gene expression during mitosis in Saccharomyces cerevisiae. *EMBO J* **18**: 6448–6454.

Xu L, Ajimura M, Padmore R, Klein C, Kleckner N. 1995. NDT80, a meiosis-specific gene required for exit from pachytene in Saccharomyces cerevisiae. *Mol Cell Biol* **15**: 6572–6581.

Yu G, Wang L-G, Han Y, He Q-Y. 2012. clusterProfiler: an R Package for Comparing Biological Themes Among Gene Clusters. *OMICS J Integr Biol* **16**: 284–287.

Zhao Y, Garcia BA. 2015. Comprehensive Catalog of Currently Documented Histone Modifications. *Cold Spring Harb Perspect Biol* **7**: a025064.